Investigating Lava Flow Emplacement: Implications for Volcanic Hazards and Planetary Evolution

by

Sean I. Peters

A Dissertation Presented in Partial Fulfillment
of the Requirements for the Degree
Doctor of Philosophy

Approved May 2020 by the
Graduate Supervisory Committee:

Philip R Christensen, Chair
Amanda Clarke
Jonathon Fink
Kelin Whipple
Thomas Sharp

ARIZONA STATE UNIVERSITY

August 2020

ABSTRACT

Lava flow emplacement in the laboratory and on the surface of Mars was investigated. In the laboratory, the effects of unsteady effusion rates at the vent on four modes of emplacement common to lava flow propagation: resurfacing, marginal breakouts, inflation, and lava tubes was addressed. A total of 222 experiments were conducted using a programmable pump to inject dyed PEG wax into a chilled bath (~ 0° C) in tanks with a roughened base at slopes of 0, 7, 16, and 29°. The experiments were divided into four conditions, which featured increasing or decreasing eruption rates for either 10 or 50 s. The primary controls on modes of emplacement were crust formation, variability in the eruption rate, and duration of the pulsatory flow rate. Resurfacing – although a relatively minor process – is inhibited by an extensive, coherent crust. Inflation requires a competent, flexible crust. Tube formation requires a crust and intermediate to low effusion rates. On Mars, laboratory analogue experiments combined with models that use flow dimensions to estimate emplacement conditions and using high resolution image data and digital terrain models (e.g. THEMIS IR, CTX, HRSC), the eruption rates, viscosities, and yield strengths of 40 lava flows in the Tharsis Volcanic Province have been quantified. These lava flows have lengths, mean widths, and mean thicknesses of 15 – 314 km, 0.5 – 29 km, and 11 – 91 m, respectively. Flow volumes range from ~1 – 430 km^3. Based on laboratory experiments, the 40 observed lava flows were erupted at 0.2 – 6.5x10^3 m^3/s, while the Graetz number and Jeffrey's equation when applied to 34 of 40 lava flows indicates eruption rates and viscosities of 300 – ~3.5 x 10^4 m^3/s and ~10^5 – 10^8 Pa s, respectively. Another model which accounts for mass loss to levee formation was applied to a subset of flows, n = 13, and suggests eruption rates and viscosities of ~30 – ~1.2 x 10^3

m^3/s and 4.5 x 10^6 – ~3 x 10^7 Pa s, respectively. Emplacement times range from days to centuries indicating the necessity for long-term subsurface conduits capable of delivering enormous volumes of lava to the surface.

DEDICATION

This dissertation is dedicated firstly to my grandparents, notably Frank and Evelena Curtis; and my parents, Lola and Charles Peters. Not only did they overcome decades of systemic racism, poverty, and generalized oppression, but in the backdrop of that hellscape they managed to instill in their grandson and son the importance of literacy, education, determination, justice, and fairness. They encouraged my creativity, nurtured my curiosity, loved me unconditionally, and sacrificed without question. Secondly, this dissertation is dedicated to the numerous teachers, instructors, and professors who have mentored me in all things academic and professional – providing a deeper understanding of the purpose behind education, motivating me to push my limits, and fostering a supportive network and environment to help me achieve my goals. Thirdly, but certainly not the least, this dissertation is dedicated to the fantastic friendships that have carried me through the ups-and-downs of graduate school and life. The amount of mental and emotional labor implicit in this work would not have been possible without the support of those near and far.

ACKNOWLEDGMENTS

I would like to acknowledge those outside of my committee who have contributed both directly and indirectly to this monumental effort, which includes a numerous amount of faculty, staff, and colleagues. I would like to highlight efforts by Dr. Erika Rader and Dr. Christopher Mount. Dr. Erika Rader taught me the experimental methodologies outlined in this work. Dr. Christopher Mount assisted with laboratory setup, calibration, and experimentation. Most importantly, both Drs. Rader and Mount kept me sane during long hours in the laboratory. In addition, I would like to acknowledge Dr. Christopher Haberle who was instrumental in teaching me technical aspects related to work; Jonathon Hill for teaching me the technical aspects of data processing; and Ashley Toland for organizing the logistics necessary to share my work at conferences.

TABLE OF CONTENTS

Page

LIST OF TABLES

LIST OF FIGURES

CHAPTER 1

INTRODUCTION

I. Introduction

Volcanism is one of the four fundamental geologic processes affecting the surfaces of rocky bodies, large and small, in the solar system. It is a by-product of planetary formation and evolution resulting in heat loss of a silicate body. Understanding the volcanic history and behavior of a body provides information on its formation and evolution in the context of differentiation and composition. On planetary bodies such as Mars, unravelling the volcanic history of the planet is complicated by the lack of data, the lack of human observation during volcanic activity, and sometimes a lack of analogous terrestrial terrain and processes. On Earth, there is the added complication of degradation, erosion, and plate tectonics, which has worked to erase a significant portion of Earth's geologic past. Because volcanism has occurred on every planetary body in the inner solar system, it is important to understand the role of volcanism within the context of other geologic processes (i.e. erosion/degradation, impacts, and tectonism). On Earth, there is an additional motivation produced by the 800 million humans who live within the vicinity of a volcano. Hazards prevention remains one of the driving motivations for research in volcanology. Numerical modelling and laboratory analogue experiments have attempted to qualitatively and quantitatively describe the natural phenomenon observed in relation to volcanic plumes and lava flows [e.g. Fink and Griffiths, 1990, 1992; Gregg and Fink, 2000; Sakimoto and Gregg, 2001; Vicari et al., 2011]. The phenomenology of lava flows is complex and has yet to be fully replicated by numerical modelling [e.g. Hupper and Sparks, 1987; Pinkerton, 1987; Fink and Griffiths, 1990]. A wedding of laboratory experiments

and numerical modelling would be valuable to the volcanology community, specifically those seeking to predict volcanic hazards to inform state/local officials, understand the formation/evolution of large shield volcanoes and large igneous provinces, and/or estimate prehistoric eruption conditions. An understanding of these processes on Earth can be translated to other planets with similar planetary conditions. On Mars, even with limited compositional data, volcanism is thought to behave like that on Earth albeit at different physical and temporal scales [Carr, 1973; Hulme, 1974; Hiesinger et al., 2007; Hauber et al., 2011]. Understanding the volcanic history of Mars places constraints on its interior composition, surface evolution, and subsurface environment [Wilson and Head, 1983].

Knowledge gaps persists in how the steadiness of eruption rates impacts flow morphology and propagation [*Wadge*, 1981; *Rader et al.*, 2017]. Previous studies focused on modelling and laboratory experiments have generally assumed constant eruption rates at the vent, however, the eruption rate can vary on timescales of hours to days [*Wadge*, 1981]. The relationship between these fluctuating eruption rates and modes of emplacement common to lava flow propagation (e.g. inflation and tube formation) has not been investigated in the laboratory. The results of this work will establish a framework for addressing the impact of unsteady eruption rates on flow morphology and propagation in the laboratory, which can be extended to modelling. On Mars, discerning lava flow emplacement conditions is hampered by a lack of direct observation, deposit morphology degradation, and poorly constrained planetary variables. Early studies suggested exceptionally high eruption rates and/or ultramafic lava compositions to explain the morphologies observed on Mars [*Cashman et al.*, 1998]. Recent studies, on the other hand, suggest that compositions and eruptions more analogous to terrestrial conditions are able

to explain the immense lava flows and volcanic constructs observed on Mars [*Hiesinger et al.*, 2007; *Baloga and Glaze*, 2008; *Hauber et al.*, 2011]. Variations in eruption conditions for Mars are also due to the different applied models and methods. Sampling a suite of lava flows using three models, including work derived from laboratory wax experiments, will further constrain Martian eruption conditions.

In the following chapters, I address the question of lava flow phenomenology, specifically deposit morphology and flow front propagation, with direct implications for Earth and Mars using laboratory analogue wax experiments. With these experiments, I qualitatively and quantitatively characterize the effects of unsteady eruption conditions on specific modes of emplacement (i.e. resurfacing, breakouts, inflation, and tube formation) and the effects of slope and unsteady vent conditions on said emplacement modes. These modes of emplacement directly impact the morphology and propagation of lava flows. In doing so, I provide phenomenological insights into lava flow emplacement that can be used to constrain probabilistic and physics-based models of lava flows on Earth and the quantification of prehistoric Martian emplacement conditions. Additionally, these experiments – due to the variables investigated – can inform our understanding of the processes responsible for producing plains-style volcanism, large shield volcanoes, and large igneous provinces [*Rader et al.*, 2017].

II. Background

Previous studies [*Huppert and Sparks*, 1987; *Fink and Griffiths*, 1990; *Griffiths and Fink*, 1992; *Gregg and Fink*, 1996; 2000; *Blake and Bruno*, 2000; *Soule and Cashman*, 2004; *Rader et al.*, 2017] have established the utility of laboratory analogue experimentation, in particular, the use of polyethylene glycol wax (PEG) – an edible

commercial polymer – in simulating lava emplacement due to its temperature dependent viscosity and readiness to form a crust. The usefulness of PEG as an analogue for lava flows has been demonstrated in a variety of studies aimed at understanding the fundamental phenomenology and physics of lava flows [*Fink and Griffiths,* 1990; *Griffiths and Fink*, 1992; *Gregg and Fink*, 1996; 2000; *Soule and Cashman*, 2004; *Griffiths and Fink, Rader et al.*, 2017]. *Fink and Griffiths* [1990] used PEG experiments to develop a dimensionless parameter Ψ that is used to describe the ratio of the timescales of crust formation and flow advancement. The parameter, Ψ, is an effective way of discerning the emplacement conditions of a flow, specifically how the flow transported heat, based off of its surface morphology. They found that flow behavior and morphology differed across discrete regimes of Ψ. *Gregg and Fink* [1996] applied the lessons from these experiments to extraterrestrial bodies and made predictions on the morphologies that would be observed on those planets. *Gregg and Fink* [2000] demonstrated using PEG experiments that increasing underlying slope decreases the expected Ψ value for a given morphology by increasing the flow velocity, creating an *effective* effusion rate. This results in morphologies associated with higher Ψ being produced on steeper slopes at lower Ψ. This work was extended by *Gregg and Smith* [2003] to investigate submarine lava flows on the Puna Ridge, Hawai'i. Analogous morphologies to those created in the lab were observed. The applicability of Ψ has also been investigated to determine its robustness in understanding the formation and evolution of a lava flow or flow field [*Gregg and Kesthelyi, 2004*]. Additional studies have looked at the effects of channel morphology on lava flows, crust distribution on the surface of lava flows, the stresses within a lava flow, and the formation of compound lava flows, although most assume steady conditions at the

vent [*Griffiths and Fink*, 1992; *Blake and Bruno*, 2000; *Cashman et al.*, 2006; *Garry et al.*, 2007]. Recently, the use of PEG wax experiments and Ψ has been invoked to understand the role of unsteady eruption conditions and its effects on inflation [*Rader et al.*, 2017].

Rader et al. [2017] focus primarily on the effects of unsteady effusion rates on the role of lava flow inflation in the context of large igneous provinces, such as the Deccan Traps in India. Their experiments focused on discrete Ψ regimes most conducive to inflation and applicable to the processes hypothesized to occur during the emplacement of long lava flows within large igneous provinces [*Self et al.*, 1996; *Sheth*, 2006; *Rader et al.*, 2017]. By conducting experiments across a wide range of applicable Ψ values and variable eruption rates during an eruption, my dissertation will address the effects of unsteady effusion rates at the vent on the modes of emplacement common to lava flow propagation (e.g. morphology, morphometry, inflation, tube formation, and resurfacing). This has implications for the formation of large igneous provinces, large shield volcanoes, and long lava flows like those observed on Mars [*Baloga et al.*, 2003; *Baloga and Glaze*, 2008; *Glaze et al.*, 2009; *Rader et al.*, 2017].

Gregg and Fink [1996] made testable predictions about the morphology of lava flows on Mars. We now have higher resolution visible images and moderate to high-resolution digital terrain elevation models of Mars. Like all the rocky planetary bodies in the inner solar system, a significant portion of the Martian crust has been resurfaced by effusive volcanic deposits. *Greeley and Spudis* [1980] estimated that 50–60% of the Martian surface had been resurfaced by effusive volcanic products, a number not too dissimilar from the Earth. However, most of the volcanic terrains on Mars are masked by optically thick dust cover which prevents compositional analyses and analysis of finer

detail morphology. This is especially true of the extensive lava flows in the Tharsis and Elysium Volcanic Provinces. Despite the lack of compositional data, the morphology and morphometry data of these flows suggests a basaltic to basaltic andesite composition. With the assumption of laminar flow and a Newtonian to Bingham rheology, these proposed compositions have been used to estimate the emplacement conditions (e.g. eruption rates, viscosities, and yield strengths) of observed flows [e.g., *Hulme*, 1974; *Hiesinger et al.*, 2007; *Hauber et al.*, 2011]. The body of work in my dissertation further constrains the emplacement conditions of Martian lava flows using laboratory wax experiments and the dimensionless parameter, Ψ. An aspect of my work allows constraints to be placed on Martian lava flow eruption rates, rheology, and emplacement times without morphometric data. For added value, I have also employed two additional models to estimate eruption rates and rheology. One model relies on applying equations derived from fundamental fluid dynamics to approximate flow conditions via methods outlined in *Hiesinger* et al. [2007] and *Hauber* et al. [2011]. The second model – the self-replication model for long lava flows – assumes that the entire flow is not active during emplacement, with some portion of the mass loss to levee construction which results in a lower calculated eruption rate for the emplacement of a given lava flow. Both models are outlined in Chapter IV in detail.

III. Methodology

Two approaches form the basis of addressing the research questions outlined in my dissertation: experimental volcanology and remote sensing. A brief explanation of the methodology of each is provided below.

Experimental Volcanology

To address the emplacement and subsequent morphology of lava flows, I conducted a series of experiments using polyethylene glycol (PEG) wax to simulate lava flow emplacement. I addressed the following: unsteady effusion rates at the vent over short (10s) and long (50s) pulses of decreased or increased eruption rate on a flat surface and the effects of unsteady effusion rates at the vent over long (50s) timescales across a range of slopes. The experiments were conducted in one of two plexiglass tanks, each containing a 0.001 m thick wire mesh attached to the bottom to simulate surface roughness and prevent the wax from slipping. One tank (0.6 x 0.6 m) with a flat surface atop a non-adjustable apparatus was used for the unsteady no slope condition. A second tank (0.76 m long x 0.3 m wide) was used for the unsteady slope condition and will sit atop an adjustable apparatus. High (~29˚), medium (~16˚), and low (~7˚) slopes conditions were tested. All experiments were recorded by video and/or picture. Qualitative morphology, flow dimensions, and flow thickness were recorded. The occurrence of emplacement modes (e.g. resurfacing, marginal breakouts, inflation, and tubes) were recorded for each flow.

Modeling and Remote Sensing

To apply the results of my experimental work to Mars, I utilized the Java-mission planning and Analysis for Remote Sensing (JMars) GIS platform. JMars provides access to high resolution image and elevation data collected by a variety of Mars missions over two decades. High resolution image data included the Thermal Emission Imaging System infrared (THEMIS IR) [100 m/pixel] on Mars Odyssey; the Context Camera (CTX) [~6 m/pixel] on Mars Reconnaissance Orbiter; and the High-Resolution Imaging Science Experiment (HIRISE) [~0.5 m/pixel] on the Mars Reconnaissance Orbiter. Elevation data

will include the Mars Orbiter Laser Altimeter (MOLA) [300 m/pixel] on Mars Global Surveyor; MOLA Digital terrain models (DTM) [463 m/pixel]; and the High-Resolution Science Camera (HRSC) DTM [50–70 m/pixel] on Mars Reconnaissance Orbiter. These data sets were used to map lava flows on Mars, qualitatively access their morphology, assign a Ψ regime based on morphology, and quantitatively access their morphometry. The morphometric data was used to find solutions to fluid dynamics equations in order to estimate eruption rates, yield strengths, viscosities, etc. Additionally, morphometric data was used in a model for long, self-replicating lava flows [*Baloga and Glaze,* 2008]. The values obtained by both methods were compared to the values predicted by their qualitative morphology and Ψ regime. The results of these methods were used to constrain the emplacement conditions of observed lava flows on Mars.

The following three chapters investigate lava flow propagation in the laboratory using analogue experiments and estimate eruption rates and flow rheology for lava flows on Mars. These chapters are outlined below. A final summary chapter provides the key findings.

IV. Chapter Outline

a. Chapter II: The effects of unsteady eruption rates on lava flow emplacement: insights from laboratory analogue experiments – chapter II presents the results and implications of laboratory analogue experiments used to understand the effects of unsteady effusion rates at the vent on common modes of emplacement that affect lava flow propagation

b. Chapter III: The effects of unsteady eruption rates and slopes on lava flow emplacement – chapter III presents the results and implications of

laboratory analogue experiments used to understand the effects of slope and unsteady effusion rates on common modes of emplacement that affect lava flow propagation

c. Chapter IV: Modeling lava flow eruption conditions in the Tharsis volcanic province on Mars – chapter IV presents the results of a study in which the dimensionless parameter developed in laboratory analogue experiments, Ψ, is used to estimate the eruption rates of several lava flows on Mars. The estimates are further constrained using dynamical equations.

d. Dissertation Summary: Key results and findings from Chapters II - IV and next steps

CHAPTER 2

THE EFFECTS OF UNSTEADY EFFUSION RATES ON LAVA FLOW EMPLACEMENT: INSIGHTS FROM LABORATORY ANALOGUE EXPERIMENTS

1. Introduction

1.1. Lava Flow Emplacement

Lava flows are one of the most common landforms on the Earth and one of the primary hazards of volcanic eruptions [*Crisp,* 1984; Francis and Oppenheimer, 2003]. The emplacement, propagation, and morphology of lava flows is dictated by a variety of factors, including effusion rate, changes in effusion rate, cooling, crystallization, degassing, and topography [*Fink and Griffiths,* 1990, 1992; *Pinkerton,* 1987; *Gregg and Fink,* 2000; *Belousov et al.,* 2015]. Despite their abundance, the phenomenology of lava flow emplacement remains poorly constrained due to its inherent complexity [*Pinkerton,* 1987; *Fink and Griffiths*; 1990, 1992; *Gregg and Fink,* 2000; *Rader et al.,* 2017]. Most of the world's lava flows are found on the ocean floor near mid-ocean spreading centers, with only a few subaerial locations readily accessible for study [*Gregg and Fink,* 2000; *Gregg and Smith,* 2003]. In-situ observations and studies, although hindered by some limitations, have aided our fundamental understanding of lava flow emplacement [e.g., *Walker,* 1973; *Wadge,* 1981; *Pinkerton,* 1987; *Belousov et al.*, 2015].

In order to prevent human and economic losses, numerical modelling is used extensively to simulate lava flow emplacement and predict the path of future lava flows [e.g. *Harris and Rowland,* 2001; *Felpeto et al.*, 2001; *Favalli et al.,* 2005; *de'Michieli Vitturi and Tarquini,* 2018]. However, these models do not capture the complete physics of lava flow emplacement, but instead rely on simplified propagation rules and

probabilistic assessments [*Felpeto et al.*, 2001; *Favalli et al*., 2005; *de'Michieli Vitturi and Tarquini,* 2018]. Understanding what influences the propagation rate and emplacement mode of lava flows is key to unraveling their complex phenomenology, which in turn can be used to improve existing models, their predictive capabilities, and their utility in hazards mitigation. In addition, better understanding of lava flow emplacement processes is invaluable in reconstructing the formation and evolutionary history of planetary surfaces.

The morphology of a lava flow is determined by its rheology, eruption rate, and preexisting topography [*Pinkerton,* 1987; *Fink and Griffiths*, 1990, 1992; *Gregg and Fink*, 2000; *Cashman et al.*, 2006]. *Walker* [1973] argued that the length of a lava flow is determined primarily by the eruption rate, whereas *Malin* [1980] tied lava flow length to the total volume of erupted material. *Fink and Griffiths* [1990] and *Cashman et al.* [2006] highlighted that the readiness to form a crust controls the morphology of lava flows, while *Gregg and Fink* [2000] observed that flows erupted on steeper slopes are narrower and longer (Fig. 1). Basaltic lava flows are the most common type of lava flow observed in nature by far – covering ~65% of the Earth's surface, ~90% of Venus, ~50% of Mars, and ~20% of the Moon [*Greeley and Spudis,* 1981; Francis and Oppenheimer, 2003]. Therefore, the nature of these lava flows is crucial to learning about the formation and evolution of the surface of Earth and other planetary bodies.

Our understanding of basaltic lava flows comes primarily from historical and contemporary eruptions – some of which have been witnessed, recorded, and subsequently analyzed – in Hawai'i, Iceland, Sicily, and on the seafloor [*Greeley,* 1972, 1987; *Malin,* 1980; *Pinkerton,* 1981; *Wadge,* 1981; *Gregg and Smith,* 2003]. Additionally, localities such as the Deccan Traps and Columbia River Basalts (Fig. 2) provide upper endmember

examples of the scale of the constructs that lava flows can form given enough time and volume of material [*Self et al.*, 1996; *Sheth*, 2006; *Rader et al.*, 2017]. Lava flows have a variety of morphologies which correspond to a range of emplacement modes and propagation rates, from channelized flows to pahoehoe sheet flows to pillow lavas [*Hulme*, 1976; *Hon et al.*, 1994; *Gregg and Keszthelyi*, 2004]. The morphology of lava flows is closely connected to and influenced by the mode of emplacement.

In this study, we focus on four modes of emplacement which control how lava is transported and distributed in a flow, and ultimately control propagation rate and final area covered by a flow. These modes are: resurfacing, marginal breakouts, inflation, and tube formation. Resurfacing is defined here as the process by which lava covers a preexisting flow surface during the same eruptive event (Fig. 3). Resurfacing is essentially a breakout on the surface of a lava flow, which leads to stacking of lobes or the repaving of the flow surface. Resurfacing is a component of compound lava flows, which consist of overlapping flow lobes [Walker 1971; *Blake and Bruno*, 2000]. Marginal breakouts, on the other hand, involve lava propagation under the flow crust, followed by rupturing of the crust at the flow margin and subsequent flow propagation and an increase in flow area. Breakouts occur due to overpressurization of the liquid core due to continuous lava influx causing the viscoelastic crust to rupture at the distal edges of the flow [*Hon et al.*, 1994; *Hoblitt et al.*, 2012; *Rader et al.*, 2017]. Sudden increases in flow rate also have the same effect of increasing pressure and promoting breakouts [*Hoblitt et al.*, 2012]. Marginal breakouts may be minor, manifested as small lobes, or they may be significant and advance the flow front in several directions. Breakouts tend to occur in concert with other modes of emplacement, typically following lava emplacement under a crust associated with either

inflation or tube formation. Inflation is the endogenic growth of a lava flow via the emplacement of molten lava in its core beneath the crust, which results in the thickening of the flow (Fig. 4) [*Hon et al.,* 1994; *Hoblitt et al.,* 2012]. Inflation has been observed to thicken lava flows from centimeters to tens of meters, and is thought to be responsible for many lava flows observed in the Deccan Traps and the Columbia River Basalts [*Self et al.,* 1996; *Sheth,* 2006; *Rader et al.,* 2017]. Lava tubes (fig. 5) are a common construct in lava flow fields and can form in number of ways including the roofing over of open channels and the consolidation of interconnected pathways within pahoehoe flows [*Greeley,* 1972, 1987; *Belousov et al.,* 2015]. Lava tubes are discreet pathways in a flow and the overlying crust insulates liquid lava allowing it to travel farther and retain its heat. As such, lava tubes tend to form during longer-lived eruptions and are a primary way lava flows propagate and lava flow fields expand. While lava tubes can occur in inflated pahoehoe sheet flow fields, lava tubes are localized and also occur independently of inflation [*Greeley*, 1971; *Greeley*, 1987]. Knowing under what conditions these emplacement modes operate is fundamental to aiding in hazards mitigation and establishing a framework for volcanic conditions on other planets, such as Mars [*Greeley,* 1972, 1987; *Pinkerton et al.,* 2002].

The eruption of lava flows is a dynamic process with a host of variables that evolve as the eruption progresses and the lava flow propagates away from the vent. While the average eruption rate is typically calculated and cited in the literature for a given volcanic eruption, the eruption rate at volcanic vents often varies with time [*Walker,* 1973; *Wadge,* 1981; *Tarquini and de'Michieli Vitturi,* 2007; *Rader et al.,* 2017]. Basaltic eruptions typically experience a large increase in eruption rate shortly after the eruption commences

followed by exponential decline after some maximum value is achieved, although periodic spikes in the eruption rate can occur [*Wadge,* 1981; *Belousov et al.,* 2015]. As such, the average eruption rate can underestimate the eruptive conditions at the vent early in an eruption and overestimate the conditions later in an eruption.

Eruption rates can fluctuate due to the injection of more magma into subsurface storage, widening of the conduit, thermal contraction of the magma, among other mechanisms [*Wadge,* 1981; *Bailey et al.*, 2006]. These fluctuations can be small – due to blockages within the channel itself – or large – due to activity at the volcanic vent. For example, during channelized flows on Mt. Etna cyclical fluxes in volumetric flow rates have been observed to generally involve dramatic increases in flow rates followed by a waning of the flow rate [*Bailey et al.,* 2006]. Rapid increases in eruption rate are termed *pulse* events and they can have a huge impact on flow emplacement, promoting overspills, flow blockages, breakouts, the remobilization of stationary flows, and the development of new channels [*Peterson and Tilling*, 1980; *Hon et al.*, 1994; *Baloga and Pieri*, 1986; *Bailey et al.*, 2006]. Thus, changes in eruption rate at the vent can impact the flow rate at the lava flow front, the morphology of the flow, and influence which emplacement modes are likely to occur. Previous studies suggest that, under steady flow rates, inflation tends to occur under low eruption rates, while lava tubes – depending on their formation mechanism – form at low to moderate eruption rates [*Greeley,* 1987; *Hon et al.*, 1994]. However, this framework does not account for short-term fluctuations in flow rate.

1.2. Hazards implications

Variability in lava flow dynamics remains a challenge to hazards assessment. For example, increasing effusion rates have been observed to remobilize nearly stationary aa

flows [*Peterson and Tilling*, 1980]. In the 1973 lava flow in Heimaey, Iceland, a water-cooled lava flow stopped propagating until the accumulation of material behind the flow front caused a breakout that destroyed 100 homes [*Pinkerton*, 1987]. *Dvigalo et al.* [2014] observed a similar instance of a lava flow deviating from its expected flow path during the 2012–2013 effusive eruption sequence of Tolbachik volcano in Kamchatka, Russia; as the eruption rate at the vent decreased, the flow front ceased and the flow increased in width and thickness (inflation) [*Dvigalo et al.*, 2014; *Belousov et al.*, 2015].

Numerical modelling has been used by state and local organizations for lava flow hazard assessment [*Favalli et al.*, 2005; *Vicari et al.*, 2011; *Connor et al.*, 2012]. The complexity of lava flows is difficult to simulate, so simplified models are created to understand individual aspects of lava flows and inform decision makers [*Baloga and Pieri*, 1986; *Pinkerton*, 1987]. Many models used today are probabilistic, such as MrLavaLoba [*de'Michieli Vitturi and Tarquini*, 2018, https://github.com/demichie/MrLavaLoba], in that they rely on stochastic perturbations in flow propagation based on tunable parameters which are based on physical characteristics such as substrate slope and lava rheology in order to adapt to different volcanic environments [e.g., *Felpeto et al.*, 2001; *Vicari et al.*, 2007; *de'Michieli Vitturi and Tarquini*, 2018]. The predictive capability of such models is validated by determining how well the model replicates well-documented flows. However, perfectly recreating past flows is challenging [*Bruno et al.*, 1996; *Favalli et al.*, 2005; *Connor et al.*, 2012]. That said, probabilistic models allow for the evaluation of lava flow propagation and hazards using a stochastic approach without the requirement of quantitative estimates of lava flow properties which may be unknown or difficult to estimate [*Felpeto et al.*, 2001].

Few numerical models are physics-based, although there are some that take into account physical aspects of the lava flows such as the thermo-rheological models FLOWGO [*Harris and Rowland,* 2001; *Rowland et al.,* 2004] and MAGFLOW [*Ganci et al.*, 2012; *Del Negro et al.* 2013; *Capello et al.* 2015]. FLOWGO models lava propagation by solving a steady-state force balance between a downslope driving force and viscous retarding forces in a Bingham fluid, which depend on rheologic properties of the lava flow and its flow geometry. While it accounts for a surface crust, the primary disadvantage of FLOWGO is its exclusive applicability to channelized flows with the assumption that the lava flow is confined to a channel of fixed width [*Harris and Rowland,* 2001; *Rowland et al.,* 2004]. MAGFLOW allows interaction with complex topography and consequent complex flow geometry, but like MrLavaLoba it assumes a steady flux from the vent and does not account for crust formation nor for inflation beneath a crust. MAGFLOW is typically used in hazards predictions by taking a Monte Carlo approach [*Ganci et al.,* 2012; *Del Negro et al. 2013*; *Capello et al.* 2015]. These useful yet incomplete models illustrate the key difficulties related to emplacement modes – physics-based models currently must *a priori* assume a simplified emplacement mode. Many lava flows pass through two or more crust-influenced modes during their lifetimes - resurfacing, inflation followed by toe breakout, tube formation, and channelization testifying to the complexity of numerically simulating the emplacement of real lava flows. For these reasons, laboratory analogue experiments would be beneficial to understand controls on mode of emplacement and therefore have the potential to better constrain models. While laboratory experiments also rely on simplifications and cannot recreate every aspect of a lava flow, they offer the opportunity to investigate the complex phenomenology of lava flows [*Fink and Griffiths,*

1990, 1992; *Gregg and Fink,* 2000; *Blake and Bruno,* 2000] and relate mode of emplacement to lava characteristics and effusion rate.

1.3. Laboratory Analogue Experiments

Previous studies [*Huppert and Sparks,* 1987; *Fink and Griffiths,* 1990; *Griffiths and Fink,* 1992; *Gregg and Fink,* 1996; 2000; *Blake and Bruno,* 2000; *Soule and Cashman,* 2004; *Kerr et al.,* 2006; *Rader et al.,* 2017] have established the utility of laboratory analogue experimentation, in particular, the use of polyethylene glycol wax (PEG) – a commercial grade polymer used in the production of food and pharmaceutical products – in simulating lava flows due to its temperature dependent viscosity and readiness to form a crust [*Soule and Cashman,* 2004]. *Fink and Griffiths* [1990] used PEG experiments to derive a dimensionless parameter, Ψ. Ψ describes the ability of a viscous gravity current to transfer heat either via the surface of the fluid or through lateral advection [*Fink and Griffiths,* 1990, 1992; *Gregg and Fink,* 2000]. As such, Ψ is defined as the ratio of the timescale of surface crust formation (t_s) to the timescale of flow advancement (t_a).

$$\boldsymbol{\Psi} = \frac{\boldsymbol{t_s}}{\boldsymbol{t_a}} \qquad \text{(eq. 1)}$$

Alternatively, the formula can be written with respect to the modified Peclet number (*IT*) (thermal advection rate/thermal diffusion rate), crustal cooling time ($\boldsymbol{\tau_s}$), and temperature differences among the ambient fluid, the erupted liquid, and the solidification temperature of the liquid ($\boldsymbol{\theta_s}$). The modified Peclet number includes the traditional Peclet number, thermal diffusivity, and a dimensionless timescale that quantifies the time it takes the contact temperature to decrease to that of the ambient environment.

$$\boldsymbol{\Psi} = \boldsymbol{\Pi\tau_s(\theta_s)} \qquad \text{(eq. 2)}$$

Fink and Griffiths [1990] observed that flow behavior and morphology differed across a continuum of Ψ regimes. Five flow regimes corresponding to discreet Ψ ranges were observed. Those regimes which correspond to observed morphologies, from high to low Ψ, are: No Crust, Levees, Folds, Rifts, and Pillows (Fig. 6) [*Fink and Griffiths,* 1990, 1992; *Gregg and Fink,* 2000]. Transitional morphologies are also observed, demonstrating that the morphologies are produced on a continuum. These morphologies are analogous to flow morphologies and surface textures observed in nature, with the exception of No Crust [*Fink and Griffiths,* 1990, 1992; *Gregg and Fink,* 2000]. In summary, Ψ is a powerful tool that relates the morphology of a flow to its cooling regime.

Additional studies have looked at the effects of channel morphology on lava flows, crust distribution on the surface of lava flows, the stresses within a lava flow, and the formation of compound lava flows [*Griffiths and Fink,* 1992; *Blake and Bruno,* 2000; *Cashman et al.,* 2006; *Garry et al.,* 2007]. However, many previous studies either limited their experiments to constant eruption conditions or did not account for how varying effusion rates with time affected propagation rate and morphology [*Baloga and Pieri,* 1986]. Recently, the use of PEG wax experiments and Ψ has been invoked to understand the role of unsteady eruption conditions and its effects on inflation in the context of large igneous provinces, such as the Deccan Traps [*Rader et al.,* 2017]. These experiments targeted lower Ψ regimes ($\Psi < 15$) where inflation is more likely and is thought to be more applicable to the processes hypothesized to occur during the emplacement of extensive lava flows within large igneous provinces [*Rader et al.,* 2017].

Here, we expand their work and demonstrate that variations in effusion rate at the vent has consequences for mode of emplacement, which directly controls how mass is

transported, distributed, and stored within a flow and where the flow is likely to divert that mass to propagate the flow. At the same time, we relate the full spectrum of Ψ regimes and a wide range of effusion rates to the modes of emplacement investigated here. As stated above, eruption rates vary over the course of an eruption with many eruptions initiating with a rapid spike in eruption rate which then decreases exponentially in time [*Walker*, 1973; *Wadge*, 1981; *Tarquini and de'Michieli Vitturi*, 2014]. However, eruption rate can also spike, sometimes multiple times, during this waning phase [*Wadge*, 1981]. In order to simulate these fluctuations in the lab, we constructed simplified models of eruption time-series, focusing on sudden increases and/or decreases in eruption rate. By doing so, we are able to ascertain which types of eruption rate fluctuations are favorable to different emplacement modes - flow stacking via resurfacing, flow propagation by breakouts and/or tube formation, and/or flow thickening by inflation – and how those modes ultimately affect propagation rate and total area covered by a lava flow.

2. Methodology

2.1. Experimental Setup and physical parameters

To test the effects of unsteady eruption rates at the vent on the propagation and morphology of lava flows, we performed 150 laboratory analogue experiments. The experiments were conducted in a 60 x 60 cm plexiglass tank (Fig. 7). This tank was placed on a non-adjustable apparatus with a fixed slope of 0°. The flat floor of the tank was fitted with a 0.1 cm thick metal mesh at 0.4 cm grid spacing to prevent slipping at the base of the flows [*Fink and Griffiths*, 1990, 1992; *Gregg and Fink*, 1996, 2000; *Blake and Bruno*, 2000]. A programmable, peristaltic pump was connected to the base of the tank via a 1-cm diameter rubber hose and metal attachment with a 1-cm opening secured to the base of

the tank. We used pharmaceutical grade polyethylene glycol (PEG) 600 wax to simulate lava flow emplacement. The solidification temperature of the wax was determined to be 18.4˚C. In order to explore the parameter space and determine the effects of unsteady vent conditions across a variety of eruption regimes, a range of Ψ values from very low to very high (1–70) corresponding to all five morphologies observed by *Fink and Griffiths* [1990] were tested. Care was taken to avoid running experiments with Ψ values associated with transitional morphologies, although some transitional behavior and morphologies were observed. In the laboratory, Ψ was varied by adjusting effusion rate and wax temperature, which in turn varied the advective time scale and timescale of wax solidification. All Ψ regimes were erupted from 1 – 6 cm^3/s at 1 cm^3/s increments. The tank was filled with a fresh water bath maintained at 0°C. The temperature of the wax and chilled bath was measured to a tenth of a degree. PEG wax was dispensed into 1000 mL beakers to simulate a magma reservoir and heated or cooled to a desired temperature (19.6 – 32.1˚C from low to high Ψ, respectively). Two or three batches of wax were dyed pre-experiment using food coloring in order to better visualize the flows and distinguish different stages of the eruption.

In order to simulate unsteady vent conditions, the experiments were divided into four conditions (Fig. 8). Conditions 1 and 2 feature 60 experimental runs each for a total of 120 experimental runs. Condition 1 is characterized by a decrease in the eruption rate, while condition 2 represents an increase in the eruption rate. The conditions correspond to a waning (condition 1) and waxing (condition 2) eruption. The period of time representing the second stage of increase or decrease in eruption rate is termed the *pulse*. *Rader et al.* [2017] used a range of pulse durations of 10, 20, 30, 40, and 50 seconds. They recorded

thinner, less complex flows for shorter pulses and thicker, more complex flows for longer pulses. For simplicity, the length of the pulse was either 10 seconds (short pulse) or 50 seconds (long pulse). Depending on the condition, the eruption rate during the pulse was either half the initial eruption rate (for condition 1) or double the initial eruption rate (for condition 2). There was a brief (~1s) pause at the start of each pulse to switch the rubber hose from one wax reservoir to another of the same temperature but different color. This pause had a negligible effect on morphology and emplacement and was not discernible in the data sets. After the pulse, the experiment ceased. For each experimental run in conditions 1 and 2, a volume of 250 mL of dyed PEG wax was erupted into the water filled tank at an initial rate of 1 – 6 cm^3/s during the first stage of the experiment prior to the pulse. The duration of the first stage of the eruption depended on the eruption rate and ranged from 250 – ~42 seconds for 1 – 6 cm^3/s, respectively. The eruption of this initial volume allowed the flow to mature before the onset of the pulse stage. In order to simulate unsteady vent conditions, the eruption rate was adjusted after the initial eruption of 250 mL of wax. The volume of wax erupted during the pulse was dictated by the flow rate and duration of the pulse, and ranged from 5.0 cm^3 – 3.00 x 10^2 cm^3 for all combinations described here.

Conditions 3 and 4 featured a combination of the waxing and waning eruption rates, with 15 experimental runs each for a total of 30 (Fig. 8). Condition 3 is characterized by a decrease and subsequent increase in the eruption rate. Condition 4 is characterized by an increase and subsequent decrease in eruption rate. The conditions correspond to a waning-waxing (condition 3) and waxing-waning (condition 4) eruption. The length of the pulse in the middle of the sequence was 50 seconds for every run at these conditions. For

Condition 3, the eruption rate during the pulse was half the initial eruption rate, while for Condition 4, the eruption rate was double the initial eruption rate. For each experimental run in conditions 3 and 4, a volume of 200 mL of dyed PEG wax was erupted into the water filled tank at an initial rate of 1 – 6 cm^3/s during the first stage before the pulse. The eruption of this initial volume allowed the flow to mature. For the pulse, the rubber hose was switched between wax reservoirs of different colors and the eruption rate was either decreased (condition 3) or increased (condition 4) for 50s. Once again, the volume of wax erupted during the pulse was dictated by the flow rate and pulse duration, and ranged from 25.0 cm^3 – 3.00 x 10^2 cm^3 for all combinations. After the pulse, the rubber hose was returned to the original wax reservoir and an additional 200 mL of wax was erupted. After this last stage of the eruption, the experiment ceased. The total volumes erupted during each experiment are the same across eruption rates, but differ slightly among eruption rates, ranging from 4.25 – 7.00 x 10^2 cm^3 for all combinations. In addition, the total volumes of experiments differ slightly between conditions 1 and 2 and conditions 3 and 4. When discussing flow dimensions, it is also important to note that flow depth and deposit thickness are sometimes the same but not always.

2.2. Image Processing

Experiments were either photographed and/or recorded using a digital camera and iPhone 6S. Video recordings were created by positioning a digital camera either adjacent to the tank (conditions 1 and 2) or overhead (conditions 3 and 4). For conditions 1 and 2, the camera was positioned on a tripod. For conditions 3 and 4, the camera was attached to a wood beam and positioned directly above the vent. Photographs were collected at the end of each experimental run, typically no sooner than 60 seconds after the experiment had

ceased. This allowed time for the wax to stop flowing and solidify. In order to collect morphometric data on the flows, we utilized Tracker and ImageJ. These programs allowed for the importing of videos and photographs, respectively, and quantitative analyses. Tracker is an open-source video analysis and modelling tool built in Java and utilized by introductory physics courses [https://physlets.org/tracker]. Tracker was used to measure the major axes of the active flows at various times during the eruption. ImageJ is an open source Java-based image processing program [*Abramoff et al.*, 2004], and was used to calculate the final area of the flows and the area of the flow that had been resurfaced.

2.3. Scaling

We calculated the non-dimensional Ψ value using equations (1 and 2) derived and adjusted by Fink and Griffiths [1990] and Gregg and Fink [1996]. Ψ is a ratio of the rate of heat transfer by diffusion (i.e. diffusion upward through the surface of the flow) to the rate of heat transfer by advection (i.e. forward propagation of the flow). Included in Ψ is, Π, the modified Peclet number, which is a ratio of the rate of advection and the rate of a diffusion of a temperature within the flow. Derivations and further discussion of Ψ and its associated input variables are found in Fink and Griffiths [1990, 1992] and Gregg and Fink [1996]. Primary inputs into the calculation of Ψ include temperature of the wax and ambient fluid, eruption rate, and material properties such as thermal diffusivity, heat capacity, and density.

3. Conditions 1 (waning) and 2 (waxing)

In the following subsections we detail the qualitative insights gained from the 60 experiments performed at Condition 1 and the 60 experiments at Condition 2. Ψ is based on the eruption rate at the onset of each experimental run. For the sake of brevity, we group

Very High Ψ (No Crust) and High Ψ (Levee) into one section and Low Ψ (Rifts) and Very Low Ψ (Pillows) into one section for all conditions. The qualitative observations below are followed by quantitative classification of the flows and direct comparison between Condition 1 (waning) and Condition 2 (waxing).

3.1. Condition 1 – Qualitative Observations

3.1.1. Very High and High Ψ Regime ($\Psi \geq 45$)

The very high and high Ψ regime corresponds to the no crust and levee morphologies, respectively, observed in the lab. A total of 24 experiments were conducted at 'very high' and 'high' Ψ values, with 12 experiments conducted under each regime. Of those 12 experiments, half featured the short (10 s) pulse and the other half featured the long (50 s) pulse.

At the onset, the flows erupted approximately axisymmetrically in plan form. Wax typically remained liquid with no appreciable crust forming for the first few seconds. Depending on the initial Q and T, the crust formed closer to (low Q, low T) or farther from (high Q, high T) the vent. Crust also varied in thickness and extent such that high Q and high T favored thinner patchier crusts, which were susceptible to failure via fracturing, foundering, and rifting. Low Q and low T favored thicker, extensive crusts, less prone to failure. As the flow propagated away from the vent, the local flow rate dropped and the flow front started to solidify and circumferential levees formed at the flow front. Regardless of conditions the crust was translucent during this stage.

When the lower effusion rate pulse began, the flow remained mostly molten. At high Q, this second pulse of wax (at a lower Q) encountered no crust and propagated by either pushing the still molten wax from the initial stage forward or channelizing into

sinuous preferred pathways. At low Q, the second pulse of fresh wax (at lower Q) encountered a thin, translucent crust and flowed beneath it axisymmetrically from the vent. While the same volume of wax was erupted in the first stage, at low Q the duration of the eruption was longer which allowed more time for crust development during the first stage of the eruption. Also, at low Q, the second pulse of fresh wax would either rupture through the thin crust (10 s pulse), mobilize unsolidified wax which would either rupture the crust or create breakouts (10 and 50 s pulse), or disrupt levees at the flow front and advance the flow (50 s pulse). After solidification, the flows rarely preserved a smooth, featureless morphology, counter to what one might expect at high Ψ regimes.

3.1.2. Intermediate Ψ Regime (Ψ = 21)

At the onset, intermediate Ψ-regime flows erupted asymmetrically. Due to the lower eruption temperature and therefore higher viscosity of the erupted wax relative to the high-Ψ regime, these flows spread more slowly and were thicker. The onset of crust formation was quicker in this Ψ regime, again due to the lower eruption temperature. In some flows, folds formed on the flow surface as crust solidified and propagated back toward the vent. Higher eruption rates promoted more branches of folding in the flow, while lower initial eruption rates promoted a thicker crust that inhibited fold formation. Overall, the crust was more expansive and thicker than at higher Ψ regimes.

In the second stage of the eruption wax initially spread radially from the vent remaining beneath the crust formed in the initial stage. Although the crust was thicker than higher Ψ regimes, it remained thin enough to be translucent. The thin crust allowed wax to eventually breakthrough and ooze out onto its surface in resurfacing events. In general, as with previous regimes, longer pulses promoted thicker crusts due to increased time for

wax to cool and a drop in local flow rates at the flow front. Thicker crusts tended to more effectively trap the wax erupted during the second pulse, and in turn promoted thickening of the flow via inflation and increased the likelihood of breakouts at the flow front.

3.1.3. Low and Very Low Ψ Regime ($\Psi \leq 8$)

Due to the lower eruption temperature relative to all other regimes, a thin, deformable crust formed almost immediately in these flows. The development of this crust early in the eruption sometimes prevented an axisymmetric flow plan, especially at lower Q. Eventually an extensive, semi-opaque to opaque crust developed covering most of, if not the entire, flow. Heterogeneity in the crust combined with continued injection of wax beneath it led to fracturing of the crust into large segments, exposing molten wax and allowing it to flow from beneath the crust through the fractures. This molten wax quickly developed a surface crust. The molten wax usually carried the rafted crust until a subsequent crust formed and surrounded the rafted crust.

Initial eruption rate influenced how far the flow propagated from the vent, although the flow was largely crusted over regardless. Breakouts that occurred at the flow margin quickly acquired a pliable crust which then thickened and became stiff. At the very lowest Ψ values, flows took on bulbous appearances as lobes of wax analogous to pillow lavas, such that higher eruption rates formed longer, larger lobes and lower eruption rates formed smaller lobes. As the eruption progressed, the crust in this regime thickened and became opaque. The opacity of crust hindered observation of the flow interior. Only the increasing prevalence of breakouts or inflation of the flow was observed.

During the low-eruption-rate pulse, the newly erupted wax remained beneath the crust, initially spreading radially for all conditions although in some locations at lower

eruption rates restricted by thicker crust. As a result, the wax typically exhibited three behaviors listed here from high to low eruption rate: breakout at the flow margin, rupture at a weak point in the crust and spill onto the flow surface (resurfacing), or accumulation beneath the flow, inflating the flow rather than propagating the flow. The behavior of the pulse of wax in the second stage of the eruption was learned by observing the flows in action and dissecting the flows post-eruption.

3.2. Condition 2 – Qualitative observations

3.2.1. Very High and High Ψ Regime ($\Psi \geq 45$)

Initially, the wax is erupted at low-Q and after a fixed volume is erupted, the eruption rate increases to double the initial Q. From the onset, the wax expands radially from the vent producing an approximately axisymmetric flow. Some distance from the vent levees develop around the circumference and a crust starts to form across most of the flow. Note that because the first stage erupts a fixed volume, stage one in condition 2 lasts longer than stage one in condition 1. As a result, flows created under condition 2 display a systematic behavior of lower Ψ regimes closer to the vent relative to condition 1. Crusts formed during the initial stage of the eruption were generally translucent and extensive in area.

The second stage of the eruption – the pulse – creates different flow regimes not observed in condition 1. The 2Q pulse of molten wax initially spreads radially from the vent, and then eventually ruptures any crust and/or displaces any molten wax near the vent. This occurred for all values of Q. In runs with a more extensive crust near the vent (low Q, low T), the resurfacing flow is less extensive and less disruptive such that most of the fresh molten wax would flow beneath this crust. If a more extensive crust was present

some distance from the vent (low T), the fresh molten wax would either flow over it, flow under it, and/or disrupt it by rupturing it and flowing over it or tearing it apart. Wax that flowed under the crust ultimately erupted at the flow front as breakouts, sometimes disrupting pre-existing levees, expanding the flow front and increasing the areal extent of the flow rapidly.

For long duration pulses (50 s), molten wax tended to develop preferred pathways that seemed to develop into tubes in the presence of an extensive, coherent crust and less molten wax. The fresh molten wax issued during the pulse did not form a crust on timescales similar to the preceding flow, in fact, generally a crust did not form until the pre-existing flow had been severely disrupted.

At lower Q, the flow was more asymmetric due to a stronger crust from the initial eruptive stage forcing the pulse wax to find irregular pathways. This asymmetry limited the ability of the pulse of fresh wax to disrupt the flow and spread radially at the flow front. At higher Q, the entire flow was disrupted by the pulse and the flow was more axisymmetric due to the ability of the fresh wax of the pulse to disrupt the crust and expand radially at the flow front. Sometimes the entire flow was overprinted by wax erupted during the pulse – an overall resurfacing. In fact, the fresh wax in the second stage more resembled an ideal No Crust regime than the initial stage of the eruption due to partial insulation of the wax and the decreased flow times due to the higher eruption rate.

3.2.2. Intermediate Ψ Regime ($\Psi = 21$)

Initially, wax erupts radially from the vent but rapid and widespread formation of a crust usually prevented true axisymmetric flow. The crust buckled as the faster flow near the vent encountered the locally slower flow at the distal portions of the flow, forming

compression ridges, or folds. The decreasing local velocities far from the vent led to locally lower Ψ regimes and corresponding morphologies, progressing from folds to rifts, rift-pillows, to pillows with increasing distance from the vent.

The fresh molten wax erupted in the second stage of the eruption was restricted by the competent crust and generally tended to flow beneath it, commonly leading to rupturing of the pre-existing crust. At higher Q, if the crust was ruptured, the pulse of fresh wax would destroy or overprint the pre-existing flow via a wholesale resurfacing event. At lower Q, a rupture of the crust was gentler, leading to wax oozing out from fractures. At very low Q, this rupture and resurfacing process resembled that observed for pillow morphology (very low Ψ) observed in condition 1. Wax flowing beneath the pre-existing crust tended to erupt at the flow margin, pushing any remaining molten wax forward as well. For short pulses, the preceding paragraph description generally holds. For long pulses, the effects were more extensive. For instance, the areal extent of the flow doubled during every 50 second pulse.

3.2.3 Low and Very Low Ψ Regime ($\Psi \leq 8$)

Wax initially emerged from the vent radially, but the rapid formation of semi-opaque to opaque crust typically resulted in nonuniform propagation of the flow front. Wax propagating at the flow front readily formed a crust and as the crust strengthened, the flow of wax would sometimes rupture this crust. Sometimes the flow would rift, rafting portions of the crust apart. Other times, the crust would fracture along a rift margin and wax would push the crust up and ooze out over the pre-existing crust. This rupturing frequently resembled a precursor to the bulbous growth usually associated with the pillow

morphology. As the wax continued to flow away from the vent, the flow transitioned to lower Ψ morphologies (i.e. rift-pillows, pillows).

For the lowest Ψ values, the evolution of the crust into a thicker, more rigid crust retarded the spreading of the flow, limiting the flow of wax and promoting a few preferred pathways. In some runs transportation of wax to the flow front, and thus the propagation of the flow front, was halted until the pulse. In other runs, the flow would propagate forward via bulbous breakout lobes. These breakouts most resemble pahoehoe lavas in the field, with a lobe of wax erupting from a fracture in the crust, forming a thin crust, and oozing onto the flow surface. At high Q, the processes of fracturing the crust and forming lobes was more vigorous. At low Q, the rate of these processes was slower, although the value of Q did not appear to have any effect on whether these processes occurred or not.

At lower Ψ there was a stronger time dependence on the impacts of the second stage of the eruption. In general, the strong crust over the vent remained intact and thus disruption of the crust tended to occur farther from the vent. The pulse of fresh wax flowed less vigorously from any ruptures in the crust. For the short pulse, the limited volume of fresh, molten wax tended to flow beneath the crust and erupt at the flow front via toes. Any rupturing of the crust was small in scale. For flows erupted at lower Q, the thicker crust retarded the effects of the pulse further, usually leading to a thickening of a flow via inflation as wax pooled beneath the crust.

At the lowest Ψ the pulse of material either pushed the flow upward or forced the wax through limited fracturing of the crust which produced bulbous lobes. For flows erupted at lower Q, the thicker crust retarded the effects of the pulse, such that the wax tended to erupt from a point of crustal weakness at the flow margin, propagate some

distance until the formation of a crust retarded its own progress. However, the preferred pathway created by this breakout would continue to supply molten wax to this region of the flow which could promote more breakouts. Breakouts from the preexisting crust during the long pulse were usually sustained, with molten wax using this preferred pathway until either the flow ceased and/or another more ideal pathway developed. This fresh wax oozed out sometimes as independent lobes and other times as narrow streams of flow. This tended to increase the areal extent of the flow.

3.3. Quantitative Analysis: Flow Morphology and Emplacement of Conditions 1 and 2

The observational data above for conditions 1 and 2 were further analyzed to identify eruption conditions most favorable to resurfacing, inflation, tubes, and marginal breakouts. Resurfacing was identified as wax rupturing the crust and repaving the preexisting flow surface. Inflation is defined as the endogenic growth of the wax flows. Through experiments performed prior to the study, the standard flow depth is ~0.5 cm on slopes of 0˚, which agrees with previous studies [*Rader et al.*, 2017]. On slopes, flows are thinner at ~0.3 cm. Therefore, any flow thicker than 0.5 cm is interpreted as having inflated, only if it was also observed to have increased in thickness over time, while simultaneously displaying little to no growth in areal extent and no evidence of meaningful contribution to its thickness via resurfacing.

Tubes were observed by slicing through the flows post-experiment, removing them from the chilled bath, and rotating them upward to inspect the interior, and are characterized by sinuous, semi-circular channels carved into the solidified wax. Flows displaying none of the aforementioned complex modes of emplacement were considered

to have been emplaced as sheet flows, and are denoted as such. Here we present the results of these analyses by comparing results for conditions 1 and 2.

3.3.1. Observed emplacement modes

Figure 10 displays the frequency of the modes of emplacement for conditions 1 and 2, noting that this figure accounts for any experimental run where a particular mode of emplacement was observed regardless of the duration or impact of that mode; if the mode was observed, it was 'counted' here. In condition 1, despite being common, resurfacing is highly dependent on Ψ such that resurfacing occurs more frequently at higher Ψ. The frequency of resurfacing is slightly increased during long pulses, suggesting a very minor dependence on pulse duration. Conversely, in condition 2, resurfacing is not dependent on pulse duration and not dependent on or very weakly dependent on Ψ regime, as resurfacing occurs readily across all Ψ values for both pulse durations in condition 2.

While resurfacing is common it is a relatively minor process in terms of the percent of the flow area resurfaced (Fig. 11). The percent of a particular flow that is resurfaced is weakly dependent on the duration of the pulse, especially for condition 1 (Fig. 11, left panel). For condition 1, approximately 80% of the flows with a 10 s pulse that experienced resurfacing had less than 5% of the area resurfaced. For flows with the 50 s pulse, only 48% had less than 5% of the area resurfaced. In general, the overwhelming majority of flows that experienced resurfacing had less than 15% of their areas resurfaced.

Resurfacing is a relatively minor process for condition 2 as well, although the areal extent of resurfacing is slightly higher than in condition 1 (Fig. 11, right panel). For instance, only ~38% of flows (10s pulse) and ~31% of flows (50s pulse) have resurfacing areas under 5%. A small dependence on pulse duration and the percentage of resurfacing

is observed, albeit less than for condition 1. Again, the vast majority of flows have <15% of their flow areas resurfaced: ~66% (short pulse) and ~79% (long pulse).

For condition 1, inflation was highly dependent on pulse duration with significantly more instances of inflation during experiments with 50s pulses (Figure 10b, left panel). Inflation is also more likely at lower Ψ values. In contrast, for condition 2, while inflation is much more common in experiments with low Ψ values, it is not dependent on pulse duration (Figure 10b, right panel).

Tubes have the lowest frequency of occurrence in condition 1 (Fig. 10c, left panel). Like inflation, the formation of tubes is strongly dependent on pulse duration and favored in long-pulse experiments. A dependence on Ψ is weak, with tubes seemingly preferred at intermediate-to-high Ψ for short-pulse experiments, but occurring equally for all Ψ values for long-pulse experiments. These trends suggest a complicated relationship between pulse duration, Ψ, and Q. Tubes are slightly more likely to occur in condition 2 than in condition 1 (compare Fig. 10c, left and right panels). Tubes are not dependent on Ψ or pulse duration in condition 2, with tubes nearly equally likely for all experimental conditions.

Marginal breakouts were very common, occurring in most runs for condition 1 and nearly all runs at condition 2 (Fig. 10d). Breakouts were characterized as localized (discreet points of eruption), circumferential (multiple points of eruption that comprise the majority of the flow front), and circum-localized (multiple points of eruption that comprise roughly half of the flow front). The majority of marginal breakouts were localized in condition 1, although some flows displayed transitional behavior exhibiting both circumferential and localized breakouts (Fig. 10d, left panel). There is not clear dependence on Ψ in condition 1. In condition 2, roughly half of the flows experienced localized

marginal breakouts while the other half were circumferential. The type of breakout in condition 2 is dependent on Ψ, such that localized breakouts were more common at lower Ψ and circumferential breakouts were more common at high Ψ values.

The dimensions of the flow, notably depth and area, are governed by Ψ and Q (Fig. 12). Not surprisingly, thicker flows are smaller in area, while thinner flows are larger in area. Thicker, smaller flows are found at lower Ψ, while thinner, larger flows are produced at higher Ψ. As expected, flows produced with a pulse duration of 50 seconds are slightly larger in area than those produced at 10 seconds due to the slightly larger total volume erupted. Condition 2 flows (Fig. 12, right panel), in general, are larger in area than condition 1 flows. The difference in area between flows produced during the long pulse and short pulse is greater in condition 2 than in condition 1, due to the greater difference in total volume erupted between waxing flows at pulse durations of 10s vs. 50 s.

Figure 13 displays flows where a single dominant emplacement mode was observed, including sheet flows. Note that this data is slightly different from that presented in Figure 10, which counts all occurrences of emplacement mode regardless of whether or not it dominated the emplacement of the experiment in question. Flows dominated by inflation are more common in condition 1 than in condition 2, and the condition 1 inflated flows tend to be considerably thicker (up to 2.5x thicker) than those observed in condition 2. Sheet flows are not thicker than the nominal 0.5 cm, while flows displaying only tubes are not thickened throughout because tube formation is a localized process. Resurfacing is generally a localized process as well, typically occurring over <15% of the flow surface. However, at low Ψ resurfacing can contribute more to flow thickening because the erupting

lobes are thicker. That said, resurfacing is nonetheless a localized process relative to inflation, which thickens the entire flow.

The interplay of Ψ, flow area, and single dominant emplacement mode is highlighted in Figure 14 (left panel). Resurfacing occurs predominantly at high Ψ, while inflation occurs predominantly at intermediate to low Ψ. In condition 1, tubes occur at intermediate and high Ψ but in condition 2, tubes occur exclusively at high Ψ. Sheet flows occur at low Ψ for condition 1, but high Ψ for condition 2. Note also that flow area is not exclusively dependent upon Ψ, particularly for condition 2. In general the flow area increases. Flows with Inflation & Resurfacing or Resurfacing, Inflation, & Tubes tend to be smaller in area. All of the flows with multiple emplacement modes are smaller in area than those with singular emplacement modes.

Figure 15 maps these dominant modes of emplacement in terms of eruption rate and Ψ (Fig. 15, left panels). It is important to note that the eruption rate used on the Y-axis corresponds to the mean eruption rate, and there is no indication of the specific time when these emplacement modes might be occurring. Ψ value, however, corresponds to the initial eruption rate of the flow. The data illustrate that inflation tends to occur in the lower-left sector of the plot for both conditions, whereas resurfacing tends to occur in the upper-right portion of the plot. Sheet flows are less common and in condition 1 tend to occur in the same field as inflation. The data also highlight the point that these modes show no dependence on eruption rate, each occurring across a range of eruption rates. Tubes are also rare and generally appear at the transition between the lower left and upper right quadrant.

More than one mode of emplacement was observed in many of the flows owing to the complexity of viscous flows (Fig. 15, right panels). Flows exhibiting multiple modes of emplacement, in other words the most complex flows, occur almost exclusively in the lower-left sector for both conditions 1 and 2.

3.4 Summary of Condition 1 and 2 findings

- Waxing (condition 2) flows favor resurfacing over inflation, although inflation is more common in waxing flows than waning flows (condition 1).
- Resurfacing is favored at high Ψ for waning flows (condition 1).
- Inflation tends to occur more readily at low Ψ values for both waxing and waning flows.
- Tube formation is uncommon in general, but is more common in waxing flows (condition 2).
- Marginal breakouts are almost always localized in waning flows (condition 1), whereas they are both localized and circumferential in waxing flows (condition 2). In waxing flows, high Ψ values favor circumferential breakouts, whereas low Ψ values favor localized breakouts.
- When mean eruption rate is plotted as a function of Ψ, resurfacing is favored at the upper right of the space, whereas pure inflation or complex flows featuring some component of inflation are favored at the lower left portion of the plot.

4.0 Conditions 3 and 4

In the following subsections we summarize qualitative observations from the 15 experiments performed at Condition 3 and the 15 experiments at Condition 4. Ψ is based on the initial and final eruption rate. For the sake of brevity, we group Very High Ψ (No Crust) and High Ψ (Levee) into one section and Low Ψ (Rifts) and Very Low Ψ (Pillows) into one section for all conditions. The qualitative observations are followed by quantitative classification of the flows and direct comparison between Condition 3 (waning-waxing) and Condition 4 (waxing-waning), and then by a general comparison among waxing or waning flows (conditions 1 & 2) and fluctuating flows (conditions 3 & 4).

4.1 Condition 3 – Qualitative Observations

4.1.1 Very High and High Ψ Regime ($\Psi \geq 45$)

In the initial stage of eruption, axisymmetric crustless flows are produced. The symmetry is eventually perturbed by the introduction of a crust initially in the form of circumferential levees followed by a crust that develops over the flow itself. Levees form close to the vent for low-Q experiments which then tended to affect subsequent flow morphology, limiting the formation of multiple morphologies and resulting in thicker crust, although in general, the crust for condition 3 runs at these Ψ values was transparent to translucent. Because of the duration of the eruption, multiple Ψ morphologies were produced as local Q decreased at the flow margins at increasing distances from the vent.

During the low-Q pulse, fresh molten wax erupts radially from the vent, again producing axisymmetric flow, beneath a tenuous crust, if present. However, depending on the strength of the crust, the wax would sometimes ooze out and flow over the crust, both

proximal and distal to the vent in 2 of the 3 runs. Wax at the new low flow rate acted to propagate the flow forward by either advancing the entire existing flow front or producing break outs at the flow front. A crust is generally slow to form on the pulsed wax, likely due to the high eruption temperature in these high Ψ experiments. In one run – at low Q – the pulse wax ruptures the thick crust and produced a channelized leveed flow that increased the extent of the flow field.

In the third stage of the eruption the eruption continues at the higher initial Q (reference rate). This increase tends to be equally or more disruptive to any crust than the low-Q pulse promoting resurfacing, breakouts, and channelization of the flow. In 2 of the 3 runs, fresh wax produces channelized flow that either resurfaced the pre-existing flow or punctured through the levees and increased the aerial extent of the flow, producing more complex morphologies reminiscent of observed flow fields in nature. At high Ψ, any pathways created during the low-Q pulse such as ruptures in the crust and breakout channels continued to be utilized during the final high-Q stage. Despite persistent localized disruptions to the crust, all runs preserved a majority of the crust which had formed during the initial eruption and thickened during the pulse.

4.1.2 Intermediate Ψ Regime (Ψ = 21)

Initially the wax propagates axisymmetrically, but within seconds of eruption onset an extensive crust formed both at the flow front (as levees) and across the flow surface retarding flow propagation and promoting formation of compression ridges or folds atop the flow. For all runs, by the time the low-Q pulse occurs, the entire flow is completely covered by a translucent, and in some areas opaque, crust. As the crust develops, the flow becomes less axisymmetric. Localized low eruption rates at the flow front result in local

production of lower Ψ morphologies and eventually the cessation of wholesale flow propagation, although the flow continued to expand via smaller breakouts or flow lobes where the crust was weaker.

During the low-Q pulse, the fresh wax erupts beneath a stable crust for all runs. However, the crust is also more rigid than in high Ψ runs, which made it more susceptible to brittle failure. In all runs, the pulse wax ruptures the crust proximal to the vent, seemingly along fractures perpendicular to flow direction, and as a result, the molten wax pours out and resurfaces the pre-existing flow surface sometimes as sheets and sometimes as channels. Additional ruptures sometimes occurred more distal to the vent. Some of the molten wax remains flowing beneath the crust and produced breakouts at the flow front. The wax in the channels and at the flow front sometimes repeat the Ψ morphology continuum, producing levees, folds, etc.

After the pulse when Q returned to the higher reference rate, the new wax takes advantage of any pathways created during the pulse producing a complex flow consisting of breakouts at the flow front, resurfacing via sheets and channels, and thickening of the flow due to inflation. The dependence on Q is less prominent in these runs than in higher Ψ runs, with the main effect being that a more stable crust formed at low Q than in the high-psi runs.

4.1.3 Low and Very Low Ψ Regime ($\Psi \leq 8$)

Pure rift morphology was difficult to produce. As a result, only 1 of the 3 low- and very low- Ψ experimental runs allotted for rift experiments actually produced rifting during the run. Even then, the rifting displayed was not as overt as in conditions 1 and 2. Initially, flows produce sub-axisymmetric flows with little or no crust present. However, flows do

not propagate far before a crust forms at the flow margins and atop the flow immediately affecting the morphology of the flow, frequently producing a preferred flow direction. This condition results in less axisymmetric flow morphologies early in the eruptions as the crust increased in thickness and extent atop the flow. Crust at flow margins is subject to repeated breakouts and disruption. At the lowest Ψ, an opaque crust forms almost immediately upon eruption of the wax which controlled the subsequent propagation and morphology of the flow by retarding forward advancement in favor of thickening. When propagation occurs, it was in the form of bulbous lobes or toes. At high Q, flow advance appears in equilibrium with crust formation. Flows achieved a pillow-like morphology of rounded lobes and were noticeably thicker than for other regimes.

During the low-Q pulse, molten wax spreads beneath the crust producing an initial axisymmetric flow of fresh wax. Resurfacing and marginal breakouts occur primarily at the vent or the flow margins, respectively, at weak points in the crust. The molten wax erupts from fractures in the crust, sometimes producing catastrophic disruption of the crust and formation of new active preferred pathways. In this case, resurfacing adds appreciably to the thickness of the flow as new lobes are emplaced and overlapped older lobes.

In the final stage, returning to high-Q, the fresh wax utilizes any pathways created during the pulse or created its own via resurfacing or breakouts, although breakouts were larger volumetrically than during the low-Q pulse. Separate flow lobes produced by breakouts initially start with no crust. These new flow lobes form a crust and cycle through the Ψ morphology continuum. The final flow morphology resembles either the morphology produced by traditional rifting, even though the mode of rifting was different

from all previous conditions or resembled a morphology similar to pillow lavas to first order depending on Ψ.

4.2 Condition 4 – Qualitative observations

A total of 15 experimental runs were completed at Condition 4 (waxing-waning), with 3 runs for each Ψ regime. The following section represents summaries of general flow behavior during each Ψ regime.

4.2.1 Very High and High Ψ Regime ($\Psi \geq 45$)

Initially flows are axisymmetric but become more irregular once levees began to form at the flow margin. Margin levees form closer to the vent for lower Q and farther from the vent for higher Q. The introduction of a crust at the margin restricts the flow from flowing outward in all directions, thus creating preferred orientations of flow controlled by radial fracture locations. Once a thin, translucent crust forms at the flow margin, it propagates back towards the vent. This process of crust formation is more pronounced and faster for lower Q. As the eruption expands approximately radially, the flow transitioned down the Ψ continuum due to decreasing local flow rates.

During the pulse or second stage of the eruption, the effusion rate doubles to 2Q for 50 seconds, violently disrupting the extensive crust. The pulse wax pushes aside any liquid wax from the first stage of the eruption, which acts to propagate the flow forward and/or promote breakouts at the flow margin. The fresh wax also disrupts the tenuous crust on the surface by rafting pieces away or melting the crust. The fresh wax spills over any coherent crust, producing widespread resurfacing. In all runs, the magnitude of the breakouts produced by the pulse doubles the areal extent of the flow. As the pulse progressed, the widespread breakouts end and molten wax is transported from the vent to

the flow front via preferential pathways. Crust forms on the fresh wax and localized Q drops as it propagates away from the vent. Crust from the first stage of the eruption – though generally disrupted by the higher eruption rate at the start of the second stage of the eruption – acts to produce preferred pathways which turn into channelized leveed flows. These leveed channels allow wax to travel past the flow margin, increasing the areal extent of the flow and its overall complexity.

In the third stage of the eruption, the effusion rate drops to the reference rate, Q. Initially, the newly erupted wax takes advantage of preexisting pathways (i.e. channels, breakouts, etc.) during the pulse. The new wax will either extend these pathways propagating the flow out farther or create new pathways via breakouts/resurfacing resulting in minimal disruption to any crust present. The lower Q in addition to cooling wax from the previous eruptive stages promote formation of a more extensive and coherent crust on the flow surface and at the flow edges, ultimately slowing flow propagation, although the flows continue to propagate and grow through limited resurfacing and localized breakouts.

4.2.2. Intermediate Ψ Regime ($\Psi = 21$)

Again, flows initially propagate radially and crust forms closer to the vent than high-Ψ experiments such that a crust forms nearly simultaneously on the surface of the flow and at the flow margin. The crust restricts radial flow, creating discrete sub-crust pathways and preventing the flow from maintaining an axisymmetric shape. These discrete pathways produce breakouts, usually near the toe of the flow. Once the wax from a breakout solidifies, wax will breakout from a different location. The crust continues to thicken – translucent to semi-opaque – and the propagation of the flow as a whole slows.

When the high-Q pulse initiates, the surface crust is not catastrophically disrupted as with higher-Ψ experiments. Instead, voluminous breakouts occur at the flow margins and resurfacing was therefore minor in terms of volume and area. Fresh, molten wax mobilizes any remaining liquid wax from the first stage of the eruption pushing it toward the edge of the flow. The lower the Q, the more spatially concentrated the breakouts are. For all runs, the breakouts double the area of the flow. Crust forms more quickly in this Ψ regime than for higher regimes, which restrict the breakout after some time leading to smaller and more discrete breakouts of wax, giving the flow and almost leaky appearance.

By the third stage of the eruption, an extensive crust forms across the flow. For the experimental run with the lowest Q, this crust is almost opaque. Thus, fresh wax takes advantage of pathways utilized during the pulse. As a result, wax either pools beneath the crust or breaks out at the flow margin. These breakouts are much smaller and less dramatic than those produced during the high-Q pulse. Flow growth slows until the eruption ceases.

4.2.3 Low and Very Low Ψ Regime ($\Psi \leq 8$)

In these flows a crust forms readily – sometimes instantaneously – across the surface of the flow and at the flow edges. As the flow propagates forward, the crust proximal to the vent thickens and flows did not achieve an axisymmetric shape in plan form. At high Q, the flow propagates in an irregular radial pattern due to crust at the flow margin retarding uniform radial flow. At low Q, the flow propagates along in discrete lobes or via breakouts. At the lowest Ψ, the formation of a crust across the entire flow leads to repeated rifting of the crust as the flow propagates from the vent, producing irregularly shaped flows. As the eruption progresses, the crust in any given location thickens turning opaque in color forcing wax to pool beneath the crust and causing a transition from rifting

crust to repeated small-volume breakouts at a variety of weak points in the crust. The wax oozes, or rather leaks out, in a manner that resembles the formation of pillow basalts. This oozing continues until the pulse which eventually leads to more axisymmetric planform shapes.

During the high-Q pulse, fresh, molten wax mobilizes any wax stored beneath the crust from the initial stage of the eruption. Both the older and new wax erupts at the flow margins in large breakouts. Although large in volume, these breakouts are more localized than those in the intermediate Ψ regime. Once breakouts form, wax pours out and doubles the size of the flow with higher-Q flows leading to higher flux at the breakouts. Typically crust forms readily on the breakouts eventually restricting the flow to smaller breakouts and leading to wax pooling beneath the crust. For intermediate to low Q, the wax will breakout and 'ooze' at the flow margin, form a crust, and then break out again with repeated breakouts occurring at the toe of preceding breakouts.

In the third stage of the eruption when flow returned to the original low-Q value, the fresh wax takes advantage of pathways created by previous breakouts. However, breakouts at the flow margin decrease in volume and became more episodic again pooling wax beneath the crust, while opaque wax continues to thicken across the flow. At low Ψ and the run with the lowest Q, fresh wax breaks out and takes advantage of a pathway formed during the pulse, erupting onto the surface of the flow to form a leveed channel. The breakouts occur at fractures in the crust where two plates of crust met and they immediately form a crust upon contact with the ambient water. The flow grows very little in area. The leaking, oozing breakouts and flow thickening continue until the eruption ceased.

4.3 Quantitative analysis: Comparison of singular modes of emplacement for conditions 3 and 4

Conditions 3 and 4 represent full pulse cycles that include both decreasing and increasing eruption rates. Each condition featured 15 experimental runs. These experiments are longer in duration due to the 50-second pulse and the additional eruption stage. As a result, the volume of wax erupted is greater which precludes direct comparison of flow dimensions with conditions 1 and 2.

Figure 16 displays the frequency of the three emplacement modes investigated and compares them across conditions 3 and 4. Resurfacing is common in both conditions (Fig. 16a). In condition 3, resurfacing is not dependent on Ψ and occurs in every experimental run. In contrast, resurfacing is dependent on Ψ in condition 4 occurring primarily at intermediate to low Ψ. Resurfacing is a more significant emplacement process for both conditions 3 and 4 in terms of the areal extent although there are fewer instances of expansive resurfacing than in conditions 1 and 2. Approximately 60% of flows (condition3) and 80% of flows (condition 4) experienced <15% of areal resurfacing (Fig. 16d).

For condition 3, inflation is also common and not highly dependent on Ψ, although no inflation occurs at very high Ψ (Fig. 16b). For Condition 4 inflation is more likely at lower Ψ values. Tubes are rare in conditions 3 and 4 (Fig. 16c), with no clear dependence on Ψ in either condition although the data suggests a slightly higher occurrence at lower Ψ. Marginal breakouts occurred in every flow for conditions 3 and 4 (Fig. 16e, f). Marginal breakouts were dependent on Ψ for condition 3, with localized breakouts favored at low Ψ and circumferential breakouts favored at higher Ψ regimes. There is no dependence on Ψ

for marginal breakouts observed in condition 4, however, circumferential breakouts were twice as common as localized breakouts. No transitional (circum-localized) breakout behavior was observed in these conditions.

The flow dimensions are governed by Ψ and Q (Fig. 17a) and there is no observable difference in flow area or depth between conditions 3 and 4. For both conditions, as expected, thicker flows are smaller in area, while thinner flows are larger in area. Thicker, smaller flows are found at lower Ψ values, while thinner, larger flows are produced at higher Ψ values. All inflated flows are thicker than 0.5 cm, while flow displaying resurfacing and rare sheet flows are not thickened (Fig 17b).

Figure 18 illustrates the relationship between flow area and Ψ for flows displaying a singular mode of emplacement along with flows displaying multiple modes of emplacement. For both conditions, area is roughly dependent on Ψ for sheet flows and those exhibiting only resurfacing or inflation. Resurfacing as a single mode occurs primarily at high Ψ and inflation only occurs at intermediate to low Ψ. Flows with only tubes are not observed in either condition. Sheet flows were observed only in condition 4 and occur at high Ψ and are large in area. Flows with multiple emplacement modes are smaller in area than flows displaying a singular mode of emplacement, and that area appears to be not dependent upon Ψ value as the range in area for those flows with multiple emplacement modes is narrow.

In Figure 19 the eruption rate used on the Y-axis corresponds to the initial and final eruption rate, or reference rate, and does not take into account the eruption rate during the pulse. For flows in condition 3 (Fig. 19a) flows with only the inflation emplacement mode plot in the upper left portion of the figure, at mid-to-high Q and low to intermediate values

of Ψ. Resurfacing dominates flows at high Ψ value over the entire range of Q. The lower-left of the figure is dominated by flows with multiple modes of emplacement, complex flows all of which exhibit inflation along with other modes. Condition 4 flows plot similarly, although the trends are less clear (Fig. 19b). Sheet flows are rare and, contrary to the condition 1 field, tend to occur at moderate to high values of Ψ.

4.3 Summary of Condition 3 and 4 findings

- Resurfacing is more common and more extensive in conditions 3 & 4 than in conditions 1 & 2.
- In condition 4, both resurfacing appear to be more common at low Ψ values.
- Inflation tends to occur more readily at low Ψ values for both waxing and waning flows.
- Tube formation is very rare in fluctuating flows (3 & 4), even more uncommon than in waxing or waning flows (1 & 2).
- Marginal breakouts are more commonly circumferential than localized in fluctuating flows, especially in condition 4 (waxing-waning) where there is little dependence on Ψ value. In condition 3 (waning-waxing), high Ψ values favor circumferential breakouts, whereas low Ψ values favor localized breakouts.
- In an eruption rate vs. Ψ plot resurfacing and/or sheet flows are favored at high Ψ values across all values of Q. Pure inflation dominates low Ψ values at high values of Q and appears to be less common than in waxing or waning flows (conditions 1 and 2).

- Complex emplacement modes appear to be more common in fluctuating flows (3 & 4) than in waxing or waning flows (1 & 2) and dominate the field at low Ψ and low Q.

5.0 **Discussion and Implications:** Modes of Emplacement

Resurfacing

Resurfacing – or surface breakouts – is commonly observed on active flows, specifically pahoehoe flow fields. Resurfacing differs from lateral breakouts at the flow margin, because it occurs on the surface of a flow and it can occur at any location proximal or distal to the flow source. However, at a smaller scale in the flow interior, resurfacing might manifest as lava erupting from the margin of lobes (for instance, a pahoehoe toe) and repaves a small portion of the preexisting flow surface. Breakouts at any location in lava flows generally occur when the crust insulating the lava flow ruptures, which could be due to overpressurization induced by an increase in flow rate or continued inward solidification of the flow crust [*Hoblitt et al.*, 2012].

Resurfacing requires a crust – not necessarily coherent and insulating, but perhaps immobile – and the ability for molten wax to rupture that crust and flow over it. Here, resurfacing was observed in the majority of experiments for every condition regardless of Ψ, Q, experiment duration, or how the effusion rate varied (waxing, waning, fluctuating). Generally, for condition 1 (waning), resurfacing occurs at intermediate to high Ψ but it is very limited in extent. The resurfacing in these flows occurs either toward the end of the initial stage of the eruption or during the pulse – the wax taking advantage of any weak points in newly formed crust. For condition 2 (waxing), resurfacing is greater in areal extent and occurred primarily during the pulse when Q was higher. In Condition 3

(waning-waxing), resurfacing was more extensive in terms of percent area re-covered, partially owing to the longer duration in the experimental run, and tended to occur when the flow rate increased again after the low-Q pulse. In Condition 4 (waxing-waning), resurfacing was even greater in areal extent than condition 3, and occurred primarily during the high-Q pulse. It is important to note that once resurfacing created a pathway through the surface crust it was not uncommon for subsequently erupted wax to take advantage of this pathway at any point after its creation.

Resurfacing commonly occurred as the primary mode of emplacement and in concert with other emplacement modes. Based on our results resurfacing is much more likely when there is a sudden increase in eruption rate, however, in general, the mass of the wax devoted to resurfacing is very small. Far more wax is mobilized in inflation and marginal breakouts (see below). For that reason, resurfacing did not contribute much to flow thickness, except at low / very low Ψ when it occurred mostly as overlapping bulbous lobes. Instead, the majority of the flow thickness is achieved either when the flow is initially emplaced or when it is inflated. Some of the conditions that favor resurfacing (such as a sudden increase in flow rate) also favor increasing spreading rates, although the resurfacing itself does not contribute very much to the increase in spreading rate, but is instead a side effect of an increased spreading rate that may directly cause crust ruptures. In experimental runs with a larger degree of resurfacing, sometimes that wax flowed passed the flow margin and increased the size of the flow, typically at very low to intermediate Ψ values.

Resurfacing was found to be dependent on Ψ only for conditions 1 and 4. In condition 1, resurfacing was less likely at low and very low Ψ. At short pulses (10

seconds), there was an observed decrease in resurfacing for intermediate Ψ, however at long pulses (50 seconds) this was not observed suggesting that the longer pulse length gave the flow time to produce resurfacing. For condition 1, this suggests that the formation of a coherent, insulating, and immobile crust produced at lower Ψ prevented wax from escaping to the surface. The decreased flow rate also reduced the pressure under the crust which may have also precluded resurfacing in some cases. However, the slight increase in frequency of resurfacing for experimental runs with a long pulse suggest that if given enough time, the molten wax is able to fracture the crust and resurface the flow. For condition 4, the opposite was observed – resurfacing was less likely for high and very high Ψ regimes. Condition 4 was observed to have the highest degree of crust disruption during the pulse, especially at higher Ψ. The relative lack of resurfacing at higher Ψ suggests that resurfacing failed to occur because the crust was torn apart by the increased flow rate and/or flow primarily occurred beneath the crust. This wax flowed toward the distal reaches of the flow and erupted at the margin.

The lack of a dependence on Ψ for conditions 2 and 3 offers a more complicated story. Condition 2 – which is essentially the first half of condition 4 – shows no resurfacing dependence on Ψ. This suggests that although the flow rate increases and the crust is disrupted, there is still an opportunity for resurfacing during the uptick in Q. On the other hand, in condition 3 – of which the first half is condition 1, shows no trend similar to that observed for condition 1. Instead, the trend for condition 3 resembles that for condition 2, which indicates that resurfacing is occurring primarily in the second half of condition 3 when the eruption rate increases, which closely resembles condition 2.

At this stage, we also consider the extent of resurfacing – that is, what percentage of the flow surface is resurfaced during these events. For condition 1, the vast majority of instances of resurfacing resurfaced <10% of the flow area. The areal extent of resurfacing increased with decreasing Ψ. For example, at very low Ψ, ~20 – 50% of the flow was resurfaced. For condition 2, the vast majority of flows that experienced resurfacing had <15% of the flow area resurfaced, representing an increase in the average degree of resurfacing overall relative to condition 1. A dependence on Ψ was also observed with low and very low Ψ regimes, with half of the flows in the low Ψ regime having resurfacing percentages 13 – 30%, and those at very low Ψ, ~20 – 60%. At these lower Ψ values, it is important to note that the resurfacing takes on a different manifestation with the flow becoming more conducive to the stacking of overlapping lobes. For conditions 3 and 4, the majority of the flows have resurfacing percentages of <15% and <20% respectively. Therefore, although resurfacing is frequent it is not necessarily the dominant emplacement mode in a given flow.

Marginal breakouts

Marginal breakouts occurred in nearly every observed experiment, except for several at condition 1 (waning flows), where the crust at the flow margins solidified and prevented continued flow propagation. The number of marginal breakouts and whether or not the breakouts widespread, localized, or some combination of both depended on Ψ and pulse duration in condition 1. The longer pulse duration allowed more time for wax to flow beneath the crust and emerge at the flow front. In most cases these breakouts where localized, meaning most of the flow front was not active at any given time. This means that waning flows are more likely to produce a few significant breakouts than many,

smaller breakouts in most flow situations. Semi-widespread breakouts – those that resulted in ~50% of the flow margin experiencing breakouts – were most common at the lowest Ψ values which has implications for pahoehoe fields for which this Ψ regime is an analogue. These observations suggest that even at decreasing eruption rates, a significant portion of the flow front could remain active.

Marginal breakouts occurred in every experimental run in condition 2 (waxing) except one. The likelihood of marginal breakouts in this condition had no dependence on pulse duration, however, whether or not the breakouts were widespread or localized depended on Ψ. The stronger crust present at lower Ψ regimes prevented widespread breakouts at the flow margin and instead favored eruptions of wax from beneath the crust at discreet locations. Pulse duration did play in role in the extent of marginal breakouts. Widespread marginal breakouts occurred almost exclusively for long pulses (50 s), with the effect being greatest for low and very low Ψ. Given a long enough pulse at higher eruption rates, the strength of the wax could be overcome and activity at the flow front increased.

Marginal breakouts occurred in every experiment for conditions 3 and 4. For condition 3, widespread breakouts occurred almost exclusively at high eruption rates and high Ψ, while localized breakouts occurred for intermediate and low eruption rates and low Ψ. These trends are directly related to the strength of the crust, which increases with decreasing Ψ, and the force exerted by the propagating wax to rupture that crust, which increases with increasing Q. For condition 4, the relationship is similar such that widespread breakouts occur at high and intermediate eruption rates, with localized marginal breakouts relegated to the lowest eruption rates. There is no dependence on Ψ

for condition 4 flows suggesting complete control by eruption rate. The difference between conditions 3 and 4 likely reside in the experimental design. The increase in eruption rate in condition 4 drives wax at higher flow rates beneath the crust. Combined with the long duration of the pulse, this provides ample opportunity for marginal breakouts to occur. These breakouts are continuously fed by new wax even after the pulse ends and the eruption rate decreases. On the other hand, in condition 3, the eruption rate drops during the pulse giving the crust time to expand and strengthen. The increase in eruption rate occurs after this solidification time and has less time to affect the flow front relative to condition 4.

Inflation

Inflation of lava flows is thought to be a primary way that many non-channelized lava flows achieve deposit thicknesses of meters to tens of meters, especially in large igneous provinces such as the Deccan Traps and Columbia River Basalts [*Hon et al.*, 1994; *Self* et al., 1996; *Sheth,* 2006; *Rader et al.*, 2017]. Complimenting, inspired by, and expanding the design used by *Rader et al.* [2017] our experiments investigated how unsteady eruption rates impact inflation. Inflation requires a coherent, insulating crust. A lower effusion rate, while amenable, may not be strictly required. In nature, inflation can occur in pahoehoe flow fields with relatively low effusion rates due to interconnected pockets of melt [*Hon et al.,* 1994]. However, those flow rates can increase gradually or spike due to changes of the vent flux or local flow conditions.

In our experiments, inflation occurred whether or not the eruption rate increased or decreased, as long as the crust was strong enough to contain the majority of the still molten wax. However, in many instances a dramatic increase in the eruption rate led to rupturing of the solid wax leading to breakouts which diverted mass from inflation into resurfacing

events. This is supported by condition 1 and 2 data. Inflation is rare in condition 1 (waning) for the 10-second pulse experimental runs because there was insufficient time for a coherent crust to form and a detectible volume of wax to accumulate beneath it. For 50-second experimental runs in condition 1, inflation is much more frequently observed. In condition 2 (waxing), the frequency of inflation is the same for 10 and 50-second experimental runs indicating that the lower initial eruption rates allowed a coherent, insulating crust to form, thus promoting conditions favorable to inflation during the later high-Q pulse.

Inflation also occurred in most runs at conditions 3 and 4 (fluctuating flows: waning-waxing & waning-waxing). The main differences between conditions 1 and 2 and conditions 3 and 4 are *when* inflation occurs. For conditions 1 and 3, it occurs during the decrease in flow rate during the 50-second pulse. For conditions 2 and 4, inflation occurs either during the initial stage of the eruption when flow rates are low and a crust can form and inflate simultaneously or during the final stage of the eruption – after the pulse in condition 4 – when the flow rate returns to the initial low-Q. Inflation also depends heavily on Ψ. For conditions 1, 2, and 4, inflation is more frequent in lower Ψ – with inflation hardly occurring at very high Ψ. This is expected. In order to produce higher Ψ regimes in the lab, we increased the erupted temperature of the wax. Higher Ψ values describe regimes where the timescale of crust formation is long and horizontal propagation of the flow is fast. Thus, these are conditions that do not favor the formation of a coherent, insulating crust.

Inflation commonly thickened flows by 2 – 3x their non-inflated counterparts, with some flows inflating even more. The final thickness of the flows was correlated with Ψ

regime, with thicker flows observed at lower Ψ. This reflects the readiness for flows in low and very low Ψ regimes to produce and maintain an immobile crust. This is a testament to the strength, but flexibility, of the crust. Inflated flows tended to be smaller in area as spreading rates at the margin were lower due in part to the storage of wax beneath the crust.

Inflation frequently occurred in the presence of other emplacement modes. Inflation and resurfacing were commonly observed together. This is most evident at very low Ψ, where flows analogous to pahoehoe or pillow lavas would inflate but bulbous lobes would erupt from the flow surface to resurface the flow.

Tubes

The tubes produced in our wax flows most closely approximate the morphology and formation process of tubes formed in pahoehoe sheet flows. Tubes produced via roofing over of open channels did not occur in our experiments. The rarity of tubes likely lies in the conditions needed to produce tubes: steady effusion rates, low effusion rates, the formation of a roof of crust, and generally longer eruption durations [*Greeley*, 1971; *Malin*, 1980]. By the nature of our experimental design, the effusion rate was not constant during the duration of the run and pulse durations were short. The frequency of tubes was higher in condition 1 for the 50 second pulse because there was more time for the flow to reach equilibrium at a lower effusion rate. Tubes were even more likely to form in condition 2 (for both 10 and 50 second pulses) when initial effusion rates were half that of the initial value for condition 1. On the other hand, tube production was exceedingly rare for conditions 3 and 4, with slightly more tubes produced in condition 3. This suggests that the added instability of the eruption with more unsteadiness, or more fluctuations, discourages tube formation and perhaps promotes a different emplacement mode.

Low effusion rates more commonly produced tubes in conditions 3 and 4; however, tubes were produced at low and high eruption rates for conditions 1 and 2. This observation suggests that – at least in our experiments – a low effusion rate is not necessary to initiate tube formation. Instead the presence of a roof crust followed by lower eruptions rates may be more important to promoting discreet pathways beneath said crust. In condition 1, those tubes formed after the crust had solidified and when eruption rates decreased. In condition 2, the reverse occurred with tubes initiating during the first stage of the eruption when flow rates were low, and then when flow rates increased, the tubes were already formed and seemed to persist. For conditions 3 and 4, the formation of a coherent crust was hindered by the unsteadiness of the eruption. Perhaps in some runs, tubes had begun to form but were halted or destroyed when the eruption rates increased and ruptured the overlying crust. Regardless of condition, the frequency of tube production was rare compared to the frequency of inflation or resurfacing. Tubes did not appear to be correlated with flow depth; were observed in flows that had experienced no thickening; and were typically produced in conjunction with resurfacing and/or inflation. These correlations suggest that the conditions favorable to tubes were sometimes also favorable for resurfacing and/or inflation.

5.3 Hazards applications and Modelling implications

The primary downside of the inability of numerical models to simulate the phenomenology of lava flows is risk mitigation and hazards prevention. As stated in the introduction, many models tend to be probabilistic or random walk scenarios. While these models can do a reasonable job of reproducing historical flows and provide a beneficial first-order analysis, they often do not simulate the complexities associated with the

different emplacement modes. Because the predictive capability of numerical models is frequently benchmarked by the reproduction of historical flows, it is important that these models are able to reproduce historic flows. While current models cannot fully capture the entire intricacy of a natural lava flow, models that account for more complexity will produce more realistic results. Laboratory experiments, while still not as complex as actual lava flows, can reproduce natural processes that are still poorly constrained. Using analogue experiments to inform models is a key step in developing models that account for the complexity of lava flows, and thus, have better predictive capabilities. Better models result in a more efficient response to natural hazards and a more efficient allocation of resources.

Modelling lava flows remains challenging due to the multiphase nature of the fluid and complicated physics associated with the phenomenology of the flow. As a result, there is a dearth of physics-based models that simulate the complicated mechanics and conditions of flowing lava, which include crystallization, degassing, topography, and variable effusion rates [*Pinkerton,* 1987]. FLOWGO and MAGFLOW – both thermorheologic models – are physics-based models that account for a variety of competing factors related to heat loss during the emplacement of a lava flow [*Harris and Rowland,* 2001; *Del Negro* et al., 2013]. Other models, such as FLOWPULSE, are simple analytical models aimed at addressing specific processes that affect lava flows emplacement. In the case of FLOWPULSE, the fluctuating supply rate at the vent in channelized flows is investigated [*Tarquini and de'Michieli Vitturi,* 2014]. Many models are deterministic or probabilistic scenarios, in which the flow's likely path is predicted

based on a few key parameters – typically underlying topography or effusion rate [*de'Michieli Vitturi and Tarquini*, 2018].

In MrLavaLoba, slope is the primary variable that affects where the next parcel of lava will flow. It models the lava flow's progression as a series of elliptical lobes and is aimed at determining the most likely zone of inundation by a given lava flow [*de'Michieli Vitturi and Tarquini*, 2018, https://github.com/demichie/MrLavaLoba]. Mr LavaLoba relies on two variables, ε_{az} and α, to determine in which direction the flow will propagate. ε_{az} is the probability distribution of a random perturbation and takes into account α and slope, θ. α is a dimensionless input parameter that varies from 0 to 1 depending on θ. If $\theta=0$, then $\alpha = 0$, which means that the generation of the next lobe will be from some random point in the flow. For $\theta>0$, then $\alpha >0$, which means that the next lobe will likely erupt from a lobe on the steepest slope. While slope is important (see Chapter 3) to the propagation of the flow, other processes can impact the propagation of a lava flow especially at shallower slopes. Based on our experiments α is not strictly random, but tied to the preexisting flow conditions which include Ψ, Q, and eruption tempo (waxing, waning, or fluctuating). In addition, the term lobe exponent in MrLavaLoba – which also ranges from 0 to 1 – describes the likelihood of the most recently emplaced lobe to become the parent of the next lobe to form. A lobe exponent value of 0 indicates that the youngest lobe will produce the next lobe, resulting, over time, in a chain of singular lobes. A value of 1 would give equal probability to any lobe producing a new lobe and results in wider, stacked, more complex flows. According to our results, a lobe exponent closer to 1 than 0 is more realistic for waxing, waning, or fluctuating flows on low or zero slopes. Depending on Ψ, Q, and eruption tempo, new lobes (breakouts) may be surficial and lead to: 1) stacking or

resurfacing, most common during waxing moments of flows, at a combination of high Ψ and high Q; 2) discreet lobes at one or two locations at the flow front, most common at low Ψ, low Q, and favored during waxing periods of flow; or 3) widespread propagation of most of the flow front, favored during waxing moments, at high Q and low to intermediate Ψ. On the other hand, low Ψ, low or high Q, and well-developed strong crust favor inflation over new lobe formation.

6.0 Conclusions

We have demonstrated that the tempo of an eruption – increasing and/or decreasing the eruption rate for a period of time – has implications for the formation and preservation of lava flow emplacement modes, specifically resurfacing, inflation, tube formation, and marginal breakouts. This provides valuable insight into lava flow dynamics and constraints for probabilistic and physic-based models which seek to replicate existing and predict future lava flows. The conclusions of this study are as follows:

1. The formation and sustainability of a coherent, insulating crust determines whether or not resurfacing, inflation, and tube formation will occur, fundamentally determining how the lava flow appropriates its own mass during emplacement.
2. Increasing (waxing) eruption rates at the vent disrupt the crust promoting marginal breakouts, resurfacing, and sheet flows. However, the stronger the crust, the less disruptive increasing eruption rates will be and modes of emplacement such as inflation could occur.
3. Decreasing (waning) eruption rates preserve the crust and allows for the crust to spread and thicken. These conditions favor inflation and tube formation as the wax beneath the crust forms discreet pathways while propagating to the flow front.

4. Breakouts via resurfacing are most likely to occur on the surface when crust is stable, at the margins circumferentially when eruption rate increases, flow rate is high, and crust is weak (high Ψ), and at the margins discreetly when flow rate is low and crust is strong (low Ψ).
5. Inflation occurs when an extensive, coherent crust is present. While favored at low and intermediate eruption rates, inflation can occur or survive increased eruption rates when a strong crust is present (low Ψ).
6. Tubes were difficult to form in the laboratory. Tubes required the formation of a stable crust that allowed flow beneath it. The inability to reproduce tubes may lie in the intended unsteadiness of the experiment, which appears to disrupt or inhibit lava tube formation.

CHAPTER 3

THE EFFECTS OF SLOPE AND UNSTEADY EFFUSION RATES ON LAVA FLOW EMPLACEMENT: INSIGHTS FROM LABORATORY ANALOGUE EXPERIMENTS

4. Introduction

4.1. Lava Flow Morphology and Emplacement

Lava flows are one of the primary hazards of volcanic eruptions [*Crisp*, 1984; Pinkerton, 1987] and their emplacement mode, propagation rate and distance, and morphology of lava flows are interdependent and controlled by a variety of factors, including composition, rheology, eruption rate, cooling rate, and preexisting topography [*Walker* 1973; *Malin*, 1980; *Hon et al*., 1994; *Fink and Griffiths*, 1990, 1992; *Gregg and Fink*, 2000; *Griffiths*, 2000; *Harris and Rowland*, 2001]. Despite the abundance of lava flows on Earth and other planets, the phenomenology of lava flow emplacement remains poorly constrained due to its inherent complexity [*Carr*, 1973; *Pinkerton*, 1987; *Fink and Griffiths*; 1990, 1992; *Gregg and Fink*, 2000; *Sakimoto and Gregg*, 2001; *Bleacher et al*., 2007; *Rader et al.*, 2017]. Numerical modelling is used extensively to simulate lava flow emplacement and predict the path of future lava flows in order to understand lava flow emplacement and mitigate the risks associated with hazards [e.g., *Harris and Rowland*, 2001; *Vicari* et al., 2011; *de' Michieli Vitturi and Tarquini,* 2018]. However, these models rarely capture lava flow physics with fidelity. Instead they rely on probabilistic approaches and many simplifying assumptions that simulate lava flow emplacement using tunable statistical parameters loosely based on underlying topography [*de' Michieli Vitturi and Tarquini*, 2018], or restrict the emplacement mode to simple channel flow [*Harris and Rowland*, 2001], ignoring other complex modes of emplacement observed in nature such

as resurfacing, toe breakouts, inflation and tube formation. Understanding what influences the propagation and emplacement of lava flows - both conceptually and quantitatively - is key to unraveling their complex phenomenology which will improve existing models and therefore aid in their predictive capabilities and response efficiency led by organizations tasked with hazards prevention.

The emplacement modes of lava flows determine how the flow accommodates mass [*Pinkerton*, 1987; *Hon et al.*, 1994; *Griffiths*, 2000]. This study focuses on propagation rate and four modes of emplacement: resurfacing, marginal breakouts, inflation, and tube formation. These emplacement modes are frequently observed in lava flow emplacement [*Greeley*, 1987; *Pinkerton*, 1987; *Hon et al.*, 1994; *Hoblitt et al*., 2012; *Rader et al.*, 2017]. Resurfacing is defined here as the process by which lava covers a preexisting flow surface during the same eruptive event (Fig. 1a). Resurfacing is essentially a breakout on the surface of a lava flow and can produce stacking of lobes of lava or repave flow surfaces. Marginal breakouts occur when molten lava is transported beneath the crust and erupts out at the flow margin. Marginal breakouts occur at the edge of a flow and can be minor or advance the flow front, however exact mechanisms that control the location and timing of breakouts is not well constrained [e.g., *Farrell et al., AGU Abstract*, 2019]. Inflation is the endogenic growth of a lava flow via the emplacement of molten lava in its core beneath the crust, which results in the thickening of the flow (Fig. 1b) [*Hon et al.*, 1994]. Inflation likely played a role in the emplacement of the tens of meters thick lava flows observed in large igneous provinces such as the Colombia River Basalts and Deccan Traps [*Self et al*., 1996; *Sheth*, 2006; *Rader et al.*, 2017]. Lava tubes (Fig. 1c) are a common construct in basalt lava flow fields and can form via the roofing over of open channels or by

consolidation of interconnected pathways within pahoehoe flows [*Greeley,* 1972, 1987; *Belousov et al.,* 2015]. Lava tubes insulate lava allowing it to travel farther and retain its heat [*Greeley,* 1972, 1987; *Malin,* 1980; *Sakimoto* et al., 1997]. As such, lava tubes tend to form during longer-lived eruptions and are a primary way lava flows propagate and lava flow fields expand [*Malin,* 1980; *Sakimoto* et al., 1997; *Bleacher* et al., 2007]. Understanding the conditions conducive to these emplacement modes is fundamental to aiding in hazards prevention and establishing a framework for classifying effusive eruptions [*Greeley,* 1972, 1987; *Pinkerton et al.,* 2002; *Bleacher et al.,* 2007].

4.2. Unsteady Eruption Conditions

While the average eruption rate is typically cited for a given volcanic eruption when considering lava flow emplacement, the instantaneous volumetric flow rate at a volcanic vent, also known as eruption rate or effusion rate, varies with time [*Walker,* 1973; *Wadge,* 1981; *Pieri and Baloga,* 1986; Lipman and Banks, 1987; *Tarquini and Vitturi,* 2014; *Rader et al.,* 2017]. Effusive dominant eruptions typically experience a large increase in eruption rate shortly after the eruption commences followed by an exponential decline in eruption rate over time after some maximum value is achieved [e.g., *Wadge,* 1981; *Belousov et al.,* 2015]. Therefore, average eruption rate can underestimate the eruptive conditions at the vent early in an eruption and overestimate the conditions later in an eruption. During the exponential decline, the eruption rates can fluctuate due to the injection of more magma into subsurface storage, widening of the conduit, and thermal contraction of the magma, among other mechanisms [*Wadge,* 1981; *Bailey et al.,* 2006; *Tarquini and Vitturi,* 2014]. Rapid, short-lived changes in the bulk eruption rate are *pulse* events and they can have a huge impact on flow emplacement, promoting overspills, flow blockages, breakouts, the

remobilization of stationary flows, and the development of new channels [*Peterson and Tilling*, 1980; *Baloga and Pieri*, 1986; *Hon et al.*, 1994; *Bailey et al.*, 2006; *Rader et al.*, 2017]. Additionally, fluctuations in the eruption rate can result in errors when calculating average eruption rates, lava viscosity, and emplacement times of lava flows [*Wadge*, 1981; *Baloga and Pieri*, 1986; *Bailey et al.*, 2006]. The change in eruption rate at the vent can also affect the flow rate at the flow front, propagation rate and style at the front, flow morphology, and emplacement mode [Chapter 2].

4.3. Slope

Slope is a variable that exerts fundamental control on the propagation of lava flows (Fig. 2) [e.g., *Gregg and Fink*, 2000; *Sakimoto and Gregg*, 2001]. Slope creates an *effective* effusion rate by increasing the flow velocity due to the added component of gravity ($F = mg*sin\theta$). This increased velocity can rupture surface crust, promote overspills onto levees when present, and generally narrows the width of the flow [*Gregg and Fink*, 2000; *Tarquini and Vitturi*, 2014; *Tarquini*, 2017]. Lava flows commonly flow over slopes 1 – 10˚ on the flanks of subaerial volcanoes and even steeper slopes on the flanks of mid-ocean spreading ridges [*Pinkerton*, 1987; *Gregg and Smith*, 1993; *Vicari* et al., 2007; *Tarquini*, 2017]. At Kilauea, many of these lava flows flow over an escarpment in Hawaii Volcanoes National Park on their way to the sea. On Mars, innumerable lava channels and lava tubes are observed to have been emplaced down the flanks of broad shield volcanoes with average slopes of 5 – 8˚ [*Carr*, 1973; *Plescia*, 2004; Bleacher et al., 2007]. At Olympus Mons, Mars, lava channels and lava tubes are observed having flowed over its steep escarpment, with 25 – 30˚ slopes [*Carr*, 1973; *Sakimoto et al.*, 1997; *Plescia*, 2004; Bleacher et al., 2007]. A number of studies have documented the effects of slope on the propagation of

lava flows in the field [e.g., *Pinkerton*, 1987; *Gregg and Smith*, 1993; *Belousov et al.*, 2015]. In the laboratory, analogue experiments have been conducted to simulate the emplacement of lava flows on constant slopes and at slope breaks [*Hallsworth et al.*, 1987; *Gregg and Fink*, 2000; *Garry et al.*, 2006; *Kerr et al.*, 2006; *Dietterich et al*. 2017]. Most numerical modelling of lava flows assume that slope is a primary influence on determining how and in which direction a lava flow will propagate [e.g., *Favalli et al.*, 2005; *de' Michieli Vitturi and Tarquini*, 2018]. While most models assume slope is the primary driver in the probability of flow propagation, other factors such as emplacement mode, heavily controlled by crust formation and by unsteady eruption conditions (Chapter 2) at the vent, can influence flow propagation. These additional factors in combination with slope could impact whether or not the flow propagates primarily at the toe or not.

4.4. Numerical modelling and hazards mitigation

The complexity of lava flows remains a challenge to modelling and hazards prevention. Crystallization, degassing, topographic effects, and effusion rate can vary over the course of a single eruption [*Wadge*, 1981; *Pinkerton*, 1987; *Griffiths*, 2000; *Belousov et al*., 2015]. Due to the inherent difficult in simulating the complexity of lava flows, simplified numerical models are utilized to understand individual aspects of lava flows and mitigate risks [*Pinkerton*, 1987; *Felpeto et al*., 2001; *Connor* et al., 2012]. The predictive capability of models is often validated by determining how well the model replicated well-documented flows [*Connor* et al., 2012; *de' Michieli Vitturi and Tarquini*, 2018]. Probabilistic models (Fig. 3) are commonly used to simulate flow emplacement in order to evaluate hazards without the requirement of numerical parameters for lava flow properties, which may be unknown or difficult to estimate [*Felpeto et al*., 2001; *Favalli* et al., 2005;

de' Michieli Vitturi and Tarquini, 2018]. Physics-based models, such as FLOWGO and MAGFLOW account for temporal variations and thermorheologic aspects of lava flows, but these are rare [*Ganci et al.*, 2012; *Harris and Rowland*, 2001; *Del Negro et al*., 2013], a testament to the difficulty of simulating the emplacement of actual lava flows. Laboratory analogue experiments provide an opportunity to investigate the complex phenomenology of lava flows and inform numerical models [*Fink and Griffiths*, 1990, 1992; *Gregg and Fink*, 2000; *Blake and Bruno*, 2000].

4.5. Laboratory Wax Experiments

Numerous studies have demonstrated polyethylene glycol (PEG) wax – a commercial grade polymer with a temperature dependent viscosity and readiness to form a crust –as a useful analogue in simulating lava flow emplacement in the laboratory [*Huppert and Sparks*, 1987; *Fink and Griffiths*, 1990; *Griffiths and Fink*, 1992; *Gregg and Fink*, 1996; 2000; *Blake and Bruno*, 2000; *Sakimoto and Gregg*, 2001; *Soule and Cashman*, 2004; *Kerr et al.*, 2006; *Rader et al.*, 2017]. *Fink and Griffiths* [1990] used PEG experiments to derive a dimensionless parameter, psi, hereafter denoted by Ψ, which describes the ability of a fluid – a viscous gravity current in this case – to transfer heat in the system either via the surface of the fluid through convection and/or radiation or by lateral advection of melt [*Fink and Griffiths*, 1990, 1992; *Gregg and Fink*, 2000]. As such, Ψ relates the timescales of surface crust formation (t_s) to the timescales of heat advection within the flow (t_a) [*Gregg and Fink*, 2000].

Fink and Griffiths [1990] observed that flow behavior and morphology differed across a continuum of Ψ regimes. Four primary flow morphologies corresponding to discreet Ψ ranges were observed, although transitional morphologies were also observed.

Those morphologies, from high to very low Ψ, are: Levees, Folds, Rifts, and Pillows (Fig. 4) [*Fink and Griffiths,* 1990, 1992; *Gregg and Fink,* 2000]. These morphologies are analogous to surface morphologies and textures observed in nature [*Fink and Griffiths,* 1990, 1992; *Gregg and Fink,* 2000]. In summary, Ψ is a powerful tool that relates the morphology of a flow to its cooling regime. Additional studies have investigated the effects of slope on flow morphology, channel morphology on lava flows, crust distribution on the surface of lava flows, and the formation of compound lava flows [*Griffiths and Fink,* 1992; *Blake and Bruno,* 2000; *Gregg and Fink,* 2000; *Sakimoto and Gregg,* 2001; *Gregg and Smith,* 2003; *Cashman et al.,* 2006; *Garry et al.,* 2006, 2007]. *Gregg and Fink* [2000] demonstrated using PEG experiments that an increase in underlying slope had the same effect as increasing the effusion rate – an effective effusion rate – which decreases the expected Ψ value for a given morphology. This shift results in high Ψ morphologies being produced at lower vent-defined Ψ values on steeper slopes. This work was extended by *Gregg and Smith* [2003] and *Garry et al.* [2006] to investigate submarine lava flows on the Puna Ridge, Hawai'i and the East Pacific Rise. Analogous morphologies to those created in the lab were observed in the natural environment. The applicability of Ψ has also been investigated to determine its robustness in understanding the formation and evolution of a lava flow or flow field [*Gregg and Kesthelyi, 2004*].

However, previous studies either limited their experiments to constant eruption conditions or did not account for how varying eruption rates with time affected flow propagation and morphology [*Baloga and Pieri,* 1986]. Recently, *Rader et al.* [2017] used PEG wax experiments and Ψ to understand the role of unsteady eruption conditions on inflation in the context of large igneous provinces, such as the Deccan Traps [*Rader et al.,*

2017]. They were able to correlate experimental data with observational field data of inflating lava flows in Hawaii. In addition, *Rader* et al. [2017] found that inflation can occur in low viscosity lavas under pulsating conditions and that the instantaneous effusion rate can be 3x higher than the average effusion rate during an eruption. The effects of slope and unsteady eruption rates on mode of emplacement - resurfacing, breakouts, inflation, and tube formation – while recorded in some aspects in the field, have not undergone scrutiny in the laboratory. The majority of laboratory studies of lava flows on slopes have been conducted under steady conditions. Therefore, to extend that work we investigate here how unsteady vent conditions and slope affect the emplacement of lava flows using results from laboratory analogue experiments. Our results demonstrate that varying the eruption rate in combination with underlying slope influences the formation and preservation of certain emplacement modes common to lava flows.

5. Methodology

5.1. Experimental Setup and physical parameters

To test the effects of unsteady eruption rates at the vent and slope on the propagation and morphology of lava flows, we performed 72 laboratory analogue experiments. The experiments were conducted in a 76 cm long x 30 cm wide plexiglass tank (Fig. 5). The distance from the vent to the back of the tank measured 50 cm. This tank was placed on an adjustable apparatus in order to vary the slope. In addition, the tank had a 3.8 cm offset attached to the base near the opening, which added to the underlying slope. For this study, we conducted experiments at ~7˚, ~16˚, and ~29˚ above horizontal, which represent low, medium, and high slopes. Additional experiments, with the same source conditions but on a flat surface are considered here for comparison [Chapter 2,

Conditions 3 & 4 suite]. The floor of the tank was fitted with a 0.1 cm thick metal mesh at 0.4 cm grid spacing to simulate surface roughness typical of that experienced by lava flows flowing over pre-existing terrain and to ensure a no-slip condition at the base of the flow [*Fink and Griffiths*, 1990, 1992; *Gregg and Fink*, 1996, 2000; *Blake and Bruno*, 2000]. The tank was filled with a fresh water bath maintained at 0°C by mixing freshwater ice. A programmable pump was connected to the base of the tank via a 1-cm diameter rubber hose and metal attachment with a 1-cm opening secured to the base of the tank. We used pharmaceutical grade polyethylene glycol (PEG) 600 wax to simulate lava flow emplacement. The solidification temperature of the wax was determined to be 18.4˚C. PEG wax was dispensed from 1000 mL beakers to simulate a magma reservoir

Ψ was varied by changing the effusion rate and wax temperature. All experiments were erupted from 1–6 cm^3/s at 1 cm^3/s intervals for each Ψ regime. PEG was heated or cooled to a desired temperature between 19.6 – 29.6˚C, according to the corresponding eruption rate to achieve the desired Ψ. The tank was filled with a fresh-water bath maintained at 0°C measured continuously to a tenth of a degree. The wax was dyed using food coloring in order to distinguish different phases of the eruption. In order to explore the parameter space and determine the effects of unsteady vent conditions across a variety of eruption regimes, we conducted experiments across a range of Ψ values from 1–45, representing very low to high Ψ, which correspond to four of the primary morphologies observed by *Fink and Griffiths* [1990]. Care was taken to avoid running experiments with Ψ values associated with transitional morphologies, although some transitional behavior and morphologies were observed. We also avoided very high Ψ values (No Crust) to avoid

redundancy due to similar behavior observed at high Ψ which are exacerbated by the added effect of slope.

In order to simulate unsteady vent conditions, the experiments were divided into two conditions (Fig. 6). Conditions 3 and 4 featured a combination of waxing and waning eruption rates, with 36 experimental runs each for a total of 72 [see Chapter 2 for condition nomenclature]. Condition 3 is characterized by an instantaneous decrease in the eruption rate from a reference rate, followed by an instantaneous increase returning to the reference rate (waning – waxing). Condition 4 is characterized by an instantaneous increase in eruption rate from a reference rate, followed by an instantaneous decrease returning to the reference rate (waxing – waning). The period of time representing the increase or decrease in eruption rate in the middle of the experiment is termed the *pulse*. In natural eruptions, the period of heightened or lessened eruption rate can range from hours to days, but are typically a fraction (less than half) of the overall eruption duration [*Wadge,* 1981]. At channelized flows on Mt. Etna, cyclical fluxes in volumetric flow rates generally involved dramatic increases in flow rates followed by a waning of the flow rate, which is similar schematically to that of condition 4 [*Bailey et al.*, 2006]. The *Rader et al.* [2017] experiments used a range of pulse durations of 10, 20, 30, 40, and 50 seconds. They recorded thinner, less complex flows for shorter pulses and thicker, more complex flows for longer pulses. We utilized a pulse length of 50 seconds in order to give the flow time to adjust to the new eruption rate at the vent, and because short pulses have a much smaller impact on flow emplacement [Chapter 2]. For Condition 3, the eruption rate during the pulse was half the initial eruption rate, while for Condition 4, the eruption rate was double the initial eruption rate. There was a brief (<1s) pause at the start of the pulse to switch the

rubber hose from one wax reservoir to another of the same temperature but different color. This pause had a negligible effect on morphology and emplacement, as was demonstrated in the lab during the experimental procedure's development phase.

For each experimental run in conditions 3 and 4, an initial volume of 200 mL of dyed PEG wax was erupted into the water filled tank at an initial rate of 1 – 6 cm^3/s. The eruption of this initial volume allowed the flow to mature. For the pulse, the rubber hose was switched between wax reservoirs and the eruption rate was either decreased (condition 3) or increased (condition 4) for 50s. After the pulse, the rubber hose was returned to the original wax reservoir and an additional 200 mL of wax was erupted. After this last phase of the eruption, the experiment ceased. While the volume of wax erupted during the initial and final stages of the eruption were the same for both conditions, the volume of wax erupted during the pulse was a function of flow rate. For condition 3, the volume of wax erupted per experiment is the same for a given eruption rate, but varies between eruption rates. Condition 4 experiments are slightly larger in volume – but similar in magnitude – compared to condition 3 owing to the lower initial and final eruption rates. The volume of erupted wax for experiments at condition 4 is also the same for a given eruption rate but different between eruption rates. Table 1 presents the run conditions for each of the 72 runs. After each eruption, we measured the length, width, and depth of the wax flows. Length and width measurements were obtained by fixing a measured grid to the base of the tank with demarcated measurements. Flow depth, or thickness, was obtained by inserting a ruler into multiple locations of the flow.

5.2. Image Processing

Experiments were either photographed and recorded using a digital camera and iPhone. In addition, two GoPro video cameras were submerged in the chilled bath for some experimental runs to record the flow progression. Video recordings were created by positioning a digital camera attached to a wooden beam across the opening of the tank. At the steepest slopes, this hindered recording of the distal flow front. Photographs were collected at the end of each experimental run, typically no sooner than 60 seconds after the experiment had ceased. This allowed time for the wax to stop flowing and solidify. Videos were analyzed to record resurfacing, breakouts, inflation, front propagation through time, and other aspects of flow phenomenology.

6. Qualitative Observations

3.1 Conditions 3 and 4

The observations of flow phenomenology gleaned from video recordings were compiled in detailed qualitative observations for each condition and were further divided by slope setting. From these observations, patterns emerged across different emplacement modes, flow processes, and crust behavior. For condition 3, a total of 36 experimental runs were completed, with 9 runs (3 runs at each of the 3 slope settings) for each of the four Ψ morphologies. In order to produce the high, intermediate, low, and very low Ψ, the wax temperature was adjusted as needed. Figure 7 provides an example of flows erupted during condition 3 on a low, medium, and high slopes for high Ψ. Full qualitative descriptions are provided in Appendix A. For condition 4 experimental runs, a total of 36 experimental runs were completed, with 9 runs for each of the four Ψ morphologies. Figure 7 provides

an example of flows erupted during condition 4 on a low, medium, and high slopes for high Ψ. Full qualitative descriptions are provided in Appendix B.

In general, for both conditions, all flow rates, and all values of Ψ, increasing the slope narrows the flow width and decreases flow depth, simplifying the overall channelized morphology. Condition 4 flows tend to be more complex than condition 3 flows under all conditions, such that the channel width is narrower in condition 4 flows but their overall width is greater due to compound and complex growth of the levee system.

7. Quantitative Observations

7.1. Flow Propagation

A total of 72 experiments at two eruptive conditions were conducted across a range of eruption rates (1–6 cm^3/s), Ψ values (1–45), and slopes (~7˚, ~16˚, and ~29˚) in order to determine the effects of slope and unsteady eruption conditions on flow propagation and to determine which conditions were most favorable to resurfacing, breakouts, inflation, and tubes. During all of the experiments, the eruption rate changes during the pulse (increasing and then decreasing, or vice versa) and as a result the Ψ also fluctuates during the pulse (increasing or decreasing in value by 0.1–8 during the pulse). Varying the eruption rate – and by extension, the Ψ, impacts how the wax flows propagate, solidify, and accommodate additional erupted wax. The order in which the eruption rate is varied – denoted by the condition – was also tested to determine whether or not the favorability of emplacement modes changed during the eruption. Resurfacing was defined by wax rupturing the crust and repaving the preexisting flow surface. Marginal breakouts were either at the flow front (toe) or the flow margins (lateral). Inflation involved the endogenic growth of the wax flows which resulted in flow thickening without resurfacing. Through experiments

performed prior to the study, the standard flow depth is ~0.5 cm on slopes of 0˚, which agrees with previous studies [*Sakimoto and Gregg*, 2001; *Rader et al.*, 2017; see Chapter 2]. We observed a thinner standard flow depth at ~0.3 cm, which is expected for flow on slopes [*Gregg and Fink*, 2000]. Once the experiment ended, we interpreted any flow deposit >0.3 cm, which was also observed to have increased in thickness over time, while simultaneously displaying little to no growth in areal extent and no evidence of meaningful contribution to its thickness via resurfacing, as having inflated. Tubes – documented by slicing through the flows after the experiment finishes, removing them from the chilled bath, and rotating them upward to inspect the subsurface – were characterized by sinuous, semi-circular channels carved into the solidified wax. Below we present the results of these analyses.

7.1.1. Comparison of flow behavior between Conditions 3 and 4

Emplacement Modes

Figure 8 displays the frequency of emplacement mode as a function of Ψ (plots on the left, top to bottom) for conditions 3 and 4 independent of slope. The role of slope is addressed in detail later in this document, although we mention general relationships between emplacement mode and slope here as part of the discussion of data in Figure 8. In condition 3, the occurrence of resurfacing is weakly dependent on Ψ (slightly more common at low Ψ), is not dependent on slope, and occurs in most experimental runs, although to varying degrees of prominence. Inflation was relatively uncommon and dependent on Ψ, increasing with decreasing Ψ value. Inflation does not occur at the steepest slopes. Tubes are rare in Condition 3, with no clear dependence on Ψ, and occur only at the lowest slopes. Observations for condition 4 are similar to those for condition

3. For comparison, resurfacing – although occurring in most experimental runs to varying degrees – is only weakly dependent on Ψ with some preference for low Ψ values. Inflation was uncommon, increasing with decreasing Ψ, with no inflation observed at high Ψ. As with Condition 3, tubes are rare in Condition 4, with only weak dependence on Ψ, seemingly more likely to occur at the lowest Ψ values.

In general, flow depth decreases with increasing slope (Figure 9, Condition 3, left; Condition 4, right), although the effect of slope is stronger in Condition 3. Generally, flows produced at higher Ψ produce the thinnest flows, however, flows at lower Ψ produce a wide range of flow depths. Figure 10 plots flow depth against flow area and color codes by dominant emplacement mode for both Conditions 3 and 4 (left and right, respectively). Flows emplaced as sheets or that are dominated by resurfacing are the thinnest flows. Flows that display inflation or tube formation, with or without other emplacement modes, are at least double in height, with the highest (or thickest) flows being those where resurfacing, inflation, and tubes are all present. The separation in height between resurfacing/sheet flows and other modes appears to be more evident for Condition 3.

Figure 11 details the dependence of emplacement mode on Ψ and flow area (Condition 3 left; Condition 4 right). Flow area functions as an approximate proxy for flow rate and slope such that area increases for a given value of Ψ as Q increases and/or slope decreases. Flow area and Ψ value show no dependence upon one another. In other words, Ψ value does not appear to control final flow area, but rather other factors such as eruption rate and slope do. Resurfacing to some degree occurs at all values of Ψ, as do sheet flows. Flows displaying inflation either as the dominant emplacement mode or alongside other

modes occur only at low or low-to-moderate Ψ values and tend to produce low to moderate flow areas, and never produce the largest flow areas.

Figure 12, a regime diagram which does not account for slope, plots mean flow rate against Ψ value while symbols indicate emplacement modes. Condition 3 is the top panel; Condition 4 is the bottom. For condition 3, high Ψ values and/or high effusion rates favor simpler flow propagation, that is, predominantly one mode of emplacement, which is typically resurfacing or, less commonly, simple sheet flows. In contrast, multiple modes of emplacement, including inflation and tubes, dominate the lower left of the diagram as they are occurred only at low mean eruption rates and/or low Ψ values. Note the lines in the figure roughly show the division between the two regimes. For condition 4, a similar trend is observed with more complex flow propagation and multiple emplacement modes dominant at low mean eruption rate and/or low Ψ, while only resurfacing is observed at high mean eruption rate and/or high Ψ. However, simple sheet flows plot in the lower region of Figure 12 for condition 4. These trends closely resemble those observed in Chapter 2 for experiments performed on flat surfaces.

Figure 13 is a regime diagram that plots slope against Ψ value, while symbols indicate emplacement modes. In condition 3, high slopes and/or high Ψ promote resurfacing and simple sheet flows, while low slopes and/or low Ψ favor multiple emplacement modes including inflation. Condition 4 displays similar patterns to condition 3. Resurfacing, simple sheet flows, and tubes are observed at high Ψ and/or high slope. Note the sheet flows, originally located at the bottom in Figure 12 at low mean eruption rates, are now located in the upper right corner similar to previous trends. This demonstrates the effect of slope on flow propagation, in this case, producing a simple sheet

flow at lower eruption rates on a steeper gradient. At low slope and/or low Ψ, inflation and multiple emplacement modes are generally observed. The observation of tube-fed flows at high slopes and high Ψ is curious. Tubes had not been observed to occur at higher Ψ in previous experiments performed on flat surfaces.

Flow Propagation

We tracked the progression of the flow with time, quantifying how the flow length changed with each stage of the eruption. This data provided additional information on how and where the wax is deposited and when certain emplacement modes are occurring. Figure 14 (a,b,c) was produced by measuring the major axis of each flow at the end of each eruptive stage (i.e. initial, pulse, and final) and recording the corresponding time since experiment onset. The major axes are plotted as a function of time and subdivided into different panels by Ψ-value range and slope. We also include data from experiments from Chapter 2 on a flat surface (0^o slope) with the same source conditions. The plotted curves cluster into distinct populations according to eruption rate and the inflection points in the curve tend to correspond to transitions between eruptive stages. The shape of each curve is controlled by processes inherent to the propagation of the flow, especially mode of emplacement.

For high Ψ values on a flat surface, we observe three distinct populations of curves (Fig. 14, top two panels). In each panel, the leftmost population of curves represents flows produced at high eruption rates, while the middle and rightmost curves represent mid- and high-Q runs. For condition 3 (waning-waxing), the difference between experiments 1 and 4 is stark. In experiment 1, the first stage of eruption shows flow growing quickly but during the low-Q pulse spreading rates slow as expected. After the pulse, the flow

continues to propagate forward at similar velocity despite an increase in eruption rate highlighting the effect of the decreased localized flow rate at the flow front. Resurfacing was the only mode of emplacement observed in experiment 1. However, in experiment 4, resurfacing and inflation was observed. The flow spreads quickly during the initial stage of the eruption. During the pulse, the curve flattens – a characteristic of inflation. The flow does not propagate at the same rate as flows without inflation because wax is being stored beneath the crust. After the pulse, the eruption rate increases and the spreading rate increases as wax is transported to and erupted at the flow margin. We observe a similar trend for experiments 2 and 5 erupted at moderate Q. Experiment 2, in which only minor resurfacing was observed, has a straighter curve caused by the decrease in eruption rate during the low-Q pulse, and a decrease in localized flow rate during the final high-Q stage of the eruption when the flow edge is most distal from the vent. This decrease in propagation rate in the final stage despite the increase in eruption rate also demonstrates that in widespread flows the front does not necessarily 'feel' an eruption rate increase immediately (or ever) due to spatially variable local flowrates. Experiment 5, on the other hand, has greater changes in slope at the points of inflection, albeit the pattern is similar to that of Experiment 2. Resurfacing, inflation, and tubes occurred during this flow which have impacted the propagation rate of the flow front and the flow area.

At low eruption rates (experiments 3 and 6), the differences are more subtle. The flows spread more slowly and are smaller in area. The flattening of the curve, in these instances, is also due to the addition of a more coherent crust and overall lower flow rates. However, there is a subtle difference in the curves specifically in the third stage of the eruption. Experiment 3 (only resurfacing) flows a little farther and a little faster than

experiment 6 (resurfacing, inflation, and tubes). Once again – except for lowest Q – none of the flows spread as fast in the third stage of the eruption as observed in the first stage of the eruption. This is due primarily to decreased localized effusion rates at the flow margin, despite increased eruption rates at the vent, and secondarily to emplacement modes.

The curves for condition 4 at high Ψ differ from those observed in the same regime for condition 3. We note the overall convex character of most curves, despite the increase in Q during the high-Q pulse in the middle stage. Counter to what might be expected, that increase in Q typically does not steepen the slope of the curve during the pulse, indicating that the increase in eruption rate is not felt at the flow front over these timescales. Again, for widespread flows, localized flow rate at the margins will be lower than those nearer the vent. At high eruption rates, the decrease in slope after the inflection points is not as great as in condition 3. In other words, the spreading rates do not decrease as much. Both experiments, 1 and 4 in this case, most closely resembled sheet flows. The flattening observed at moderate eruption rates for experiment 5 is likely due to a bias in our measurements; while the flow continued to grow, it did not propagate along its major axis. Only in experiment 3 do we see a concomitant increase in propagation rate and eruption rate at the vent.

We compare these results to those at high Ψ on a 7˚ slope. The curves are again easily discriminated by eruption rate, Q, whereas the kinks in the curves reflect changes in Q during the low-Q pulse and the effects of crust solidification. In condition 3, at high eruption rates, the flows propagate rapidly downslope until the pulse, as observed for experiment 1. During the pulse, the propagation speed slows due to the decreased eruption rate. In the case of experiment 1, the flow hit the back of the tank by the end of the pulse.

At the moderate eruption rate of experiment 2, the curve flattens to nearly horizontal during the pulse, due in part to the reduction in flow rate during the low-Q pulse, but also due to observed resurfacing and some overspill of wax from the main channel.

Equivalent results for Condition 4 on a 7˚ slope are shown on the middle-right of Figure 14a. The curves are again easily discriminated by eruption rate, Q. Here, a progression in the bend of the curves is accentuated by differences in Q. At high eruption rates, the flows propagate rapidly downslope until the high-Q pulse, when the propagation rate increases suddenly due to the increased eruption rate. Once eruption rate decreased after the pulse, the flow began to propagate much more slowly. In the case of experiment 1, the flow hit the back of the tank by the end of the pulse. The curve of experiments 1 - high Q – exhibited broad channelized flow bounded by levees and only the resurfacing mode of emplacement, and no inflation, tube formation, or marginal breakouts. At moderate eruption rates as in experiment 2, a flattening of the curve is observed during the final stage of the eruption. This segment is longer than for higher eruption rates due to the longer duration of the experiment as a result of the lower initial eruption rates. Experiment 2 recorded only resurfacing and no inflation, tube formation, or marginal breakouts. Experiment 3 in condition 4 is an example of an experiment conducted at the lowest initial eruption rate on a 7˚ slope. The lengthening of the curve is a result of the lower eruption rate and a characteristic increase in propagation rate is observed during the high-Q pulse. Resurfacing and tube formation were observed for experiment 3. Figure 14a (bottom right) illustrates an experimental run conducted at a 16˚ slope for condition 4. In the case of experiment 6, high Ψ, low Q, the flow channelized and reached the back of the tank by the end of the pulse. No resurfacing, inflation, or tube formation were observed but the

increase in eruption rate during the high-Q pulse was seen in the propagation rate as noted by the increased slope.

All of the flows in Figure 14b (left panel, condition 3 runs at intermediate Ψ values flat and 7^o slopes) experienced inflation and resurfacing. Hence, all of their curves demonstrate a noticeable flattening during the low-Q pulse, or second stage of the eruption. The shallower rebound of the propagation rate in the last stage of the eruption observed in experiment 9 is tied to a stronger crust which hinders the propagation of the flow. Experiment 9 is also the thickest of the three flows here. Compare these experiments to the ones observed in condition 4 for intermediate Ψ, all of which underwent inflation. Note that at high and intermediate eruption rates (exp 7, exp 8), the curve does not show an increase in propagation rate during the high-Q pulse despite the increase in eruption rate at the vent. Experiment 9, on the other hand, does show an increase in propagation rate during the high-Q pulse. In all cases, the pulse is followed by flattening during the final stage of the eruption reflecting the decrease in eruption rate and decreasing local flow rates at the front as the flow increases in area. We note here that the enhanced crust formation in the intermediate-Ψ value runs increased the liklihood of inflation and therefore led to more pronounced decreases in propagation rates as q dropped.

On a 7^o slope, experiments with mid-psi and mid-Q exhibit a greater slope increase during the high-Q pulse than equivalent runs on a flat surface, indicating that the increase in eruption rate at the vent more evidently impacts flow front propagation for flows on slopes, consistent with the trends for condition 4 at high psi values.

At low and very low Ψ for condition 3 (Fig. 14c), inflation occurred in all of the flows at low Ψ, except for experiment 11 where a flat curve during the pulse stage is notably

absent. The lack of inflation in condition 3, experiment 11 is due to the occurrence of a large localized marginal breakout. The drastic reduction in propagation rate evident in experiments 10 and 13 are a result of the inflation. For these flows, however, the curves during the pulse are not as flat owing to the higher eruption rate of these experimental runs. After the low-Q pulse when eruption rate increases to the reference rate, only some flows show a corresponding increase in propagation rate. It is important to note that because major axis is the metric it would only record circumferential breakouts at the flow margin and not localized breakouts that may have not occurred near the measured section.

For condition 4 at low Ψ, the curves are generally concave upward, like condition 4 flows at high and intermediate values of Ψ. Many flows do not show an increase in propagation rate during the high-Q pulse, either due to inflation or resurfacing (e.g., exp. 13), or due to the fact that local flow rate decreases with distance from vent as the flow spreads. In the final stage of the eruption, the curve flattens. At moderate eruption rates, many of the curves reach their flattest during the final stage of the eruption, due to a combination of decreasing eruption rate, decreasing local flow rates, and resurfacing (specifically at low – very low Ψ).

As slope increases, flows at condition 3 generally exhibit more constant propagation rates, event through the low-Q pulse, with the exception of experiment 20 that experienced inflation which doubled flow depth. The final stage of the experiments when the eruption increased to the reference rate generally exhibit higher propagation rates on slopes than on flat surfaces primarily due to channelized flow. The exception is Experiment 33; the only run conducted at the lowest eruption rate of the study. Due to the lower effusion rate, the flow propagated at a slower but steady rate during the initial phase of the

eruption, then decreased slightly during the pulse, and further slowed in the final phase of the eruption although never hitting the back of the tank. The much slower propagation rate in the final stage of the eruption is due to crust formation and inflation.

For condition 4 on slopes, Experiment 31 is an example of a flow discharged at a high eruption rate, has a noticeable bench during the pulse. This bench was caused by widespread resurfacing during the pulse when wax erupted from the vent, broke through the crust at the vent, and flowed over (i.e. resurfaced) the preexisting flow. Experiment 32, also conducted at very low Ψ but at moderate Q, displays a different shaped curve. A flattening of the curve in Exp 32 is mainly observed during the final stage of the eruption when the effusion rate returns to the lower initial value. Note that very low Ψ values for Condition 4 produce propagation plots reminiscent of those for Condition 3, indicating that the increased flow rate during the pulse is accommodated largely by inflation or widespread resurfacing when a robust crust forms during the first stage of the experiment (as can be expected for very low Ψ values).

8. Discussion and Implications

8.1. Emplacement mode and the role of slope

8.1.1. Resurfacing / Marginal Breakouts

As observed in chapter 2, resurfacing was a common process in flow development. The differences in resurfacing on a slope were primarily due to how it manifested during flow emplacement and the degree of resurfacing. For condition 3, resurfacing was generally a dominant process except at the steepest slopes. On steep slopes, resurfacing occurred proximal to the vent and generally involved the spilling of wax onto and over levees (overspill) proximal to the vent. This increased the width of the levees and

sometimes the height negligibly. In condition 4, resurfacing was inhibited by steeper slopes – with those experiments generally producing channelized leveed flows. However, the areal extent of resurfacing was minor for very low Ψ regardless of slope – a trend not observed in condition 3. This probably relates to the stronger crust created under this regime which limited the number of breakouts and controlled the eruptible volume as well. Resurfacing occurred in response to the changing eruption rate, although the extent of resurfacing was greater when the eruption rate increased (condition 4).

Marginal breakouts were surprisingly rare especially compared to chapter 2, occurring primarily in the lowest Ψ regime. This affect was likely due to or enhanced by slope. The preexisting slope acted to funnel the wax downslope and discouraged lateral spread. In the lowest Ψ regime, the flow propagated more slowly due to the rapidly solidifying crust. The crust also acted as a barrier to downslope movement, which allowed the wax to pool beneath the crust. This provided an opportunity for breakouts to occur at locations other than the flow toe. Marginal breakouts were observed more in condition 3, although this could be an observational bias due to decreased GoPro functionality for condition 4 experiments. However, the overhead camera captured few signs of marginal breakouts in condition 4 which leads us to conclude they were more common for condition 3.

8.1.2. Inflation

Inflation was most affected by substrate slope. Introducing slope added a gravitational component which increased the effective effusion rate and lateral flow velocity. Therefore, as expected, the wax preferred to flow downslope. Inflated flows were more frequently observed at shallower slopes, although inflation is more common at

lower Ψ even on steeper slopes. In both conditions, inflation was dependent on Ψ and more likely to occur at lower Ψ. At very low Ψ, the competency of the crust retarded flow propagation in any direction and allowed for the storage of wax beneath the crust. Many flows which inflated during eruptions later deflated due to the drain out. In some cases, the inflation was partially preserved, in other cases it was not. Inflated flows were generally smaller in area, a result of the importance of a crust in promoting conditions suitable to inflation.

Experiments performed under no slope conditions [see Chapter 2] yield a much higher occurrence of inflation for conditions 3 and 4, which recorded the same number of occurrences in each condition. For example, in no slope experiments, inflation occurred in 11 out of 15 runs, or ~73% of the total runs in that condition. For condition 3 in this study, inflation occurred in 9 of 36 runs, or 25%. We interpret this decrease in observed inflation as a result of slope, which promotes flow downhill and decreases crust competency due to higher flow rates. In nature, inflated flows are generally observed on shallow slopes, such as those observed in the Deccan Traps and Columbia River basalts [*Hon et al.*, 1994; *Sheth*, 2006].

8.1.3. Tube formation

Tubes were a rare occurrence, although they were slightly more common for condition 4. Tubes tended to form under lower Ψ conditions, which reasserts the importance of a coherent, insulating crust to tube development. The dearth of observed tubes may be a direct result of the experimental parameters. *Greeley* [1971, 1987] highlighted the formation of lava tubes and necessary eruption conditions, which included long-lived steady low to moderate effusion rates. Other studies have used the observation

of lava tubes on extraterrestrial volcanoes to reconstruct their eruptive histories and highlight changes in emplacement conditions through time [*Sakimoto* et al., 1997; *Bleacher et al.*, 2007]. By incorporating a pulse into our experimental design, we have advertently made the eruption conditions not steady and hindered a long-lived eruption. By doing so, we have inhibited tube formation. Conducting longer experiments, which would involve erupting larger volumes of wax into a larger tank, might better simulate the conditions for tube formation and development. Regardless, we did observe some tube development and those tubes occurred under expected conditions – mainly those that allowed the formation of a coherent crust.

Perhaps more important were the formation mechanisms observed for tubes. Experiments performed on a flat substrate [see Chapter 2] produced tubes that form under conditions analogous to those of a pahoehoe sheet flow. This is one mechanism of tube formation. Tubes also form by roofed over lava channels. We observed this mechanism of tube formation during some of our experimental runs on slopes. Rafted pieces of crust in the flow channel would accrete to the levees and over time form a roof to cover the channelized wax. In one experimental run, this process started at the vent with a crust rapidly forming over newly erupted wax. As the wax propagated away from the vent, this roof was no longer stable and the flow transitioned into open channel flow. Some of the observed tubes formed as the flows propagated as single toes with rapidly solidifying crusts where molten wax would continue to flow in the interior while the outer crust hardened. These flows were narrower and sinuous. The minor propensity for tubes under condition 4 likely reflects the lower initial effusion rate which creates conditions conducive to the formation of a stable crust early in the eruption. Those conditions, while interrupted during

the pulse, occur afterwards as well. In condition 3 – except at low initial Q – these conditions would not occur until the low-Q pulse and then would be disrupted by the increase in Q afterwards. Tubes had a negligible impact on flow height, which is consistent with results in Chapter 2, although flows were thicker when tubes occurred in the presence of other emplacement modes such as inflation.

8.2. Modelling & Hazards Implications

Because most observed lava flows originate on or are emplaced on slopes, such as near the summit of a volcano, slope is often a fundamental variable affecting the propagation of a lava flow in addition to composition, rheology, exsolution of volatiles, and cooling. Previous studies have noted the relatively narrow channelized flows, fast flow rates, and relatively crust-free surface of lava propagating on sloped substrates [*Hallsworth et al.*, 1987; *Gregg and Fink*, 2000; *Kerr et al.*, 2006]. *Gregg and Fink* [2000] conducted experiments on slopes ranging from 0 – 60˚ at steady vent conditions and recorded narrowing of flows at steeper slopes and a shift in flow morphologies to those associated with higher Ψ values. The observation of higher Ψ morphologies at lower Ψ values, but steeper slopes is due to the added velocity attributed to underlying slope, which is not incorporated into Ψ.

Many of the qualitative aspects of our flows had been previously observed by *Hallsworth et al.* [1987] who sought to understand the phenomenology of flow emplacement on slopes. The complexity of lava flows in combination with slope has given rise to various numerical models which work to simulate flow emplacement. Due to the inherent difficulty in modeling lava flows, many of these models have been simplified to either deterministic or 1-D thermorheological models and assume that slope – when present

– is the primary driver in downhill flow. MrLavaLoba, a probabilistic model, for instance, contains a dimensionless variable (α) whose value is assigned depending on the underlying slope [*de' Michieli Vitturi and Tarquini*, 2018]. While slope is indeed very important to flow direction and propagation, especially at steeper slopes, it is not the only variable affecting flows. Our experiments demonstrate that at shallower slopes (≤16˚) unsteady conditions at the vent and the cooling regime of the flow can promote emplacement modes that affect flow morphology and therefore affect propagation rate and direction.

The incorporation of flow phenomenology observed in laboratory analogue experiments into numerical models is a powerful way to analyze and predict lava flow emplacement. The complexity of experiments lends to better understanding of natural processes which cannot be accurately modeled at present. This will increase the robustness of both statistical and physics-based models. Better models will result in enhanced predictive capabilities which means a more efficient response to hazards. Our experiments have direct implications for assumptions and variables used in models that simulate lava flow emplacement. In the probabilistic model, MrLavaLoba, there are three variables of interest: ε_{az}, α, and *lobe exponent* [*de' Micheili Vitturi and Tarquini*, 2018]. MrLavaLoba simulates the emplacement of a lava flow as a series of elliptical parcels, or lobes. ε_{az} is the probability of a random perturbation in the flow and incorporates slope (θ) and α. α is a dimensionless parameter varying from 0 to 1 depending on slope. Increasing the slope tends α towards 1, which increases the probability the flow will not propagate randomly, but instead flow downhill. According to our results, for slopes <16˚ and especially those <7˚ this approach may be too simplistic. However, for slopes >16˚ our study and others suggest that this assumption is valid and robust [*Gregg and Fink*, 2000]. The variable, *lobe*

exponent, which varies from 0 to 1, outlines the likelihood of a daughter lobe becoming the parent of a subsequent lobe. A lobe exponent value of 1 will result in a flow of singular lobes linked together resembling a chain link, while an exponent of 0 results in a wider, more complex flow of propagation occurring at random lobes. The lobe exponent approximates the processes of resurfacing, inflation, and marginal breakouts. A value of 0 will cause "stacking" as subsequent lobes are erupted atop previous lobes. According to our results, stacking is more likely to occur at shallower slopes and during periods of increasing flow rate. Increasing the slope should increase the lobe exponent and promote more downflow propagation. Decreasing the flow rate, on the other hand, increases the likelihood of flow thickening via inflation (which may also be approximated as stacking) and slows forward propagation of the flow front. Other models which can easily incorporate fluctuation in eruption rate at the vent could incorporate our findings to produce more realistic flow behavior. Wedding laboratory analogue experiments and numerical modelling is the next frontier of lava flow modelling and hazards prevention.

9. Conclusions

We performed 72 experiments using polyethylene glycol (PEG) 600 wax to simulate lava flow emplacement on ~7˚, 16˚, and 29˚ slopes with unsteady eruption rates at the vent. We divided these experiments into two conditions that simulated decreasing-increasing and increasing-decreasing eruption rates in order to simulate tempos observed in actual eruptions. We observed the morphology and emplacement modes (resurfacing, marginal breakouts, inflation, and tubes) of the wax flows. The goal of the study has been to better understand the distribution of mass within an active flow when there are unsteady

vent conditions and flows are emplaced on a sloped substrate. The following findings are a result of this study.

1. Although slope is important to flow direction and propagation, unsteady vent conditions and the presence of a coherent crust impact emplacement modes which also affect flow morphology and propagation. Slope promotes flow in the downhill direction and inhibits lateral spread of the flow, especially at steeper slopes. However, unsteady effusion rates and the surface crust can impact how and when that mass moves downslope.
2. Slope impacted the manifestation of emplacement modes, resulting in varieties of emplacement modes not observed in experiments performed on flat surfaces. Resurfacing manifested as overspilling onto levees and wholesale re-pavement of previous flow surfaces from the vent. Tubes formed via processes observed in nature, such as the roofing over of open channels and as propagation of toes with rapidly solidifying crust similar to that observed in pahoehoe flow fields.
3. Inflation was inhibited by increasing slope as excess mass was preferentially moved downhill. Only ¼ of flows experienced inflation relative to the ¾ of flows that experienced inflation when no slope was present. Deflation of flows were also observed in some runs.
4. Marginal breakouts were inhibited by slope, except at very low Ψ. Although slope reduced the likelihood of breakouts away from the active flow front, at very low Ψ the presence of a strong, coherent crust acted to slow propagation down slope and allow for the concentration of molten wax under the crust. This increased the likelihood of marginal breakouts.

5. On flat surfaces, increases in eruption rate do not commonly increase propagation rate, due to the combined effects of resurfacing, inflation, and decreasing local flow rates far from the vent as flows increase in area. However, an increase in eruption rate is more likely to be manifest as an increase in propagation rate as substrate slope increases.
6. Laboratory analogue experiments can have a direct impact on numerical models. Models should incorporate unsteady vent conditions, if possible, and account for more dynamic emplacement processes. Our conclusions suggest that slope remains an important variable in flow propagation especially at steeper slows. Nevertheless, unsteady vent conditions play a large role in how lava flows are emplaced. Additionally, unsteady vent conditions affect when conditions are favorable for certain emplacement modes to occur. As a result, at shallower slopes other processes such as resurfacing or inflation become important to flow emplacement.

CHAPTER 4

LAVA FLOW ERUPTION CONDITIONS IN THE THARSIS VOLCANIC PROVINCE ON MARS

10. Introduction

Volcanism is a fundamental geologic process that has created and shaped the surfaces of the terrestrial planets in our solar system [*Carr,* 1973; *Carr,* 1974; *Greeley and Spudis,* 1981; *Wilson and Head,* 1983; *Pieri et al.*,1984; *Gregg and Fink,* 2000; *Plescia*, 2004; *Werner,* 2009; *Spudis et al.*, 2013]. Understanding the volcanic history of a planetary body provides information on its formation and evolution [*Carr,* 1973; *Carr,* 1974; *Greeley and Spudis*, 1981; *Wilson and Head*, 1983; *Spudis et al.*, 2013]. On Mars, study of the volcanic history of the planet is complicated by the sparsity of compositional data, the lack of human observation during volcanic activity, and sometimes a lack of analogous terrestrial terrain and processes. Nevertheless, a mafic composition of much of the Martian crust is suggested by surface mineralogy of less dust covered regions [*Rogers and Christensen*, 2007]. Although a variety of volcanic landforms have been preserved at the surface, effusive volcanic eruptions have dominated throughout much of Martian history, resurfacing 50–60% of the crust and producing vast lava plains, voluminous lava flows, sinuous rilles, and massive shield volcanoes [*Carr,* 1974; *Greeley and Spudis*, 1981; *Plescia*, 2004; *Werner*, 2009; *Hauber et al.*, 2009, 2011; *Hiesinger et al.*, 2009; *Xiao et al*., 2012]. The bulk of Martian volcanism appears to have occurred early in the planet's history during the Noachian (>3.7Ga) and Early Hesperian (>3.5Ga), with decreasing volcanic fluxes through time [*Werner,* 2009; *Tanaka et al.*¸2014]. In the absence of direct observations, the eruption conditions can only be estimated based upon the morphology of

preserved deposits. Using flow morphology to estimate eruption conditions has been a goal of terrestrial and planetary volcanology for decades and has fueled a number of studies [e.g., *Wilson and Head,* 1983; *Fink and Griffiths,* 1990; *Gregg and Fink,* 1996; *Cashman et al.*, 1998; *Mallonee et al*., 2017]. Previous studies have estimated lava flow eruption rates, viscosities, and yield strengths using combinations of simplified fluid mechanics, numerical models, and morphometry [e.g. *Glaze and Baloga*, 2006; *Baloga and Glaze*, 2008; *Glaze et al.,* 2009; *Hauber et al.,* 2011; *Hiesinger et al.,* 2009].

For this study, we have quantitatively characterized and modelled the emplacement of 40 lava flows in the Tharsis Volcanic Province on Mars in order to calculate eruption rates, viscosities, yield strengths, and emplacements times. These 40 lava flows occur in the volcanic plains and in proximity to or on central volcanoes. High resolution images up to 0.4 m/pixel and digital terrain models at ~50 – 70 m/ pixel have enabled detailed analyses of these lava flows [*Jaumann* et al., 2007; *Malin* et al., 2007; *McEwan* et al., 2007]. We have applied three lava flow emplacement models that utilize flow morphology and morphometry to constrain eruption rates, rheology, and emplacement times. The suite of models consists of 1) a standard cooling limited rheologic treatment outlined in *Hiesinger et al.* [2007]; 2) the utilization of Ψ derived from laboratory analogue experiments; and 3) the self-replication model outlined in *Baloga and Glaze* [2008]. The calculated volumes, eruption rates, viscosities, and emplacement times have implications for the eruption conditions of relatively recent volcanic activity on Mars, the composition of lavas erupted on Mars, and the subsurface pathways that transport magma in the Martian crust. An application of this method to lava flows on other volcanic bodies, such as Io or Venus, could also prove useful.

11. Background

The eruption conditions of lava flows on Mars have implications for understanding its composition, interior, and evolution. The morphology of terrestrial and extraterrestrial lava flows has long been used as a proxy for the eruptive conditions at the time of emplacement [e.g., Walker 1971, 1973; *Carr*, 1973, 1974; *Wilson and Head*, 1983; *Griffiths and Fink*, 1992; *Gregg and Fink*, 1996; *Cashman et al.*, 1998; *Bleacher et al.*, 2007; *Hiesinger et al.*, 2007; *Baloga and Glaze*, 2008; *Hauber et al.*, 2011]. A number of studies have used the morphology and morphometry of lava flows on Mars to estimate effusion rates, viscosities, and yield strengths by applying cooling limited and rheologic models [*Wilson and Head*, 1983; *Glaze and Baloga*, 2006; *Bleacher et al.*, 2007; *Hiesinger et al.*, 2007; *Hauber et al.*, 2011]. These studies have made a variety of simplifying assumptions about lava flow rheology, composition, and environmental conditions during emplacement. Using these methods, earlier studies invoked either exceptional eruption rates never observed in terrestrial lava flows or exotic compositions to explain the very large dimensions of Martian lava flows [*Wilson and Head*, 1983; *Cashman et al.*, 1998; *Giacomini et al.*, 2009]. These analyses were partly predicated on the assumptions that the length of lava flows is controlled exclusively or largely by eruption rate, the entire flow front is active at all times and the flow moves as a coherent mass, and/or lava behaves as a Newtonian fluid [*Nichols*, 1939*; Bruno et al.*, 1996; *Baloga et al.*, 1998; *Baloga and Glaze*, 2008]. Although studies have demonstrated a Newtonian rheology may be assumed for the hot interior of a lava flow, *Hulme* [1976] demonstrated that the behavior of lava flows on Olympus Mons, Mars, and elsewhere, were better approximated by a Bingham rheology due to the significant yield strength of most lavas, particularly as they propagate and cool.

Subsequent studies followed suit [e.g. *Bruno et al.*, 1996; *Hiesinger et al.*, 2007; *Glaze and Baloga*, 2006; *Baloga and Glaze,* 2008; *Hauber et al.*, 2011]. Recent works have accounted for more complex processes that occur during the emplacement of lava flows such as levee construction and overspills [*Baloga et al.*, 1998; *Baloga and Glaze*, 2008; *Glaze et al.*, 2009]. Most studies aimed at constraining lava composition and effusion rates on Mars have focused on the Tharsis and Elysium volcanic provinces where some of the best-preserved lava flows on the planet are located. Due to dust cover, however, compositional data is sparse to nonexistent in these localities [*Christensen*, 1986; *Hiesinger et al.*, 2007; *Baloga and Glaze,* 2008; *Hauber et al.*, 2011].

Laboratory analogue experiments have provided a fundamental understanding of lava flow emplacement processes and their relationship to propagation rate and morphology, and have thus been used to make predictions of lava flow behavior on other planets [*Hallsworth et al.*, 1987; *Fink and Griffiths,* 1990; *Griffiths and Fink*, 1992; *Gregg and Fink,* 1996; 2000; *Blake and Bruno,* 2000; *Soule and Cashman,* 2004; *Rader et al.*, 2017]. Previous laboratory studies have examined lava flow morphologies by extruding substances analogous to lava into controlled environments under controlled source conditions [*Hallworth et al.*, 1987; *Fink and Griffiths,* 1990, 1992; *Gregg and Fink,* 1996, 2000]. Polyethylene glycol (PEG) wax has been demonstrated to be a useful analogue to real lava flows due to its temperature dependent viscosity and timescale of crust formation [*Hallsworth et al.*, 1987; *Fink and Griffiths,* 1990, 1992; *Gregg and Fink*, 1996, 2000; *Soule and Cashman*, 2004]. *Fink and Griffiths* [1990] derived a dimensionless parameter, Ψ, which is a ratio of the characteristic time scale of crust formation, which is controlled

by surface cooling, to the characteristic time scale of lateral thermal advection, for which flow propagation rate is a proxy.

Fink and Griffiths [1990] observed five morphologies produced in the laboratory: no crust, levees, folds, rifts, and pillows, which occur on a continuum from high to low Ψ values, respectively (Fig. 1). Analogous morphologies have been observed in nature [*Fink and Griffiths,* 1990, 1992; *Griffiths and Fink,* 1992; *Gregg and Fink,* 1996, 2000; *Gregg and Keszthelyi*, 2004; *Garry et al.*, 2006]. *Gregg and Fink* [2000] extended this work and demonstrated the effect of slope on Ψ and associated morphologies. Other studies utilized PEG experiments to address the formation of channelized flows, surface crust distribution, and surface textures of submarine lava flows which are analogous to morphologies produced in the lab [*Hallsworth et al.*, 1987; *Gregg and Smith*, 2003; *Kerr et al.*, 2006; *Garry et al.*, 2006]. Extrapolating laboratory experiments to other terrestrial bodies such as Mars has been attempted in order to constrain eruption parameters and predict expected morphologies, although the image resolution at the time of these studies was limited to >150 m/pixel [*Fink and Griffiths*, 1992; *Gregg and Fink*, 1996]. Laboratory experiments, in conjunction with rheologic modelling and remote sensing geomorphology, therefore provide an additional constraint on prehistoric eruption conditions on Mars.

12. Study Area

12.1. Tharsis Volcanic Province

Tharsis is the largest volcanic province on Mars (Fig. 2), containing the tallest volcano in the solar system (Olympus Mons at ~22 km), one of the largest volcanoes on the planet in areal extent (Alba Mons at ~1.15 x 10^6 km^2), and the Tharsis Montes [*Carr,* 1973; *Carr,* 1974; *Crumpler and Aubele*, 1978; *Greeley and Spudis*, 1981; *Scott and*

Tanaka, 1981; *Plescia*, 2004]. The Tharsis Volcanic Province dominates the western hemisphere of the planet and occupies a region from ~60° N to ~40° S and 210° E to 300° E and ~4000 x 6000 km. Volcanic activity began ~4 Ga and has occurred within the last ~100 Ma [*Carr*, 1973; *Carr*, 1974; *Scott and Tanaka*, 1981; *Plescia*, 2004; *Werner*, 2009]. The region contains innumerable lava flows and small shields, in what is sometimes characterized as plains-style volcanism [*Greeley*, 1977; *Baloga and Glaze*, 2008; *Glaze et al.*, 2009; *Hiesinger et al.*, 2007; *Hauber et al.*, 2009, 2011]. The 40 lava flows featured in this study occur throughout the Tharsis Volcanic Province, primarily on and around Olympus Mons, in the volcanic plains surrounding the Tharsis Montes, and Daedalia Planum. A brief summary is given of each region.

12.1.1. Olympus Mons

Olympus Mons is 600 km across and is situated northwest of the Tharsis Montes and southwest of Alba Mons (Fig. 2) [*Carr*, 1973; *Greeley and Spudis*, 1981; *Plescia*, 2004; *Werner*, 2009]. It features a summit caldera complex approximately 90 x 60 km in size, an encircling basal escarpment ranging in height from 3 – 8 km, and massive landslide deposits derived from the volcano, that extend up to 800 km away [*Carr*, 1973; *Plescia*, 2004; *Tanaka et al.*, 2014]. To the northeast and southwest, lava has flowed over the escarpment and obscured its topographic expression, creating two distinct aprons [*Greeley and Spudis*, 1981; *Plescia*, 2004]. Olympus Mons displays a flat summit plateau, steeper upper flanks (~5 – 9°), and gentler sloping lower flanks (~4°), with the steepest slopes (~25 – 40°) restricted to the basal escarpment [*Plescia*, 2004; *Byrne* et al., 2013]. Extensive dust cover prohibits compositional analyses of Olympus Mons, but the volcano is morphologically similar to Hawai'i and the Galapagos shield volcanoes and a basaltic

composition has been inferred for its erupted lavas [*Hulme*, 1974; *Christensen*, 1986; *Bleacher* et al., 2007]. Although construction of the Olympus Mons edifice is believed to have started ~3.6 Ga in the Late Noachian or Early Hesperian, most of the shield's surface has been dated to < 700 Ma based on crater count modeling [e.g. *Neukum* et al., 2004; *Werner*, 2009; *Xiao et al*., 2012]. Effusive volcanic activity dominated in recent Martian history, as evidenced by abundant lava tubes and channels [*Sakimoto et al*., 1997; *Bleacher* et al., 2007; *Werner*, 2009; *Peters and Christensen*, 2017]. Some of the youngest features on Olympus Mons include lavas on the floors of the nested calderas (~100–200 Ma), lava flows on the volcano's southwestern flanks (≤ 50 Ma), and small satellite vents and arcuate graben [*Neukum* et al., 2004; *Werner*, 2009; *Tanaka et al*., 2014; *Peters and Christensen*, 2017].

12.1.2. Volcanic plains & Daedalia Planum

Volcanic plains formed by countless overlapping lava flows cover much of the terrain within the Tharsis Volcanic Province (Fig. 2) producing a monotonous topography of gentle slopes, punctuated by low shields, cinder cones, graben, and the central volcanoes [*Carr*, 1973, 1974; *Greeley and Spudis*, 1981; *Hauber et al*., 2011; *Peters and Christensen*, 2017]. The lava plains surround the major volcanic constructs in Tharsis and individual flows can extend hundreds of kilometers from their sources [*Carr*, 1973; *Carr*, 1974; *Greeley and Spudis*, 1981; *Baloga and Glaze*, 2008]. The sources include dozens of low shield volcanoes, the Tharsis Montes, and buried vents [*Carr*, 1973, 1974; *Crumpler and Aubele*, 1978; *Greeley and Spudis*, 1981; *Hiesinger et al.*, 2007; *Glaze et al.*, 2009; *Werner*, 2009; *Hauber et al.*, 2011]. Daedalia Planum – an example of this terrain – is an 18 x 10^6 km^2 volcanic plain on Mars located southwest of Arsia Mons, one of the Tharsis Montes

[*Plescia*, 2004; *Werner*, 2009; *Giacomini et al.*, 2012]. It too hosts very long lava flows (>200 km in some cases), with many believed to be sourced by activity related to Arsia Mons [*Scott and Tanaka*, 1981; *Giacomini et al.*, 2009, 2012; *Crown and Ramsey*, 2016]. Arsia Mons is approximately 460 x 320 km across and 12 km high and interpreted to be the oldest of the Tharsis Montes [*Plescia*, 2004; *Werner*, 2009]. Recent studies on Daedalia Planum have measured average thicknesses of 35 – 70 m for some lava flows using high resolution image and elevation data, observed inflation in lava flows using possible lava rises and tumuli, and attempted compositional analysis via spectral mapping [*Giacomini et al.*, 2009, 2012].

13. Methodology

13.1. Datasets & Analyses Criteria

We used image data from the Mars Reconnaissance Orbiter (MRO) Context Camera (CTX: ~5 m/pixel), [*Malin* et al., 2007], the Mars Odyssey Thermal Emission Imaging System in the infrared (THEMIS IR: 100 m/pixel), [*Christensen* et al., 2004], and the MRO High Resolution Imaging Science Experiment (HiRISE: ~0.5 m/pixel) instruments [*McEwan* et al., 2007]. We utilized topographic data from the Mars Global Surveyor (MGS) Mars Orbital Laser Altimeter (MOLA: ~463 m/pixel) digital elevation model (DEM) [*Zuber* et al., 1992] dataset, as well as Mars Express High-Resolution Stereo Camera (HRSC) DEM (DEM cell size: 50 – 75 m) [*Jaumann* et al., 2007]. While the region has extensive CTX and localized HiRISE coverage, high resolution HRSC DEMs did not cover the entire study area. As a result, some flows were characterized using the MOLA DEM [*Glaze et al.*, 2003]. Due to the resolution of the MOLA DEM, larger and thicker lava flows were given priority when HRSC DEM coverage was not available. This

prioritization could lead to bias toward reporting lava flow conditions capable of producing thicker flows. All datasets were accessed and analyzed using the Java Mission Planning and Remote Sensing (JMARS) GIS software.

For this study, we considered lava flows in the Tharsis Volcanic Province because of the large number of well-preserved flows and extensive overlapping datasets. We selected 40 lava flows based on the following criteria: 1) morphology and 2) data coverage. We prioritized flows with relatively unobstructed flow along their lengths and relatively well-defined margins. In all cases, the full extent of the original flow was not preserved due to superimposed lava flows, impact craters, or erosion/degradation. These processes reduced the available flow area for study and also resulted in the erasure of the flow source. As a result, our flow volumes and volumetric flow rates represent minima. We also prioritized lava flows with adequate data coverage. Every selected lava flow had CTX visible image coverage and at least partial HRSC and/or MOLA DEM coverage. Despite the ~1 m dust mantle that blankets the Tharsis Volcanic Province, lava flow surface texture is relatively well preserved and discernible [*Christensen,* 1986]. Compression ridges are visible on a number of lava flows, owing to the resilience of these features in the face of erosion, degradation, and dust cover. However, finer scale morphologies, such as pahoehoe lava lobes (which tend to be meter-scale features), if originally present, are not visible due to limited spatial resolution. Overall, the morphologies and morphometric properties of lava flows in the Tharsis Volcanic Province suggest a basalt to basaltic andesite composition [*Carr,* 1974; *Hulme,* 1974; *Bleacher et al.,* 2007; *Hiesinger et al.,* 2007]. We measured the length, mean width, mean height, surface area, and mean slope for each of the 40 lava flows in this study. The length of each flow was measured using a

centerline. The mean width and height of each flow were calculated using multiple cross-sectional profiles. We calculated the volume by multiplying surface area by mean height. These data are listed in Table 1. We applied the three models discussed above to the 40 lava flows in this study in order to estimate volumetric flow rates, bulk viscosities, and emplacement times. Each model and the methodology for each application is detailed in the following section.

13.2. Models for interpreting the datasets

13.2.1. *Cooling-limited and Rheologic Model*

We applied a standard rheologic treatment to 34 of 40 lava flows using methods outlined by *Hiesinger et al.* [2007], and references therein, to calculate the eruption rate and viscosity. We did not apply this model to 6 of 40 lava flows, which represent lava ridges observed on Olympus Mons, Ascraeus Mons, and in the lava flow plains, because those flows produced prominent ridges likely formed through repeated overspills from a channel or tube during emplacement. Although perhaps initially emplaced as channelized flows, the flow eventually roofed over and formed tubes which may or may not have operated at steady conditions. The stark difference in the emplacement mechanism of these ridges (e.g. lava tubes) renders the application of this approach inappropriate [*Sakimoto et al.*, 1997]. The method uses 1) the Graetz number (G_z), a dimensionless number that characterizes the ratio of the time scale of cooling by conduction at the edges or surface of the flow, to that of fluid advection downstream for laminar flow in a conduit; and 2) Jefferey's equation, which is a steady-state momentum equation reduced to a force balance between downslope gravitational forces which drive the flow and viscous forces which

impede the flow and can be expressed in terms of flow velocity and geometry, and fluid viscosity [*Jeffreys*, 1925; *Wilson and Head*, 1983].

Cooling exerts a strong control on lava flow emplacement and the Graetz number characterizes the temperature distribution across the flow and at any given point within a flow [*Pinkerton and Sparks*, 1976; *Hulme and Fielder*, 1977]. Initially derived to describe cooling fluid in a cylindrical pipe, the Graetz number can be applied to lava flows by assuming the surface of the lava flow exposed to ambient atmospheric conditions cools in the same way as the boundary of the fluid being cooled at pipe margins [*Pinkerton and Sparks*, 1976; *Hulme and Fielder*, 1977]. According to a suite of observations of cooling-limited lava flows at Mt. Etna, *Pinkerton and Sparks* [1976] found that they ceased advancing at Gz of approximately 300, when crust formation was sufficient to prevent the continued propagation of the small amount of melt remaining in the core of the flows.

Application of this approach requires some assumptions for the 34 lava flows we studied, consistent with previous investigations [*Hiesinger et al.* 2007; *Hauber et al*., 2011]. These assumptions include: laminar flow, due to the generally high and increasing viscosity of silicate lavas during emplacement; steady-state emplacement at low velocities; flow dimensions reflect rheological properties of the flow [*Wilson and Head*, 1983; *Hiesinger et al.*, 2007; *Hauber et al.*, 2011]; and that flow propagation halts at a Graetz number of 300 as in the observations of Pinkerton and Sparks [1976]. *Gues*t et al. [1987] questioned the value of 300 because Pinkerton and Sparks [1976] did not take into account branching of lava flows or the possibility of volume-limited flows. However, for cooling-limited flows, Guest et al. [1987] place the halting Graetz number at approximately 230, very close to the assumed value of 300. The Mars flows studied here exhibit limited to no

branching, and given their large volumes (see below), they were unlikely to have been volume-limited. We therefore assume that they were cooling-limited and proceed with a halting Graetz number value of 300.

The following equation is an expression for Graetz number,

$$G_z = Q/(\kappa x)\ (h/w) \qquad \text{(Eq. 1)}$$

where G_z is the Graetz number, Q is the effusion rate, κ is thermal diffusivity of the lava which is a function of its composition ($m^2\ s^{-1}$), x is flow length, w is mean flow width (Table 1), and h is mean flow height (Table 1) [*Wilson and Head*, 1983]. This equation is a modification from the Graetz number for pipe flow such that the aspect ratio w/h of the flow accounts for the fact that thinner flows cool faster than deeper flows [*Hulme and Fielder*, 1977]. Effusion rate Q was obtained by rearranging Eq. 1, assuming a halting Graetz number of 300, using the flow geometries measured from the previously described data sets, and applying the thermal diffusivity of basalt, $5.00 \times 10^{-7}\ m^2/s$ [*Wilson and Head*, 1983; *Hon et al.*, 1994; *Pasckert et al.*, 2012].

Jeffrey's equation – which assumes a Newtonian rheology – can be used to relate the effusion rate of a flow to its viscosity, density, and flow dimensions. It is derived for flow on an infinitely wide plane and is described as follows for broad flows [*Jeffreys*, 1925].

$$\eta = \rho g h^3 w \sin\alpha\ /3\mathrm{Q} \qquad \text{(Eq. 2)}$$

In this equation, η is the effective dynamic viscosity of the flow during emplacement and propagation, ρ is the lava density during emplacement, w and h are the flow dimensions as described previously, Q is volumetric effusion rate, α is the underlying slope, and 3 is a constant used for flows that are much wider than they are deep Our calculations utilized an *n* value of 3 because all of our flows are much wider than they are thick [*Jeffreys*, 1925]. As most flows have been truncated by other flows, impacts, and erosion/degradation, our area and volume estimates represent minima. We assumed a density of 2700 kg/m^3 which is consistent with estimates from previous studies and within the range of terrestrial basalt values [*Rowland et al.*, 2004; *Hiesinger et al.*, 2007; *Hauber et al.*, 2011; *Pasckert et al.*, 2012]. Q from Eq. 1, along with flow geometry, underlying slope, and magma density were used in Eq. 2 to calculate dynamic viscosity η. We used the calculated Q from Eq. 1 and individual flow volumes to calculate minimum emplacement times.

13.2.2. *Laboratory experiments and* Ψ

We classified each of the 40 observed lava flows by dominant surface morphology, which corresponds to a particular Ψ regime [*Fink and Griffiths,* 1990; *Gregg and Fink*, 1996]. Ψ is a powerful way of understanding the dynamics of flow emplacement using only flow morphology. Because it is a dimensionless parameter, Ψ can be applied to flows of any composition, rheology, and scale so long as reasonable emplacement constraints (e.g. ambient conditions or properties of the flowing liquid) can be assumed. Five flow morphologies corresponding to discreet Ψ ranges have been observed. Those morphologies from high to low, Ψ >55 to Ψ ~1, are: No Crust, Levees, Folds, Rifts, and Pillows (Fig. 1) [*Fink and Griffiths,* 1990, 1992; *Gregg and Fink,* 2000]. Transitional morphologies are also observed in the lab and on Mars, demonstrating that the

morphologies are produced on a continuum. And, as stated previously, the textures observed in the laboratory are observed in nature – from terrestrial felsic lava flows to sulfur flows [*Fink et al.*, 1983; *Pieri et al.*, 1984; *Griffiths and Fink*, 1992; *Gregg and Fink*, 1996].

In the analysis presented, we assumed that the predominant morphology observed represents the dominant Ψ regime at the time of emplacement (Fig. 1). This has been demonstrated in the laboratory to the extent possible [*Fink and Griffiths*, 1990, 1992; *Gregg and Fink*, 2000]. And, despite the possibility that flows pass through a number of morphological regimes during the emplacement process (e.g., Chapter 2, this thesis), the final morphology preserved in the rock record is the only source of data we have for the surface of Mars. We proceed with this caveat in mind, and thus assume that our calculations based on Ψ regime best represent the final stages of flow emplacement when the flow exhibited the last morphology before ceasing due to extensive cooling. Furthermore, because Ψ morphologies observed in the laboratory occur on a continuum, each flow was assigned a Ψ value range corresponding to the observed morphology. Some transitional morphologies (i.e. levee-fold) were observed, while no pillow morphologies were definitively observed. We interpreted the lava ridges, previously observed on Olympus Mons, Alba Mons, and other localities, and interpreted as lava tubes by [*Sakimoto et al.*, 1997; *Bleacher et al., 2007*], to represent rift morphology. This interpretation is based on laboratory analogue experiments using PEG wax performed on slopes, which yielded ridge-like structures produced by lava tubes [see Chapter 3].

Ψ can be written in terms of a modified Peclet number, Π, crustal cooling timescale, τ_s, and differences among the ambient, solidification, and liquid temperatures, θ_s [Fink and Griffiths 1990, Eq. 10].

$$\Psi = \Pi\tau_s(\theta_s) \quad \text{(Eq. 3)}$$

Π, like a traditional Peclet number (Pe), is a ratio of characteristic velocity in the flow propagation direction and characteristic thermal diffusion rate at the surface of the flow, and can be written as a function of the Peclet number, gravity, viscosity, and thermal diffusivity [Fink and Griffiths, 1990, Eq. 11]. This expression is given as

$$\Pi = \left(\frac{g'}{\nu}\right)^{\frac{2}{3}} \kappa^{\frac{1}{3}}\lambda Pe^{\frac{1}{3}} \quad \text{(Eq. 4)}$$

Where g' is a reduced gravity (difference in wax and ambient densities divided by wax density), ν is the kinematic viscosity of the wax, κ is the thermal diffusivity of the wax, and λis a timescale of wax cooling during propagation.

Ψ can also be written as a ratio of the solidification and advection time scales, which is more descriptive when observing and describing qualitative morphology of flows.

$$\Psi = \frac{t_s}{t_a} \quad \text{(Eq. 5)}$$

Here, t_s represents the timescale of solidification of the surface crust and t_a represents the timescale of horizontal advection. Using the relationships in Equation 3, we can calculate a range of effusion rates corresponding to the Ψ ranges for each flow morphology of assumed Mars eruption and ambient conditions. From those effusion rates and measured flow volumes, we can also calculate a range of emplacement times for each flow.

However, in order to translate the Ψ ranges to eruption rates, we are required to make simplifying assumptions about the ambient environment and the erupted liquid. In the lab, the ambient environment corresponds to the chilled bath or a sucrose solution and the erupted liquid refers to the PEG wax. For Mars, these values correspond to the ambient environment of the Martian surface and the lava flow. We also assumed that radiation is the primary way a lava flow loses heat on Mars based on previous work, which found that radiant heat loss is an order of magnitude greater than that for convection or conduction [*Griffiths and Fink,* 1992; *Gregg and Fink,* 1996; *Rowland et al.,* 2004; *Garry et al.,* 2006]. As a result, convective and conductive losses are considered to be negligible. In addition to the flow properties mentioned previously (i.e. density, thermal diffusivity), we assumed an ambient environment temperature of 210 K, an atmospheric density of 0.02 kg/m^3, a solidification temperature of 900˚C, and gravity of 3.71 m^3/s [*Peck,* 1978; *Rowland et al.,* 2004]. The ambient environment temperature, atmospheric density, and gravity represent the average values for Mars [*Rowland et al.,* 2004]. For values related to the Martian atmosphere, specifically kinematic viscosity, we assumed pure CO_2 [*Chemical Rubber Company*, 1984; *Crane Company*, 1988]. The basalt solidus is cited as 980˚C; however, the internal temperature of barely mobile basalt flows has been measured at temperatures as low as 800˚C and basalt flows on Mt Etna have been typically modeled with

solidification temperatures of ~870 ˚C [*Peck*, 1978; *Pinkerton et al.*, 2002; *Vicari et al.*, 2007; *Belousov et al.*, 2015]. The solidification temperature is complicated by the melt composition, which contains multiple minerals that crystallize across a range of temperatures [*Peck*, 1978]. We find a value of 900˚ C reasonable and within the range of previous studies. Terrestrial basalts typically erupt between 1100 – 1250˚C [*Pinkerton*, 1987; *Pinkerton et al.*, 2002; *Harris and Rowland*, 2015]. We assumed the lava flows in our study erupted at 1150˚C, which is similar to the erupted temperature of basalts at Hawaiian volcanoes and Mt. Etna [*Harris and Rowland*, 2001; *Vicari et al*., 2007]. These values are further explored later in the discussion, where a range of each is considered along with the sensitivity of results to that range.

13.2.3. Self-replicating lava flow model

Many of the lava flows observed in the major Martian volcanic provinces of Tharsis and Elysium display a similar repetitive morphology. These lava flows have morphologic characteristics that repeat over the length of the flow, have relatively constant channel and levee dimensions, and have a single channel that is visible for most of its length (Fig. 3). As a result of these consistent dimensions that produce a repeated morphology, *Baloga and Glaze* [2008] termed these lava flows "self-replicating lava flows" and developed a model that takes into account the removal of mass from the active molten lava flow that is deposited into the formation of levees at the flow front as it propagates. The model assumes that levees are created at the flow front due to a vertical parabolic velocity profile in which the top of the flow is traveling downslope faster than its base (Fig. 4) [*Glaze and Baloga*, 2006; *Baloga and Glaze*, 2008]. The mass flux that enters the levees is calculated as a product of the excess flow velocity, (Q_{ex}), at the top of the flow and the, nondeformable

crust atop the flow [*Baloga and Glaze*, 2008, Eq. 10]. The excess mass is then left behind as the flow front advances at the average downstream velocity of the molten core (u_c). In addition, the model takes into account the formation of a surface crust and assumes that the molten core behaves as a Newtonian fluid. Only a subset of lava flows in this study – 13 of 40 – met the criteria of self-replicating flows.

Using methods outlined in *Baloga and Glaze* [2008] and references therein, which include measuring levee and channel dimensions and assuming the conductive cooling law used by *Hon et al*. [1994], we calculated eruption rates (Q_{ex}) and the resultant viscosities and emplacement times for 13 lava flows across the Tharsis Volcanic Province. To do so, we first calculated the levee widths (w_l) according to the following:

$$wl = \frac{Q_{ex}}{u_c * h_l} \quad \text{(Eq. 6)}$$

where h_l is the levee thickness. The crust thickness is assumed to be the difference in thickness between the total flow and the liquid core (h_c). The total flow thickness is approximated by the height of the levees, such that the crust thickness is $h_l - h_c$. This crust thickness was found as a function of distance downstream and the data was smoothed as in Baloga and Glaze (2008) [*Baloga and Glaze*, 2008 Eqs. 12 & 13, Figure 8]. A cooling time for the crust to form was calculated using solidification by radiant cooling following [*Hon et al.*, 1994]. The emplacement duration of the flow was assumed to be the same time required for crustal growth. Average effusion rate was calculated for each flow using its total volume and the emplacement time.

2.2.4 Yield strength calculation

Our use of Eqs. 1 and 2 above assume Newtonian behavior, thus producing a viscosity from Jeffrey's equation (Eq.2). However, many suggest that most lavas, especially those cooling during emplacement, behave more as a Bingham fluid. For example, yield strengths for the Earth, Moon, and Mars have been predicted by *Moore* et al. [1978]. In order to explore this rheology further, we estimate the yield strength (τ) of each flow using underlying slope (α), flow thickness (h), and an assumed lava density of 2700 kg m^{-3} (following the procedure of *Heisinger* et al. 2007 and references therein).

$$\tau = \rho g \sin(\alpha) h \quad \text{(Eq. 7)}$$

14. Results

14.1. Classification of Qualitative Flow Morphologies

14.1.1. Channelized flows – high Ψ

Channelized lava flows – a common feature of high-volume eruptions – are widely observed in the plains and shield volcanos of the Tharsis volcanic province [*Carr,* 1973, 1974; *Greeley and Spudis,* 1981; *Baloga and Glaze,* 2008]. These flows are characterized by clearly defined (usually wide) channels and levees (Fig. 4). The sources of these flows are obscured by the superposition of later flows and the termination of the flow is marked by a reduction of channel visibility and the fanning out of the flow into a smooth, featureless flow surface. Of the 40 lava flows in this study, 27 are considered channelized flows. Several of these flows display the self-replicating morphology described in *Baloga and Glaze* [2008]. Channelized lava flows are particularly common on Olympus Mons,

the Tharsis Montes, Alba Mons and in the volcanic plains including Daedalia Planum. Channelized lava flows on central volcanoes tend to be smaller in length and width than those in the volcanic plains, and appear to correspond to the high Ψ regime and, in the lab, are produced on slopes >5˚ or on shallower slopes at high eruption rates [*Peiterson and Crown*, 1999; *Gregg and Fink*, 2000; *Garry et al.*, 2006; chapters 2 & 3, this thesis].

14.1.2. Corrugated (folded) flows – intermediate Ψ

Corrugated flows – which are analogous to the fold morphology observed in PEG wax experiments performed in the laboratory – are a variation of channelized flows [*Fink and Griffiths*, 1990, 1992; *Gregg and Fink*, 2000; chapters 2 & 3, this thesis]. Typically, these flows display a broad, open channel and clearly defined levees. However, the inside of the channel and terminus of the flow is characterized by a corrugated surface texture (Fig. 5). This corrugated or folded texture is interpreted as the physical manifestation of compression ridges on the surface crust. This texture has also been observed on submarine and subaerial terrestrial flows. In this study, these flows are observed on Olympus Mons and in the volcanic plains surrounding Ascraeus Mons. Of the 40 lava flows observed in this study, five display this morphology. Of those five, four display a transitional morphology between channelized and corrugated flows. The same behavior has been observed in the laboratory and, in those cases, Ψ value ranges corresponding to transitional morphologies were assigned [*Fink and Griffiths*, 1990, 1992; *Gregg and Fink*, 2000].

14.1.3. Smooth flows – very high or low Ψ morphology

Many lava flows on Mars display a smooth, featureless texture that some believe represent sheet flows emplaced by high eruption rates and/or low viscosity lavas, although some of these flows might instead represent inflated pahoehoe flows [*Hon et al.*, 1994;

Bleacher et al., 2017]. In our study, we avoided smooth lava flows due to an inability to distinguish between those flows which might represent wholesale emplacement at high eruption rates and those which might have been emplaced as pahoehoe flow fields that have undergone inflation. Nonetheless, some of the flows in our study, found in the volcanic plains, display smooth textures along certain lengths of the flow. In these instances, a long-channelized portion of the flow is also observed, and we therefore interpret these flows as transitional between channelized and sheet flows. This morphology corresponds to high / very high Ψ values. Two of the flows in this study have segments with a smooth surface morphology and the morphology of these flows is treated as transitional between channelized and smooth.

14.1.4. Lava ridge flows – low Ψ on slopes

Lava ridges have been observed on and around central volcanoes, specifically Alba Mons, Olympus Mons, and in the fan associated with Ascraeus Mons [*Sakimoto et al.*, 1997; *Bleacher et al., 2007*]. These features have been interpreted as tube-fed flows, or lava tubes. Lava ridges generally produce a broad triangular shaped feature in longitudinal profile. Skylights are observed on some of the ridges, where portions of the roof have collapsed into the void space below. We interpret the tube-fed flows as being associated with low Ψ values, since analogue features have been reproduced in the lab on a slope only at low Ψ values. Six of the 40 studied flows are classified as lava ridges.

14.2. Flow geometries

We measured the dimensions – length, width, and thickness – of 40 lava flows in the Tharsis volcanic province on Mars. From these flow dimensions, we calculated flow volumes. Flows occurred in three subregions: on central volcanoes (i.e. Olympus Mons

and Ascraeus Mons), in close proximity of central volcanoes (i.e. Olympus Mons and Ascraeus Mons), and in the volcanic plains of Tharsis. The 40 lava flows ranged in length from ~15 – 314 km. The longest flows occurred in the volcanic plains. Mean flow widths ranged from ~0.5 – 29 km, with the narrowest flows occurring on Olympus Mons. Flow thicknesses ranged from ~11 – 91 m. Flow areas and volumes ranged from ~14 – 11,180 km^2 and ~1 – 430 km^3, respectively. The smallest flows in areal extent and volume are observed on Olympus Mons and Ascraeus Mons, while the largest flows occur in the volcanic plains of Tharsis surrounding the Tharsis Montes and Daedalia Planum. The lava flows were emplaced on slopes ~0.3 – 6.6˚, with the steepest slopes occurring on the flanks of Olympus Mons. Slopes in the volcanic plains typically ranged from ~0.3 – 1˚.

14.3. Rheological analyses

For 34 of 40 lava flows in Tharsis investigated in this study, using methods outlined in *Hiesinger et al.* [2007] and described above, we estimated the effusion rate using Eq. 1. Emplacement times were calculated by dividing the total flow volumes (Table 1) by the calculated effusion rate, which represents the average rate of flow emplacement. Effective emplacement viscosity was then estimated by substituting these effusion rates and measured geometries into Jeffrey's equation (Eq. 2). And, although this method of calculating effusion rates and viscosities treats the lava flows as Newtonian fluids [*Hiesinger et al.*, 2007], we also calculate the yield strength of the lava flows, treating them as Bingham fluids (Eq. 4) [Moore 1978; *Wilson and Head*, 1983].

The 34 flow lengths range in mean thickness from ~11 – 55 m, mean widths ~0.5 – 29 km, and calculated volumes range from ~1 – 430 km^3 (Table 1). Although not considered in this analysis, the calculated volumes for the six lava ridges also fall within

this range. Volumetric flow rates, or effusion rates, for the 34 lava flows ranged from 3 x 10^2 – ~3.5 x 10^4 m^3/s (Fig. 6 and 7; Table 2). Higher effusion rates were estimated for the intervolcanic plains and Daedalia Planum, while lower effusion rates were estimated for flows on Olympus Mons. We calculated effective flow viscosities of ~ 10^5 – 10^8 Pa s and yield strengths of ~800 – 3 x 10^4 Pa. Viscosities and yield strengths were highest for flows observed on Olympus Mons and lowest for those in the volcanic plains. Modeled emplacement times for the lava flows ranged from 9 days to ~1 year.

14.4. Application of Ψ

We used assigned Ψ to calculate eruption rates and emplacement times for all 40 lava flows (Figure 6). Assuming a solidification temperature of 900˚C and an eruption temperature of 1150˚C, calculated effusion rates using Eqs. 3–5 ranged from 0.2 – 6500 m^3/s (Table 3). However, each Ψ regime had a specific range of effusion rates. The following are effusion rates for each morphology observed: smooth-levee flows (~6500 m^3/s); levee flows (950 – 6500 m^3/s); levee-fold flows (575 – 950 m^3/s); folded flows (35 – 575 m^3/s); rift, or tube-fed, flows (0.2 – 20 m^3/s). The kinematic viscosity was an input instead of an output in this model, but we used a value of ~10^2 Pa s [*Nichols*, 1939; *Hon et al.*, 1994;]. Yield strengths are not an output of Ψ and were not calculated. Emplacement times range from ~2 days–2200 years. The largest emplacement times (180 – 2200 years) were exclusively for the tube-fed flows and were calculated using the lowest effusion rate of the range – 0.2 m^3/s. If the tube-fed flows are removed, the emplacement times range from ~2 days – 9.5 years.

14.5. Self-replicating lava flow model

We utilized the self-replication model as outlined by *Baloga and Glaze* [2008] on a subset of lava flows (i.e. 13 of 40) in Tharsis to calculate effusion rates and emplacement times as described above in the Methods section. As stated previously, effusion rates were calculated by removing the levee volume from the flow dimensions and assuming a Newtonian rheology for the molten lava core in the channel. Viscosities were then calculated by treating the lava as a Newtonian fluid and using Jeffrey's equation again (Eq. 2). Yield strengths were calculated by treating the flow as a Bingham fluid (Eq. 4). Using this model, we calculated effusion rates of ~30 – ~1200 m^3/s (Figures 6–7; Table 4). Eruption rates were highest for lava flows observed in the volcanic plains. Viscosities ranged from 4.5×10^6 – ~3×10^7 Pa s and yield strengths ranged from ~10^3 Pa – 3.6×10^4 Pa. No appreciable difference – given the sample size – was observed between the Tharsis subregions. The time of emplacement for these flows ranges from 4.5 months – 9 years. No dependence of emplacement time on subregion was observed.

5.5 Summary

While there is some overlap of calculated volumes, eruption rates, viscosities, yield strengths, and emplacement times with terrestrial values, some of the calculated values are much larger for Mars in many cases. The measured flow lengths, mean widths, and mean thicknesses for 40 lava flows on Mars were ~15 – 314 km, ~0.5 – 29 km, and ~11 – 91 m, respectively. Calculated flow volumes ranged from ~1 to 430 km^3. Volumetrically smaller flows were observed on Olympus Mons and in the flow fields associated with Ascraeus Mons, while the largest volumes were calculated for flows in Daedalia Planum and the

volcanic plains around the Tharsis Montes. Depending on the applied model, the eruption rates – and subsequent emplacement times – can vary by orders of magnitude.

Using a standard rheologic approach, which utilizes the Graetz number and Jeffrey's equation, on 34 of 40 applicable lava flows, we calculated effusion rates, viscosities, and yield strengths of 300 – ~3.5 x 10^4 m^3/s, ~10^5 – 10^8 Pa s, ~800 – 3 x 10^4 Pa, respectively. Emplacement times ranged from 9 days – ~1 year. The highest eruption rates occurred in Daedalia Planum and the Tharsis plains, while lower values were observed on Olympus Mons.

All 40 lava flows were assigned a Ψ based on flow morphology. Because a given Ψ represents a range in conditions, the eruption rates and emplacement times are also a range of values. We calculated eruption rates and emplacement times of ~0.2 – 6.5 x10^3 m^3/s and ~2 days – 2.2 x 10^3 years, respectively.

The self-replication model for long lava flows takes into mass loss to levee construction thereby further constraining flow emplacement conditions [*Baloga and Glaze*, 2008]. For the 13 lava flows considered for this model, relative to the previous methods, we calculated a lower range of eruption rates (~30 – ~1.2 x 10^3 m^3/s); comparable viscosities (4.5 x 10^6 – ~3 x 10^7 Pa s); comparable yield strengths (10^3 Pa – 3.6 x 10^4 Pa); and similar emplacement times (4.5 months – 9 years). Although these flows represent ~33% of the flows in this study, we find similar trends of higher calculated eruption rates in the Tharsis plains and lower values elsewhere.

15. Discussion and Implications

15.1. Martian volcanism

15.1.1. Volumes, eruption rates and distribution of lava flows

Martian volcanism has decreased in spatial extent and frequency. According to a number of studies that have used crater counts, geomorphology, and modelling, the bulk of Martian volcanism occurred >3 Ga during the Noachian and Early Hesperian [e.g. *Plescia*, 2004; *Werner*, 2009; *Tanaka et al.*, 2014]. Early volcanic activity consisted of plains-style volcanism, possible explosive eruptions, and the construction of the large shields [*Carr*, 1973, 1974; *Plescia*, 2004]. Subsequent observations have also suggested that the volume of volcanism has decreased with time [*Xiao et al*., 2012]. As Mars has cooled, the number of volcanoes erupting and the volumes of erupted magma have decreased [*Greeley and Spudis*, 1981; *Bleacher et al.*, 2007; *Werner*, 2009]. The flows in our study are among the most recent examples of effusive volcanism in the Tharsis Volcanic Province and on Mars. Studies by *Tanaka et al*. [2014] and *Werner* [2009] suggests these flows were emplaced in the Late Amazonian and range in age from 10s – 100s of millions of years old. There is some variability among sub-regions within Tharsis. The flows on the flanks of Olympus Mons are ~500 – 700 Ma, with localized areas < 50 Ma [*Neukum et al.*, 2004]. The volumes of eruptions are also less on Olympus Mons relative to the volcanic plains [*Bleacher et al.*, 2007; this study].

Figure 7a shows the volume of our flows in km^3 vs. area covered in km^2. In terms of volume and corresponding area, flows on the central volcanoes of Ascreaus Mons (AM) and Olympus Mons (OM) (stars) are distinct from and smaller than flows associated with

plains volcanism (squares). A similar relationship can be seen in Figure 8b where lava flow length (km) is shown as a function of total volume.

In Figure 7a, we also compare the Mars flows to well-documented terrestrial flows. We first note that in terms of volume / area, the Mars flows follow the same trend as terrestrial flows and sit directly between Hawaiian flows (Puu Oo, 1983-84, Wolfe et al. 1987) and flows from the Columbia River Basalts (CRB) (Self et al. 1997). Further, the OM and AM flows sit close to the Puu Oo flows whereas the plains flows extend over a greater range, reaching but not overlapping with the CRB flows. We also note that the plains flows are longer than flows erupted from central vents (Fig. 7b).

In Figure 8c, we note that the relationship between volume and length follows a power law for both terrestrial and Mars flows. The terrestrial flows follow a relationship with a power-law exponent of roughly 0.5. According to Malin [1980] a power-law exponent of 0.33 would indicate that flow length, width, and depth are equally controlled (and proportional to) the volume erupted, whereas an exponent of 1 would indicate that the cross-sectional area of the flow does not vary with volume, and thus only the length is controlled by volume. Malin [1980] interprets the exponent of 0.5 to indicate that both the length and cross-sectional area (depth, width) of the flows are controlled by the volume, but that volume has a slightly greater control on length than on cross-sectional area. The Mars flows appear to have a similar exponent (0.4) indicating that in these flows the cross-sectional area and length are controlled by total volume, with nearly equal sensitivity.

Our effusion rates calculated above support the interpretation that differences in eruption rate play some part in differentiating the subregions (Figure 8a), with the highest rates estimated for the plains regions and the lowest values estimated for AM and OM. The

application of the halting Graetz number (Gz = 300) and the self-replicating model of Glaze and Baloga [2006] produce Q results for AM and OM that match well to terrestrial values (Fig. 8b). Q values for the plains regions on Mars exceed many Hawaiian and Etna eruption rates but are consistent with some of the highest eruption rates measured at the Puu Oo vent [1983-84, *Wolfe et al*., 1987] and Mauna Loa [1984, *Lipman and Banks*, 1987]. Lower eruption rates are estimated when flow morphology and mass allocation to levees are taken into account in the self-replicating model [*Glaze and Baloga*, 2006; *Baloga and Glaze*, 2008]. Overall, our results are consistent with other studies [*Hiesinger et al*., 2007; *Baloga and Glaze*, 2008; *Hauber et al.*, 2011]. For example, our calculated eruption rates for the 25 young flows observed by Hiesinger et al. [2007] are ~23 - ~404 m^3/s. These values fall within range of those calculated in our study using all three models. The values for tube-fed flows in our study (0.2 – 20 m^3/s) falls at the very low end of the range proposed by *Sakimoto et al.* [1997] of $2 – 10^5$ m^3/s. Despite the long runouts of lava flows in the Tharsis region of Mars, the necessity for unrealistically high effusion rates or exotic lavas to explain them is no longer valid.

The flows on Olympus Mons are smaller in size than those observed in the volcanic plains of Tharsis and tend to be open channel flows, which may suggest short-lived volume-limited eruptions [*Bleacher et al.*, 2007]. The flows in the volcanic plains are larger in areal extent than flows observed on Olympus Mons or the Tharsis Montes. The variability in flow volume by subregion suggests different eruption conditions, specifically differences in subsurface pathways and magma sources. The volumetrically larger flows were likely erupted to the surface by large dikes and remaining active for long periods of time (Fig. 9) [*Wilson and Head*, 1983]. Meanwhile, the flows on Olympus Mons and

proximal to Ascraeus Mons were likely emplaced by smaller subsurface conduits that were active for shorter periods of time [*Bleacher et al.*, 2007; *Wilson and Head*, 1983]. We also note that the Mars flows, given the measured volumes and calculated values of Q, must have been active much longer than typical terrestrial flows from places like Hawaii, but may rather be more akin to regions like the CRB which are thought to have been active over long periods to generate voluminous fields; this is particularly likely for the Mars plains volcanism characterized here.

To further put the scale of the flows from this study into context, and potential implications, their volumes and flow areas are compared to typical terrestrial lava flows, as well as other well-documented eruptions (Figure 7). For comparison, one of the largest flows (Flow 3) represents about one tenth of the volume of magma erupted in the last Yellowstone super eruption, approximately the same volume as the last eruption of the Valles caldera (NM), and about $1/30^{th}$ of the entire Deccan Traps [*Sheth*, 2006]. In short, the individual volumes are significant and remarkable. These data and subsequent analysis here (Figures 7, 8, 9) support the notion that the volume of erupted material represents a more important control on their reach than effusion rate. These significant volumes suggest large conduits (i.e. dikes and sills) in the Martian subsurface capable of erupting such large volumes, which is in agreement with previous observations [*Carr*, 1973; *Wilson and Head*, 1983]. It is worth noting that the Mars volumes, erupted during any single event, appear to bear greater resemblance to volcanism at (young) hot spots on Earth, than to any other setting.

15.1.2. Lava composition

Earlier studies of Martian volcanism invoked ultramafic and other exotic compositions to explain the large, voluminous effusive eruptions preserved across the surface of the planet [*Cashman et al.*, 1998]. While the ranges differ depending on the model, the viscosities of $10^3 – 10^7$ Pa s calculated in this study are consistent with a basalt to basaltic andesite composition. These viscosities are similar to those calculated for 25 young lava flows observed on the eastern flank of Ascraues Mons (10^4-10^7 Pa-s) by *Hiesinger* et al. [2007] and the 8 lava flows observed in the volcanic plains of Tharsis (10^2-10^3 Pa-s) by *Hauber* et al. [2011]. The rheologic model results in slightly lower calculated viscosities, due to the estimate of effusion rate (Q) which could be an order of magnitude higher than reality because it assumes the entire flow front is active during the time of emplacement. Jeffrey's equation is particularly sensitive to the flow height. The flow heights measured in our study are taken to be the maximum heights, assuming erosion and gradation has not significantly altered the flow, as it is likely that much of the flow during emplacement operated below this height. The self-replication model produces viscosity values of $10^6 – 10^7$ Pa s that are at the higher range of basalt and more congruent with basaltic andesite. Baloga and Glaze [2008] obtained a value of 10^6 Pa-s for a very long lava flow which is the same flow as our Flow 2. We obtained a value of ~10^7 Pa-s. The difference is likely due to the flow length analyzed for Flow 2. Whereas Baloga and Glaze [2008] performed analysis on 173 km of flow length for Flow 2, whereas we analyzed 313 km of the same flow. Our range of viscosities using the self-replication model are consistent with the range of values calculated by *Hiesinger et al.* [2007].

15.1.3. Planetary evolution & interior

Martian volcanism, although widespread early in its history, has become more localized with time. The most recent episodes of volcanism have occurred near the Elysium Mons volcanic province around Cerberus Fossae and the Tharsis Volcanic Province [*Neukum et al.*, 2004; *Werner*, 2009]. The effusion rates and viscosities of recent eruptions (~10s – 100s Ma) suggest that the Martian interior has produced eruptions on par with those on Earth and has erupted less evolved magmas – despite millions of years of quiescence between eruptions. It also suggests that the Martian interior may be relatively warm and capable of producing volcanic eruptions in the present day. The sheer volume of the erupted flows implies a large supply of eruptible magma at depth had a pathway to the surface over long periods of time, particularly in the volcanic plains. Emplacement times of hours to centuries suggest that some of these subsurface conduits remained open for extended periods of time. Given the volumes calculated in this study, these pathways would have been linked to sizeable magma bodies. The observation of relatively young low shields in the volcanic plains of Tharsis (<100 Ma) might hint at a larger magma body, perhaps related to the proposed plume beneath Tharsis [*Carr*, 1973; *Hauber et al.*, 2011].

The prolonged contribution of effusive volcanism to climate has been a subject of open speculation for terrestrial and extraterrestrial systems [Figure 10; *Black and Manga*, 2016; Rader *et al.*, 2017]. At a minimum, the eruptions represented by the lava flows in our study lasted for hours to centuries and the masses are on the order of very large terrestrial eruptions. However, the masses calculated in our study are less than that for terrestrial large igneous provinces and other eruptions that had significant global impacts. While large igneous provinces typically erupt over millions of years on Earth, the Tharsis

volcanic province has produced volcanic eruptions over billions of years [*Sheth*, 2006; *Werner*, 2009; *Tanaka et al.*, 2014]. Whether or not those eruptions were continuous or volumetrically significant enough to impact the atmosphere remains an open question, although some studies have suggested millions to tens of millions of years in repose times for eruptions at the Tharsis Montes and Olympus Mons [*Werner*, 2009]. That said, the erupted mass of the flows in our study are on the order of large terrestrial eruptions that caused short term changes to the global climate.

16. Conclusions

By modelling the emplacement of 40 lava flows in the Tharsis Volcanic Province on Mars, our study has produced volumes, effusion rates, viscosities, and emplacement times that have implications for recent volcanism on Mars, lava composition, and the plumbing of the Martian subsurface. Mars – a world whose surface has been dominated by volcanism – is interpreted to have a decreasing volcanic output since its formation due to a cooling interior. Calculated volumes for the 40 lava flows range from ~1 – 430 km^3. We applied three models in order to constrain eruption conditions at the time of flow emplacement. Using the Graetz number and Jeffrey's equation, we calculated effusion rates (300 – ~3.5 x 10^4 m^3/s), viscosities (~ 10^5 – 10^8 Pa s), yield strengths (~800 – 3 x 10^4 Pa), and emplacement times (9 days - ~1 year) for 34 of 40 lava flows. Applying Ψ – a dimensionless parameter derived from analogous laboratory experiments – yields effusion rates (~0.2 – 6500 m^3/s) and emplacement times (~2 days – 2.2 x 10^3 years) for all 40 lava flows. We applied the self-replication model for long lava flows proposed by *Baloga and Glaze*d [2008] to a smaller subset of lava flows (*n*=13) and calculated effusion rates (~30 – 1200 m^3/s), yield strengths (~10^3 Pa – 3.6 x 10^4 Pa), viscosities (4.5 x 10^6 – ~3 x 10^7 Pa

s), and emplacement times (~4.5 months – 9 years). There is overlap between the values calculated for each model and between the calculated model values and terrestrial values. Additionally, sub-regional differences in flow volumes across the Tharsis volcanic province suggest different magma sources and subsurface plumbing conditions for central volcanoes and lava plains. Drawing from these data, we conclude the following:

1. Martian lava flows do not require extremely high volumetric flow rates or exotic lava compositions. Observed lava flows can be produced by terrestrial volumetric flow rates and non-exotic lava compositions with viscosities and yield strengths suggestive of basalt and basaltic andesite compositions.

2. The Martian interior – possibly the shallow crust – was capable of erupting melts for at least months to years to produce individual lava flows of remarkable length and volume. Additionally, if the ages of the flows are accurate, magma was being stored and transported throughout the Martian crust from the mantle within the last 1 Ga – and as recent as ~100 Ma during the Late Amazonian.

3. Olympus Mons has produced volumetrically smaller recent eruptions than the sources of lava flows in the volcanic plains. This suggests smaller dikes and possibly a smaller, secondary magma source within Olympus Mons. The volcanic plains may be fed directly through a thinner overlying crust by a more abundant source related to a mantle plume or an early plume head.

4. Lava flow surface morphology provides fundamental information on flow characteristics without morphometric data, which allows volumetric flow rates and eruption conditions to be estimated for places with limited data coverage.

SUMMARY OF FINDINGS AND FUTURE STEPS

The following section represents the main conclusions reached in this body work regarding the emplacement of lava flows, specifically how unsteady eruption rates affect modes of emplacement that impact lava flow propagation and the eruption rates and rheology of lava flows on Mars. In addition, the scope of the work and future directions is discussed. In chapter II, I have demonstrated that unsteady eruption rates – increasing and/or decreasing the eruption rate for a duration of time – affects resurfacing, inflation, tube formation, and marginal breakouts. The following are main results from chapter II:

- The formation and sustainability of a coherent, insulating crust determines whether or not resurfacing, inflation, and tube formation will occur, fundamentally determining how the lava flow appropriates its own mass during emplacement. The crust also mitigates the impact of fluctuating eruption rates.
- Increasing eruption rates at the vent disrupt the crust promoting marginal breakouts, resurfacing, and sheet flows. A strong crust mitigates this effect.
- Decreasing eruption rates preserve the crust and allows for the crust to spread and thicken. These conditions favor inflation and tube formation as the wax beneath the crust forms discreet pathways while propagating to the flow front.
- The crust determines the degree of mass appropriated to surficial (resurfacing) and marginal breakouts. A stronger crust inhibits the severity of breakouts.
- Inflation occurs when an extensive, coherent crust is present. While favored at low and intermediate eruption rates, inflation can occur or survive increased eruption rates when a strong crust is present.

Many probabilistic models assume location for generation of a new lava lobe depends primarily on slope. However, our work suggests that generation of a new lava lobe also depends on the variability of the eruption rate at the vent and the coherence of the crust. As a result, lava flows on shallow slopes may not propagate in a purely stochastic manner, but instead may demonstrate some general behavior tied to conditions at the vent.

For chapter III, we investigated the distribution of mass within an active flow when unsteady vent conditions and slope occur and are combined. The following findings are a result of this study.

- Although slope is important to flow direction and propagation, unsteady vent conditions and the presence of a coherent crust impact emplacement modes which affect flow morphology and propagation. Slope promotes mass movement in the downhill direction and inhibits lateral spread of the flow, especially at steeper slopes. However, unsteady effusion rates and the flow crust can impact how and when that mass moves downslope.
- Slope impacted the manifestation of emplacement modes, resulting in varieties of emplacement modes not observed in experiments performed on no slopes. Resurfacing manifested as overspilling onto levees and wholesale re-pavement of previous flow surfaces from the vent. Tubes formed via processes observed in nature, such as the roofing over of open channels and as propagation of toes with rapidly solidifying crust similar to that observed in pahoehoe flow fields.
- Inflation was inhibited by increasing slope as excess mass was preferentially moved downhill. Only ¼ of flows experienced inflation relative to the ¾ of flows that

experienced inflation when no slope was present. Deflated flows were also observed in some runs.

- Marginal breakouts were inhibited by slope, except at very low Ψ. Although slope reduced the likelihood of breakouts away from the active flow front, at very low Ψ the presence of a strong, coherent crust acted to slow propagation down slope and allow for the concentration of molten wax under the crust. This increased the likelihood of marginal breakouts.
- Models should incorporate unsteady vent conditions, if possible, and account for more dynamic emplacement processes. Our results suggest that slope remains an important variable in flow propagation especially at steeper slopes. Nevertheless, unsteady vent conditions play a large role in how lava flows are emplaced. Additionally, unsteady vent conditions affect when conditions are favorable for certain emplacement modes to occur. As a result, at shallower slopes other processes such as resurfacing or inflation become important to flow emplacement.

Unsteady vent conditions have a large impact on how lava flows distribute mass. The distribution of mass determines the propagation speed of the flow, flow height, and flow area. Under certain conditions, flow propagation may be inhibited. The addition of slope provides a preferential flow direction which acts to funnel material downhill. Slopes impact flow dimensions, propagation speeds, and emplacement modes. Incorporating the findings of laboratory analogue experiments into numerical models will result in a more accurate and realistic simulation of lava flow emplacement. These models will serve to enhance our understanding of lava flow dynamics and assist with hazards prevention and the allocation of resources.

In Chapter IV, I calculated lava flow areas, volumes, effusion rates, viscosities, and emplacement times that have implications for recent volcanism on Mars, lava composition, and the plumbing of the Martian subsurface. The main points of this research are as follows:

- Martian lava flows do not require extremely high volumetric flow rates or exotic lava compositions. Observed lava flows can be produced by terrestrial volumetric flow rates and non-exotic lava compositions with viscosities and yield strengths suggestive of basalt and basaltic andesite compositions.
- The Martian interior – possibly the shallow crust – was capable of erupting melts for at least months to years to produce individual lava flows of remarkable length and volume.
- Eruption fluxes vary between central volcanoes and volcanic plains suggesting different sources.
- Lava flow surface morphology provides fundamental information on flow characteristics without morphometric data, which allows volumetric flow rates and eruption conditions to be estimated for places with limited data coverage.

Using more complex models that account for more physical processes during the emplacement of lava flows provides a more accurate description of natural processes. Combined with laboratory analogue experiments which account for phenomenology, they represent a useful tool for estimating eruptive conditions.

Lava flows represent one of the primary volcanic hazards to property and life. Predicting the propagation of lava flows is complicated by the complex interaction of internal flow factors, which includes unsteady eruption rates at the vent. Changes in the eruption rate impact the how mass is distributed within a flow via the mode of emplacement

(e.g. resurfacing, breakouts, inflation, and lava tubes). Numerical models – often used to simulate lava flow hazards – have yet to fully replicate flow conditions. Many computational models are probabilistic, as opposed to physics-based, owing to the complexity in simulating lava flow rheology and emplacement. Laboratory simulations are a bridge toward improving models because they allow for the simulation of flow complexity. Future laboratory experiments should investigate the complexity inherent in larger flows similar to what is observed in large igneous provinces (which would require larger tanks), more complex eruption dynamics (e.g. multiple pulses of varying fluxes), and investigate how these processes might scale to larger or longer duration eruptive events.

Understanding the history of volcanism on Mars provides information on its volcanic evolution, interior, and composition. The results of this thesis suggest that the voluminous lava flows on the surface of Mars were generated not by exotic lava compositions or unnecessarily high eruption rates, but by erupting basalt-like rheologies for extended periods of time using large subsurface conduits (i.e. dikes and sills). The introduction of more complex models that account for mass loss due to common lava flow processes (such as levee formation) has helped enhance our understanding of recent volcanism on Mars. As our understanding of lava flows improves, future models and remote geomorphological studies will help further constrain eruption conditions on Mars.

REFERENCES

Abramoff, M.D., Magalhaes, P.J., Ram, S.J. (2004), Image processing with Image J. Biophotonics International 11, 36–42.

Bailey, J.E., Harris, A.J.L., Dehn, J., Calvari, S., and S.K. Rowland (2006), The changing morphology of an open channel on Mt. Etna, *Bull Volcanology*, 68, 497–515, doi: 10.1007/s00445-005-0025-6.

Baloga, S., and D. Pieri (1986), Time-dependent profiles of lava flows, *J. Geophys Res.*, 91, No. B9, 9543–9552.

Baloga, S.M., P.J. Mouginis-Mark, and L.S. Glaze (2003), Rheology of a long lava flow at Pavonis Mons, Mars, *J. Geophys. Res.*, 108, E7, 5066, doi: 10.1029/2002JE001981.

Baloga, S.M., and L.S. Glaze (2008), A self-replication model for long channelized lava flows on the Mars plains, *J. Geophys. Res.*, 113, E05003, doi: 10.1029/2007JE002954.

Baloga, S.M., Glaze, L.S., Crisp, J.A., and S.A. Stockman (1998), New statistics for estimating the bulk rheology of active lava flows: Puu Oo examples, *J. Geophys. Res.*, 103, No. B3, 5133–5142.

Belousov, A., Belousov, M., Edwards, B., Volynets, A. and D. Melnikov (2015), Overview of the precursors and dynamics of the 2012–13 basaltic fissure eruption of Tolbachik Volcano, Kamchatka, Russia, *J. Volcano Geotherm. Res.*, 307, 22–37, http://dx.doi.org/10.1016/j.jvolgeores.2015.04.009.

Black, B.A., and M. Manga (2016), The eruptibility of magmas at Tharsis and Syrtis Major on Mars, *J. Geophys. Res. Planets*, 121, 944–964, doi: 10.1002/2016JE004998.

Black, B.A., and M. Manga (2017), Volatiles and the tempo of flood basalt magmatism, *Earth Planet. Sci. Lett.*, 458, 130–140.

Blake, S., and B.C. Bruno (2000), Modelling the emplacement of compound lava flows, *Earth and Planetary Sci. Lett*., 184, 181–197.

Bleacher, J.E., R. Greeley, D.A. Williams, S.C. Werner, E. Hauber, and G. Neukum (2007), Olympus Mons, Mars: Inferred changes in late Amazonian aged effusive activity from lava flow mapping of Mars Express High-Resolution Stereo data, *J. Geophys. Res., 112*, E04003, doi: 10.1029/2006JE002826.

Bleacher, J.E., Greeley, R., Williams, D.A., Cave, S.R., and G. Neukum (2007), Trends in effusive style at the Tharsis Montes, Mars, and implications for the development of the Tharsis province, *J. Geophys. Res.*, 112, E09005, doi: 10.1029/2006JE002873.

Bleacher, J.E., Orr, T.R., de Wet, A.P., Zimbelman, J.R., Hamilton, C.W., Garry, W.B., Crumpler, L.S., and D.A. Williams (2017), Plateaus and sinuous ridges as the fingerprints of lava flow inflation in the Eastern Tharsis Plains of Mars, *J. Volcano. Geotherm. Res.*, http://dx.doi.org/10.1016/j.jvolgeores.2017.03.025.

Brown, D. (2009), Video modeling and tracker, *In: AAPT Topical Conference*: Computer Modeling in the Introductory Course. AAPT Summer Meeting.

Bruno, B.C., Baloga, S.M., and G. J. Taylor (1996), Modeling gravity-driven flows on an inclined plane, *J. Geophys. Res.*, 101, No. B5, 11,595–11,577.

Capello, A., Herault, A., Bilotta, G., Ganci, G., and C. Del Negro (2015), MAGFLOW: a physics-based model for the dynamics of lava flow emplacement, *Geologic. Soc. London Special Pub*., 426, 357–373, https://doi.org/10.1144/SP426.16.

Carr, M.H. (1973), Volcanism on Mars, *J. Geophys. Res., 78*, 4049 – 4062.

Carr, M.H. (1974), Tectonism and Volcanism of the Tharsis Region of Mars, *J. Geophys. Res., 79, no. 26,* 3942 – 3949.

Cashman, K.V., Kerr, R.C., and R.W. Griffiths (2006), A laboratory model of surface crust formation and disruption on lava flows through non-uniform channels, *Bull Volcanol*, 68, 753–770, doi: 10.1007/s00445-005-0048-z.

Chemical Rubber Company (CRC) (1984), CRC Handbook of Chemistry and Physics. Weast, Robert C., editor. 65th edition. *CRC Press, Inc*. Boca Raton, Florida. USA.

Christensen, P.R. (1986), Regional Dust Deposits on Mars: Physical Properties, Age, and History, *J. Geophys. Res., 91, no. B3,* 3533 – 3545.

Christensen, P.R., B.M. Jakosky, H.H. Kieffer, M.C. Malin, H.Y. McSween, K. Nealson, G.L. Mehall, S.H. Silverman, S. Ferry, M. Caplinger, and M. Ravine (2004), The Thermal Emission Imaging System (THEMIS) for the Mars 2001 Odyssey Mission, *Space Sci. Rev., 110,* 85 – 130.

Connor, L.J, Connor, C.B., Meliksetian, K., and I. Savov (2012), Probabilistic approach to modelling lava flow inundation: a lava flow hazard assesment for a nuclear facility in Armenia, *J. Applied Volcan.*, 1:3.

Crane Company (1988), Flow of fluids through valves, fittings, and pipe, *Technical Paper No. 410* (TP 410).

Crisp, J.A. (1984), Rates of Magma Emplacement and Volcanic Output, *J. Volcanol. Geotherm. Res.*, 20, 177 – 221.

Crown, D.A., and M.S. Ramsey (2016), Morphologic and thermophysical characteristics of lava flows southwest of Arsia Mons, Mars, *J. Volcanol. Geotherm. Res.*, http://dx.doi.org/10.1016/j.volgeores.2016.07.008.

Crumpler, L.S., and J.C. Aubele (1978), Structural Evolution of Arsia Mons, Pavonis Mons, and Ascraeus Mons: Tharsis Region of Mars, *Icarus*, 34, 496–511.

Danes, Z.F. (1972), Dynamics of lava flows, J. Geophys. Res., 77, No. 8, 1430–1432.

Del Negro, C., Capello, A., Neri, M., Bilotta, G., Herault, A., and G. Ganci (2013), Lava flow hazards at Mt. Etna: constraints impose by eruptive history and numerical simulations, *Scientific Reports*, 3:3493. doi: 10.1038/srep03493.

Diettrich, H.R., Lev, E., Chen, J., Richardson, J. A., and K. V. Cashman (2017), Benchmarking computational fluid dynamics models of lava flow simulation for hazard assessment, forecasting, and risk management, *J. Applied Volcano.*, 6:9, doi: 10.1186/s13617-017-0061-x.

Dragoni, M, and A. Tallarico (1994), The effect of crystallization on the rheology and dynanics of lava flows, *J. Volcano. Geotherm. Res.*, 59, 241–252.

Edwards, B.R., Belousov, A., and M. Belousova (2014), Propagation style controls lava-snow interactions, *Nature Communications*, 5:5666, doi: 10.1038/ncomms6666.

Farrell, J., Hamilton, C., Karson, J., and R. Wysocki (2019), Predicting Breakouts in Basaltic Lava Experiments, *2019 Amer. Geophys. Uni.*, V23C-04 abstract.

Favalli, M., Pareschi, M. T., Neri, A., and I. Isola (2005), Forecasting lava flow paths by a stochastic approach, *Geophys. Res. Lett.*, 32, L03305, doi: 10.1029/2004GL021718.

Felpeto, A., Arana, V., Ortiz, R., Astiz, M., and A. Garcia (2001), Assessment and modelling of lava flow hazard on Lanzarote (Canary Islands), *Natural Hazards*, 23, 247–257.

Fink, J.H., and R.C. Fletcher (1978), Ropy pahoehoe: surface folding of a viscous fluid, *J. Volcano. and Geotherm. Res.*, 4, 151–170.

Fink, J.H., Park, S.O., and R. Greeley (1983), Cooling and deformation of sulfur flows, *Icarus*, 56, 38–50.

Fink, J.H., and R. W. Griffiths (1990), Radial spreading of viscous-gravity currents with solidifying crust, *J. Fluid Mech.*, 221, 485–509.

Fink, J.H., Park, S.O., and R. Greeley (1983), Cooling and deformation of sulfur flows, *Icarus*, 56, 38–50.

Francis, P., and C. Oppenheimer (2003), Volcanoes 2nd edition, *Oxford Univ. Press.*

Ganci, G., Vicari, A., Cappello, A., and C. D. Nero (2012), An emergent strategy for volcano hazard assessment: from thermal satellite monitoring to lava flow modelling, *Remote Sens. Environ.*, 119, 197–207, doi: 10.1016/j.rse.2011.12.021.

Garry, W.B., Gregg, T.K.P., Soule, S.A., and D.J. Fornari (2006), Formation of submarine lava channel textures: insights from laboratory simulations, *J. Geophys. Res.*, 111, B03104, doi: 10.1029/2005JB003796.

Garry, W.B., Zimbelman, J.R., and T.K.P. Gregg (2007), Morphology and emplacement of a long-channeled lava flow near Ascraeus Mons volcano, Mars, *J. Geophys. Res.*, 112, E08007, doi: 10.1029/2006JE002803.

Giacomini, L., Massironi, M., Martellato, E., Pasquare, G., Frigeri, A., and G. Cremonese (2009), Inflated flows on Daedalia Planum (Mars)? Clues from a comparative analysis with the Payen volcanic complex (Argentina), *Planet. Space Sci.*, 57, 556–570.

Giacomini, L., Carli, C., Sgavetti, M., and M. Massironi (2012), Spectral analysis and geological mapping of the Daedalia Planum lava field (Mars) using OMEGA data, *Icarus*, 220, 679 – 693.

Glaze, L.S., and S.M. Baloga (2006), Rheologic inferences from the levees of lava flows on Mars, *J. Geophys. Res.*, 111, E09006, doi: 10.1029/2005JE002585.

Glaze, L.S., and S.M. Baloga (1998), Dimensions of Pu`u O`o lava flows on Mars, *J. Geophys. Res.*, 103, no. E6, 13,659–13,666.

Glaze, L.S., Baloga, S.M., and E.R. Stofan (2003), A methodology for constraining lava flow rheologies with MOLA, *Icarus*, 165, 26–33, doi: 10.1016/S0019-1035(03)00171-4.

Glaze, L.S., Baloga, S.M., Garry, W.B., Fagents, S.A., and C. Parchetta (2009), A hybrid model for leveed lava flows: Implications for eruption styles on Mars, *J. Geophys. Res.*, 114, E07001, doi: 10.1029/2008JE003278.

Greeley, R. (1972), Additional observations of actively forming lava tubes and associated structures, Hawaii, *Modern Geology*, 3, 157–160.

Greeley, R. (1987), The role of lava tubes in Hawaiian volcanoes, *Volcanism in Hawaii*, *USGS Proff. Paper*, chapter 59, 1589–1602.

Greeley, R., and P.D. Spudis (1981), Volcanism on Mars, *Rev. Geophys. Spac. Phys.*, 19, no. 1, 13 – 41.

Gregg, T.K.P., and J. H. Fink (1996), Quantification of extraterrestrial lava flow effusion rates through laboratory simulations, *J. Geophys. Res.*, 101, No. E7, pp. 16891–16900, 96JE01254.

Gregg, T.K.P., and J. H. Fink (2000), A laboratory investigation into the effects of slope on lava flow morphology, *J. Volcano. and Geotherm. Res.*, 96, 145–159.

Gregg, T.K.P., and L.P. Keszthelyi (2004), The emplacement of pahoehoe toes: field observations and comparison to laboratory simulations, *Bull Volcanol*, 66, 381 – 391, doi: 10.1007/s00445-003-0319-5.

Gregg, T.K.P., and D.K. Smith (1993), Volcanic investigations of the Puna Ridge, Hawai'i: relations of lava flow morphologies and underlying slopes, *J. Volcano. Geotherm. Res.*, 126, 63–77.

Griffiths, R.W. (2000), The dynamics of lava flows, *Annu. Rev. Fluid Mech.*, 32, 477–518.

Griffiths, R.W. and J.H. Fink (1992), The morphology of lava flows in planetary environments: predictions from analog experiments, *J. Geophys. Res. Solid Earth*, 97, B13, 19739–19748.

Griffiths, R.W., and J.H. Fink (1993), Effects of surface cooling on the spreading of lava flows and domes, *J. Fluid Mech.*, 252, 667–702.

Griffiths, R.W., and J.H. Fink (1997), Solidifying Bingham extrusions: a model for the growth of silicic lava domes, *J. Fluid Mech.*, 347, 13–36.

Griffiths, R.W., Kerr. R.C., and K.V. Cashman (2003), Patterns of solidification in channel flows with surface cooling, *J. Fluid Mech.*, 496, 33–62, doi: 10.1017/S0022112003006517.

Harris, A.J.L., and S.K. Rowland (2001), FLOWGO: a kinematic thermo-rheological model for lava flowing in a channel, *Bull Volcanol*, 63, 20–44, doi: 10.1007/s004450000120.

Hallsworth, M.A., Huppert, H.E., and R.S.J. Sparks (1987), A laboratory simulation of basaltic lava flows, *Modern Geology*, 11, 93–107.

Hauber, E., Broz, P., Jagert, F., Jodlowski, P., and T. Platz (2011), Very recent and wide-spread basaltic volcanism on Mars, *Geophys. Res. Lett.*, 38, L10201, doi: 10.1029/2011GL047310.

Hiesinger, H., Head III, J.W., and G. Neukum (2007), Young lava flows on the eastern flank of Ascraeus Mons: Rheological properties derived from High Resolution Stereo

Camera (HRSC) images and Mars Orbiter Laser Altimeter (MOLA) data, *J. Geophys. Res.*, 112, E05011, doi: 10.1029/2006JE002717.

Hoblitt, R.P., Orr, T.R., Heliker, C., Denlinger, R.P., Hon. K., and P.F. Cervelli (2012), Inflation rates, rifts, and bands in a pahoehoe sheet flow, *Geosphere*, 8, no. 1, 179–195, doi: 10.1130/GES00656.1.

Hon. K., Kauahikaua, J., Denliger, R., and K. Mackay (1994), Emplacmenet and inflation of pahoehoe sheet flows: observations and measurements of active lava flows of Kilauea volcano, Hawaii, *Geologic. Soc. Amer. Bull.*, 106, 351–370.

Hulme, G. (1974), The interpretation of lava flow morphology, *Geophys. J. R. astr. Soc.*, 39, 361 – 383.

Hulme, G. (1976), The Determination of the Rheological Properties and Effusion Rate of an Olympus Mons Lava, *Icarus, 27,* 207 – 213.

Hulme, G., and G. Fielder (1977), Effusion rates and rheology of lunar lavas, *Phil. Trans. R. Soc. Lond.* A., 285, 227 – 234.

Jaumann, R., G. Neukum, T. Behnke, T.C. Duxbury, K. Eichentopf, J. Flohrer., S. Van Gasselt, B. Giese, K. Gwinner, E. Hauber, H. Hoffmann, A. Hoffmeister, U. Köhler, K.-D. Martz, T.B. McCord, V. Mertens, J. Oberst, R. Pischel, D. Reiss, E. Ress, T. Roatsch, P. Saiger, F. Scholten, G. Schwartz, K. Stephan, M. Wählisch and The HRSC Co-Investigator Team (2007), The high-resolution stereo camera (HRSC) experiment on Mars Express: instrument aspects and experiment conduct from interplanetary cruise through the nominal mission, *Planet. Space Sci., 55,* 928 – 952.

Jeffreys, H. (1925), The flow of water in an inclined channel of rectangular section, *The London, Ediburgh, and Dublin Phil. Mag. J. Sci.*, 49:293, 793 – 807, doi: 10.1080/14786442508634662.

Kerr, R.C., Griffiths, R.W., and K.V. Cashman, (2006), Formation of channelized lava flows on an unconfined slope, *J. Geophys. Res.*, 111, B10206, doi: 10.1029/2005JB004225.

Leverington, D. W. (2006), Volcanic processes as alternative mechanisms of landform development at a candidate crater-lake site near Tyrrhena Patera, *J. Geophys. Res.*, 111, E11002, doi: 10.1029/2004JE002382.

Lipman, P.W., and N.G. Banks (1987), AA Flow dynamics, Mauna Loa, *Volcanism in Hawai'i,* 1527 – 1567.

Malin, M.C. (1980), Lengths of Hawaiian lava flows, *Geology*, 8, 306–308.

Malin, M.C., J.F. Bell, B.A. Cantor, M.A. Caplinger, W.M. Calvin, R.T. Clancy, K.S., Edgett, L. Edwards, R.M. Haberle, P.B. James, S.W. Lee, M.A. Ravine, P.C. Thomas, and M.J. Wolff (2007), Context camera investigation on board the Mars Reconnaissance Orbiter, *J. Geophys. Res., 112*, E05S04, doi: 10.1029/2006JE002808.

Mallonee, H.C., Kobs Nawotniak, S.E., McGregor, M., Hughes, S.S., Neish, C., Downs, M., Delparte, D., Lim, D.S.S., Heldmann, J., and the FINESSE team (2017), Lava flow morphology classification based on measures of roughness, *Lunar Plan. Sci. Conf. XLVIII*, Abstract 2992.

McEwan, A.S., E.M. Eliason, J.W. Bergstrom, N.T. Bridges, C.J. Hansen, W.A., Delamere, J.A. Grant, V.C. Gulick, K.E. Herkenhoff, L. Keszthelyi, R.L. Kirk, M.T. Mellon, S.W. Squyres, N. Thomas, and C.M. Weitz (2007), Mars Reconnaissance Orbiter's High-Resolution Imaging Science Experiment (HiRISE), *J. Geophys. Res., 112*, E05S02, doi:10.1029/2005JE002605.

Mellon, M.T., Jakosky, B.M., Kieffer, H.H., and P.R. Christensen (2000), High-resolution thermal inertia mapping from the Mars Global Surveyor Thermal Emission Spectrometer, *Icarus*, 148, 437 – 455, doi: 10.1006/icar.2000.6503.

Moore, H.J., Arthur, D.W.G., Schaber, G.G. (1978), Yield strengths of flows on the Earth, Mars, and Moon, *Proc. Lunar Planet. Sci. Conf. 9*th, 3351 – 3378.

Mouginis-Mark, P. and M.T. Yoshioka (1998), The long lava flows of Elysium Planitia, Mars, *J. Geophys. Res.*, 103. No. E8, 19389 – 19400.

Nichols, R. L. (1939), Viscosity of Lava, *J. Geology*, 47, no. 3, 290 – 302.

Neukum, G., R. Jaumann., H. Hoffmann, H., E. Hauber, J.W. Head, A.T. Basilevsky, B.A. Ivanov, S.C. Werner, S. van Gasselt, J.B. Murray, T. McCord, and The HRSC Co-Investigator Team (2004), Recent and episodic volcanic and glacial activity on Mars revealed by the High Resolution Stereo Camera, *Nature*, 432, 971 – 979.

Pasckert, J. H., Hiesinger, H., and D. Reiss (2012), Rheologies and ages of lava flows on Elysium Mons, Mars, *Icarus*, 219, 443 – 457.

Peck, D.L. (1978), Cooling and Vesiculation of Alae Lava Lake, Hawai'i, *Geologic. Surv. Pro. Paper*, 935-B.

Peiterson, M.N., and D.A. Crown (1999), Downflow width behavior of Martian and terrestrial lava flows, *J. Geophys. Res.*, 104, no. E4, 8473 – 8488.

Peterson, D.W., and R.I. Tilling, (1980), Transition of basaltic lava from pahoehoe to aa, Kilauea volcano, Hawaii: field observations and key factors, *J. Volcanol. Geotherm. Res.*, 7, 271–293.

Pieri, D.C., and S.M. Baloga (1986), Eruption rate, area, and length relationships for some Hawaiian lava flows, *J. Volcanol. Geotherm. Res.*, 30, 29–45.

Pieri, D.C., Baloga, S.M., Nelson, R.M., and C. Sagan (1984), Sulfur Flows of Ra Patera, IO, *Icarus*, 60, 685 – 700.

Pinkerton, H. (1987), Factors affecting the morphology of lava flows, *Endeavour New Series*, 11, no. 2, 73–79.

Pinkerton, H., and R.S. J. Sparks (1976), The 1975 Sub-terminal lavas, Mount Etna: A case history of the formation of a compound lava field, *J. Volcanol. Geotherm. Res.*, 1, 167 – 182.

Pinkerton, H., James, M., and A. Jones (2002), Surface measurements of active lava flows on Kilauea volcano, Hawai'i, *J. Volcanol. Geotherm. Res.*, 113, 159 – 176.

Plescia, J.B. (2004), Morphometric properties of Martian volcanoes, *J. Geophys. Res., 109*, E03003, doi: 10.1029/2002JE002031.

Rader, E., Vanderkluysen, L., and A. Clarke (2017), The role of unsteady effusion rates on inflation in long-lived lava flow fields, *Earth Planet. Sci. Lett.*, 477, 73–83.

Rogers, A.D., and P.R. Christensen (2007), Surface mineralogy of Martian low-albedo regions from MGS-TES data: implications for upper crustal evolution and surface alteration, *J. Geophys. Res.*, 112, E01003, doi: 10.1029/2006JE002727.

Rowland, S.K., Harris, A.J.L., and H. Garbeil (2004), Effects of Martian conditions on numerically modeled, cooling-limited, channelized lava flows, *J. Geophys. Res.*, 109, E10010, doi: 10.1029/2004JE002288.

Rowland, S.K., Garbeil, H., and A.J.L. Harris (2005), Lengths and hazards from channel-fed lava flows on Mauna Loa, Hawaii, determined from thermal and downslope modeling with FLOWGO, *Bull Volcanol*, 67, 634–647, doi: 10.1007/s00445-004-0399-x.

Sakimoto, S.E.H., Crips, J., and S.M. Baloga (1997), Eruption constratins on tube-fed planetary lava flows, *J. Geophys. Res.*, 102, no. E3, 6597 – 6613.

Sakimoto, S.E.H., and T.K.P. Gregg (2001), Channeled flow: analytic solutions, laboratory experiments, and applications to lava flows, *J. Geophys. Res.*, 106, no. B5, 8629–8644.

Scott, D.H., and K. L. Tanaka (1981), Mars: Paleostratigraphic restoration of buried surfaces in Tharsis Montes, *Icarus*, 45, 304 – 319.

Self, S., Thordarson T., Kesthelyi, L., Walker, G.P.L., Hon, K., Murphy, M.T., Long, P., and S. Finnemore (1996), A new model for the emplacement of Colombia River basalts as large, inflated pahoehoe lava flow fields, *Geophys. Res. Lett.*, 23, no. 19, 2689–2692.

Sheth, H.C. (2006), Large Igneous Provinces (LIPs): definition, recommended terminology, and a hierarchical classification, *Earth Sci. Rev.*, 85, 117–124.

Soule, S.A., and K.V. Cashman (2004), The mechanical properties of solidified polyethylene glycol 600, an analog for lava crust, *J. Volcanol. Geotherm. Res.*, 129, 139–153.

Spudis, P.D., McGovern, P.J., and W.S. Kiefer (2013), Large shield volcanoes on the Moon, *J. Geophys. Res. Planets*, 118, 1063 – 1081, doi: 10.1002/jgre.20059.

Tarquini, S. (2017), A review of mass and energy flow through a lava flow system: insights provided from a non-equilibrium perspective, *Bull Volcanol.*, 79:64, doi: 10.1007/s00445-017-1145-5.

Tarquini, S., and M. d' Michieli Vitturi (2014), Influence of fluctuating supply on the emplacement dynamics of channelized lava flows, *Bull Volcanol.*, 76:801, doi: 10.1007/s00445-014-0801-2.

Vicari, A., Alexis, H., Del Negro, C., Coltelli, M., Marsella, M., and C. Proietti (2007), Modelling of the 2001 lava flow at Etna volcano by cellular automata approach, *Environment. Model. Software*, 22, 1465–1471.

Vicari, A., Bilotta, G., Bonfiglio, S., Cappello, A., Ganci, G., Herault, A., Rustico, E., Gallo, G., and C. Del Negro (2011), LAV@HAZARD: a web-GIS interface for voclanic hazard assesment, *Ann. Geophys.*, 54, 5, doi: 10.4401/ag-5347.

D' Michieli Vitturi, M., and S. Tarquini (2018), Mr Lava Loba: a new probibalistic model for the simulation of lava flows as a settling process, *J. Volcanol. Geotherm. Res.*, 349. 323–334.

Wadge, G. (1981), The variation of magma discharge during basaltic eruptions, *J. Volcanol. Geotherm. Res.*, 11, 139–168.

Walker, G.P.L. (1971), Compound and simple lava flows and flood basalts, *Bull. Volcanol.*, 35, 579 – 590.

Walker, G.P.L. (1973), Lengths of lava flows, *Phil. Trans. R. Soc. Lond. A.*, 274, 107 – 118.

Werner, S.C. (2009), The global martian volcanic evolutionary history, *Icarus*, 201, 44 – 68.

Wilson, L., J.W. Head III (1983) A comparison of volcanic eruption processes on Earth, Moon, Mars, Io, and Venus, *Nature*, 302, 663 – 669.

Wolfe, E.W., Garcia, M.O., Jackson, D.B., Koyanagi, R.Y., Neal, C.A., and A.T. Okamura (1987), The Pu'u O'o eruption of Kilauea volcano, episodes 1 – 20, January 3, 1983, to June 8, 1984, 471 – 508.

Xiao, L., Huang, J., Christensen, P.R., Greeley, R., Williams, D.A., Zhao J., and Q. He (2012), Ancient volcanism and its implication for thermal evolution of Mars, *Earth and Planet. Sci. Lett.*, 323-324, 9 – 18.

Zuber, M.T., D.E. Smith, S.C. Solomon, D.O. Muhleman, J.W. Head, J.B. Garvin, J.B. Abshire, and J.L. Bufton (1992), The Mars observer laser altimeter investigation, *J. Geophys. Res., 97,* 7781 – 7797.

APPENDIX A

TABLES OF DATA COMPILED FOR CHAPTER 4

	Lat (N)	Long €	Region	Length (km)	Mean Width (km)	Flow Thickness (m)	Volume (km^3)	Observed Ψ Morphology
Flow 1	18.53	235.94	E of Olympus Mons	21	5.61	10.5	1.32	Levee (fed by)
Flow 2	11.914	244.629	Tharsis	313	18.3	46	281.80	Levees
Flow 3	14.504	248.246	Tharsis	314	28.8	39	436.18	Smooth-Levees
Flow 4	15.199	226.654	Olympus Mons	18.3	0.592	27	0.38	Levee-Folds
Flow 5	15.008	226.823	Olympus Mons	33	0.57	11.5	0.25	Levee-Folds
Flow 6	15.761	224.764	Olympus Mons	19	3	25	1.48	Levees
Flow 7	11.739	224.015	S Olympus Mons	100	6.9	26	23.40	Levees
Flow 8	11.597	222.495	S Olympus Mons	41	6.5	14	1.76	Levees
Flow 9	-19.332	243.262	Daedalia Planum	78	5.9	25	12.00	Levee
Flow 10	-20.945	240.957	Daedalia Planum	136.5	5.89	33	34.16	Levee
Flow 11	-21.733	242.555	Daedalia Planum	58	16.3	35.5	38.41	Levee-Folds
Flow 12	-23.297	242.812	Daedalia Planum	266	19.3	45	268.16	Levees
Flow 13	-22.547	244.16	Daedalia Planum	201	11.8	30	101.07	Levees
Flow 14	-23.195	237.617	Daedalia Planum	219	6	32	52.22	Levee
Flow 15	-19.081	234.684	Daedalia Planum	92	3.8	15	6.11	Levee-Folds
Flow 16	-17.307	233.48	Daedalia Planum	164.5	3.23	16	12.24	Levees
Flow 17	-22.665	237.6084	Daedalia Planum	106	4.48	17	10.17	Levees
Flow 18	8.945	257.408	Ascraeus Mons	16	4.1	15	0.99	Folds
Flow 19	15.521	261.191	Ascraeus Mons	78.5	4.19	23	8.33	Levees
Flow 20	12.102	250.046	W of Ascraues Mons	99	12	37	65.38	Levees
Flow 21	11.193	248.41	W of Ascraues Mons	121	16.5	38	73.07	Smooth-Levees
Flow 22	15.757	225.213	Olympus Mons	15	1.15	17.5	0.33	Levees

Flow 23	15.814	225.379	Olympus Mons	30.4	5.93	91	8.20	Rifts
Flow 24	15.156	225.105	Olympus Mons	27.12	1.32	18	0.77	Levee
Flow 25	14.997	225.298	Olympus Mons	59.5	6.79	68	13.74	Rifts
Flow 26	16.089	227.269	Olympus Mons	13.3	3.72	64	1.58	Rifts
Flow 27	15.91	227.239	Olympus Mons	27.6	2.2	37	1.12	Rifts
Flow 28	15.178	259.464	Ascraeus Mons	47.6	4.6	30.8	3.37	Rifts
Flow 29	15.689	259.131	Ascraeus Mons	29	7	38.4	3.90	Rifts
Flow 30	8.572	263.609	Tharsis	43.7	7.13	29	8.96	Levee
Flow 31	-12.934	239.423	Daedalia Planum	25.3	2.08	31	1.72	Levee
Flow 32	-0.879	237.326	Tharsis	77.2	5.94	30.5	15.16	Levee
Flow 33	-3.006	239.936	Tharsis	69.3	6	29	11.66	Levee
Flow 34	16.210	261.309	Tharsis	72	3.67	25	7.13	Levee
Flow 35	5.018	256.914	Tharsis	98.6	3.11	16	5.09	Levee
Flow 36	5.229	254.687	Tharsis	23	1.26	11	0.46	Levee
Flow 37	5.371	255.546	Tharsis	38.4	1.86	13	1.09	Levee
Flow 38	3.576	259.678	Tharsis	128	4.94	18.1	11.91	Levee
Flow 39	1.347	238.558	Tharsis	71.1	6.7	23	12.03	Levee
Flow 40	15.51	271.857	Tharsis	219	13.8	55	173.69	Levee

Table 1: Data on 40 lava flows in Tharsis volcanic province on Mars investigated in this study.

Calculations using Graetz number and Jeffrey's Equation			
Flows	**Eruption Rate (m^3/s)**	**Viscosity (Pa-s)**	**Yield Stength (Pa)**
1	1680	9.38E+04	7.65E+02
2	16330	2.12E+06	3.07E+03
3	34781	9.42E+05	2.24E+03
4	60	7.42E+07	3.10E+04
5	245	1.35E+06	1.32E+04
6	342	3.33E+07	1.82E+04
7	3981	7.94E+05	2.03E+03
8	2855	1.39E+05	9.33E+02
9	2761	1.38E+06	3.09E+03
10	3654	2.51E+06	4.29E+03
11	3994	6.89E+06	4.02E+03
12	17113	4.59E+06	6.03E+03
13	11859	8.96E+05	3.00E+03
14	5646	1.26E+06	3.79E+03
15	3496	1.62E+05	1.99E+03
16	4981	1.56E+05	2.81E+03
17	4190	1.96E+05	1.90E+03
18	656	9.54E+05	2.03E+03
19	2145	1.22E+06	3.53E+03
20	4816	3.78E+06	3.32E+03
21	7881	3.41E+06	3.39E+03
22	152	1.11E+07	1.40E+04
23			
24	298	6.99E+06	1.46E+04
25			
26			
27			
28			
29			
30	1612	2.79E+06	2.25E+03
31	255	1.97E+07	7.52E+03
32	2255	2.80E+06	3.43E+03
33	2151	3.19E+06	4.08E+03
34	1585	1.33E+06	2.75E+03
35	2875	2.07E+05	2.24E+03

36	395	1.62E+05	1.26E+03
37	824	2.10E+05	1.65E+03
38	5579	1.79E+05	1.74E+03
39	3107	7.02E+05	1.85E+03
40	8242	9.71E+06	5.75E+03

Table 2: Eruption rates and rheological properties of 34 lava flows on Mars using a Graetz number of 300 and Jefferey's equation.

Application of Ψ	
Flow	**Eruption Rates**
1	950 - 6500
2	950 - 6500
3	6500
4	575 - 950
5	575 - 950
6	950 - 6500
7	950 - 6500
8	950 - 6500
9	950 - 6500
10	950 - 6500
11	575 - 950
12	950 - 6500
13	950 - 6500
14	950 - 6500
15	575 - 950
16	950 - 6500
17	950 - 6500
18	35 - 575
19	950 - 6500
20	950 - 6500
21	6500
22	950 - 6500
23	0.2 - 20
24	950 - 6500
25	0.2 - 20
26	0.2 - 20
27	0.2 - 20
28	0.2 - 20
29	0.2 - 20
30	950 - 6500
31	950 - 6500
32	950 - 6500
33	950 - 6500
34	950 - 6500
35	950 - 6500
36	950 - 6500
37	950 - 6500

38	950 - 6500
39	950 - 6500
40	950 - 6500

Table 3: Eruption rate ranges for 40 lava flows on Mars by based on surface morphology, assigned Ψ value, and assumed ambient and flow properties.

	Self-replication lava flow model [Baloga & Glaze, 2008]		
Flow	**Yield Strength (Pa)**	**Eruption Rate (m^3/s)**	**Viscosity (Pa-s)**
1			
2	**3.43E+03**	**1174.39**	**9.45E+06**
3	**5.26E+03**	**335.62**	**2.85E+07**
4			
5			
6			
7			
8			
9			
10	**4.60E+03**	**52.66**	**3.17E+07**
11			
12			
13			
14	**3.30E+03**	**135.42**	**1.95E+07**
15			
16			
17			
18			
19			
20			
21	**7.91E+03**	**285.09**	**1.45E+07**
22	**1.66E+04**	**27.60**	**2.92E+07**
23			
24	**3.63E+04**	**26.90**	**1.45E+07**
25			
26			
27			
28			
29			
30	**1.39E+03**	**46.00**	**1.73E+07**
31			
32	**2.73E+03**	**236.21**	**1.58E+07**
33	**4.03E+03**	**204.30**	**2.19E+07**
34	**2.00E+03**	**50.57**	**1.03E+07**
35	**2.81E+03**	**89.26**	**2.53E+06**

36			
37			
38			
39	**1.38E+03**	**111.17**	**4.52E+06**
40			

Table 4: Eruption rates and rheologic properties of 13 lava flows on Mars using the self-replication model for long lava flows [*Baloga and Glaze*, 2008].

APPENDIX B

CHAPTER TWO FIGURES

Figure 1: Example of a pahoehoe lava flow in Hawaii during summer 2016 propagating down the slope into an inflation pit. The flow narrows while on the slope and expands in area after the slope break. Photo credit: Sean Peters.

Figure 2: Example of the Deccan Traps, a large igneous province in north-central India**.** The Deccan consists of hundreds of stacked lava flows, many of which have thickened to tens of meters. Image from Wikimedia commons.

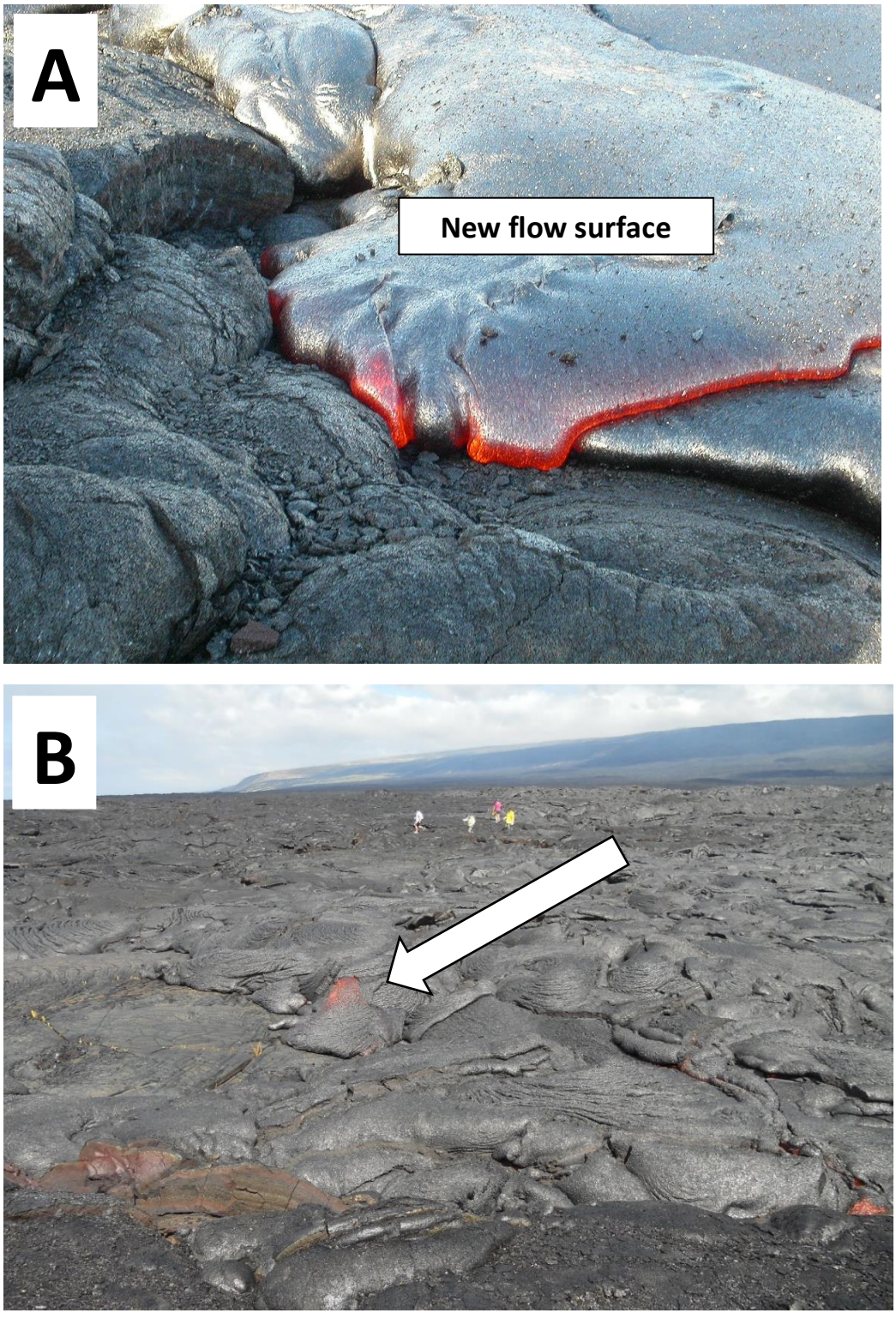

Figure 3: (a) Example of resurfacing in a pahoehoe flow. Notice how the pahoehoe lobe is repaving a previous surface of the same flow. Image credit: Wikimedia Commons. (b)

Example of a marginal breakout at the edge of a pahoehoe flow in Hawaii. Photo taken summer of 2016. Image credit: Sean Peters.

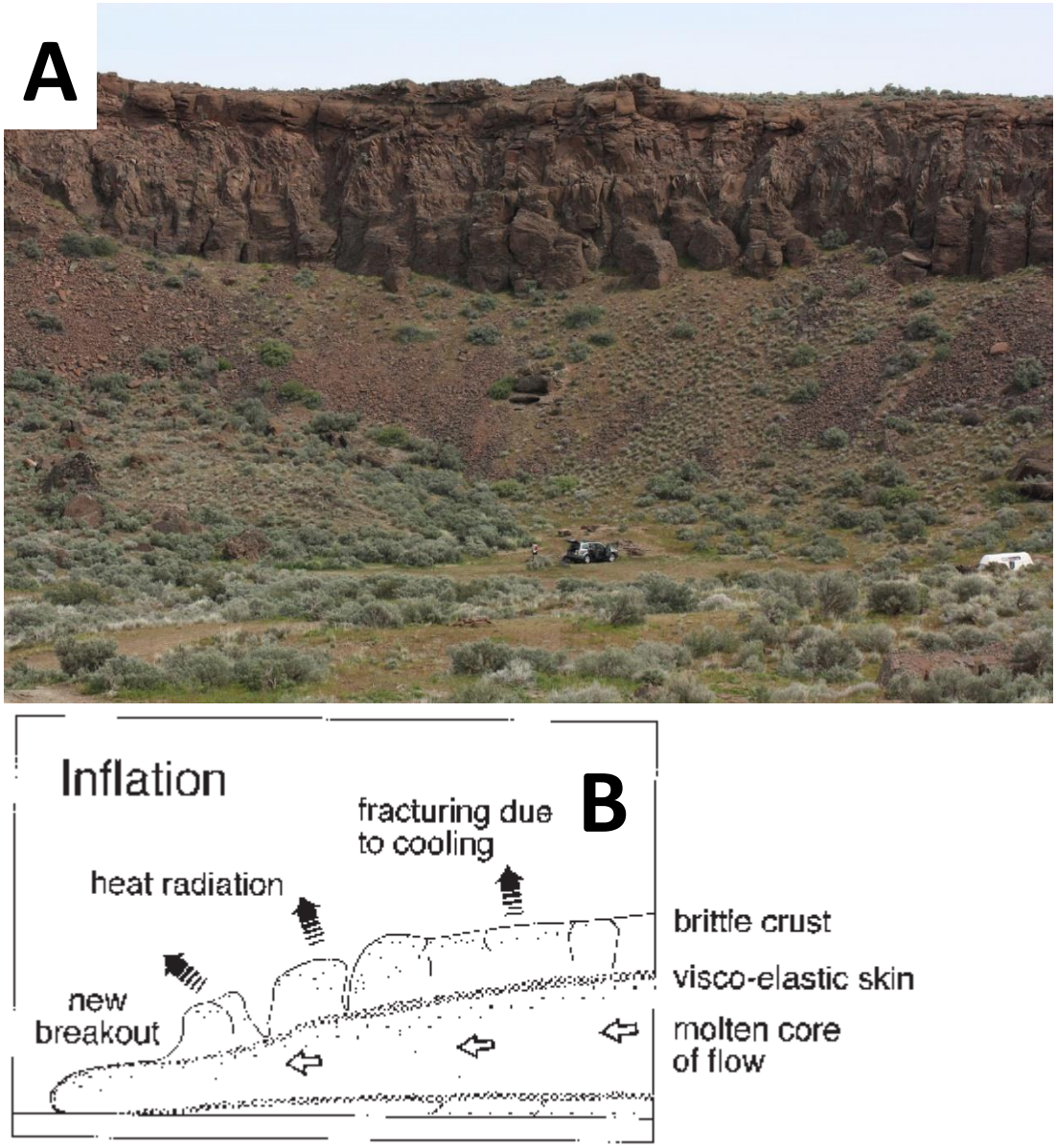

Figure 4: (a) Example of inflated lava flows of the Columbia River Basalts. Image credit: Wikimedia Commons. (b) The process of inflation involves the endogenic growth of lava flows. Marginal breakouts, as individual lobes, can also occur. Image adapted from Self et al., 1996.

Figure 5: Example of a lava tube. Raised surface at the bottom right is a benchmark that represents a lava flow surface. Featured lava tube is the Thurston lava tube in Hawaii. Image credit: Wikimedia Commons. Photo by Michael Oswald.

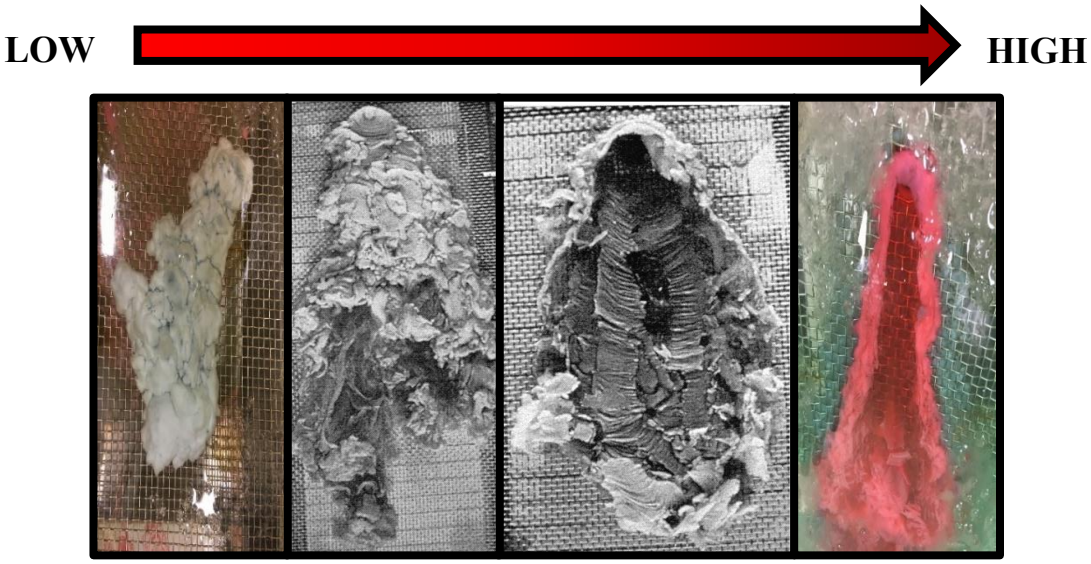

Figure 6: Four primary morphologies observed by Fink and Griffiths [1990] and their relation to Ψ. A fifth morphology (No Crust, not pictured here) was observed beyond Levees and may be appropriate to some systems. Approximate Ψ value ranges of morphologies observed in our experiments are as follows: Pillows (≤2); Rifts (4 – 12); Folds (15 – 29); Levees (34 – 54); No Crust (>55). Values in-between frequently result in transition morphologies, defined here as morphologies that form contemporaneously. Blurriness in colorized lab images due to ice. Image adapted from Fink and Griffiths [1990]. New, colorized experiments were conducted by the author.

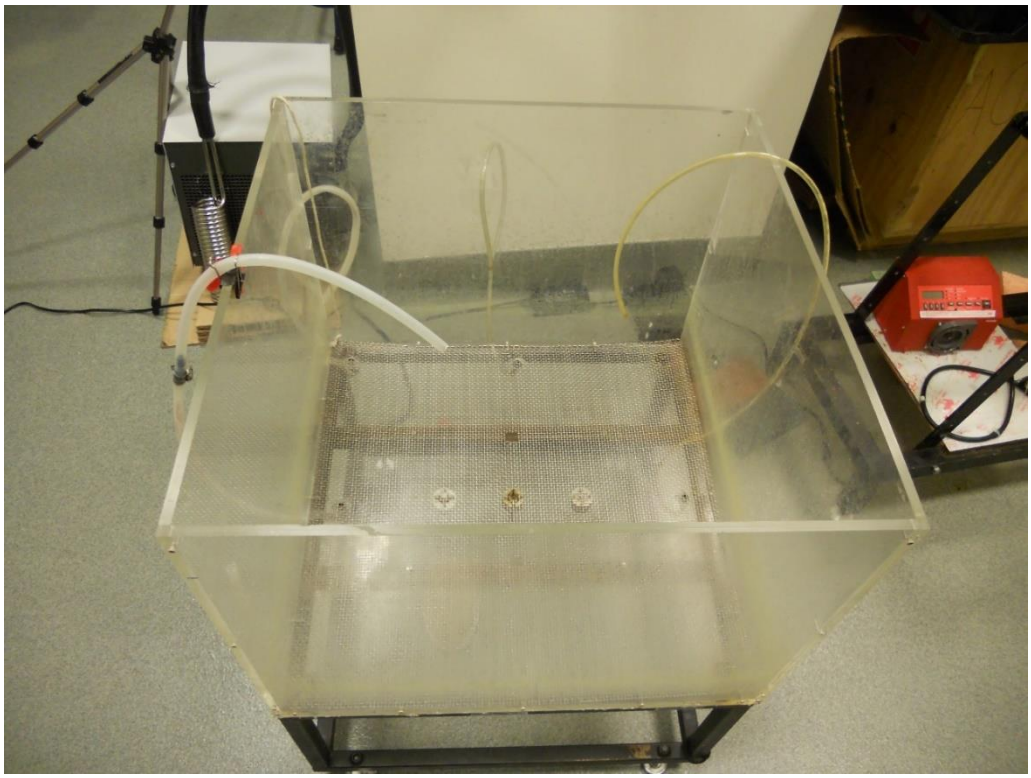

Figure 7: Tank used to perform experiments in conditions 1 – 4. Tank measures 60 x 60 cm. A 4 mm spaced steel mesh at the bottom of the tank prevents slip conditions. Hole in the center of the tank represents the vent and the epicenter of the eruption.

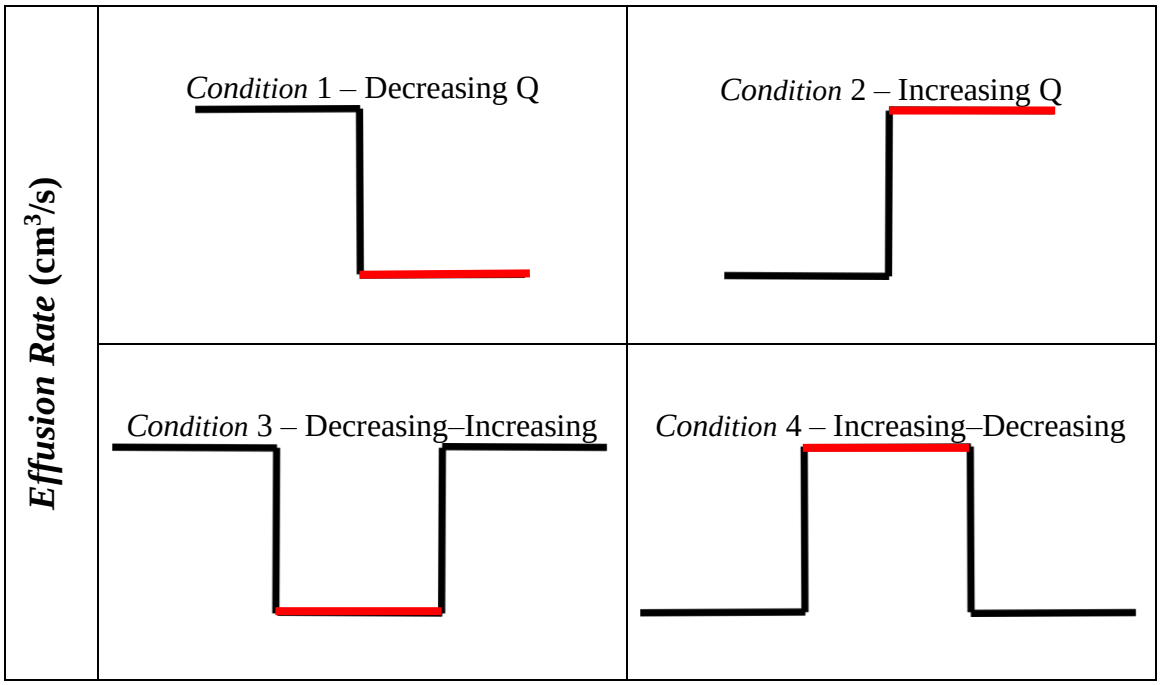

Figure 8: The experimental design consists of four conditions corresponding to decreasing (waning), increasing (waxing), decreasing-increasing (waning-waxing), and increasing-decreasing (waxing-waning) eruption rates. Red bars denote pulse during the experimental run. For conditions 1 and 2, the pulse duration was either 10 or 50 seconds. For conditions 3 and 4, the pulse duration was 50 seconds. During the initial stages of Conditions 1 & 2, 250 mL was erupted, while the amount erupted during the pulse was controlled by Q and pulse duration. During the initial and final stages of Conditions 3 & 4, 200 mL of wax was erupted, while the amount erupted during the pulse was controlled by pulse duration and Q.

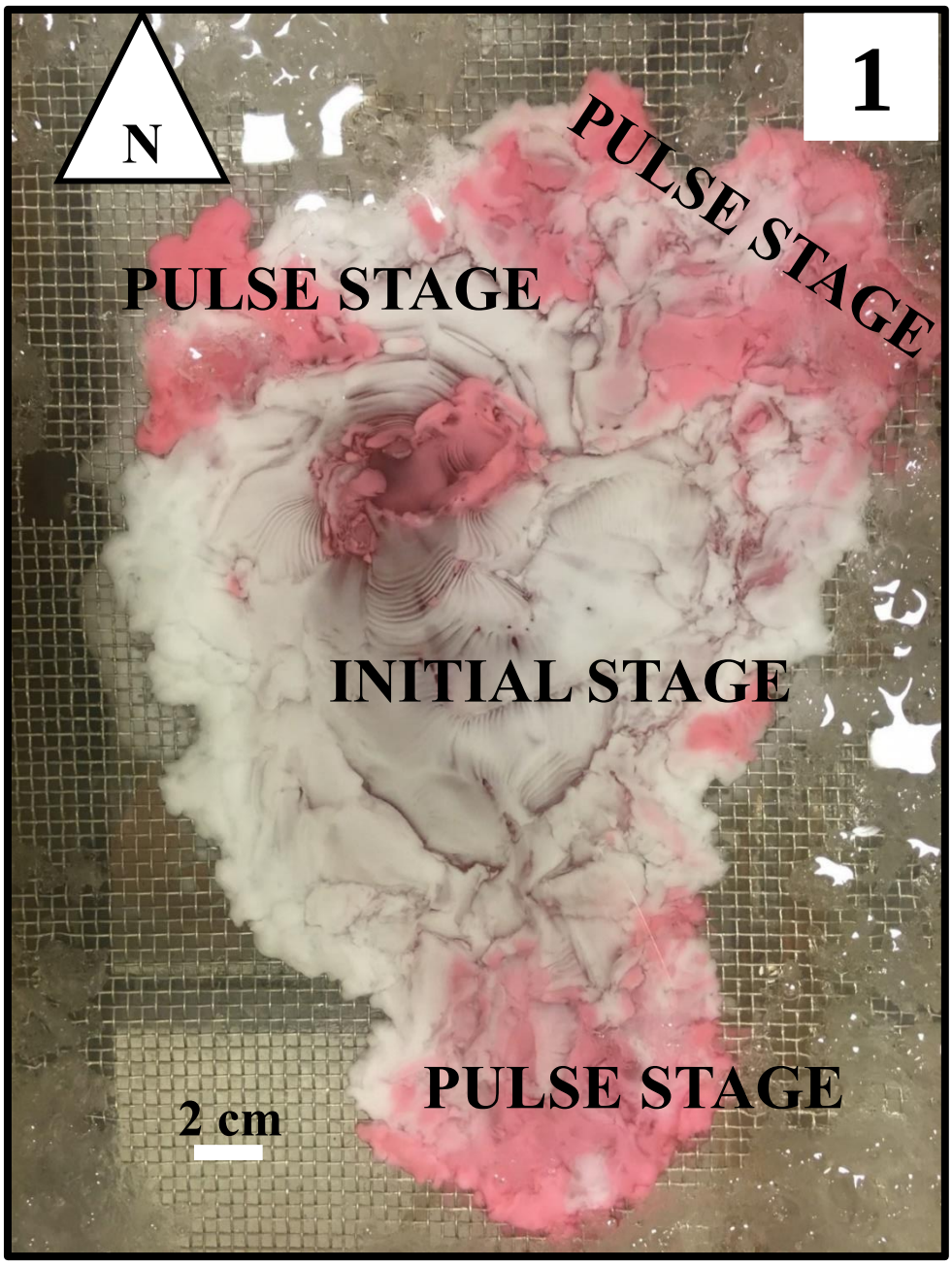
N
1
PULSE STAGE
PULSE STAGE
INITIAL STAGE
PULSE STAGE
2 cm

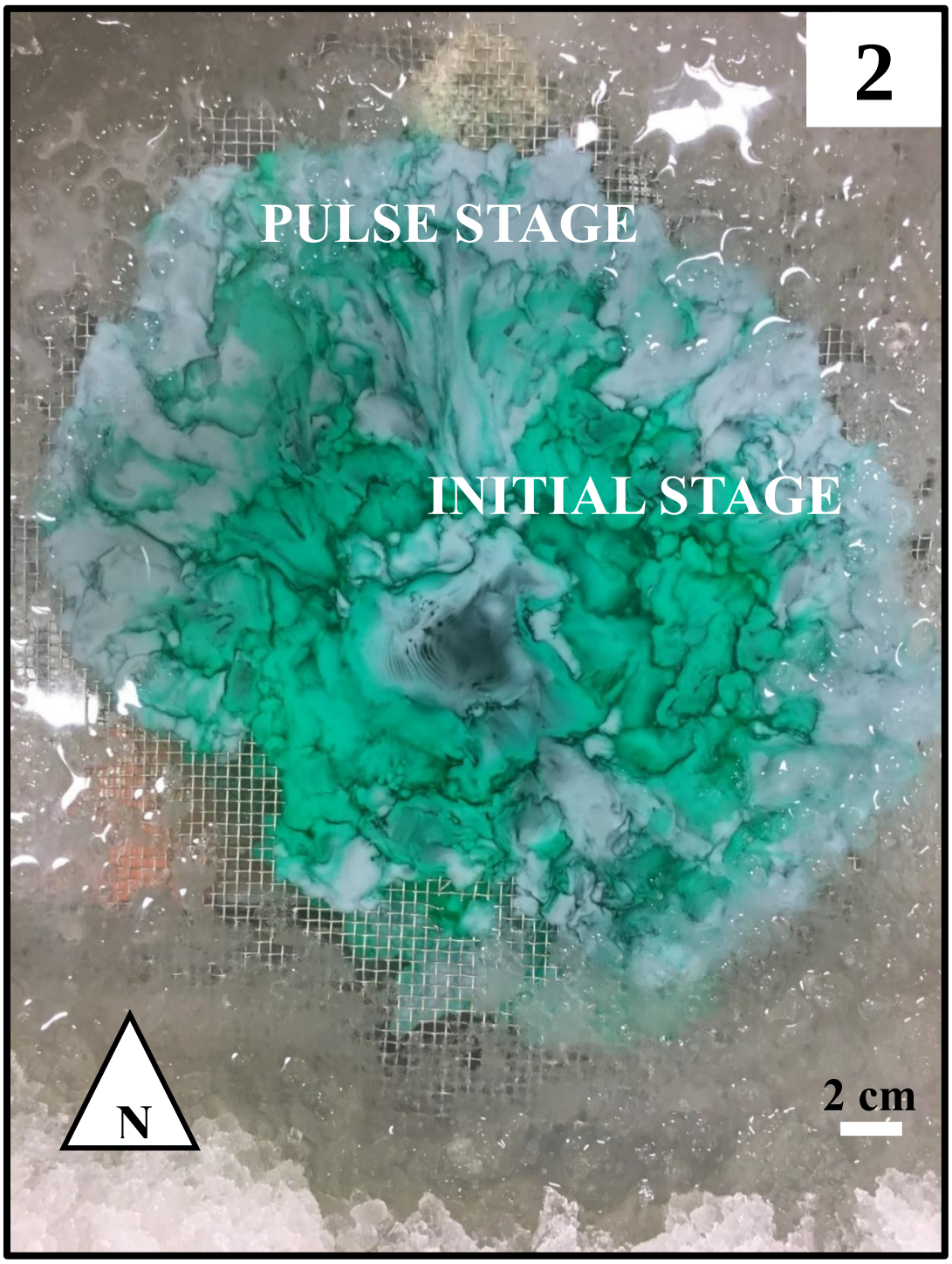
2
PULSE STAGE
INITIAL STAGE
N
2 cm

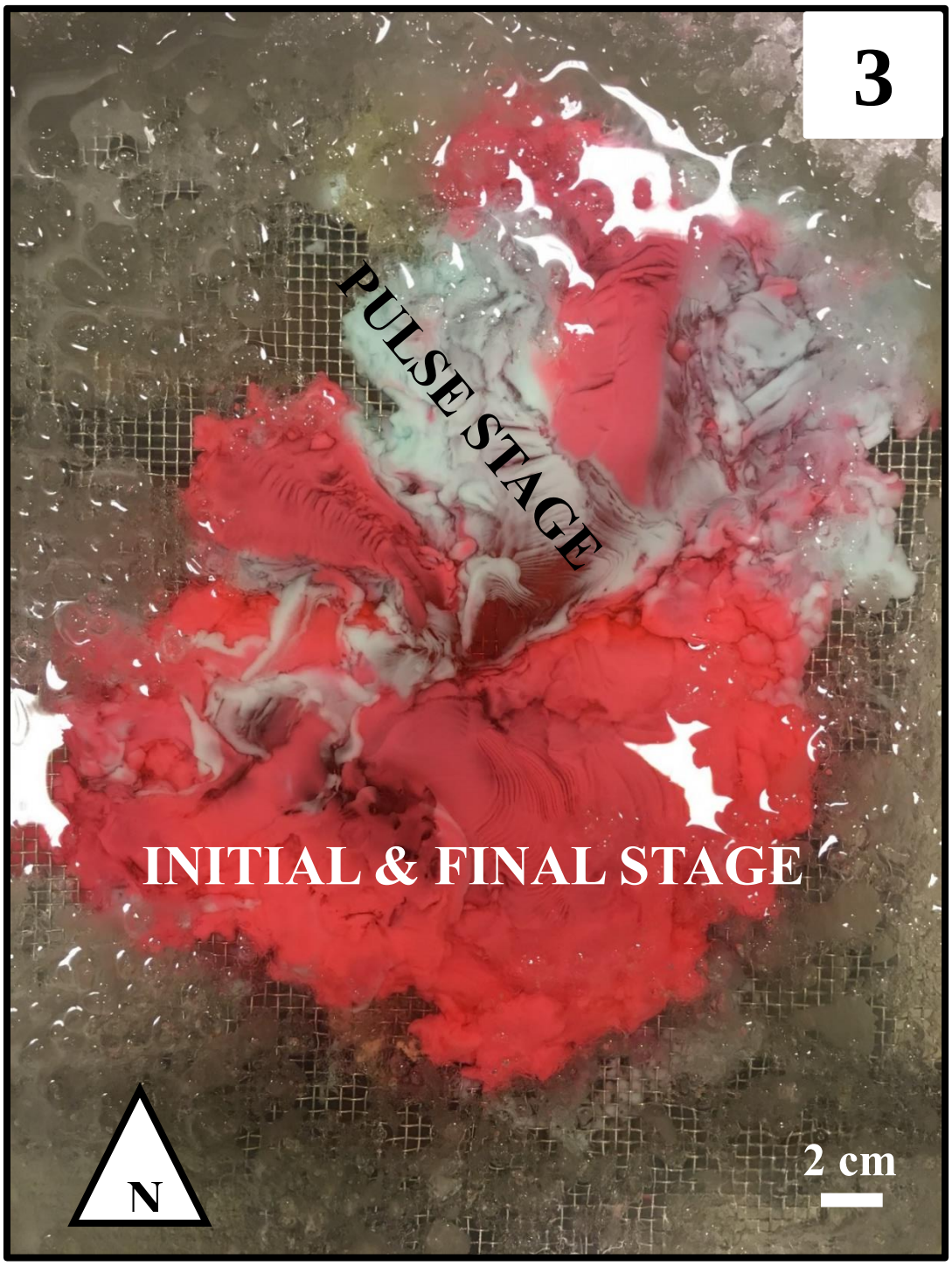
3
PULSE STAGE
INITIAL & FINAL STAGE
N
2 cm

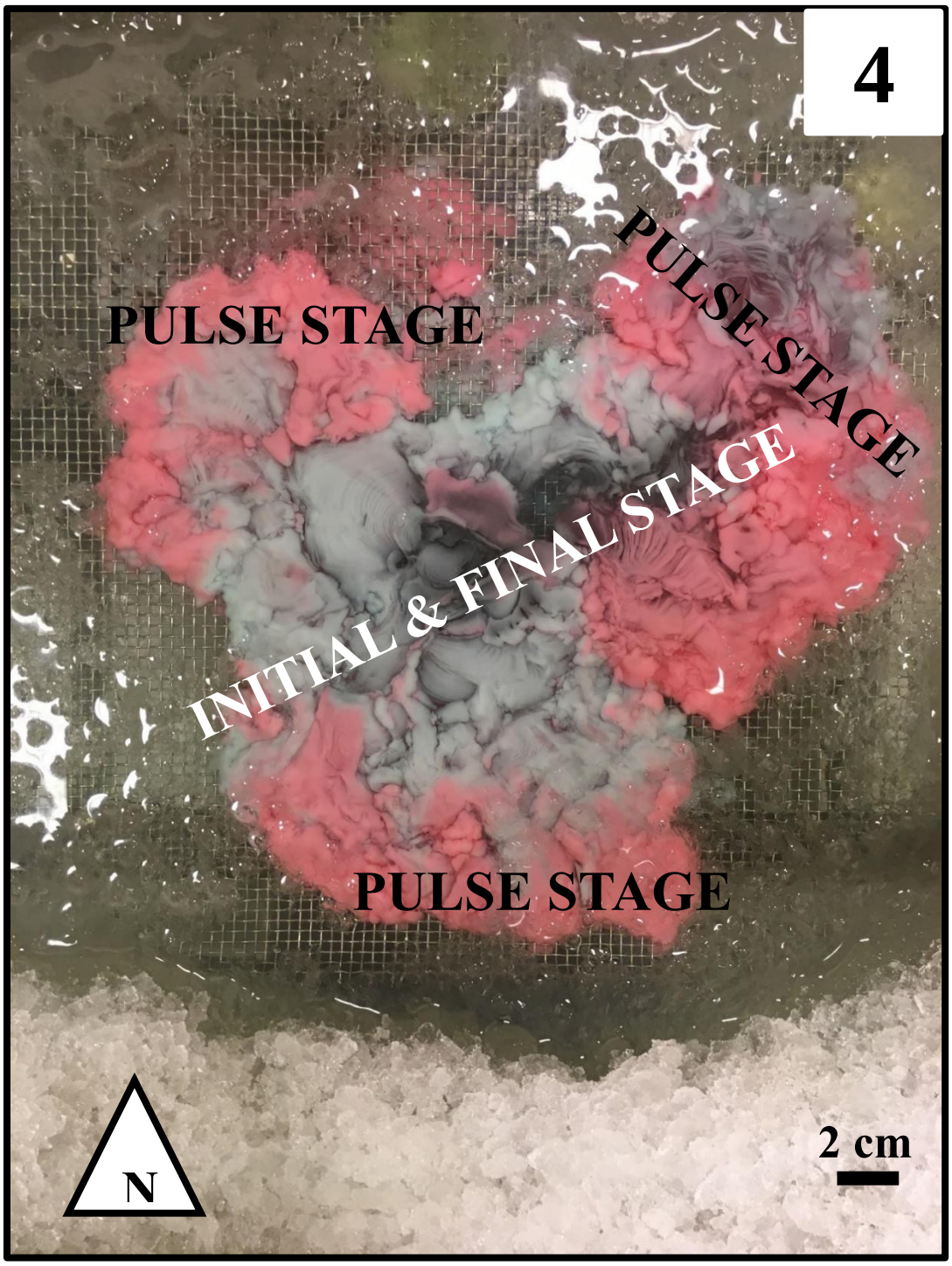

Figure 9: (1) An example of a flow produced in condition 1**.** $\Psi = 21$. Light blue wax represents wax erupted during the initial stage of the eruption. Red wax represents wax that erupted during the pulse. Note the 4 major, discreet breakout locations. Three of those breakouts originated at the flow margin, while one occurred near the vent. Most of the wax

erupted during the pulse traveled beneath the crust to the flow margin. Note: a small fraction of the pulse wax ruptured the crust near the vent and resurfaced the flow. **(2):** An example of a Condition 2 experiment. $\Psi = 21$. Green wax represents initial stage of the eruption. Light blue wax was erupted during a 50-second pulse. Flow measures 20 x 16 cm. Unlike the flow pictured for Condition 1, there are no discreet breakouts. Instead the wax erupted during the pulse has resulted in circumferential breakouts at the margin. This is the result of wholesale flow of the pulse wax beneath the crust to the flow margin. Note: a small fraction of the pulse wax ruptured the crust proximal to the vent and resurfaced the flow. **(3)** An example of a Condition 3 experiment. $\Psi = 21$. Red wax represents initial and final stages of the eruption. Light blue wax was erupted during a 50-second pulse. Flow measures 24 x 28 cm. Unlike conditions 1 and 2, the flows produced for condition 3 are more complex by design. Here, there has been a discreet marginal breakout at the northeastern edge of the flow. Resurfacing has also occurred across the southwestern portion of the flow, although it's harder to see because the wax is of the same color. The resurfacing occurred during the final stage of the eruption. **(4)** An example of a Condition 4 experiment. $\Psi = 21$. Light blue wax represents initial and final stages of the eruption. Red wax was erupted during a 50-second pulse. Flow measures 31 x 20 cm. Condition 4 flows are the largest and most complex. Here, we observe circumferential marginal breakouts that have morphed into seemingly discreet breakouts. Wholesale flow beneath the surface crust resulted into breakouts all around the margin of the flow, and gradually those breakouts coalesced into three discreet regions. Subsequent wax from the final stage of the eruption took advantage of the breakout pathway at the northeast corner of the flow.

Comparison in Emplacement Modes for Conditions 1 and 2

Condition 1	Condition 2
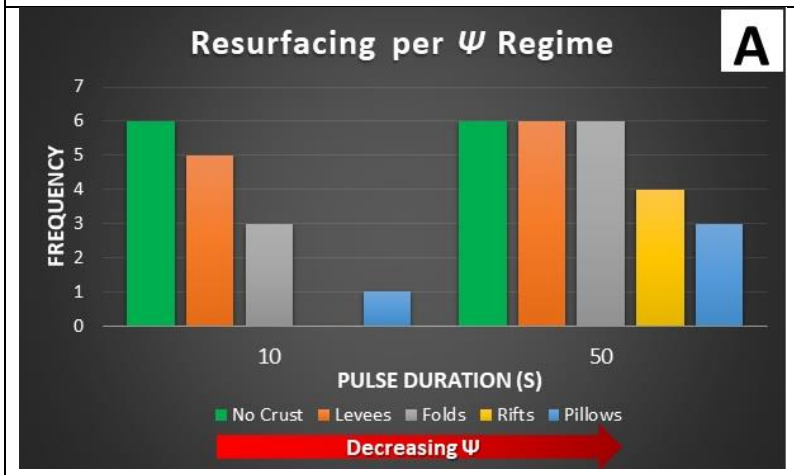	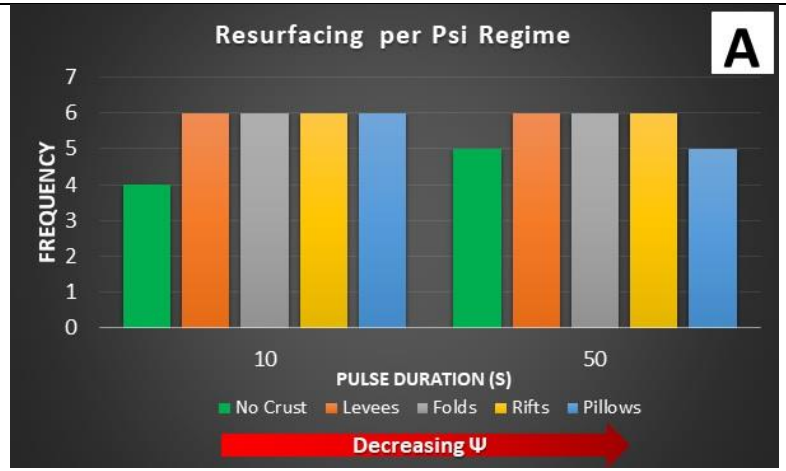
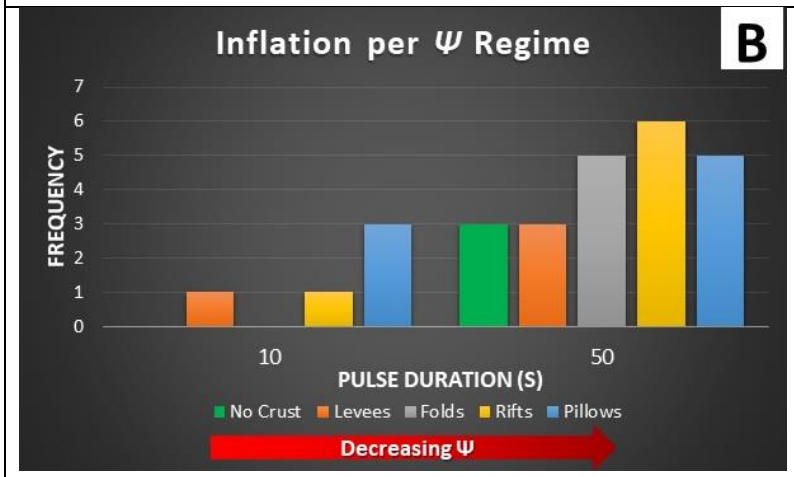	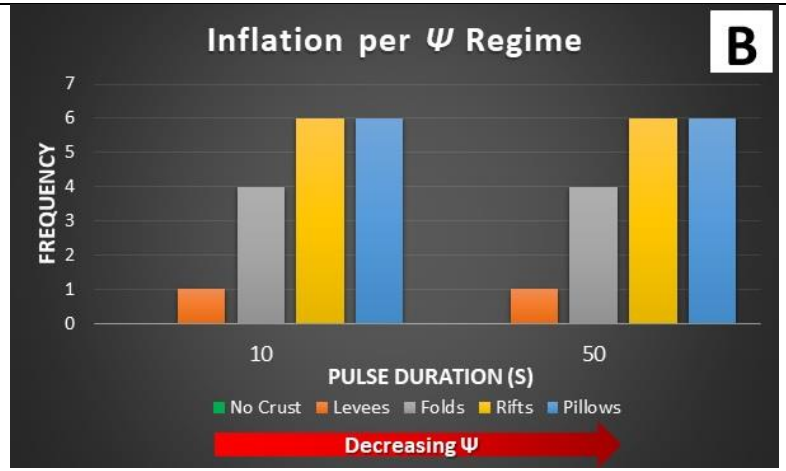

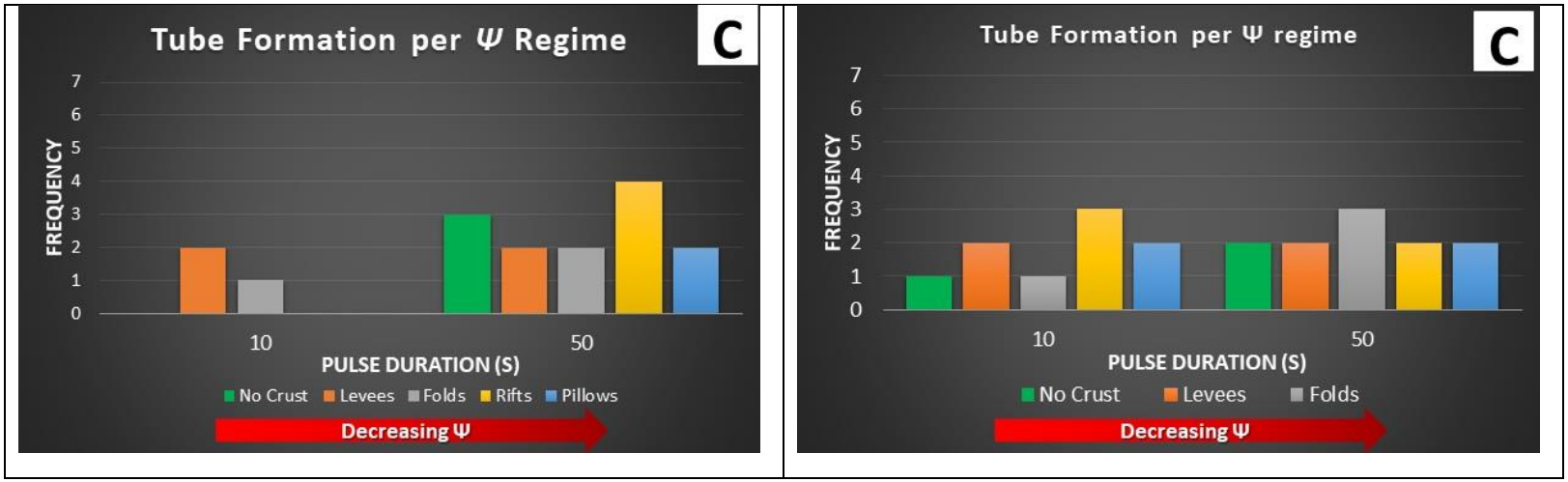

Figure 10: A comparison of the occurrence of Resurfacing, Inflation, and Tubes between conditions 1 and 2 are displayed for each Ψ regime as a function of pulse duration. **(a)** In condition 1, resurfacing – which frequently occurred –was dependent on Ψ and pulse duration. For condition 2, resurfacing had no dependence on pulse duration or Ψ morphology. **(b)** In condition 1, inflation was strongly dependent on the pulse duration and less so on Ψ morphology. For condition 2, inflation had no dependence on pulse duration, but was controlled by Ψ morphology. Inflation occurred more frequently for lower Ψ morphologies. **(c)** For condition 1, tubes were the most difficult emplacement mode to produce. The formation of tubes was strongly dependent on pulse length. For shorter pulses, tubes are favored at intermediate Ψ values/regimes, although they occurred at a similar frequency for all regimes at longer pulse durations. In condition 2, at first glance, *tubes* appear to have some dependence on pulse duration but this could also be a dependence on Ψ morphology at shorter pulse durations. There seems to be some dependence on Ψ morphology, with tubes favoring intermediate Ψ values, which correspond with intermediate flow rates.

Comparison in the percent of final flow area resurfaced for conditions 1 and 2

Condition 1

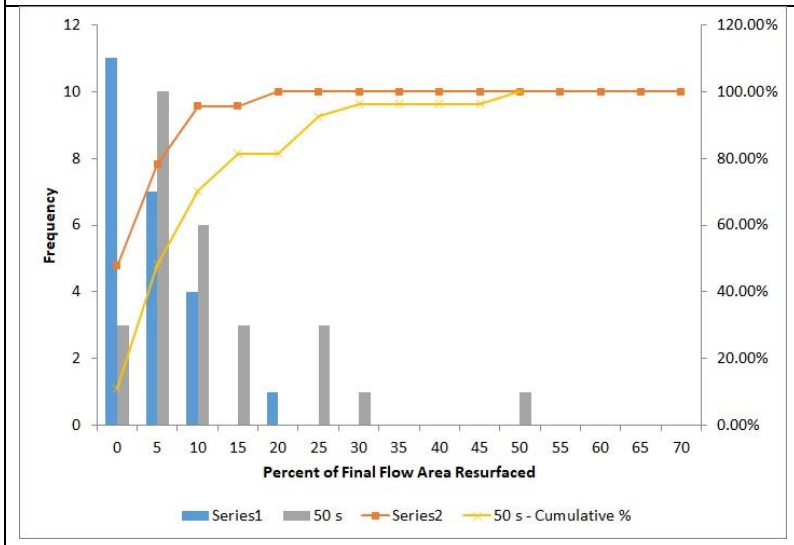

Condition 2

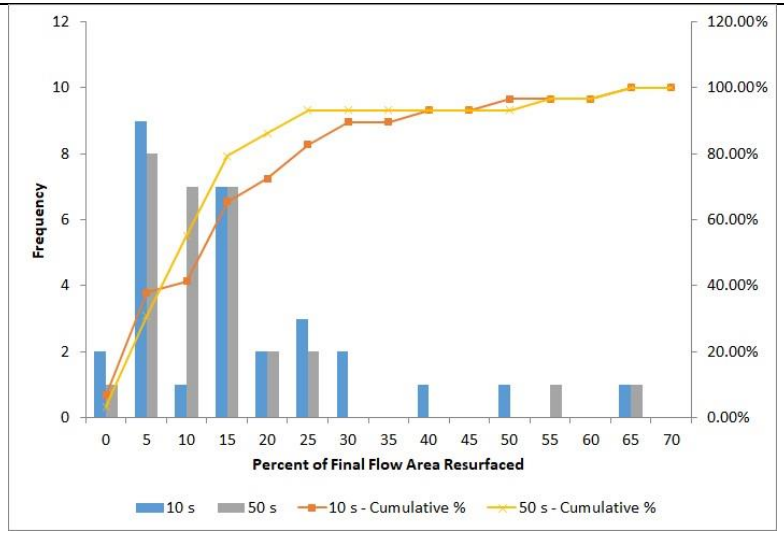

Figure 11: (Left) The percentage of final flow area covered by resurfacing is presented as a function of pulse duration for condition 1. Most flows where resurfacing is observed experience less than 20%. (Right) In condition 2, most flows – where present – experienced less than 20% of resurfacing.

Comparison of flow depth and flow area for conditions 1 and 2

Condition 1	Condition 2

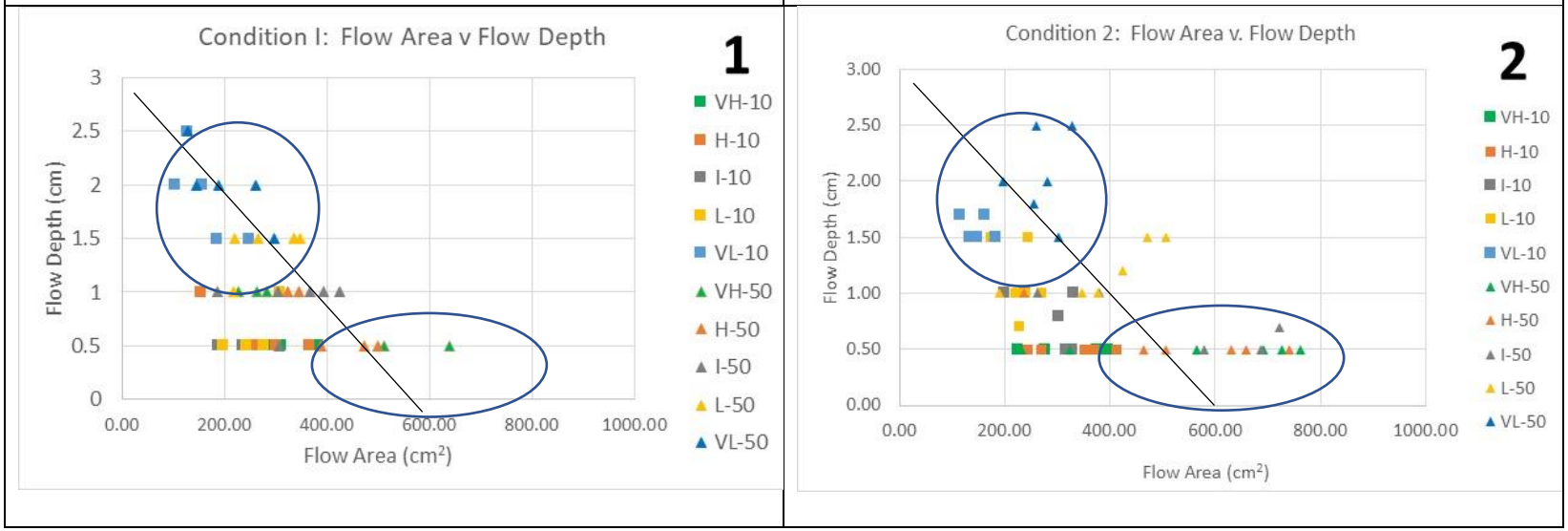

Figure 12: Letters in the legend indicate the magnitude of Ψ. Numbers in legend denote pulse duration in seconds. VH=very high; H=high; I = intermediate; L = Low; VL = very low. Trend lines highlight increase in flow area between conditions 1 and 2. Circles highlight populations in following discussion. **(1)** Longer pulse durations generally created larger flows, except at the lowest Ψ values. Higher Ψ values produced larger flows in general. There is an inverse relationship between flow depth and decreasing Ψ. In other words, lower Ψ values correspond to thicker flows. **(2)** Longer pulse durations created larger flows. Higher Ψ values produced larger flows in general. We observed an inverse relationship between flow depth and decreasing Ψ. In other words, lower Ψ values correspond to thicker flows.

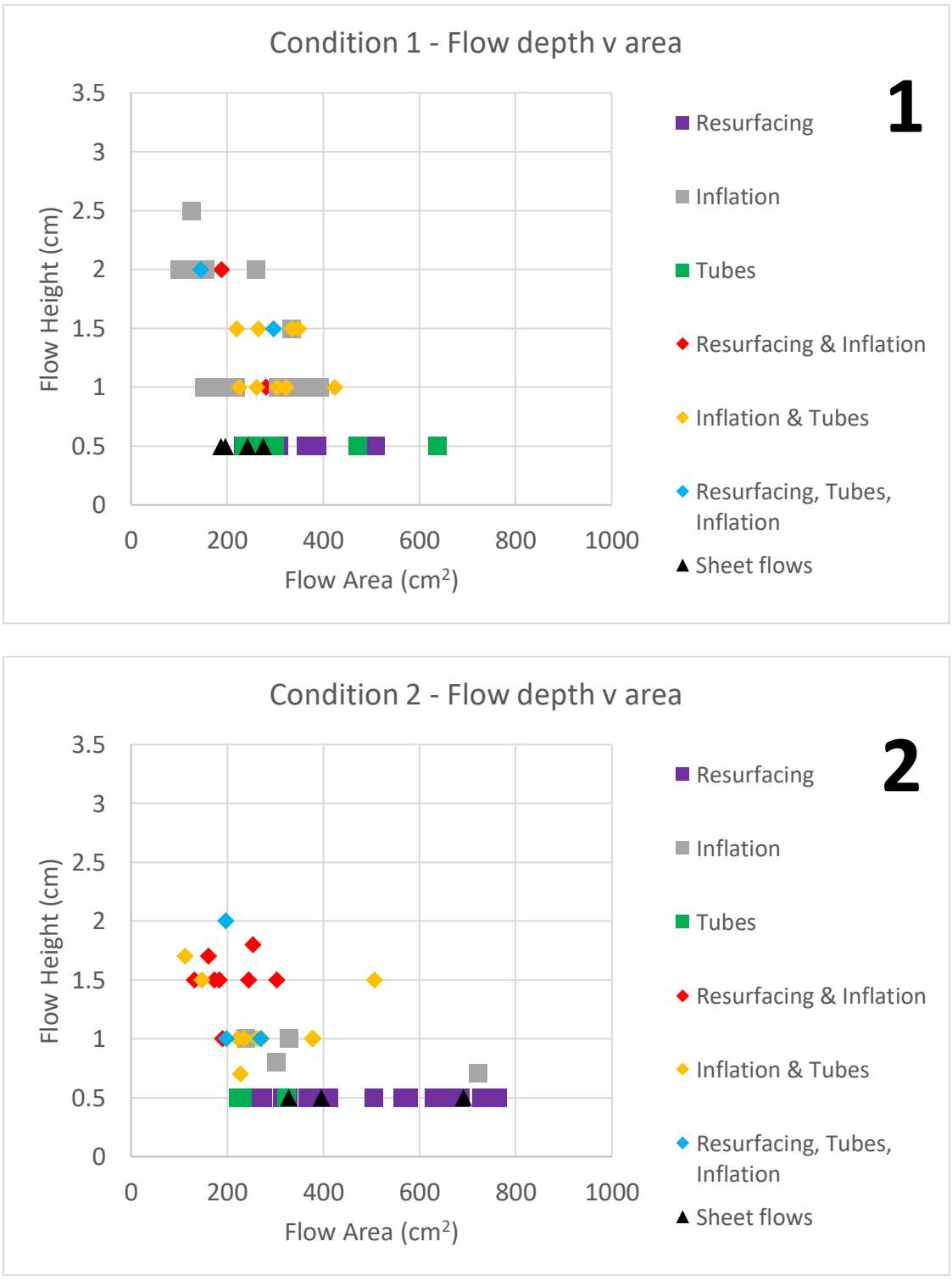

Figure 13: Slightly larger flow area for condition 2 likely reflects larger erupted volume. **(1)** The depth of a flow is dependent on the emplacement mode present. Flows displaying multiple modes of emplacement are the thickest and smallest in flow area. All

other singular emplacement modes occur in flows of standard depth. **(2)** Condition 2 flows are thinner relative to condition 1, although flows with multiple modes of emplacement are still the thickest.

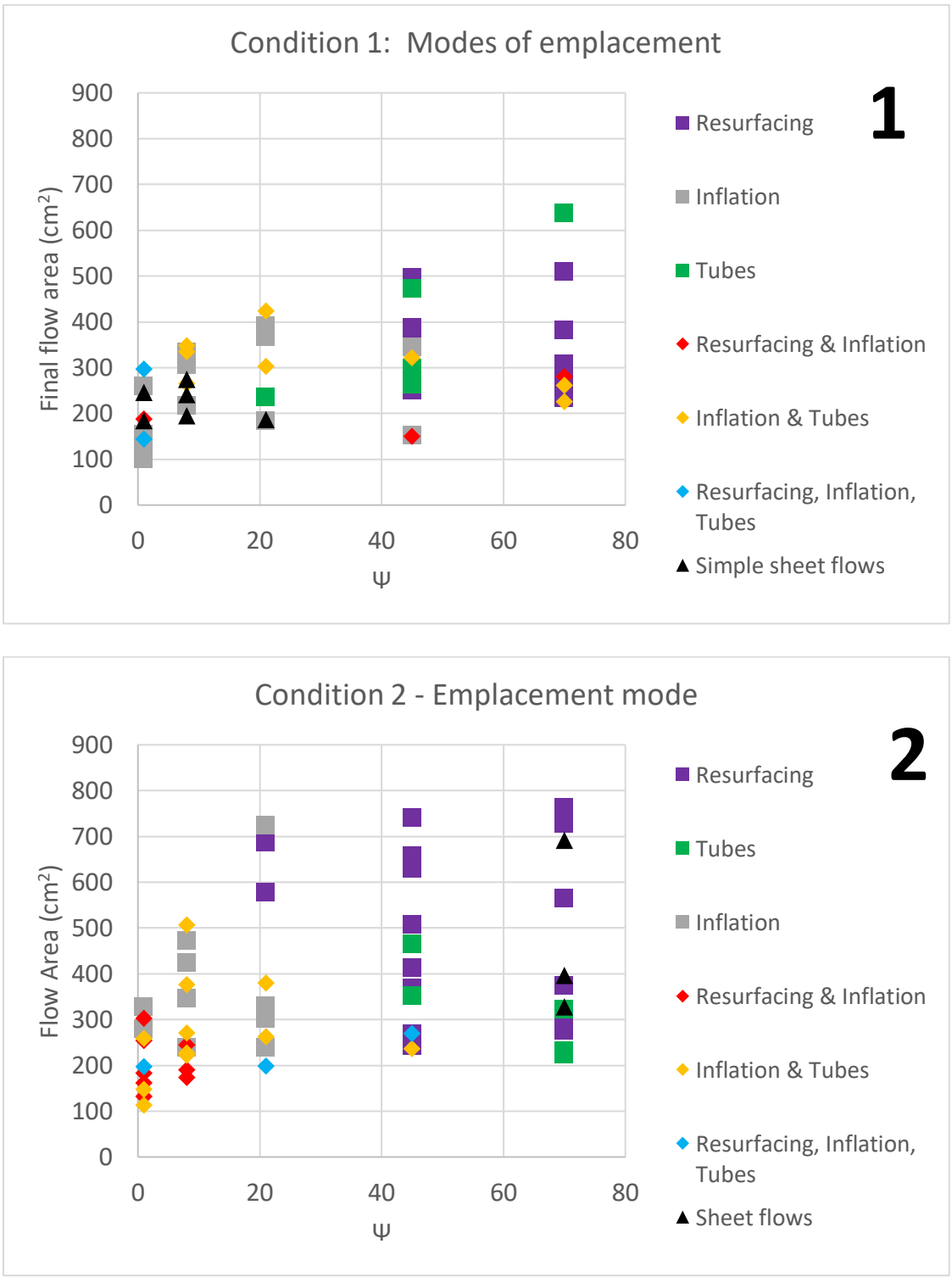

Figure 14: Flows with singular modes of emplacement have a dependence on Ψ in both conditions. Flows in condition 1 were smaller in area than those observed in condition 2 due in part to differences in erupted volumes. **(1)** Sheet flows and inflation occurred at low

Ψ regimes. Flows with tubes are present at intermediate and high Ψ. Flows with multiple modes of emplacement occur at lower to intermediate Ψ and display smaller areas. **(2)** Sheet flows and resurfacing occur at high Ψ, while inflation occurs at lower Ψ. Flows with only tubes occur at very high Ψ. More complex flows, with multiple modes of emplacement observed, occur at low to intermediate Ψ and display smaller areas.

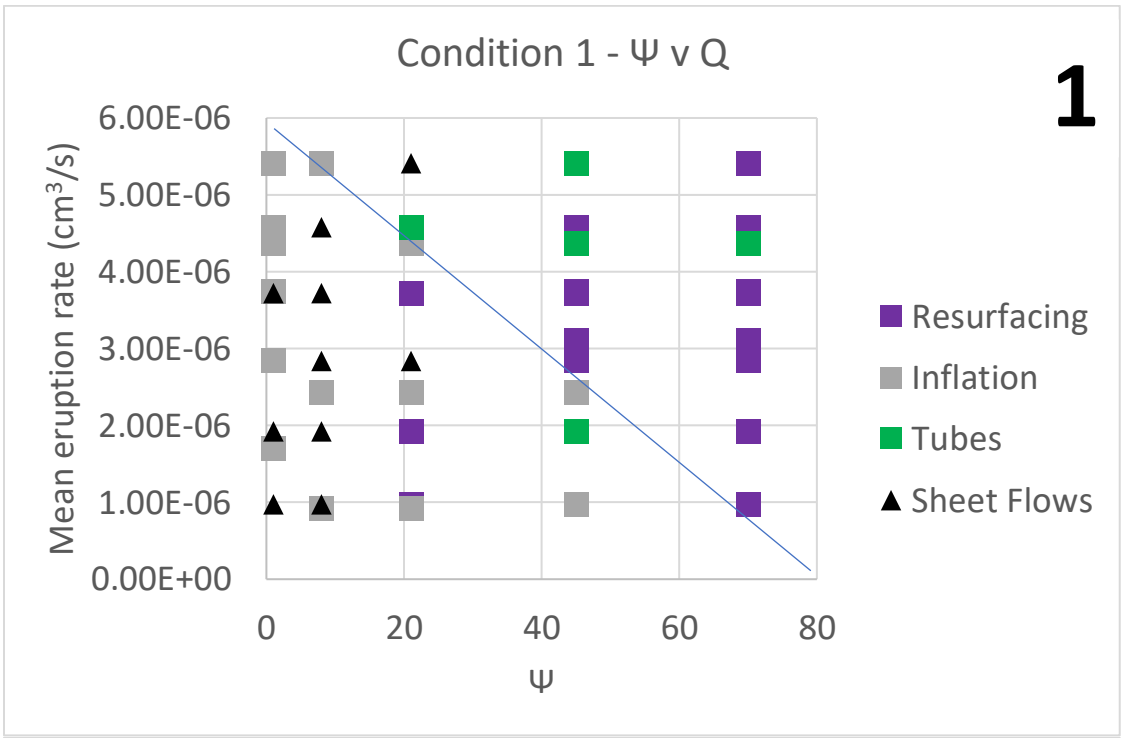
Condition 1 - Ψ v Q
1
Mean eruption rate (cm³/s)
6.00E-06
5.00E-06
4.00E-06
3.00E-06
2.00E-06
1.00E-06
0.00E+00
0
20
40
60
80
Ψ
Resurfacing
Inflation
Tubes
Sheet Flows

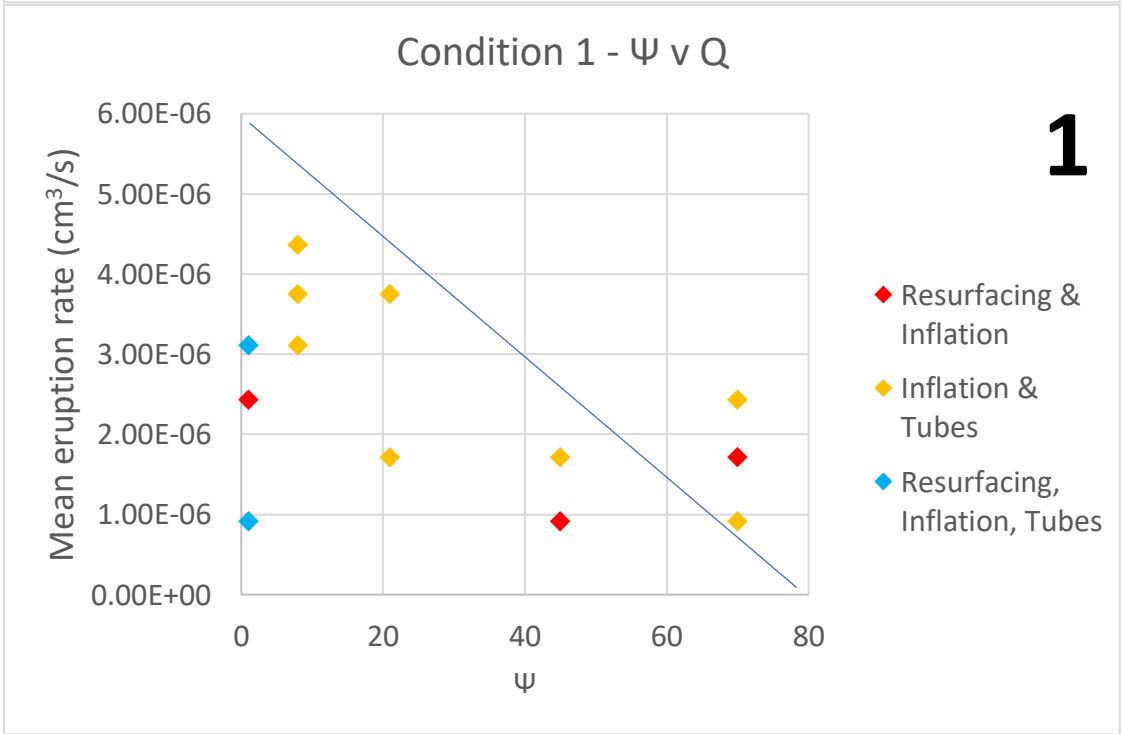
Condition 1 - Ψ v Q
1
Mean eruption rate (cm³/s)
6.00E-06
5.00E-06
4.00E-06
3.00E-06
2.00E-06
1.00E-06
0.00E+00
0
20
40
60
80
Ψ
Resurfacing & Inflation
Inflation & Tubes
Resurfacing, Inflation, Tubes

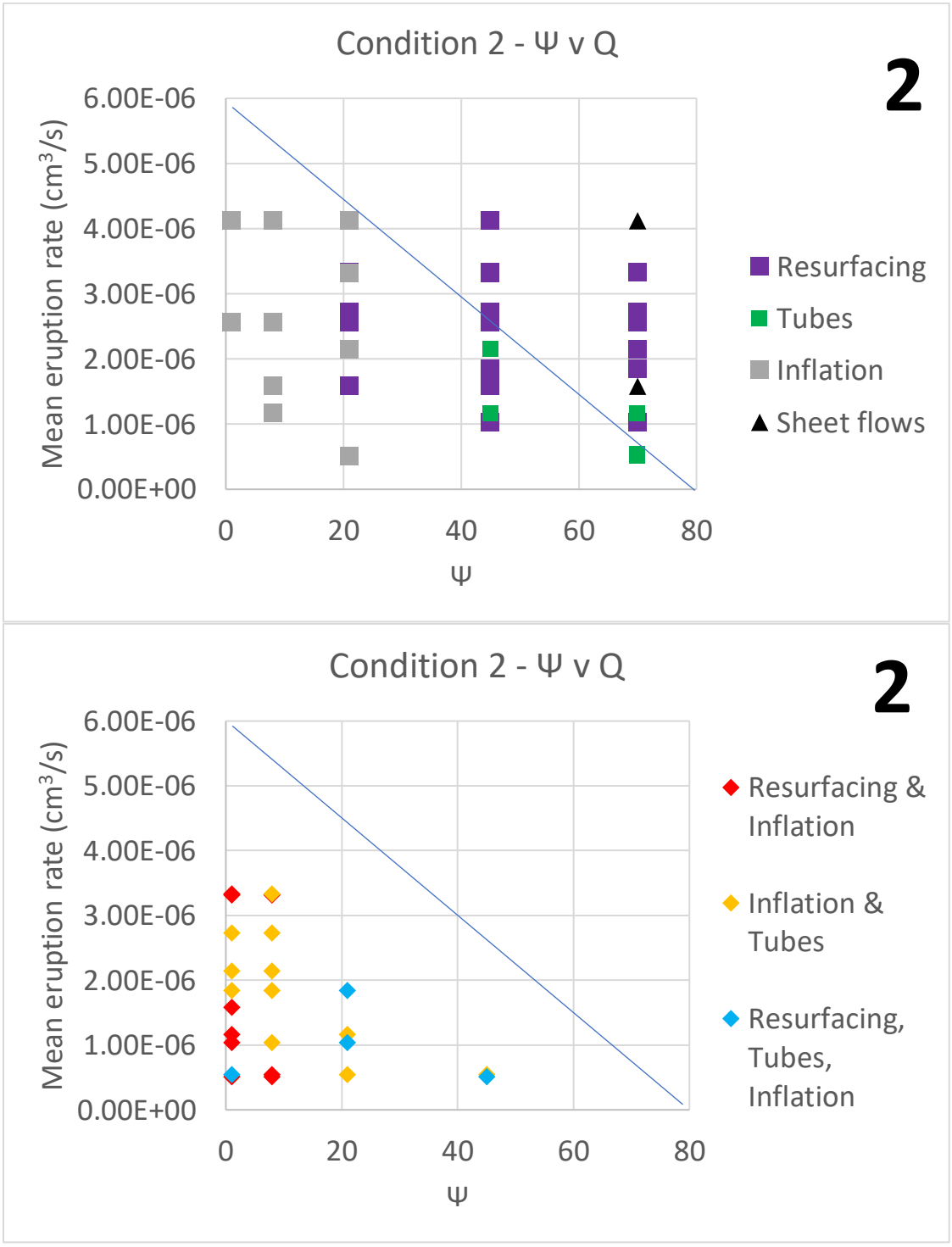

Figure 15: A divide – highlighted by the blue line – between the occurrence of modes of emplacement is evident in conditions 1 and 2. The mean eruption rate is provided on the Y-axis. **(1)** For condition 1, resurfacing and tubes occur primarily to the right of the blue line at higher Ψ and/or higher Q. Simple sheet flows and inflation occur primarily to the

left of the blue line at lower Ψ and/or lower eruption rates. Flows with multiple modes of emplacement in condition 1 tend to occur in the bottom left of the plot at lower to intermediate Ψ across a range of eruption rates. **(2)** For condition 2, resurfacing, sheet flows, and tubes occur to the right of the blue line at higher Ψ and/or mean eruption rate. The movement of the sheet flows is notable suggesting the increase in flow rate may be the cause. Flows demonstrating inflation are found to the left of the blue line at lower Ψ and/or lower eruption rates. In condition 2, flows with multiple modes of emplacement tend to occur at lower Ψ in the same zone dominated by flows displaying only inflation.

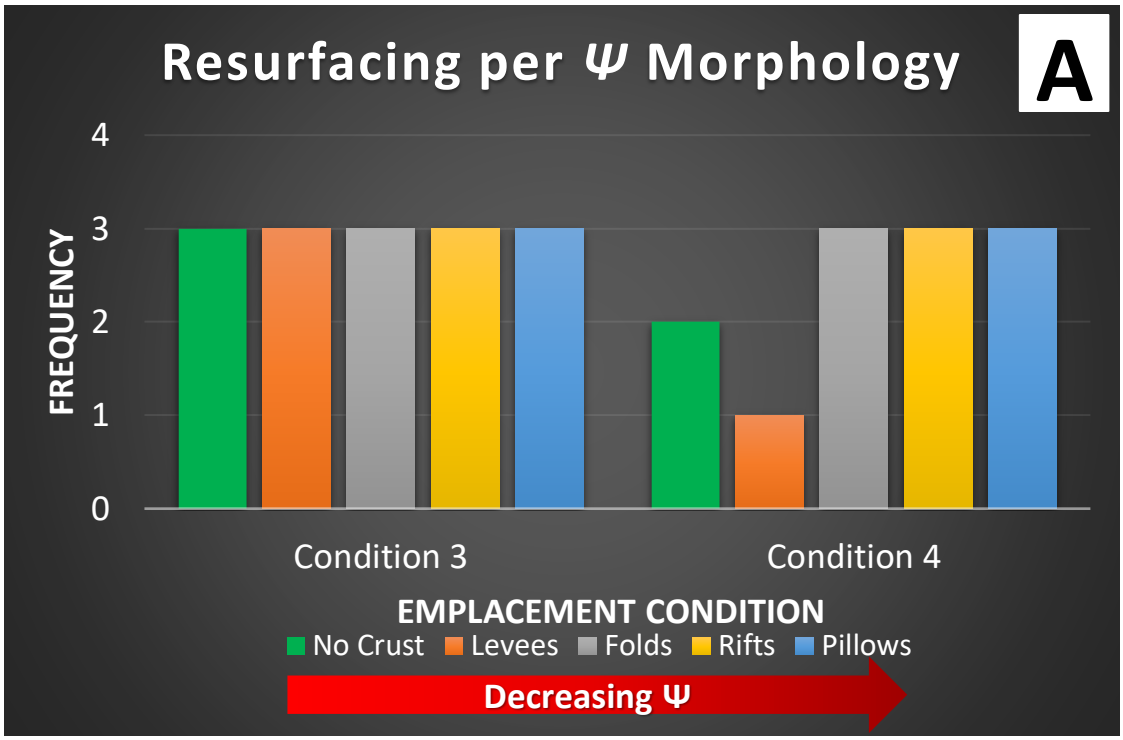
Resurfacing per Ψ Morphology
A
4
3
2
1
0
FREQUENCY
Condition 3
Condition 4
EMPLACEMENT CONDITION
No Crust
Levees
Folds
Rifts
Pillows
Decreasing Ψ

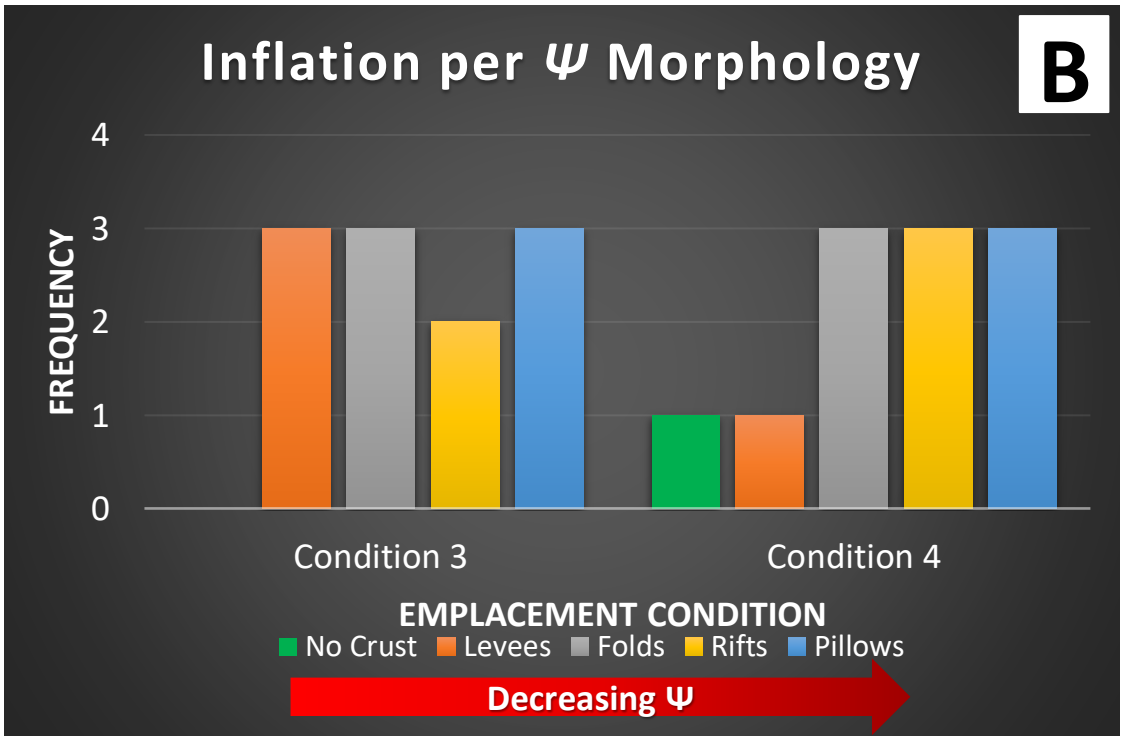
Inflation per Ψ Morphology
B
4
3
2
1
0
FREQUENCY
Condition 3
Condition 4
EMPLACEMENT CONDITION
No Crust
Levees
Folds
Rifts
Pillows
Decreasing Ψ

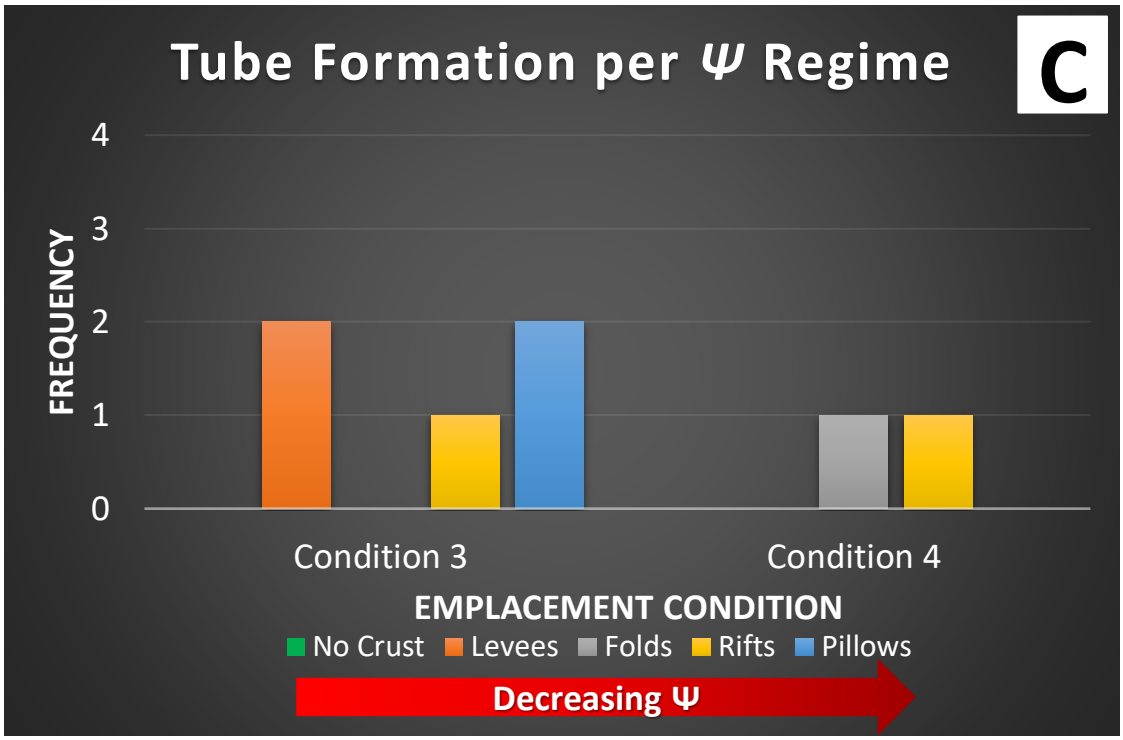
Tube Formation per Ψ Regime
C
4
3
2
1
0
FREQUENCY
Condition 3
Condition 4
EMPLACEMENT CONDITION
No Crust
Levees
Folds
Rifts
Pillows
Decreasing Ψ

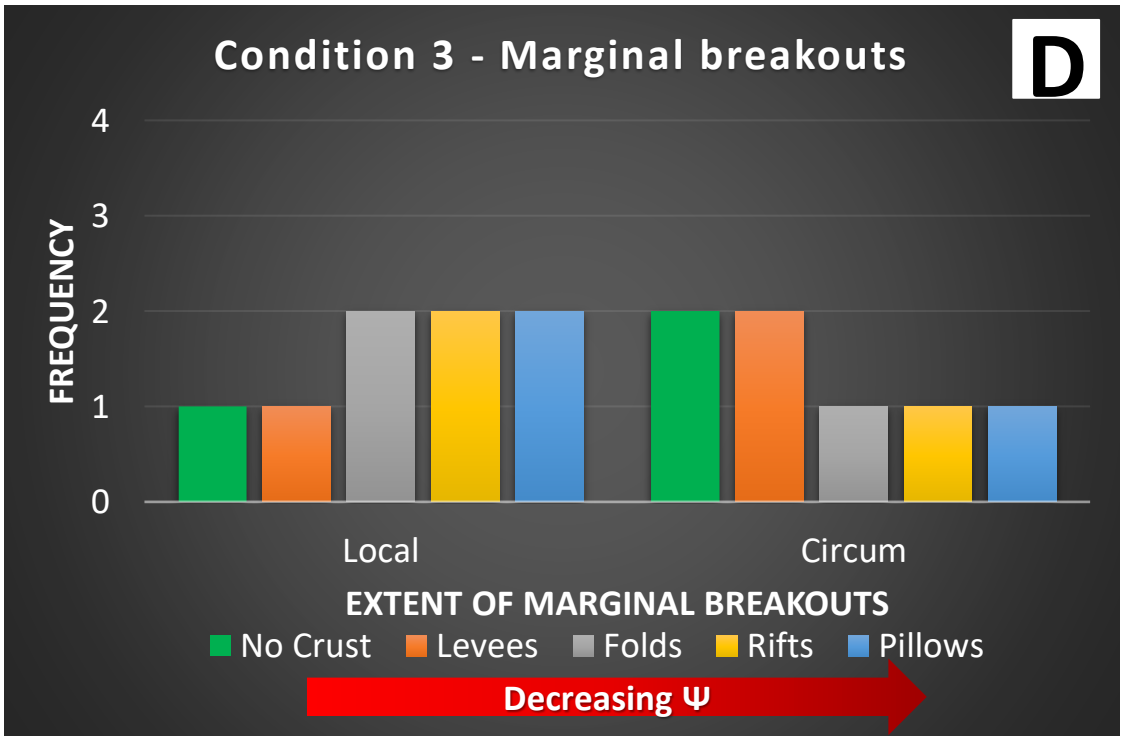
Condition 3 - Marginal breakouts
D
4
3
2
1
0
FREQUENCY
Local
Circum
EXTENT OF MARGINAL BREAKOUTS
No Crust
Levees
Folds
Rifts
Pillows
Decreasing Ψ

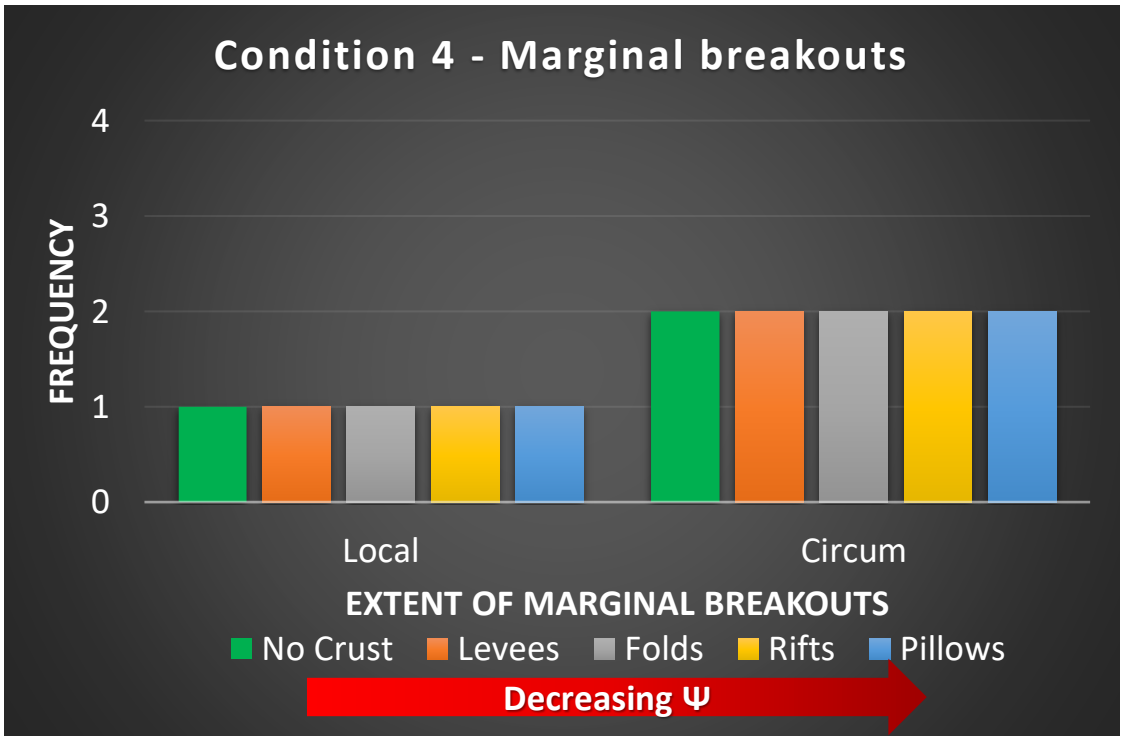

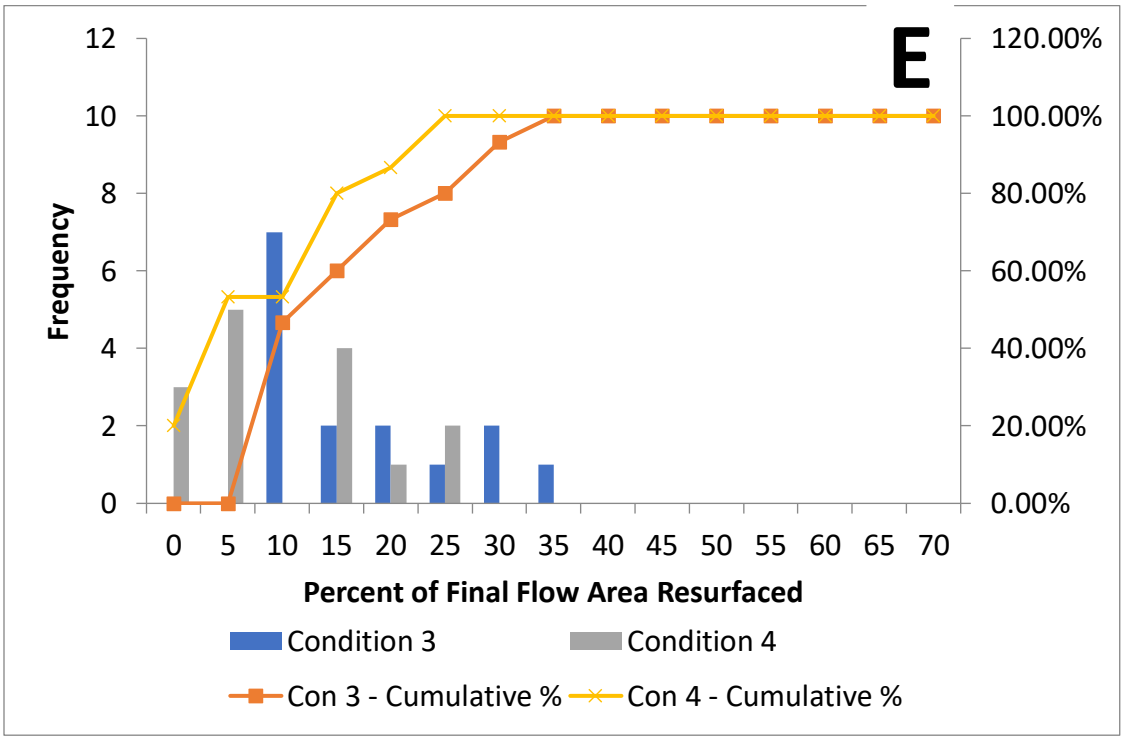

Figure 16: Note the Y-axes are different from the bar graphs for conditions 1 and 2 due to the lesser number of experiments performed for both condition 3 and condition 4. **(a)** *Resurfacing* had no dependence on Ψ morphology for condition 3; however, some

dependence at higher Ψ values for condition 4 is observed. **(b)** *Inflation* was controlled by Ψ morphology. For condition 3 this manifested in a lack of inflation observed at the highest Ψ regime. A slightly stronger dependence on Ψ was observed in condition 4. **(c)** *Tubes* appear to have a dependence on Ψ morphology, with tubes favoring intermediate to low Ψ values. There is a slight dependence on condition as well, with tubes slightly less common in condition 4. **(d)** Marginal breakouts as a function of conditions 3 and 4. Dependence on Ψ is observed in condition 3, but not in condition 4. **(e)** Greater percentages of final flow area are resurfaced in conditions 3 and 4 due to the duration of the experiments and the volume of erupted wax.

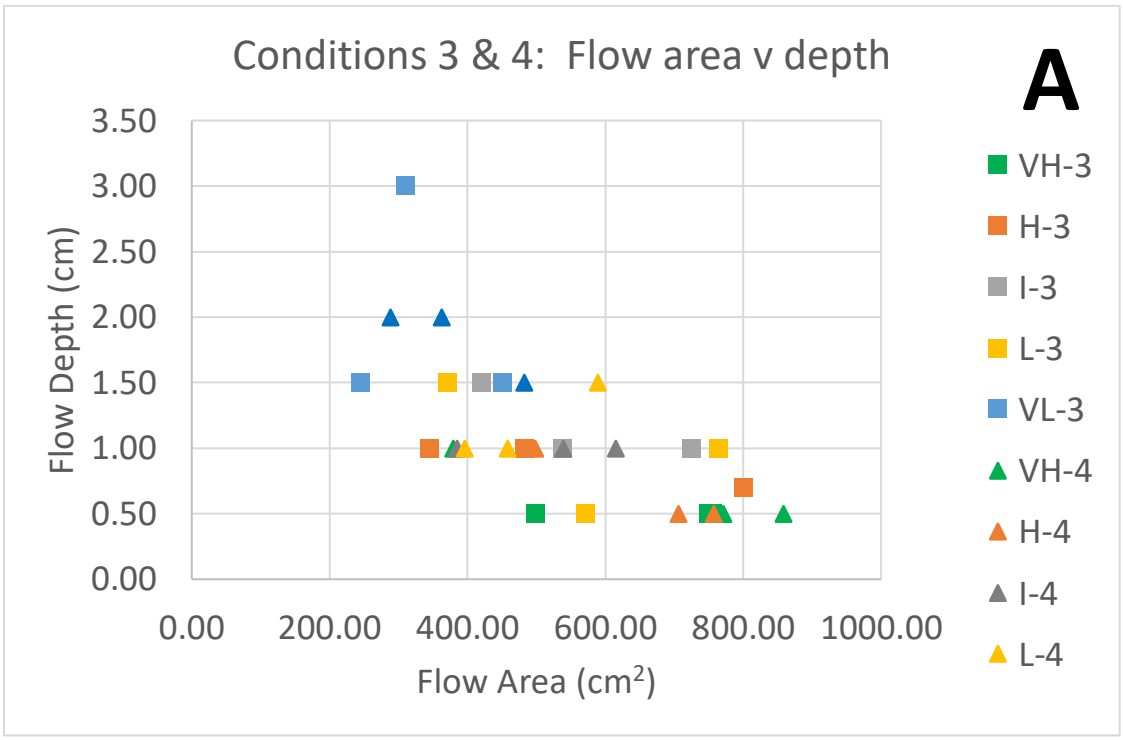
Conditions 3 & 4: Flow area v depth
A
Flow Depth (cm)
3.50
3.00
2.50
2.00
1.50
1.00
0.50
0.00
0.00
200.00
400.00
600.00
800.00
1000.00
Flow Area (cm²)
VH-3
H-3
I-3
L-3
VL-3
VH-4
H-4
I-4
L-4

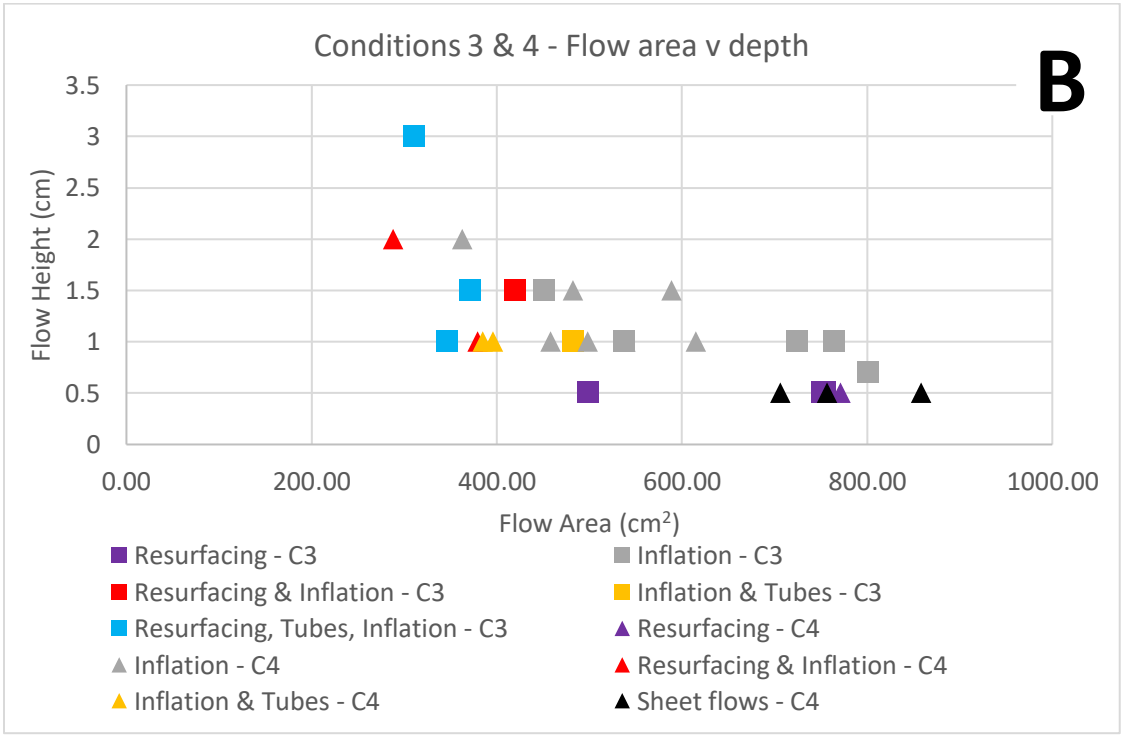
Conditions 3 & 4 - Flow area v depth
B
Flow Height (cm)
3.5
3
2.5
2
1.5
1
0.5
0
0.00
200.00
400.00
600.00
800.00
1000.00
Flow Area (cm²)
Resurfacing - C3
Inflation - C3
Resurfacing & Inflation - C3
Inflation & Tubes - C3
Resurfacing, Tubes, Inflation - C3
Resurfacing - C4
Inflation - C4
Resurfacing & Inflation - C4
Inflation & Tubes - C4
Sheet flows - C4

Figure 17: (a) Flow areas were larger for conditions 3 & 4 due to the longer length of the eruption. Flow area, however, was primarily controlled by Ψ, with lower values corresponding to smaller flows. Flow depth was also controlled by Ψ, with lower values corresponding to thicker flows. At higher Ψ values, condition 3 produced slightly larger flow areas. VH= very high; H=high; I=intermediate; L=low; VL= very low; all refer to the Ψ value. **(b)** Flows displaying multiple modes of emplacement are smaller in area and thicker. Flows displaying only resurfacing along with simple sheet flows are generally larger in area and thinner.

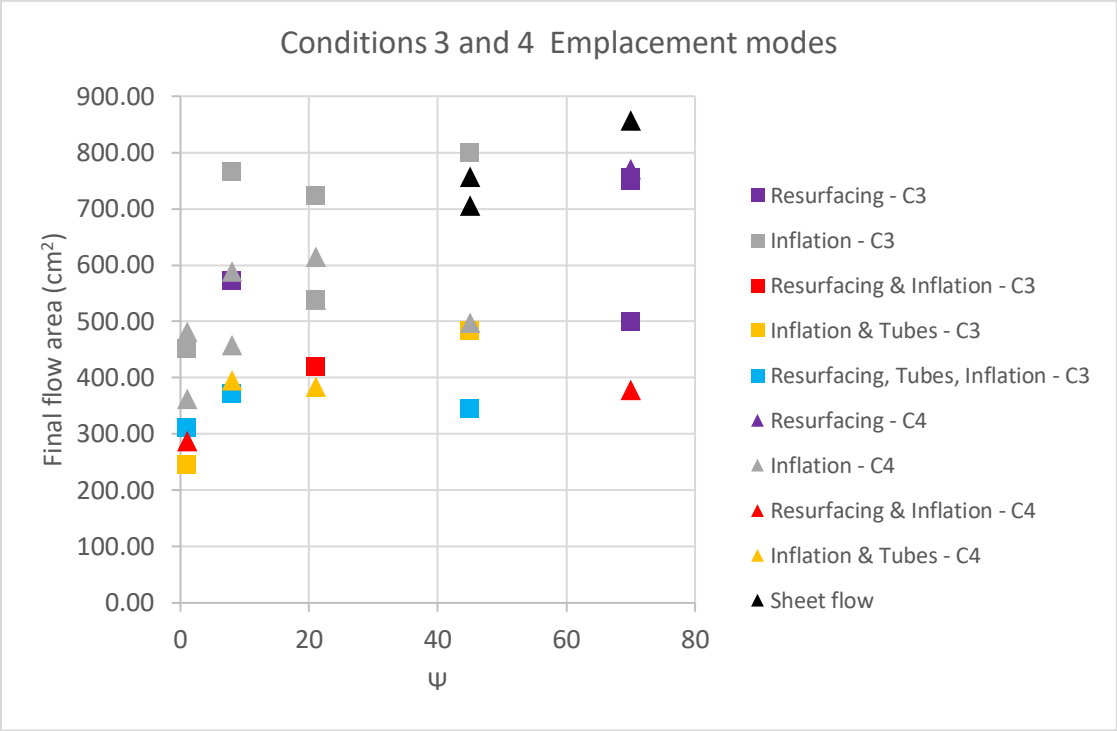

Figure 18: The flows in condition 3 and 4 are larger in flow area than those in conditions 1 and 2 primarily due to the larger erupted volume. Flows with singular modes of emplacement have a dependence on Ψ in both conditions. Flow area does not vary dramatically between conditions 3 and 4. Sheet flows and resurfacing occur at higher Ψ values, while flows displaying only inflation occur primarily at low to intermediate Ψ values. Flows with multiple modes of emplacement display smaller areas across the range of Ψ values.

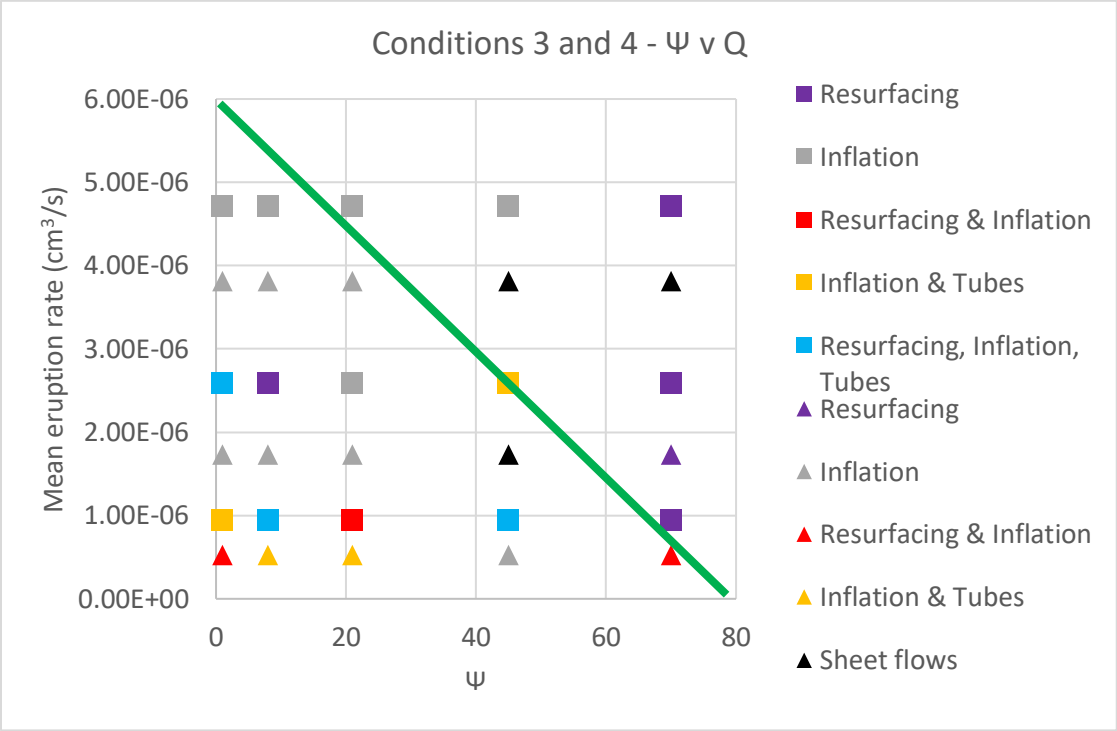

Figure 19: Emplacement mode for conditions 3 and 4 as a function of eruption rate and Ψ. Squares denote condition 3, while triangles denote condition 4. The green line indicates the degree of flow complexity – with flows displaying inflation or multiple modes of emplacement primarily to the left of the line and resurfacing and simple sheet flows to the right of the line. Flows displaying multiple emplacement modes occur at lower mean eruption rates and/or lower Ψ values. Resurfacing and inflation have a dependence on Ψ, with resurfacing occurring primarily at high Ψ and resurfacing at lower Ψ.

APPENDIX C

CHAPTER 3 FIGURES

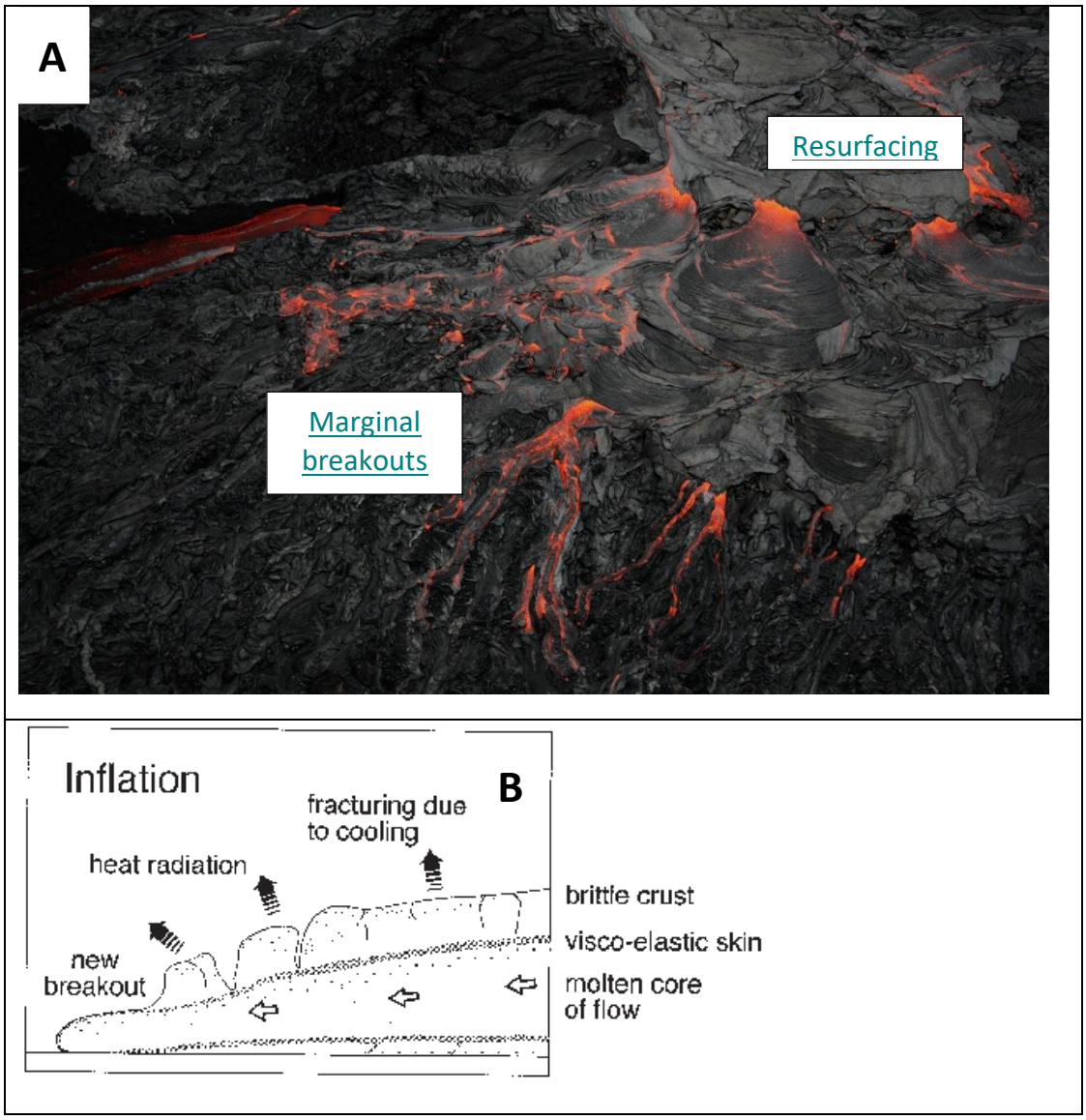
A
Resurfacing
Marginal breakouts
Inflation
B
fracturing due to cooling
heat radiation
new breakout
brittle crust
visco-elastic skin
molten core of flow

Figure 1: An example of the three modes of emplacement observed. (a) An example of resurfacing and marginal breakouts in a lava flow on Hawai'i. Image source: Wikimedia commons. (b) Inflation diagram from Self et al., 1996. (c) Lava tube photo features a lava tube in the Mojave National Preserve, California. Image credit: John Fowler via Wikimedia commons.

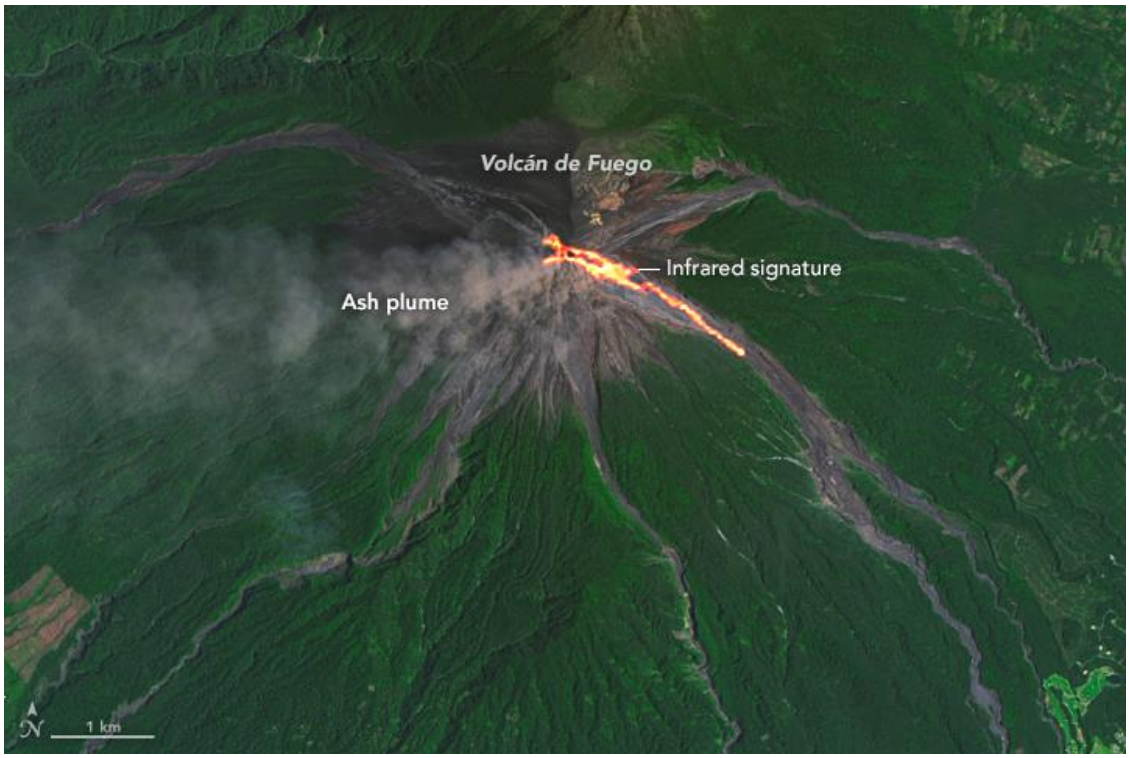

Figure 2: Examples of lava flows emplaced on slopes.

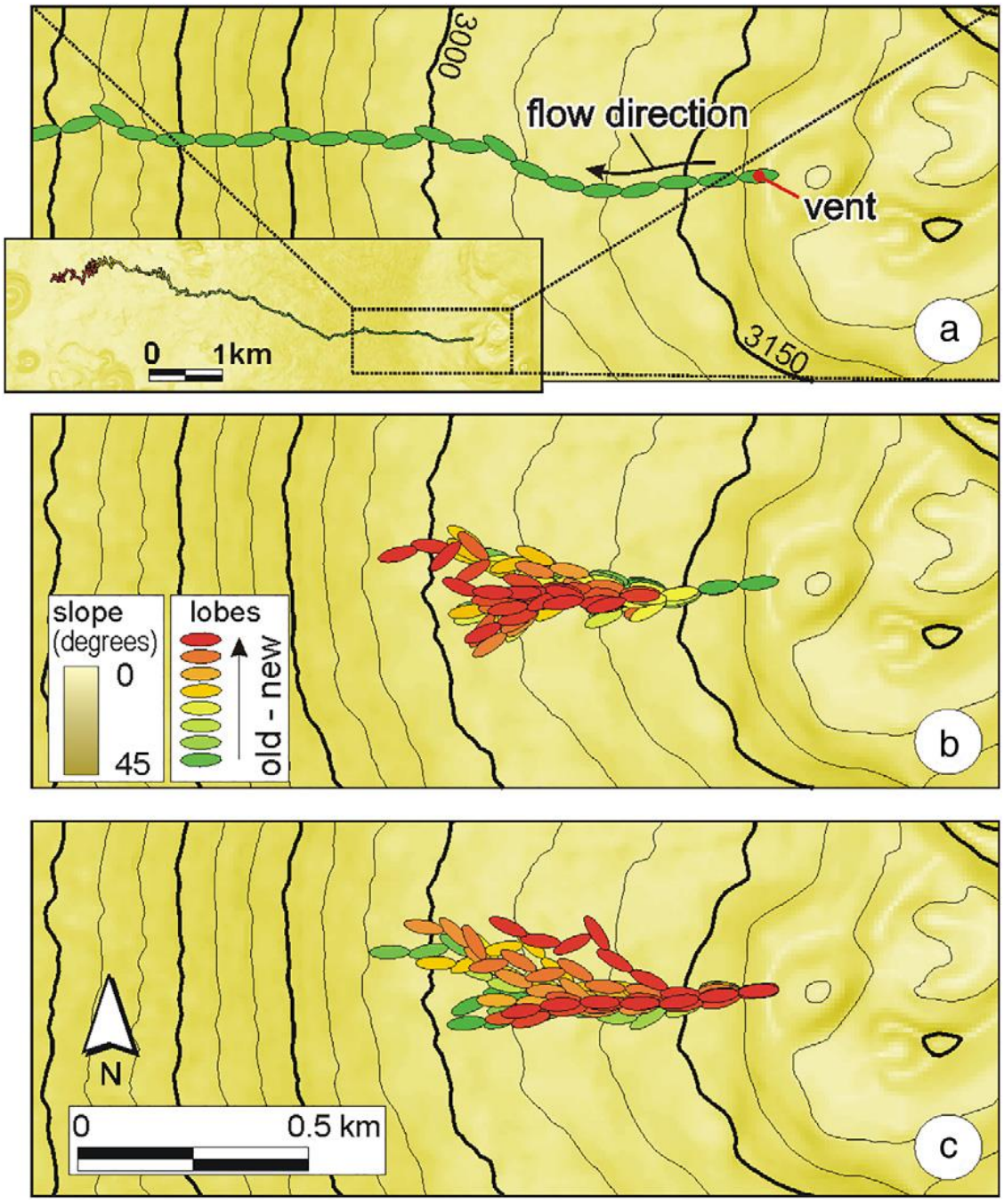

Figure 3: The probabilistic model, MrLavaLoba, assumes that underlying topography (slope) is the primary driver in prediction of flow path by determining the likelihood of where new lobes of lava will be generated. Figured from *de' Michieli Vitturi and Tarquini*, 2018.

Figure 4: Four primary morphologies observed by Fink and Griffiths [1990] and their relation to Ψ. A fifth morphology (No Crust, not pictured here) was observed beyond Levees and may be appropriate to some systems. Approximate Ψ value ranges of morphologies observed in our experiments are as follows: Pillows (≤2); Rifts (4 – 12); Folds (15 – 29); Levees (34 – 54); No Crust (>55). Values in-between frequently result in transition morphologies, defined here as morphologies that form contemporaneously. Blurriness in colorized lab images due to ice.

Figure 5: Experiments were conducted in a 76 x 30 cm plexiglass tank with a fitted 4mm grid steel mesh. The tank sat on an adjustable apparatus capable of producing the ~7, 16, and 29˚ slopes necessary. The distance from the vent to the back of the tank was 50 cm.

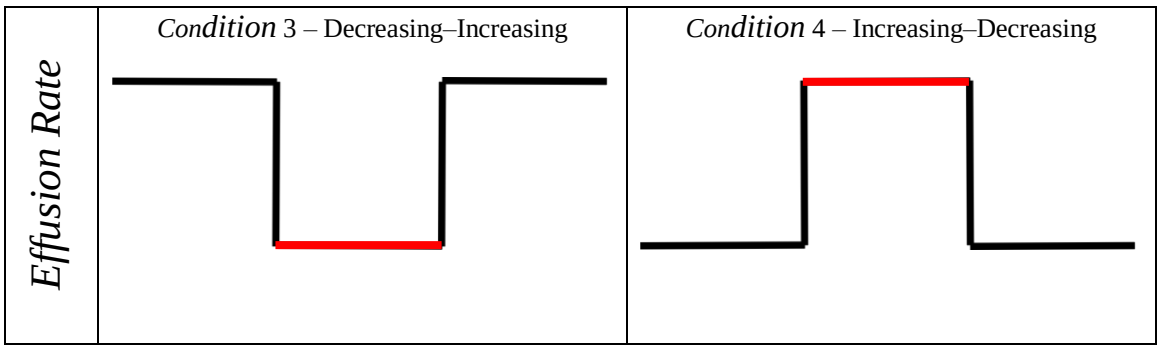

Figure 6: The experimental design consists of the two conditions tested in this study corresponding to decreasing, increasing, decreasing-increasing, and increasing-decreasing eruption rates. For conditions 3 and 4, the pulse duration was 50 seconds. Each condition was performed on 3 different slopes: ~7˚ (low), 16˚ (medium), and 29˚ (high).

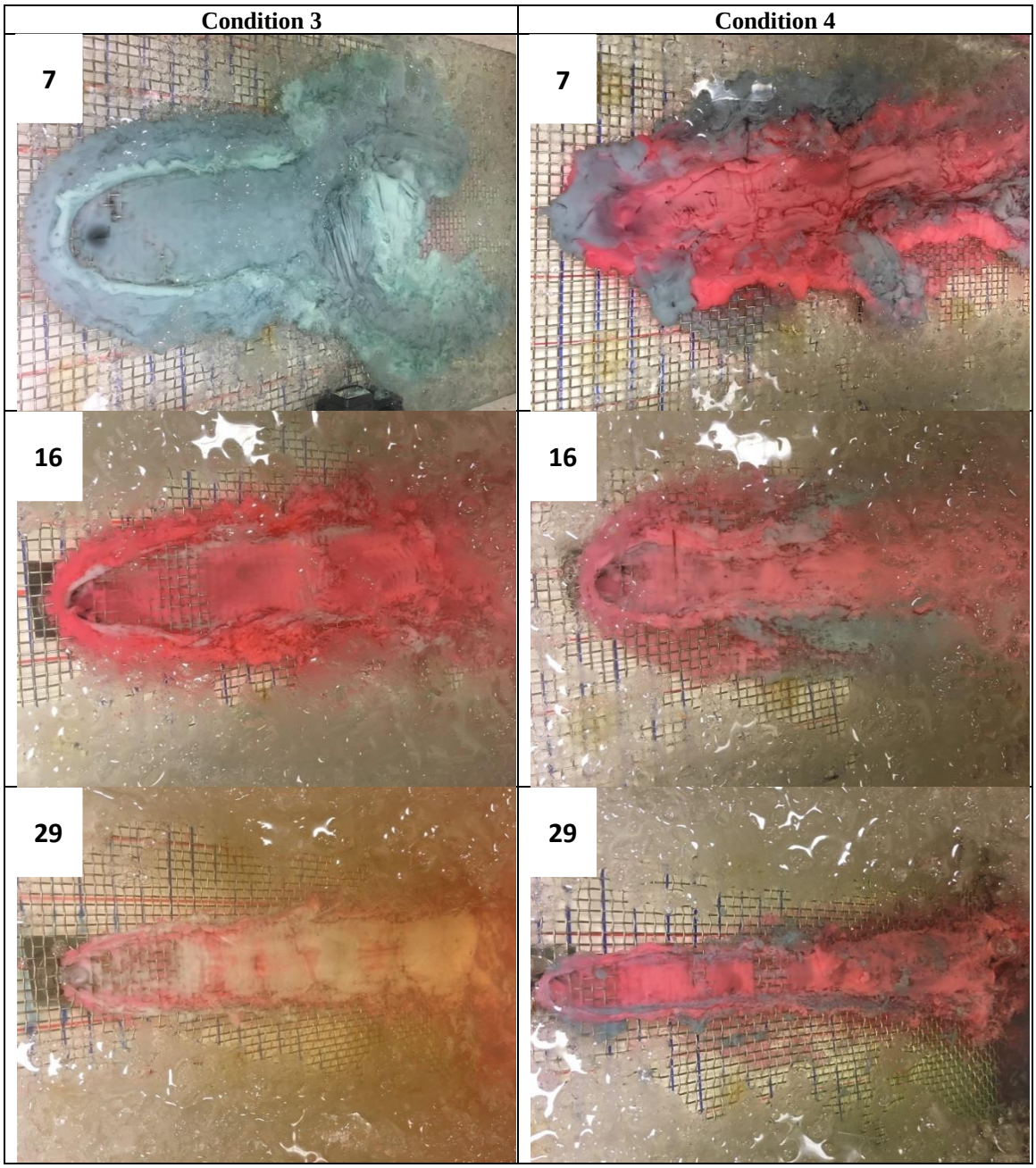

Figure 7: Examples of flows produced at low (~7˚), medium (~16˚), and high slopes (~29˚) for conditions 3 and 4. For condition 3, all flows were erupted at 3 cm^3/s and have Ψ =45, placing them in the high Ψ regime. The pulse eruption rate was 1.5 cm^3/s. For condition 4, all flows were erupted at 1.5 cm^3/s and have a Ψ=45. The pulse eruption rate was 3 cm^3/s. Increasing the slope narrows the flow width and decreases flow depth, simplifying the overall channelized morphology.

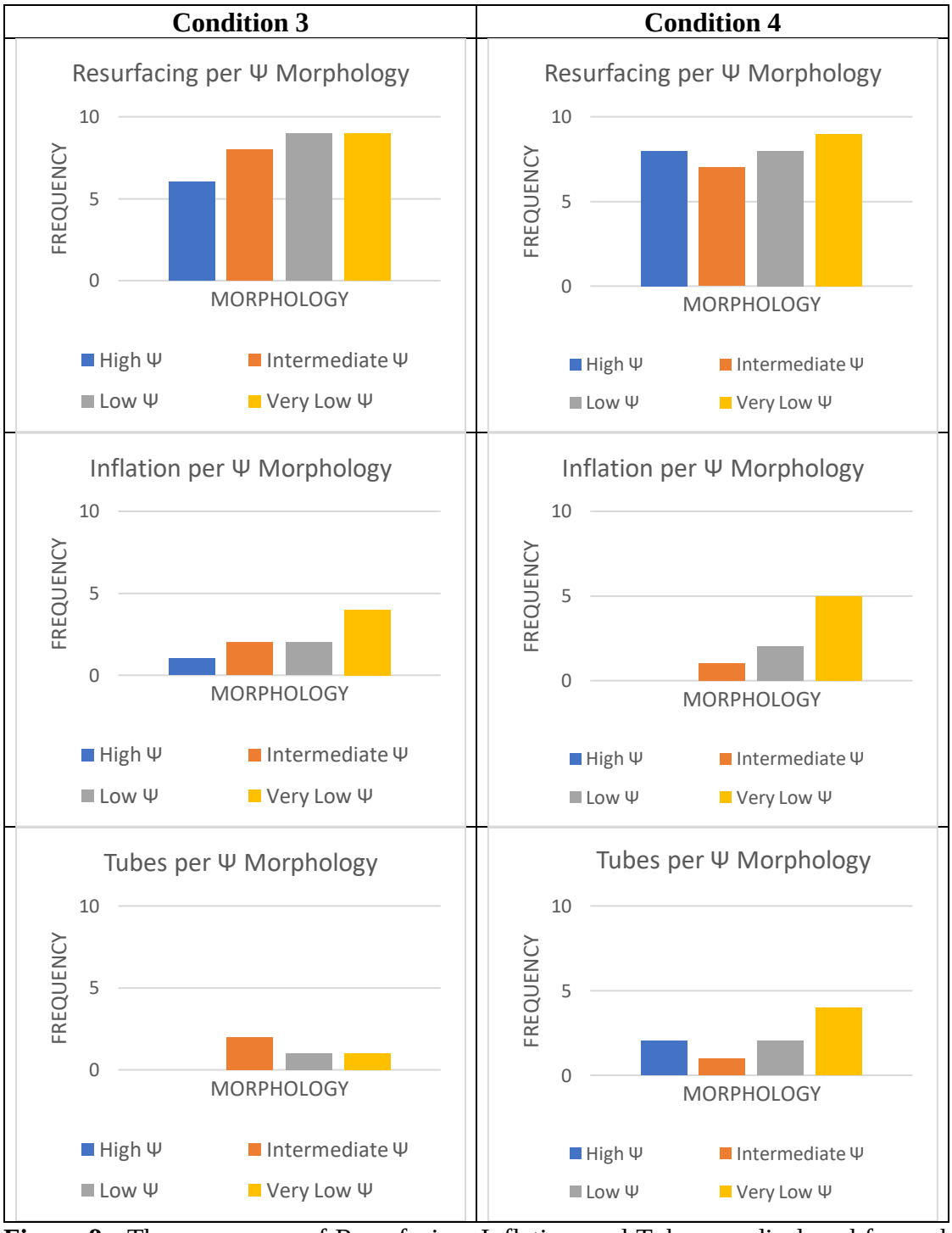

Figure 8: The occurrence of Resurfacing, Inflation, and Tubes are displayed for each Ψ regime for conditions 3 and 4. **(left – condition 3) (a)** *Resurfacing* – which frequently occurred –was dependent on Ψ. **(b)** *Inflation* was also dependent on Ψ but occurred sparingly. **(c)** *Tubes* were the most difficult emplacement mode to produce. Tubes were weakly dependent on Ψ. **(right – condition 4) (a)** *Resurfacing* is not dependent on Ψ,

occurring frequently. **(b)** *Inflation* is dependent on Ψ, being more common at lower Ψ but still relatively uncommon. **(c)** *Tubes* were more common in condition 4, than condition 3, with a weak suggestion of correlation on very low Ψ.

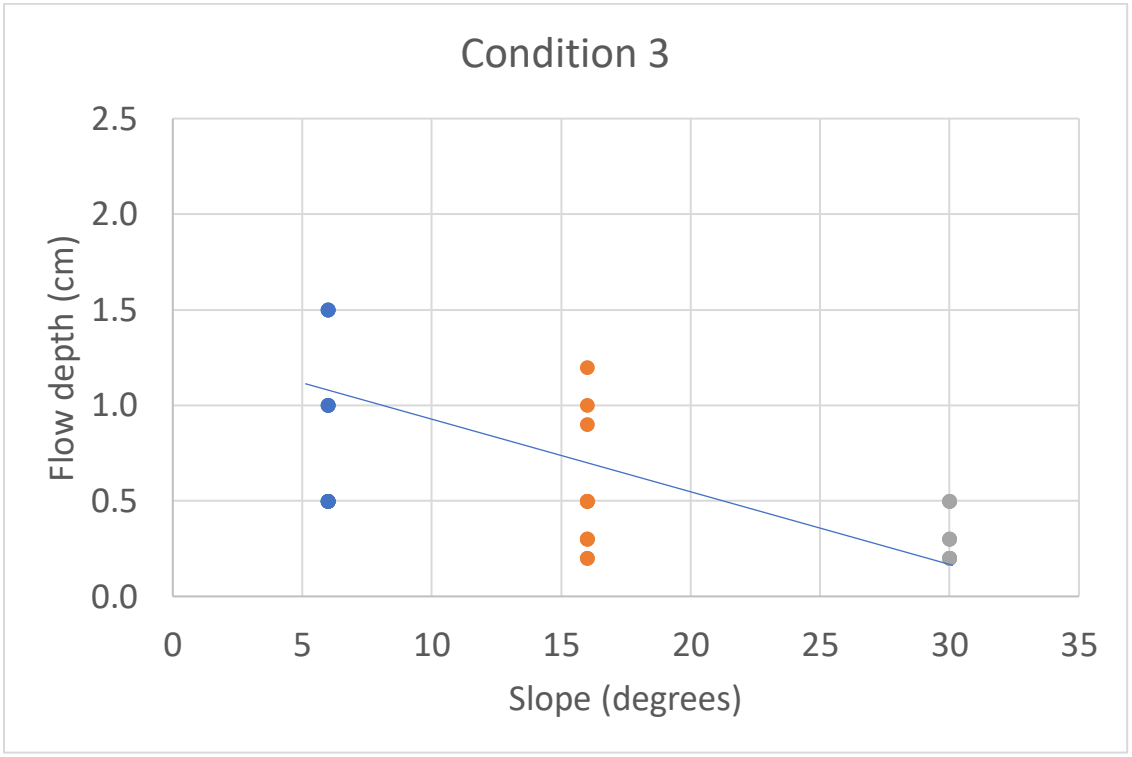

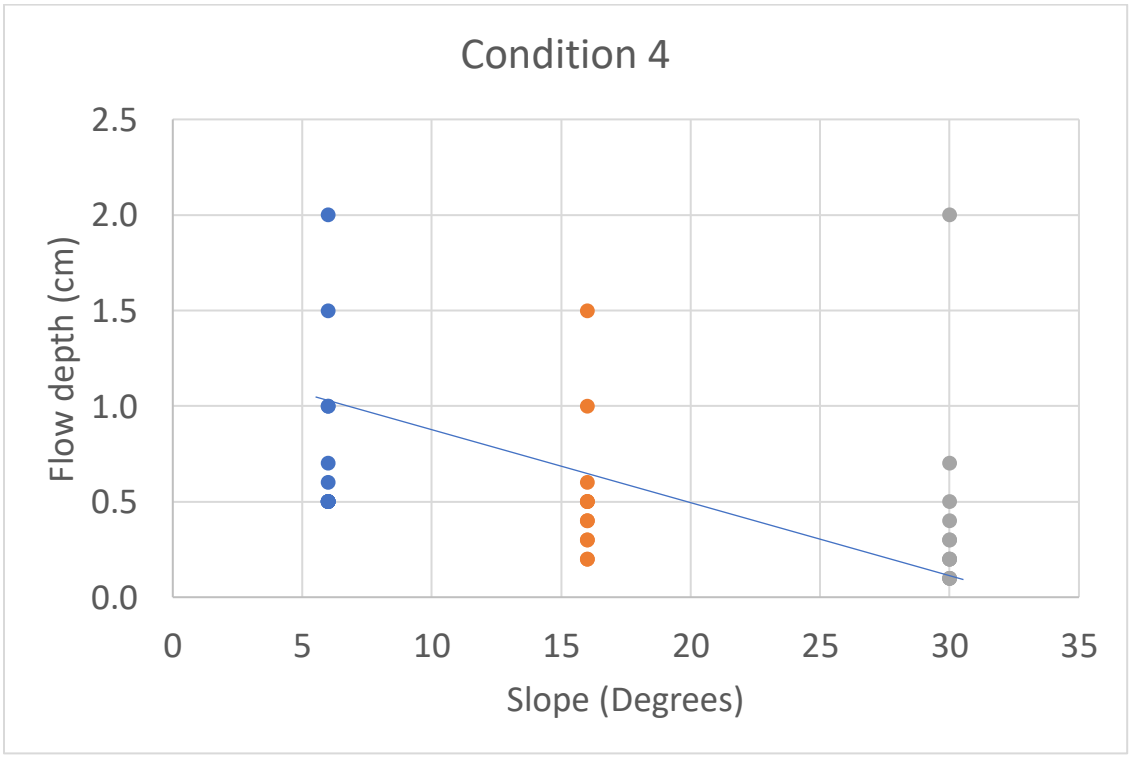

Figure 9: Slope has an impact on flow depth, with steeper slopes resulting in thinner flows. There is more spread in condition 4 but the trend holds.

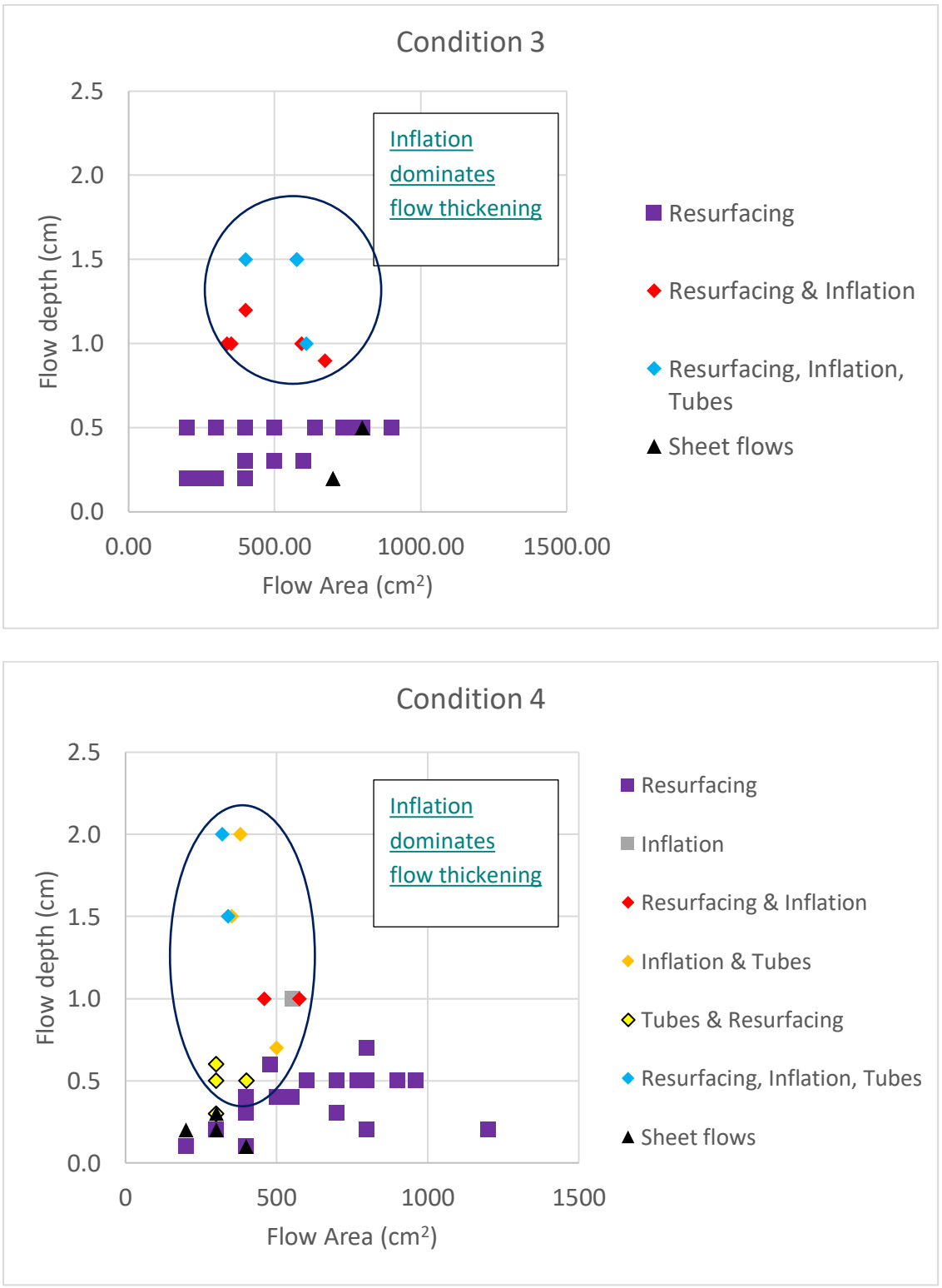

Figure 10: The flow height and area are dependent on the emplacement modes observed for conditions 3 and 4. (**top-condition 3**) Sheet flows and resurfacing are the thinnest and

their field extends to the largest areas. Inflated flows are thicker. (**bottom-condition 4**) Sheet flows and resurfacing are the thinnest. Flows displaying resurfacing are the largest in area. The smallest flows in area are sheet flows and those displaying multiple emplacement modes, including inflation. Inflated flows, with or without other modes of emplacement are the thickest.

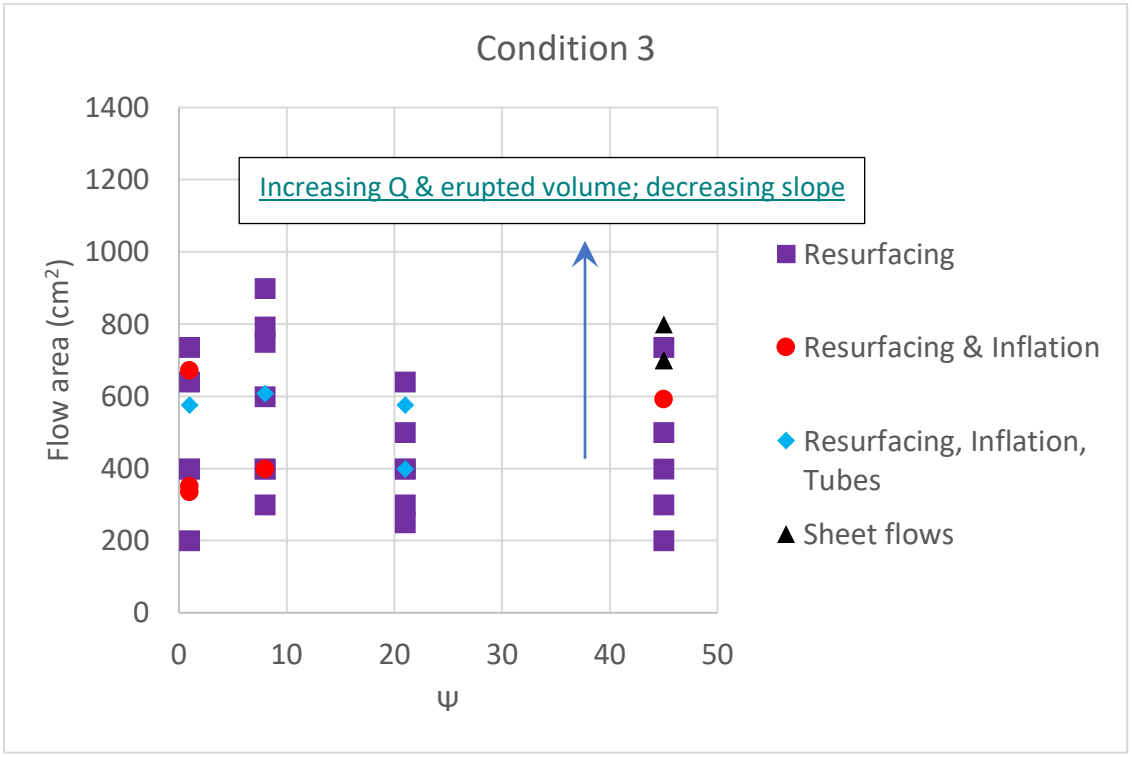

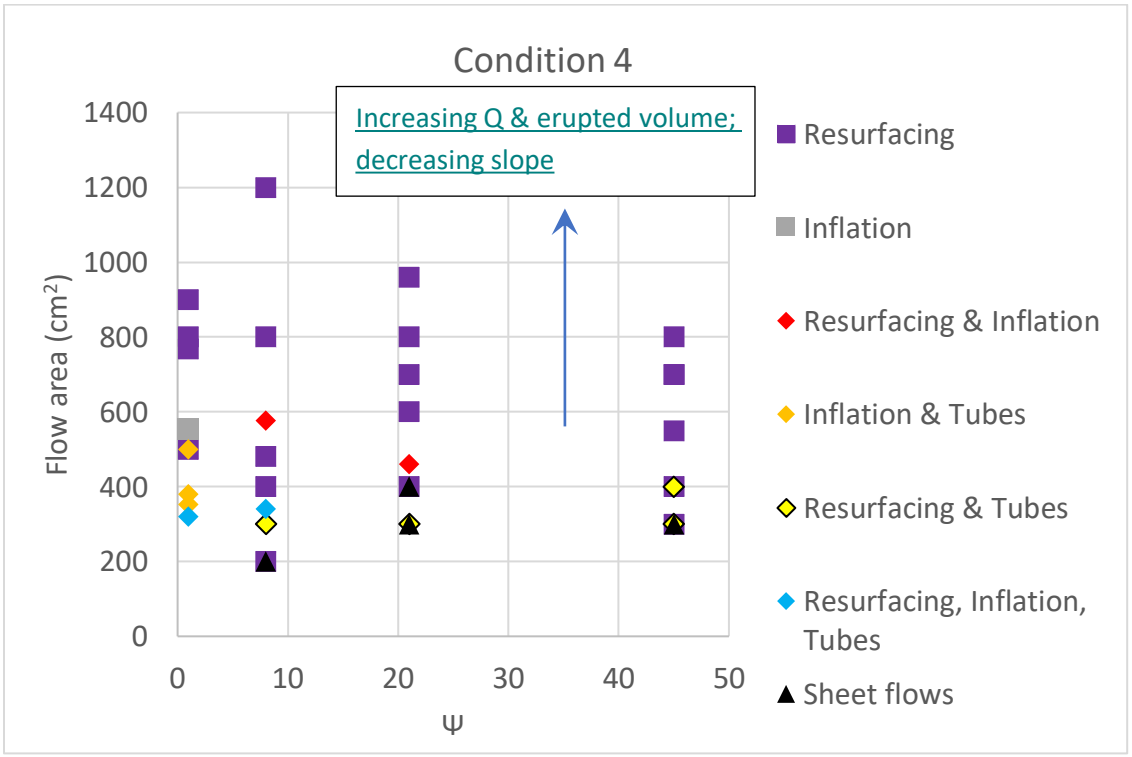

Figure 11: Emplacement modes are presented as a function of Ψ and flow area. Increasing flow area is broadly tied to increasing slope and increasing eruption rate. **(top)** Area shows

no dependence on Ψ. Sheet flows and those displaying resurfacing are the largest in area. With one exception, flows displaying more than one emplacement mode generally occur at low and intermediate Ψ and are intermediate in area. **(bottom)** Flows displaying resurfacing are the largest in area, while those with multiple emplacement modes tend to be smaller in area. Sheet flows are also small in area. Neither resurfaced nor sheet flows were dependent on Ψ. Flows that have undergone inflation occur at low and intermediate Ψ.

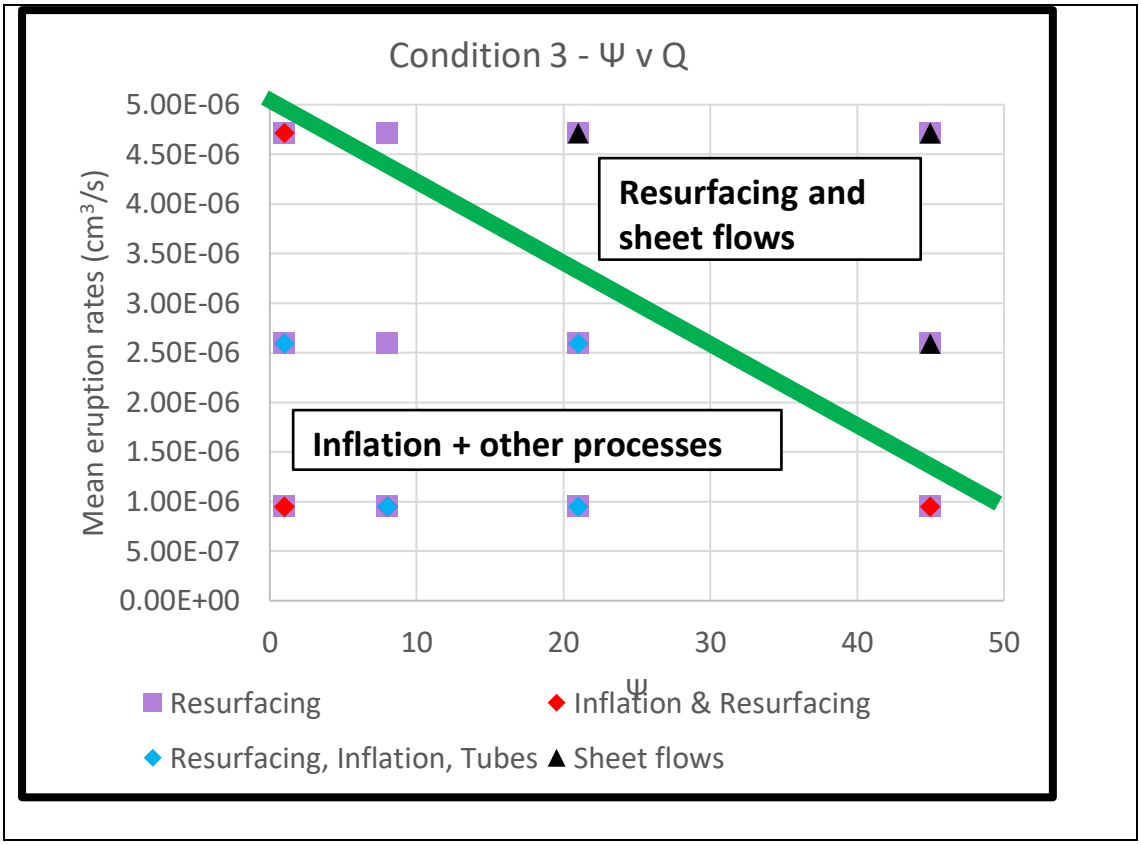
Condition 3 - Ψ v Q
Mean eruption rates (cm³/s)
5.00E-06
4.50E-06
4.00E-06
3.50E-06
3.00E-06
2.50E-06
2.00E-06
1.50E-06
1.00E-06
5.00E-07
0.00E+00
0
10
20
30
40
50
Ψ
Resurfacing and sheet flows
Inflation + other processes
Resurfacing
Inflation & Resurfacing
Resurfacing, Inflation, Tubes
Sheet flows

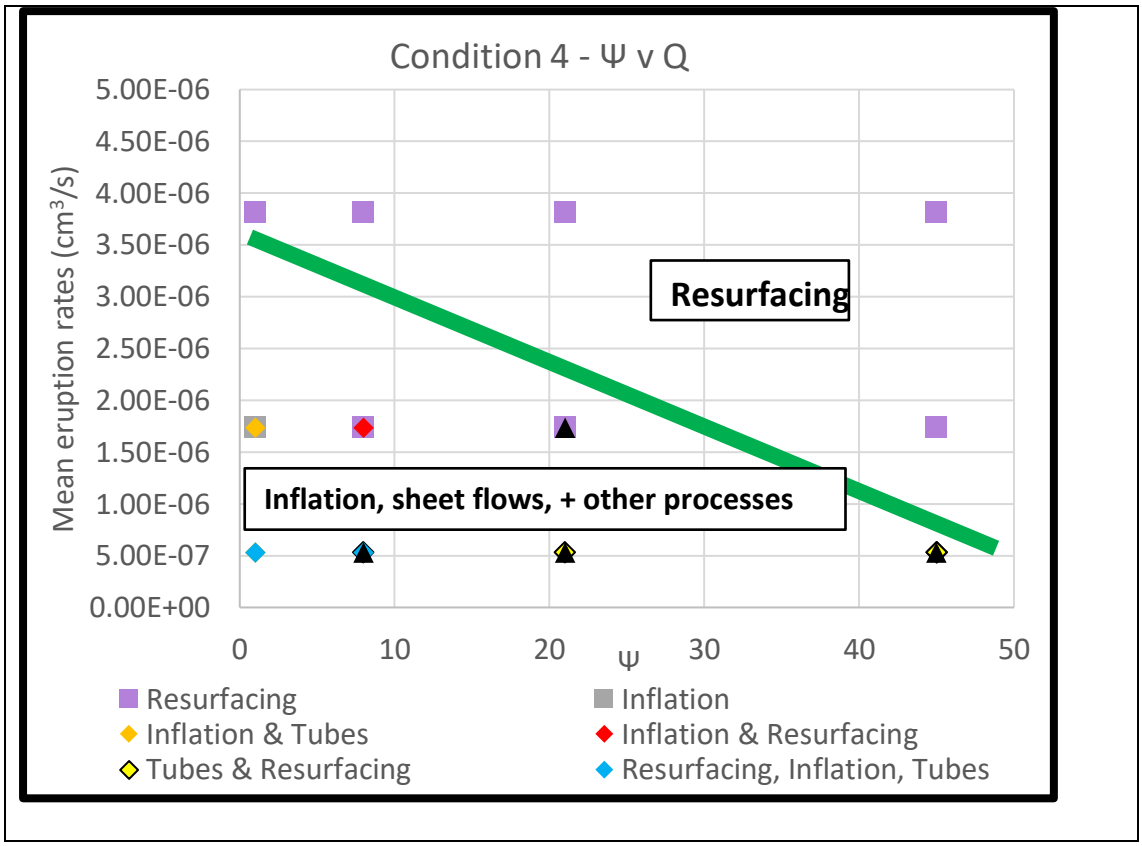

Figure 12: The relationship between Ψ, mean eruption rate, and emplacement mode is illustrated in this regime diagram. This diagram does not account for slope. As a result, trends are similar to those found in experiments performed on no slope. **(top)** For condition 3, resurfacing and sheet flows are found at increasing Ψ and increasing eruption rate. On the other hand, multiple emplacement modes and inflation are generally found at decreasing Ψ and decreasing eruption rate. **(bottom)** For condition 4, resurfacing happens primarily at increasing Ψ and increasing eruption rate. However, sheet flows – contrary to previous trends – do not. Instead, sheet flows, inflation, and multiple modes of emplacement tend to occur at decreasing Ψ and decreasing eruption rate.

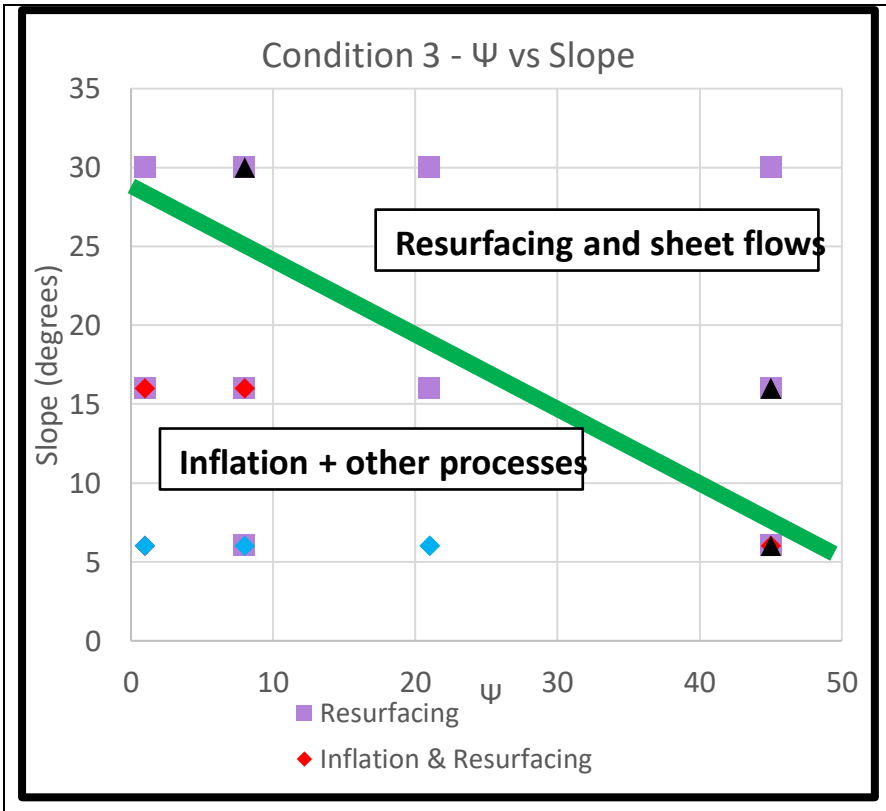
Condition 3 - Ψ vs Slope
Slope (degrees)
35
30
25
20
15
10
5
0
0
10
20
30
40
50
Ψ
Resurfacing and sheet flows
Inflation + other processes
Resurfacing
Inflation & Resurfacing

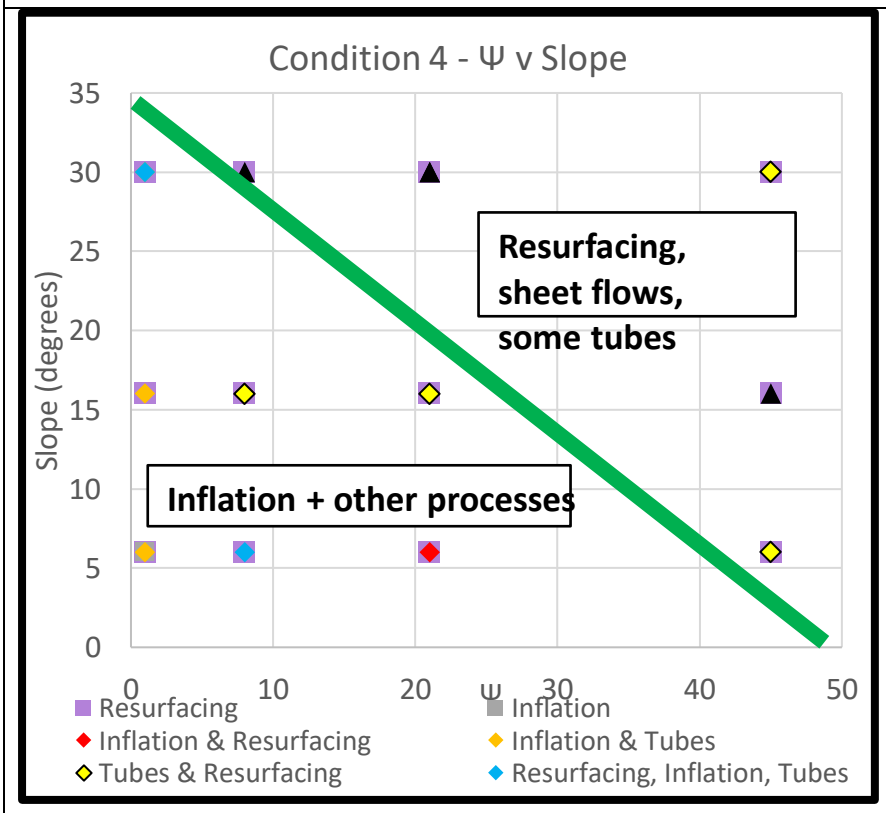
Condition 4 - Ψ v Slope
Slope (degrees)
35
30
25
20
15
10
5
0
0
10
20
30
40
50
Ψ
Resurfacing, sheet flows, some tubes
Inflation + other processes
Resurfacing
Inflation
Inflation & Resurfacing
Inflation & Tubes
Tubes & Resurfacing
Resurfacing, Inflation, Tubes

Figure 13: Emplacement mode regime diagram: Ψ and slope. **(top)** For condition 3, flows displaying resurfacing are dependent on neither Ψ nor slope. However, the upper right portion of the diagram contains almost exclusively flows that display resurfacing alone. Sheet flows also occur in this region, although the number of samples is small. Flows with multiple emplacement processes occur at shallower slopes and generally intermediate and low Ψ. **(bottom)** In condition 4, flows displaying resurfacing are dependent on neither Ψ nor slope. A similar relationship is observed with sheet flows although the sample is small. However, the upper right portion of the diagram contains almost exclusively flows that display resurfacing alone. Flows with multiple emplacement processes occur at shallower slopes and generally intermediate and low Ψ.

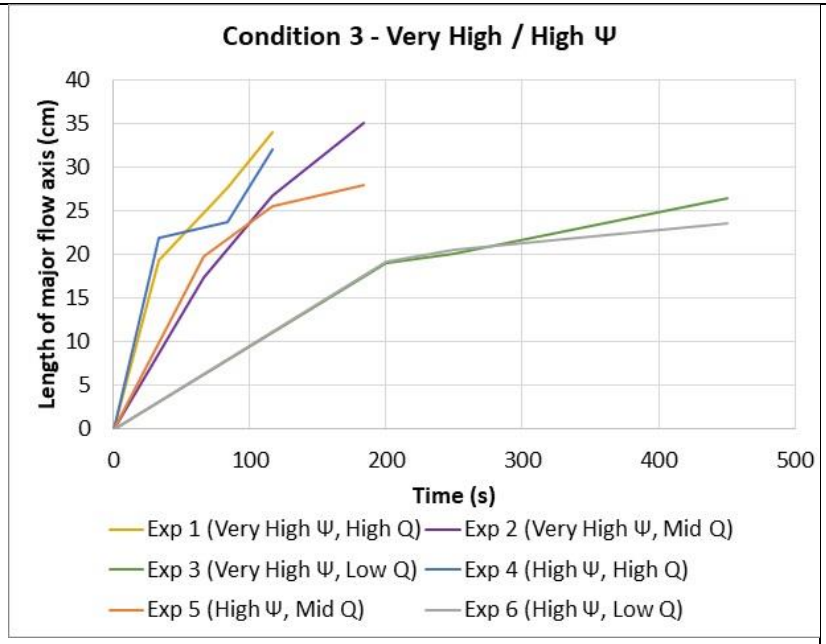
Condition 3 - Very High / High Ψ
Length of major flow axis (cm)
0
5
10
15
20
25
30
35
40
0
100
200
300
400
500
Time (s)
Exp 1 (Very High Ψ, High Q)
Exp 2 (Very High Ψ, Mid Q)
Exp 3 (Very High Ψ, Low Q)
Exp 4 (High Ψ, High Q)
Exp 5 (High Ψ, Mid Q)
Exp 6 (High Ψ, Low Q)

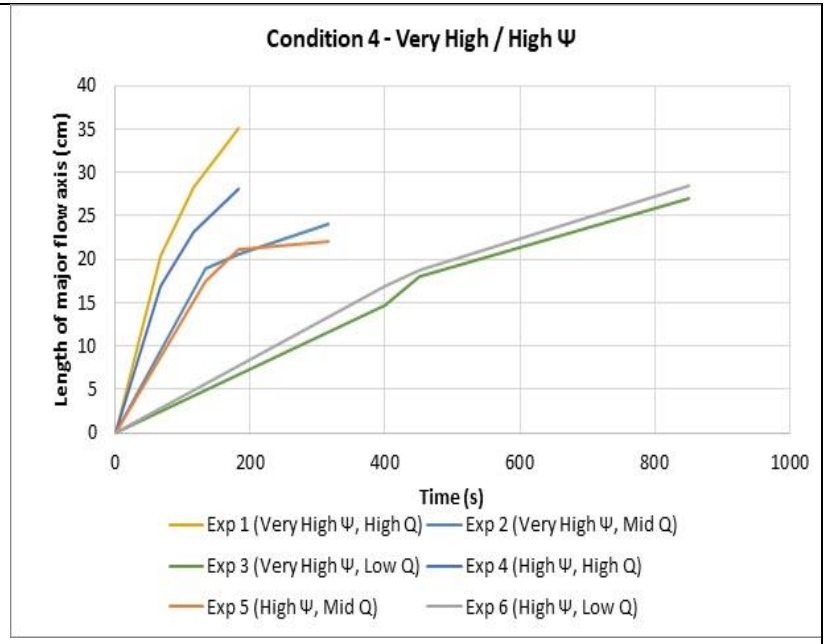
Condition 4 - Very High / High Ψ
Length of major flow axis (cm)
0
5
10
15
20
25
30
35
40
0
200
400
600
800
1000
Time (s)
Exp 1 (Very High Ψ, High Q)
Exp 2 (Very High Ψ, Mid Q)
Exp 3 (Very High Ψ, Low Q)
Exp 4 (High Ψ, High Q)
Exp 5 (High Ψ, Mid Q)
Exp 6 (High Ψ, Low Q)

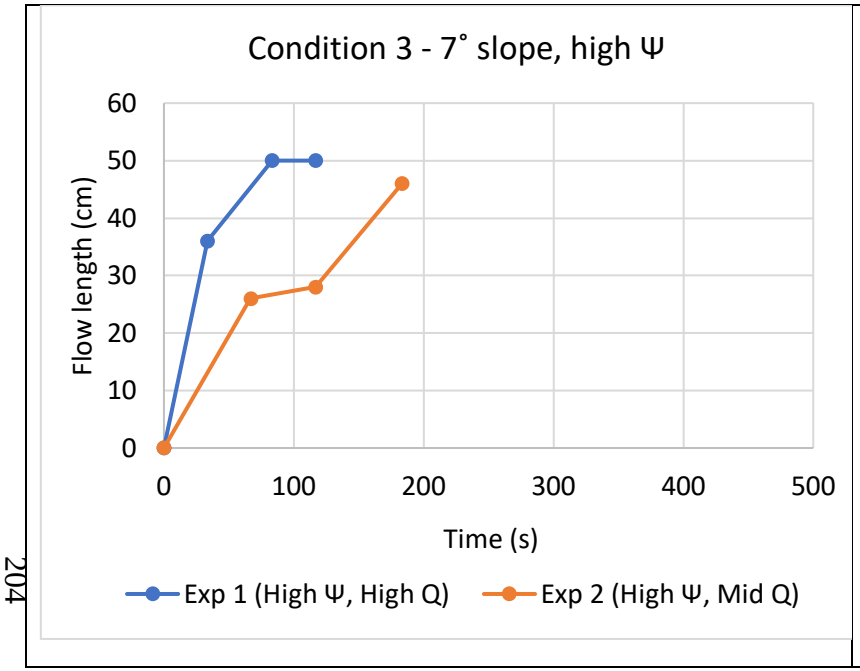
Condition 3 - 7˚ slope, high Ψ
Flow length (cm)
60
50
40
30
20
10
0
0
100
200
300
400
500
Time (s)
Exp 1 (High Ψ, High Q)
Exp 2 (High Ψ, Mid Q)

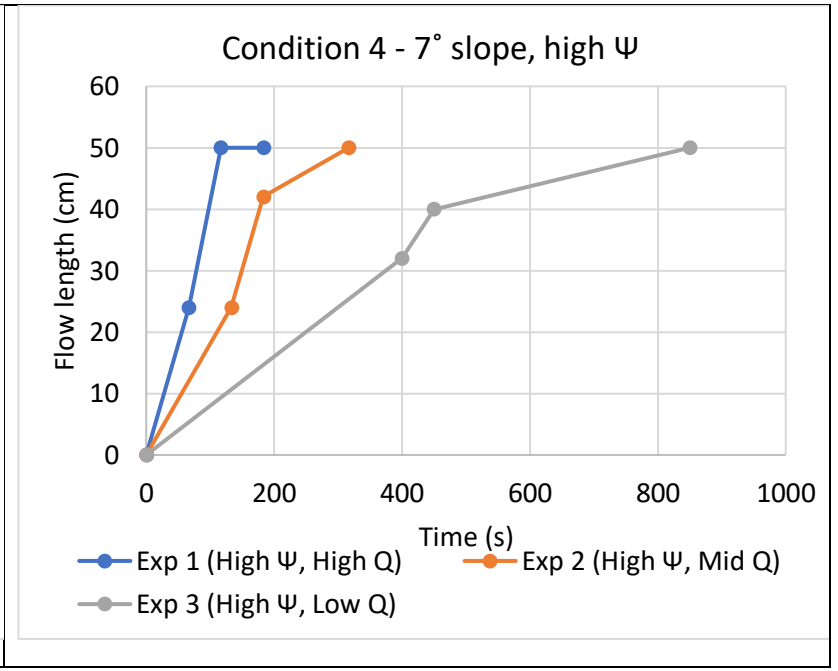
Condition 4 - 7˚ slope, high Ψ
Flow length (cm)
60
50
40
30
20
10
0
0
200
400
600
800
1000
Time (s)
Exp 1 (High Ψ, High Q)
Exp 2 (High Ψ, Mid Q)
Exp 3 (High Ψ, Low Q)

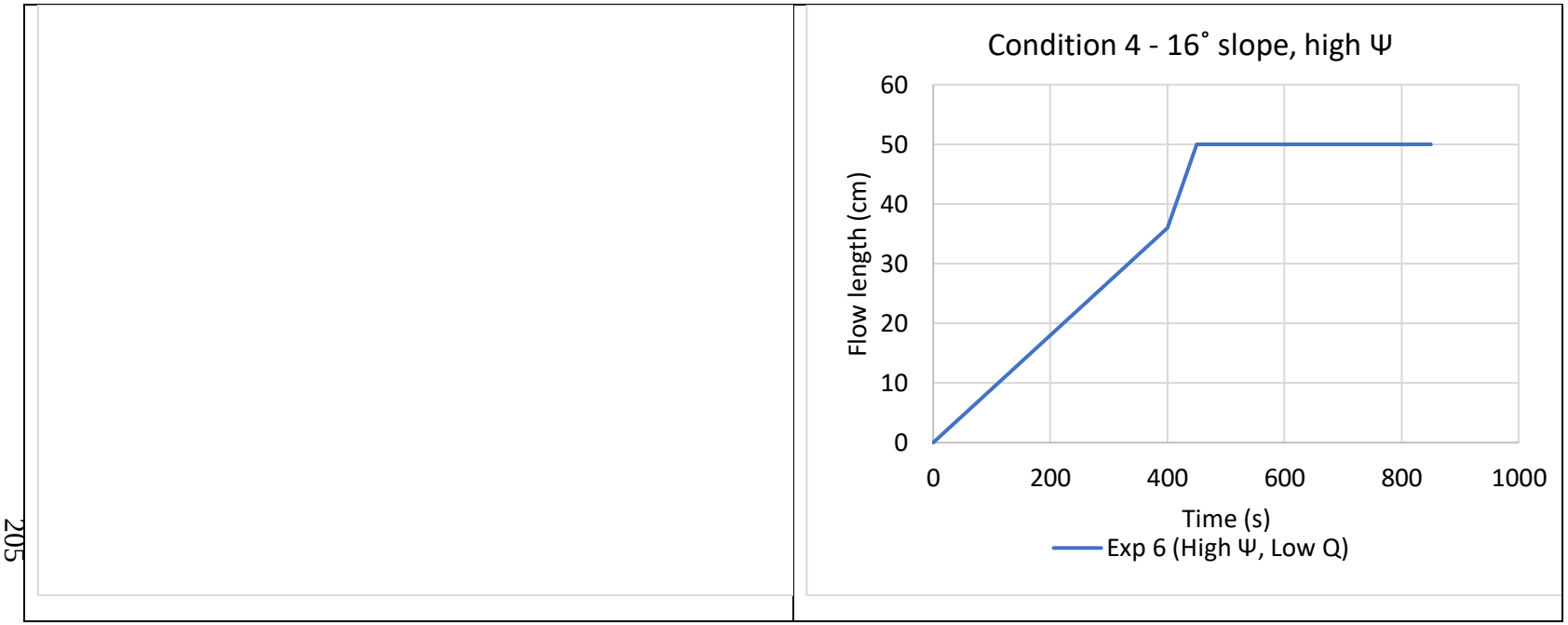

Figure 14a – high psi: Propagation profiles illustrating the length of the flows during a single experimental run as a function of time. Each profile is divided into 3 segments, representing the three stages of the eruption: first (initial), second (pulse), and third (final). Accurate length data was not obtainable for flows on 29˚ slopes. Profiles are discriminated by effusion rate, or Q. The shape of the profiles is influenced by Ψ, local flow rate, and emplacement mode. Left column features condition 3. Right column features condition 4. Note the x-axis for condition 3 is different from that of condition 4. Graphs are ordered by increasing slope as you move down the figure. **(top)** Profiles between condition 3 and 4 differ only slightly on 0˚ slopes, suggesting that high Ψ conditions are negating other effects on the flow. **(middle)** While the profiles are similar between conditions on no slope, the curves on a 7˚ slope are noticeably different with a steepening observed during the second stage of the eruption – the pulse – as flow rates increased for condition 4. The flattening observed after the pulse is due to either flow thickening or lower flow rates at the flow front. **(bottom)** A channelized flow experiencing none of the emplacement modes we investigated. The flow behaves as expected given the vent conditions, with an increase in propagation speed at the flow front during the pulse. The flow hits the back of the tank, which is 50 cm from the vent.

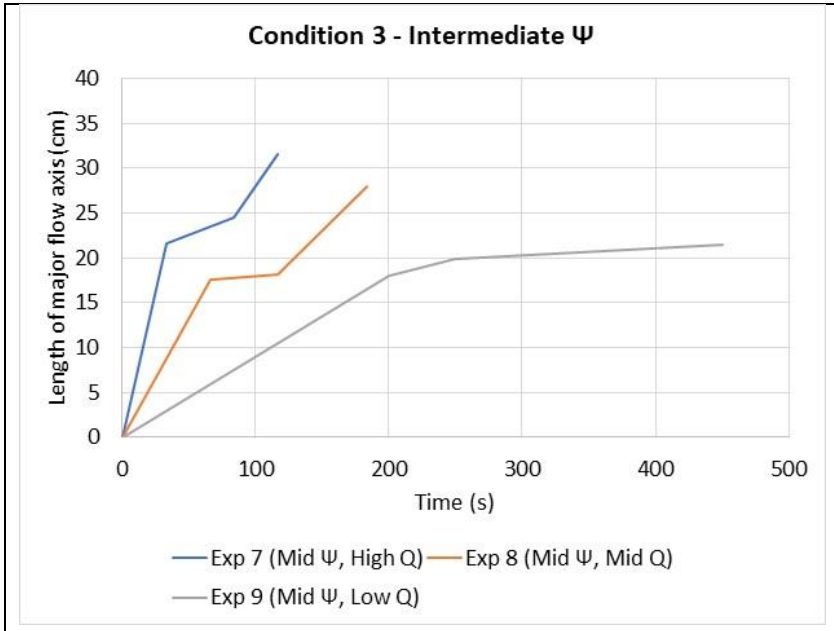
Condition 3 - Intermediate Ψ
Length of major flow axis (cm)
0
5
10
15
20
25
30
35
40
0
100
200
300
400
500
Time (s)
Exp 7 (Mid Ψ, High Q)
Exp 8 (Mid Ψ, Mid Q)
Exp 9 (Mid Ψ, Low Q)

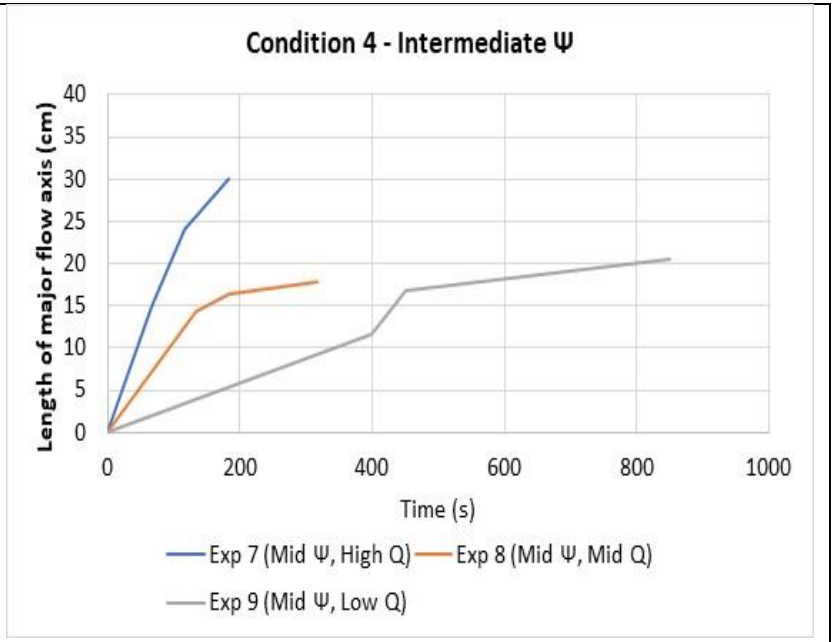
Condition 4 - Intermediate Ψ
Length of major flow axis (cm)
0
5
10
15
20
25
30
35
40
0
200
400
600
800
1000
Time (s)
Exp 7 (Mid Ψ, High Q)
Exp 8 (Mid Ψ, Mid Q)
Exp 9 (Mid Ψ, Low Q)

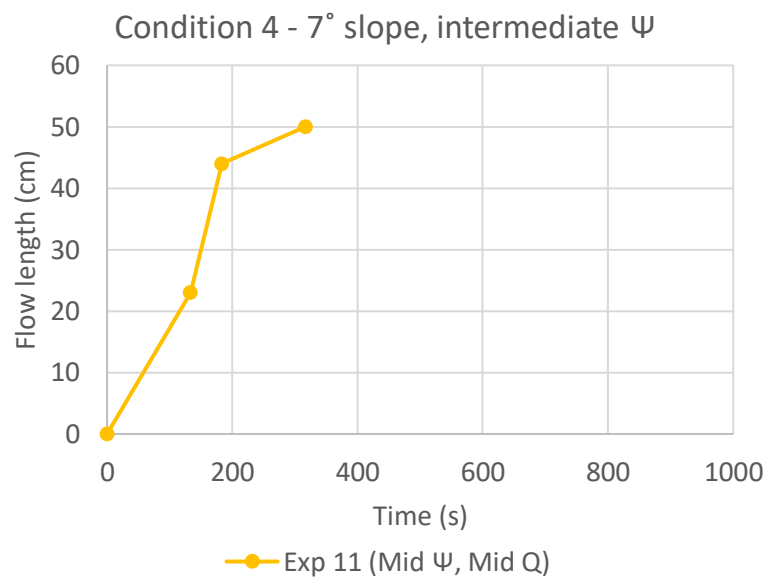
Condition 4 - 7˚ slope, intermediate Ψ
Flow length (cm)
60
50
40
30
20
10
0
0
200
400
600
800
1000
Time (s)
Exp 11 (Mid Ψ, Mid Q)

Figure 14b

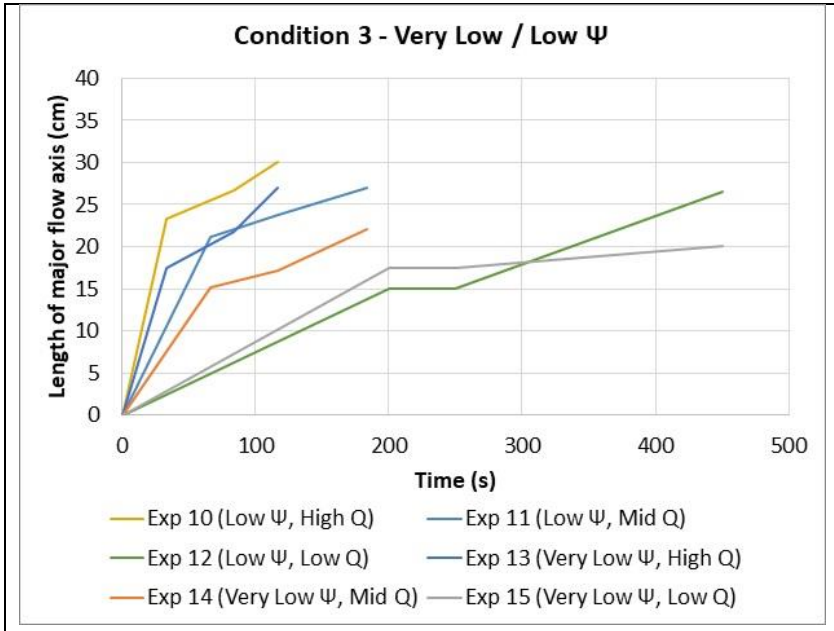
Condition 3 - Very Low / Low Ψ
Length of major flow axis (cm)
0
5
10
15
20
25
30
35
40
0
100
200
300
400
500
Time (s)
Exp 10 (Low Ψ, High Q)
Exp 11 (Low Ψ, Mid Q)
Exp 12 (Low Ψ, Low Q)
Exp 13 (Very Low Ψ, High Q)
Exp 14 (Very Low Ψ, Mid Q)
Exp 15 (Very Low Ψ, Low Q)

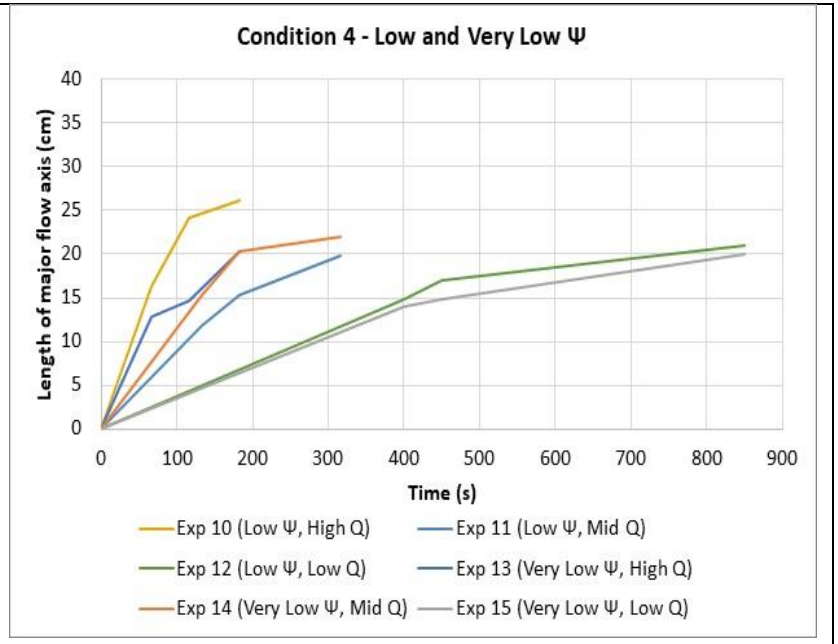
Condition 4 - Low and Very Low Ψ
Length of major flow axis (cm)
0
5
10
15
20
25
30
35
40
0
100
200
300
400
500
600
700
800
900
Time (s)
Exp 10 (Low Ψ, High Q)
Exp 11 (Low Ψ, Mid Q)
Exp 12 (Low Ψ, Low Q)
Exp 13 (Very Low Ψ, High Q)
Exp 14 (Very Low Ψ, Mid Q)
Exp 15 (Very Low Ψ, Low Q)

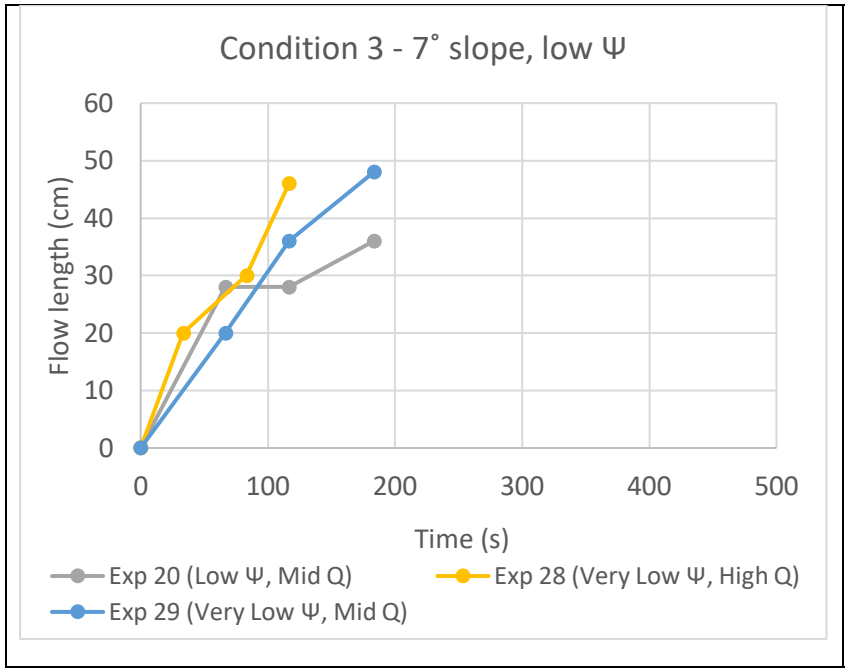
Condition 3 - 7˚ slope, low Ψ
Flow length (cm)
60
50
40
30
20
10
0
0
100
200
300
400
500
Time (s)
Exp 20 (Low Ψ, Mid Q)
Exp 28 (Very Low Ψ, High Q)
Exp 29 (Very Low Ψ, Mid Q)

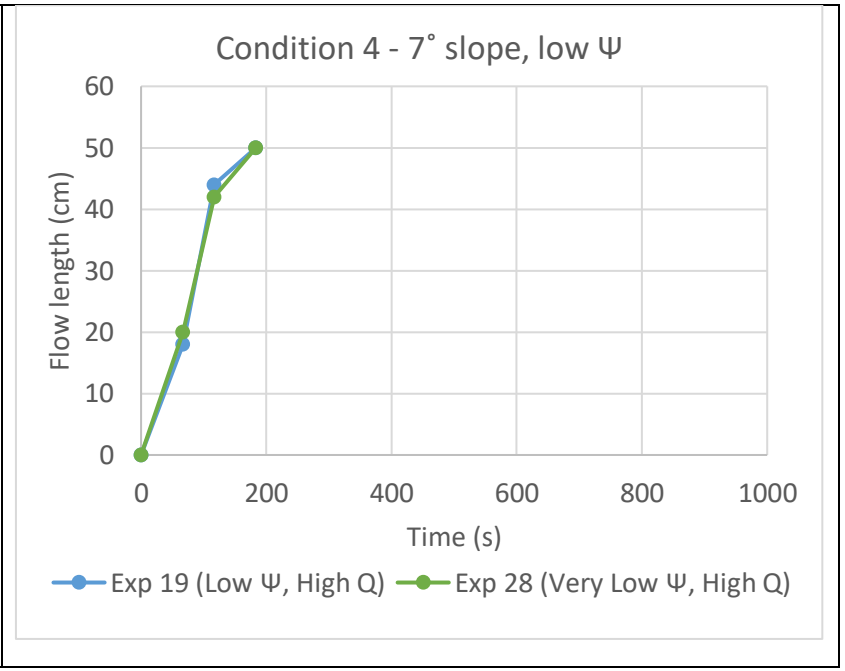
Condition 4 - 7˚ slope, low Ψ
Flow length (cm)
60
50
40
30
20
10
0
0
200
400
600
800
1000
Time (s)
Exp 19 (Low Ψ, High Q)
Exp 28 (Very Low Ψ, High Q)

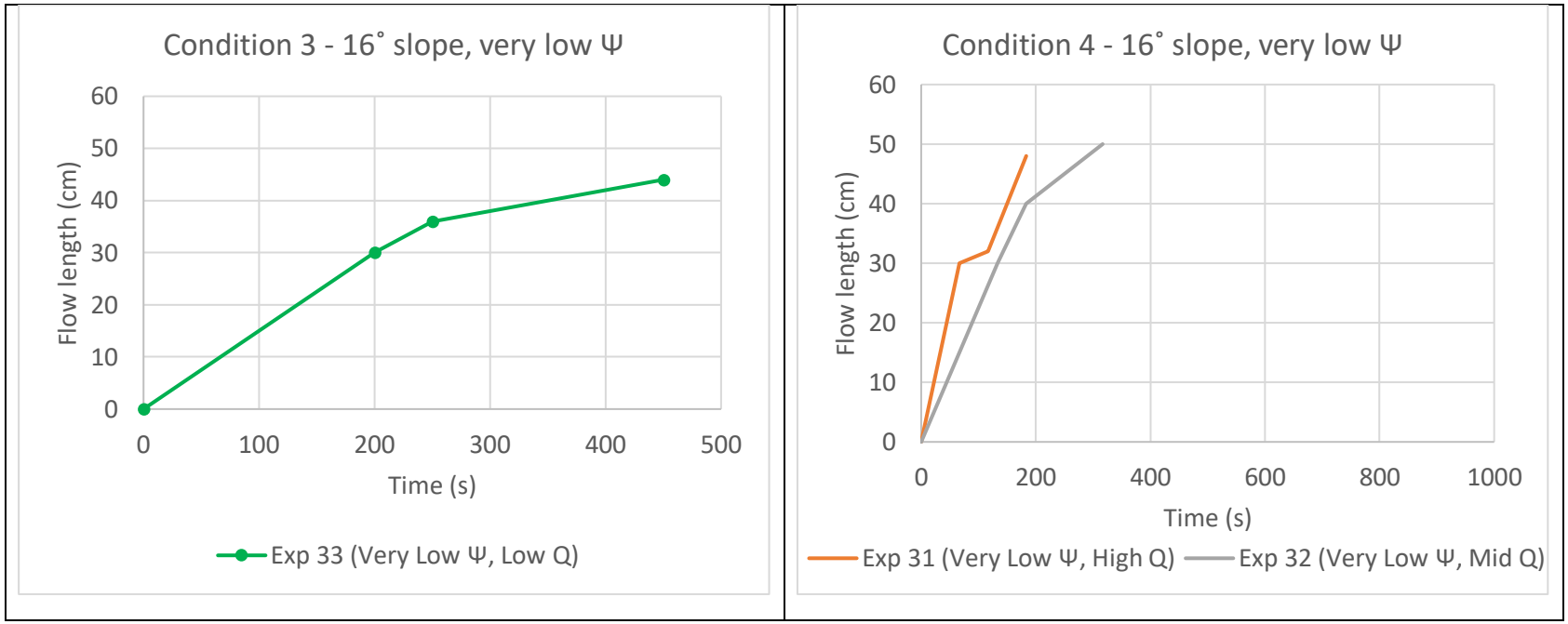

Figure 14b – moderate Ψ: Propagation profiles illustrating the length of the flows during a single experimental run as a function of time. Each profile is divided into 3 segments, representing the three stages of the eruption: first (initial), second (pulse), and third (final). Accurate length data was not obtainable for flows on 29˚ slopes. Profiles are discriminated by effusion rate, or Q. The shape of the profiles is influenced by Ψ, local flow rate, and emplacement mode. Left column features condition 3. Right column features condition 4. Note the x-axis for some condition 3 graphs is different from that of condition 4. Graphs are ordered by increasing slope as you move down the figure. **(top)** Profiles between condition 3 and 4 are noticeably different for a few on 0˚ slopes. During the second stage of condition 3 experiments 7&8, there is a dramatic flattening of the curve indicating that propagation of the flow front nearly stopped. This serves as an indication of when inflation occurred. **(bottom)** The flow produced during experiment 11 behaves as expected for condition 4, with an increase of forward propagation when eruption rate increases during the pulse.

Figure 14c – low Ψ: Propagation profiles illustrating the length of the flows during a single experimental run as a function of time. Each profile is divided into 3 segments, representing the three stages of the eruption: first (initial), second (pulse), and third (final). Accurate length data was not obtainable for flows on 29˚ slopes. Profiles are discriminated by effusion rate, or Q. The shape of the profiles is influenced by *Ψ,* local flow rate, and emplacement mode. Left column features condition 3. Right column features condition 4. Note the x-axis for some condition 3 graphs is different from that of condition 4. Graphs are ordered by increasing slope as you move down the figure. **(top)** Once again, profiles between condition 3 and 4 are differ only slightly on 0˚ slopes. For several profiles, the second stage of the eruption is hardly noticeable as flow propagation proceeds at a near constant rate. Benches in the during the second stage are due to both a decrease in local flow rate and flow thickening due to inflation or voluminous resurfacing. **(middle)** On 7˚ slopes the profiles differ between condition. For condition 4, the profiles – both at high eruption rates – display the characteristic increase in propagation rate during the second stage of the eruption corresponding to the pulse. The condition 3 profiles are more diverse, with only one (experiment 29) having inflation. The other bends in the profiles are due to resurfacing and/or changes in the flow rate at the flow front. **(bottom)** The flow produced during experiment 32 for condition 4 has a near constant propagation rate through the first two stages of the eruption. The bench in condition 4, experiment 31 is due to resurfacing in which wax repaved the flow surface instead of contributing to flow advancement during the pulse. Inflation occurs in condition 3, experiment 33 primarily during the final stage of the eruption.

APPENDIX D

CHAPTER 4 FIGURES

Figure 1: Examples of the five primary morphologies observed by *Fink and Griffiths* [1990], *Gregg and Fink* [2000], and *Chapter II* [this dissertation]. From high to low Ψ, the morphologies the No Crust, Levees, Folds, Rifts, and Pillows.

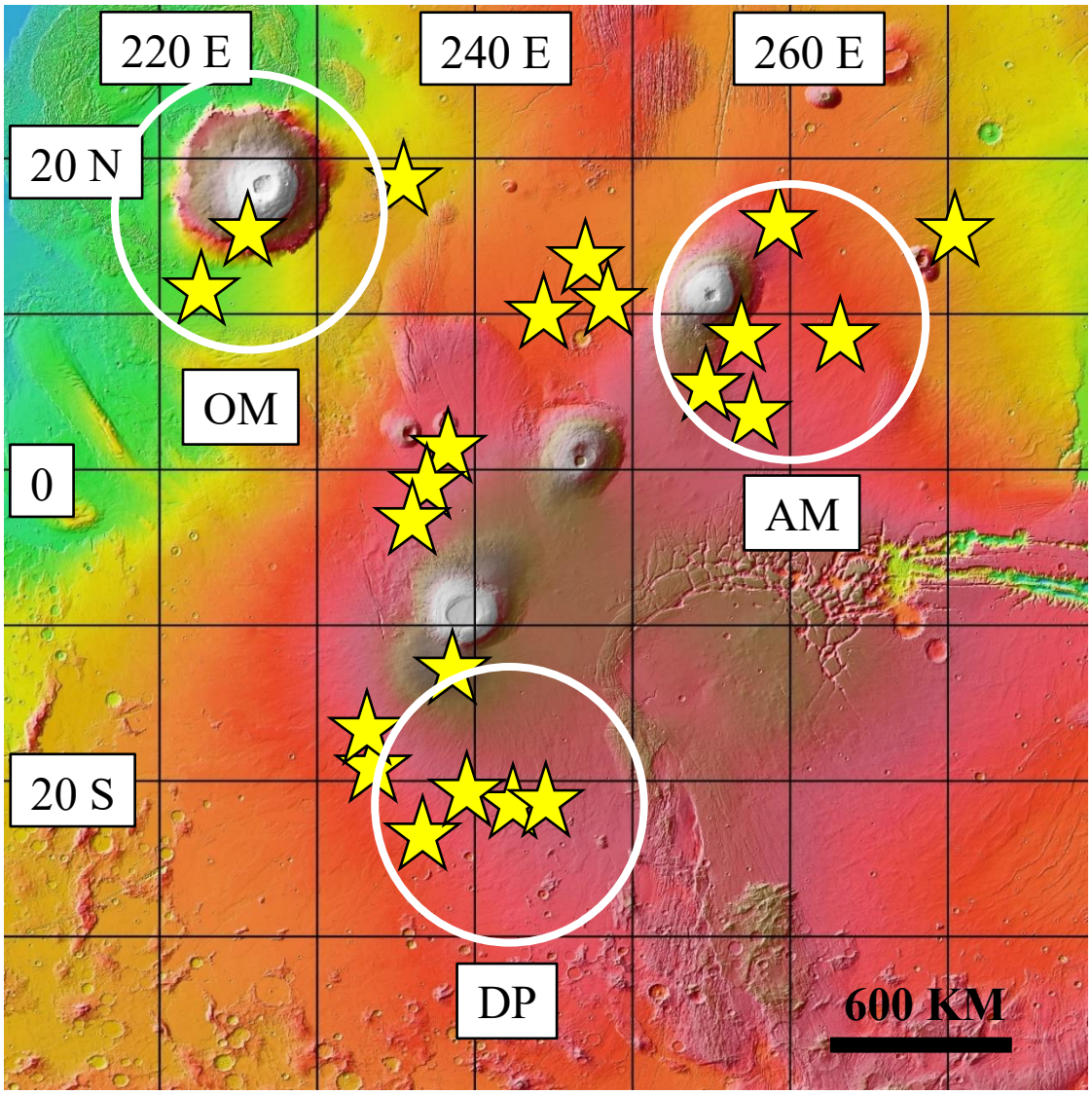

Figure 2: Map of study area, the Tharsis Volcanic Province. Base map is colorized MOLA topography, with warm colors representing areas of higher elevation. White circles indicate Olympus Mons (OM), Ascraeus Mons (AM), and Daedalia Planum (DP).

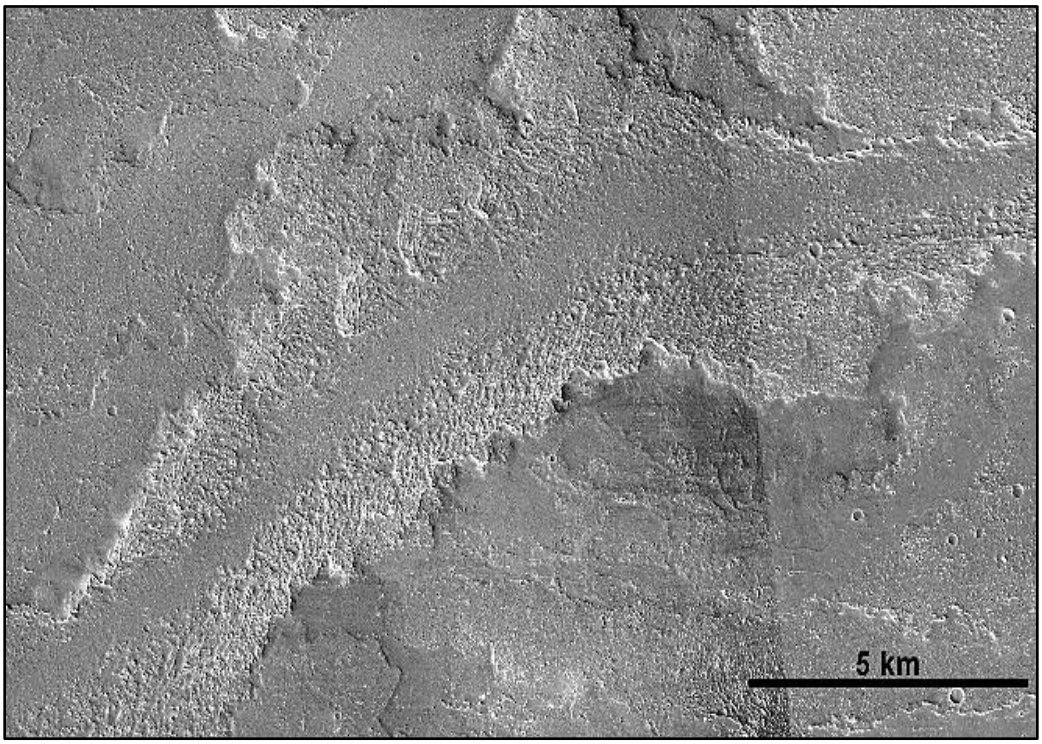

Figure 3: An example of a long, self-replicating lava flow in the volcanic plains of Tharsis south of Olympus Mons. The channel is clearly defined, has an approximately constant width, and levees are well developed and near constant width.

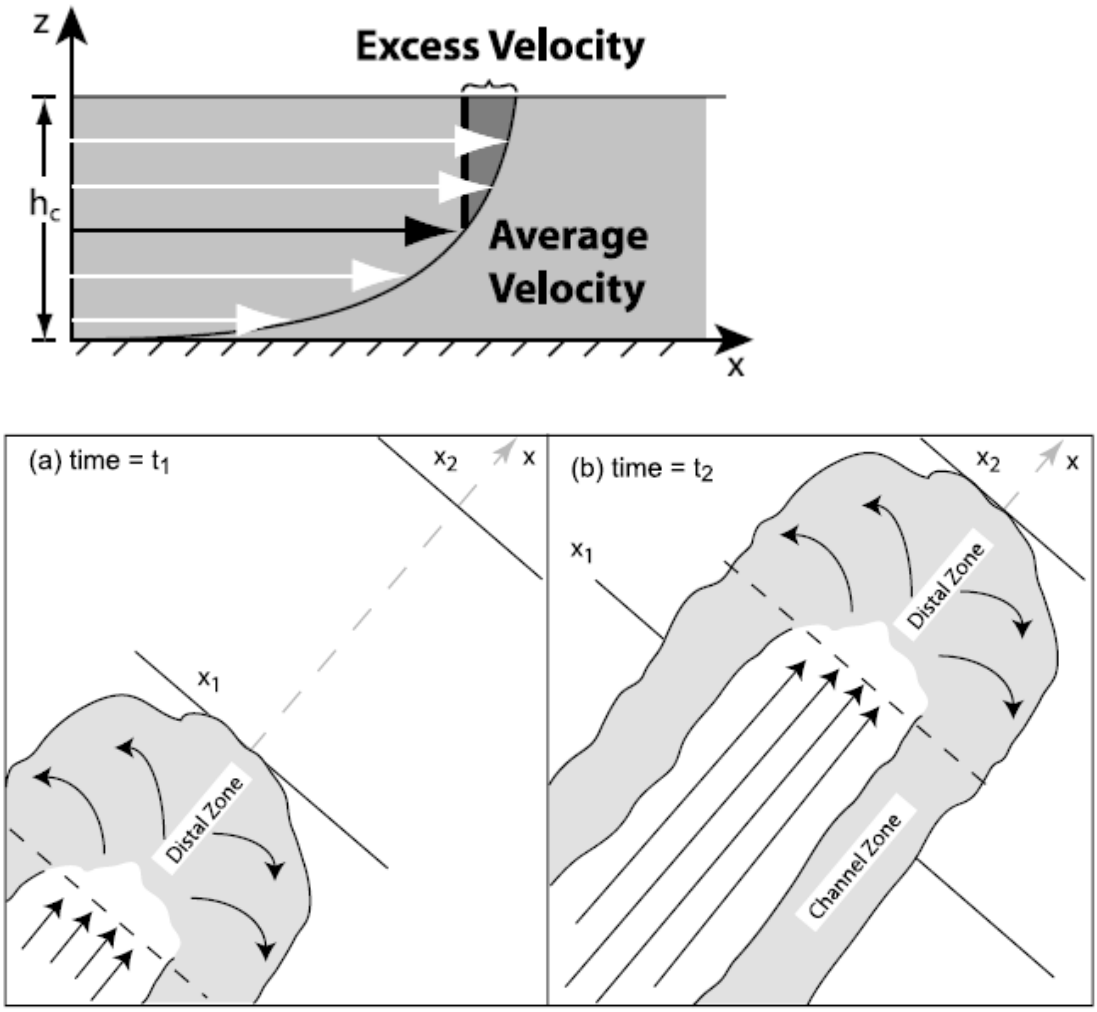

Figure 4: Figures from Baloga and Glaze [2008] explaining how "self-replicating" lava flows are produced. As the flow passes a given point, some mass of the flow at the flow front is deposited to form levees. Once the flow passes this point, the flow and channel width remain relatively constant.

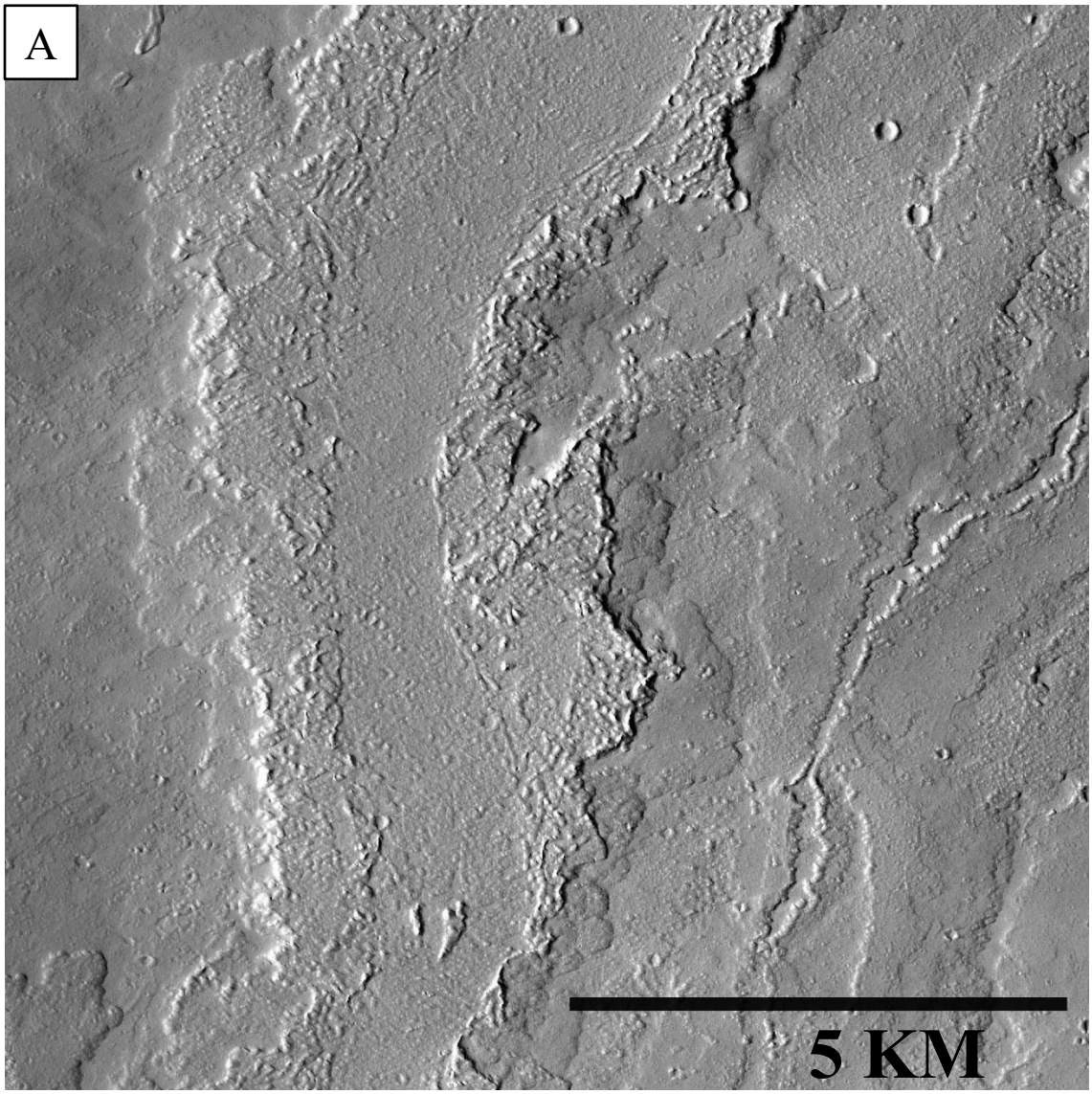
A
5 KM

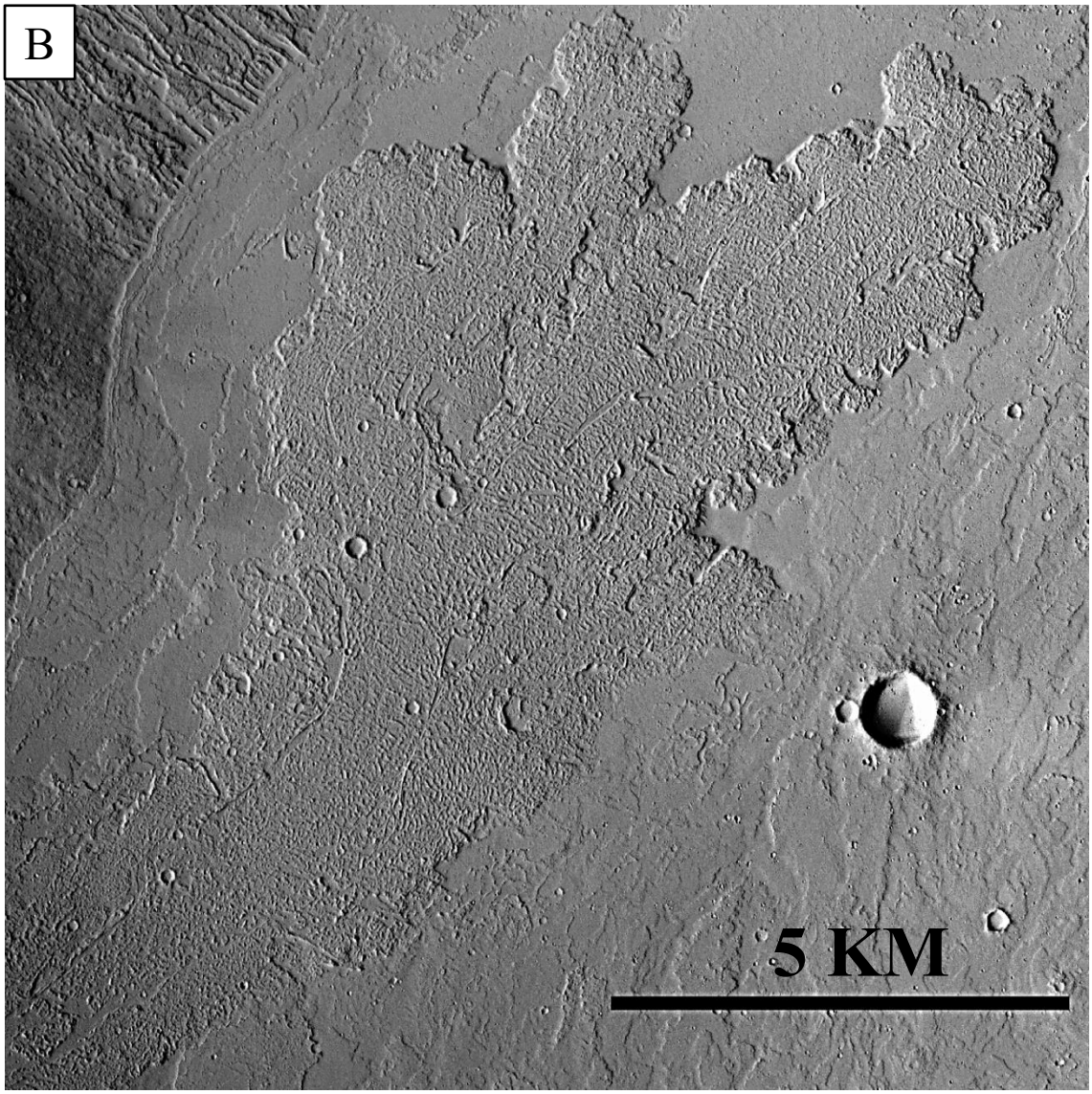
B
5 KM

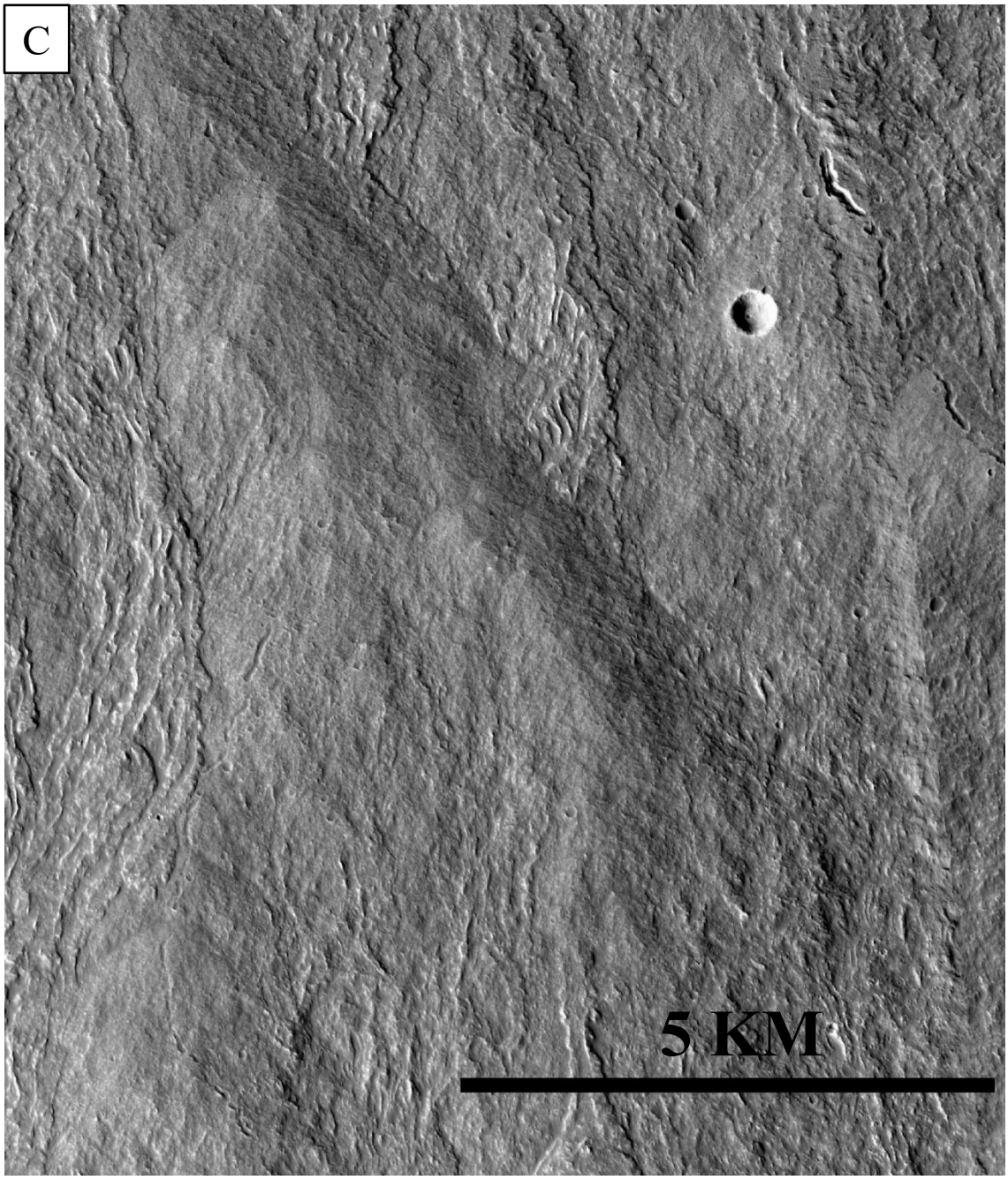

Figure 5: Examples of the three predominant flow morphologies observed in this study. (a) channelized flow (b) corrugated flow (c) ridge flow. North is up in all images. The channelized flow has likely experienced drain out leaving behind a relatively smooth inner channel and raised levees. The ridge flow is likely a channelized flow that has roofed over – a tube-fed flow. Such flows are observed across Olympus Mons, Ascraeus Mons, and Alba Mons [*Sakimoto* et al., 1997; *Bleacher* et al., 2007]

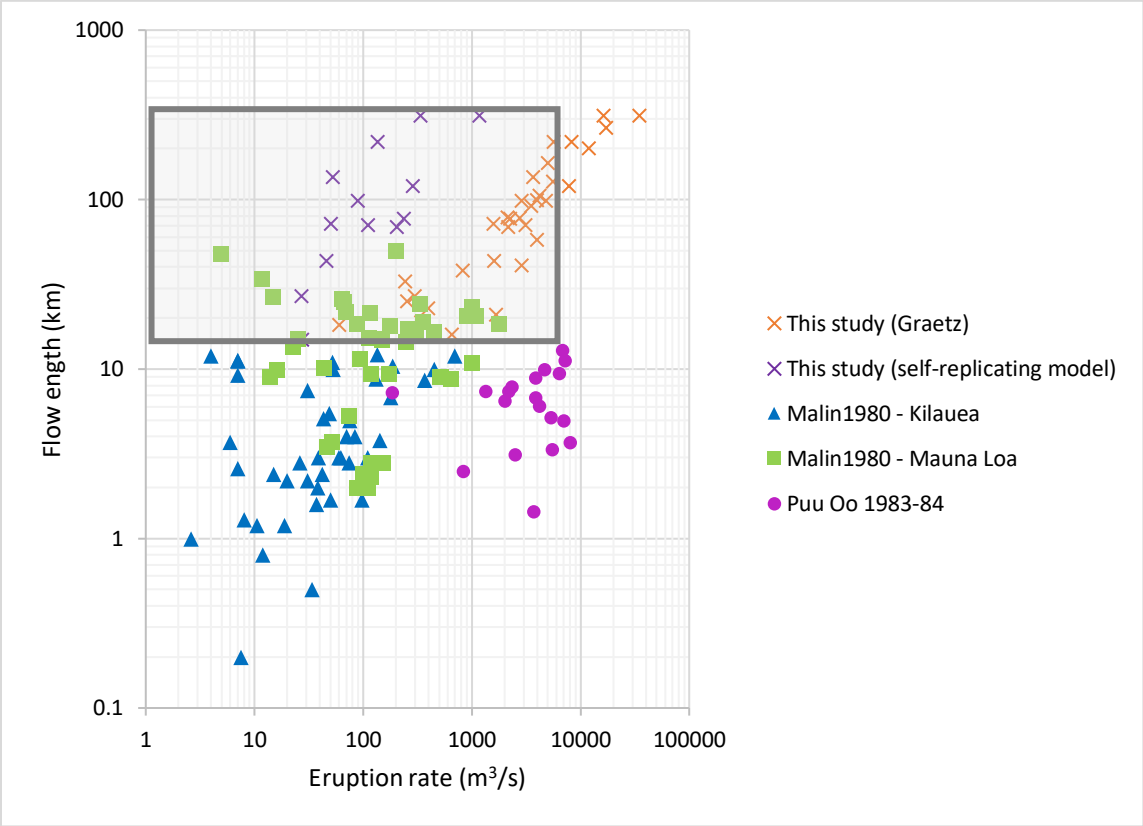

Figure 6: Figured modified from Walker [1973]. Log-log plot shows the length of lava flows as function of the eruption rate for terrestrial lava flows at Mauna Loa, Mt. Etna, and other localities. Superposed on that figure are the eruption rates calculated using the three models in this study. Blue dots are calculated eruption rates using Graetz number. Red dots are eruption rates calculated from self-replication model. Shaded gray box represents area represented by ranges of eruption rates calculated using Ψ.

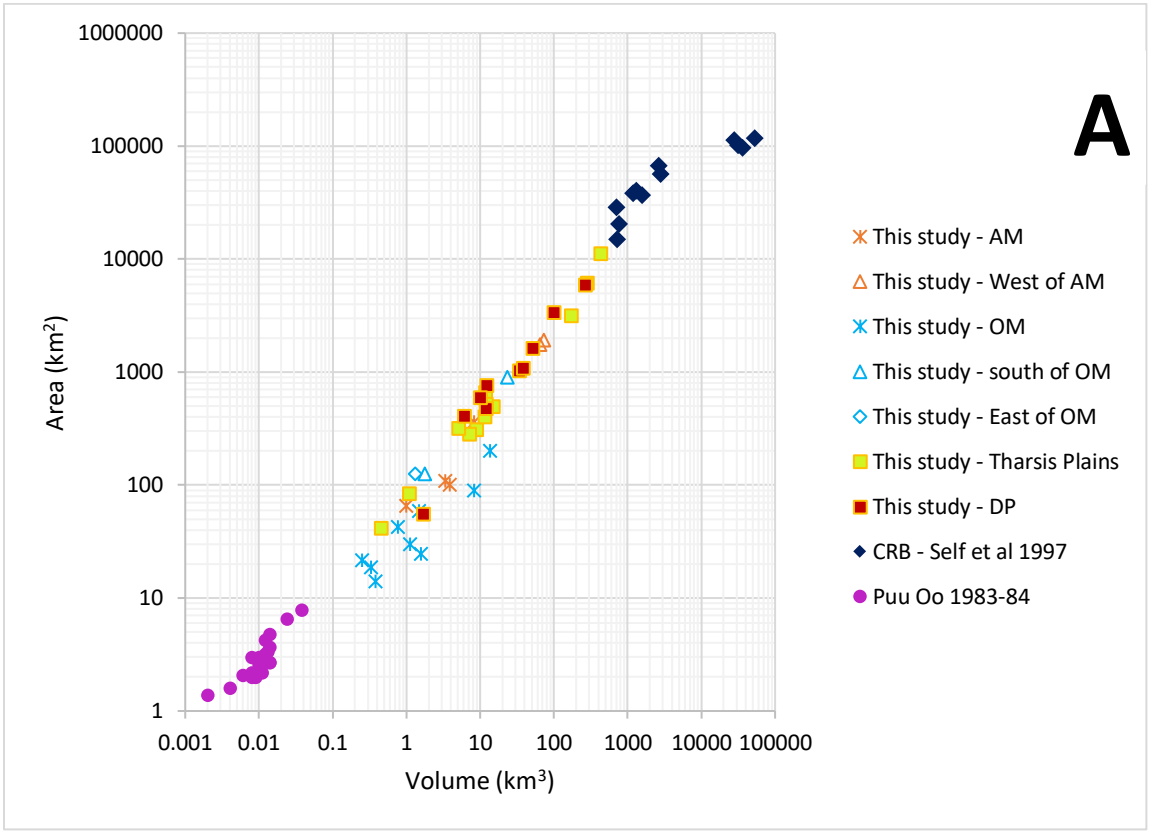
A
1000000
100000
10000
1000
100
10
1
Area (km²)
0.001
0.01
0.1
1
10
100
1000
10000
100000
Volume (km³)
This study - AM
This study - West of AM
This study - OM
This study - south of OM
This study - East of OM
This study - Tharsis Plains
This study - DP
CRB - Self et al 1997
Puu Oo 1983-84

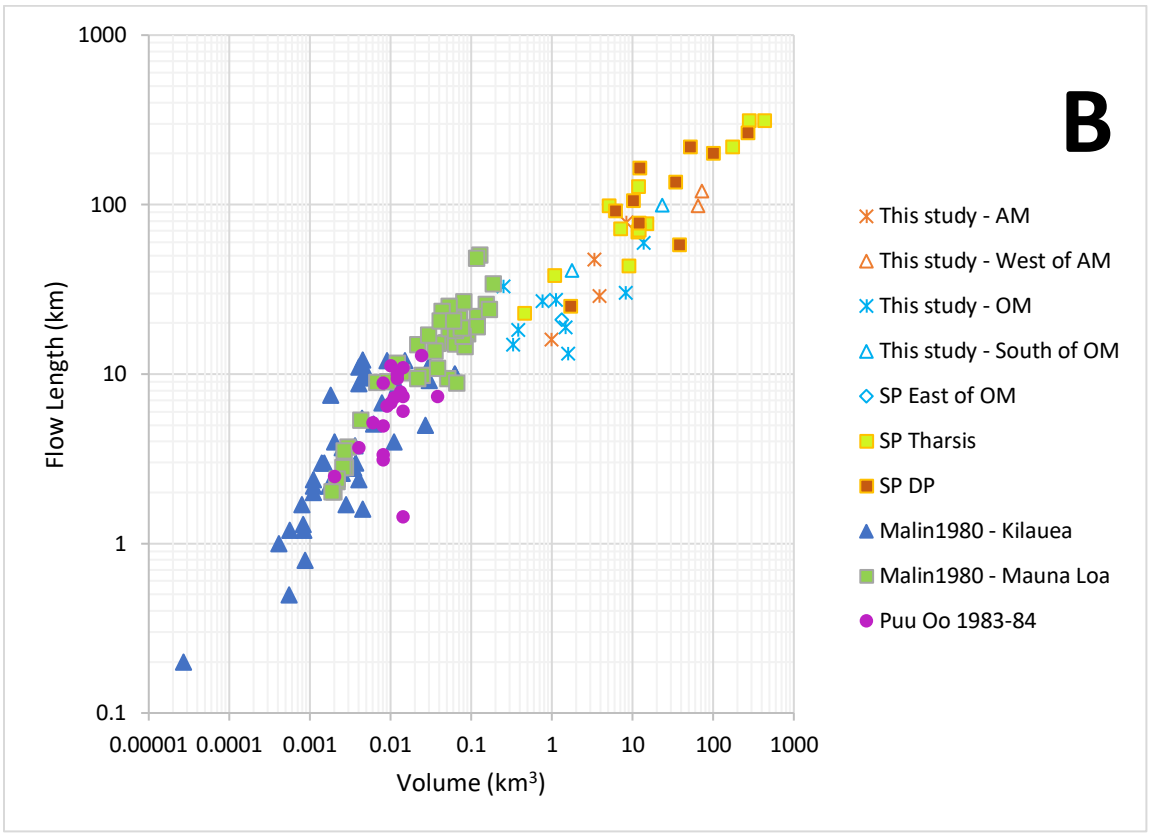
B
Flow Length (km)
1000
100
10
1
0.1
0.00001
0.0001
0.001
0.01
0.1
1
10
100
1000
Volume (km³)
This study - AM
This study - West of AM
This study - OM
This study - South of OM
SP East of OM
SP Tharsis
SP DP
Malin1980 - Kilauea
Malin1980 - Mauna Loa
Puu Oo 1983-84

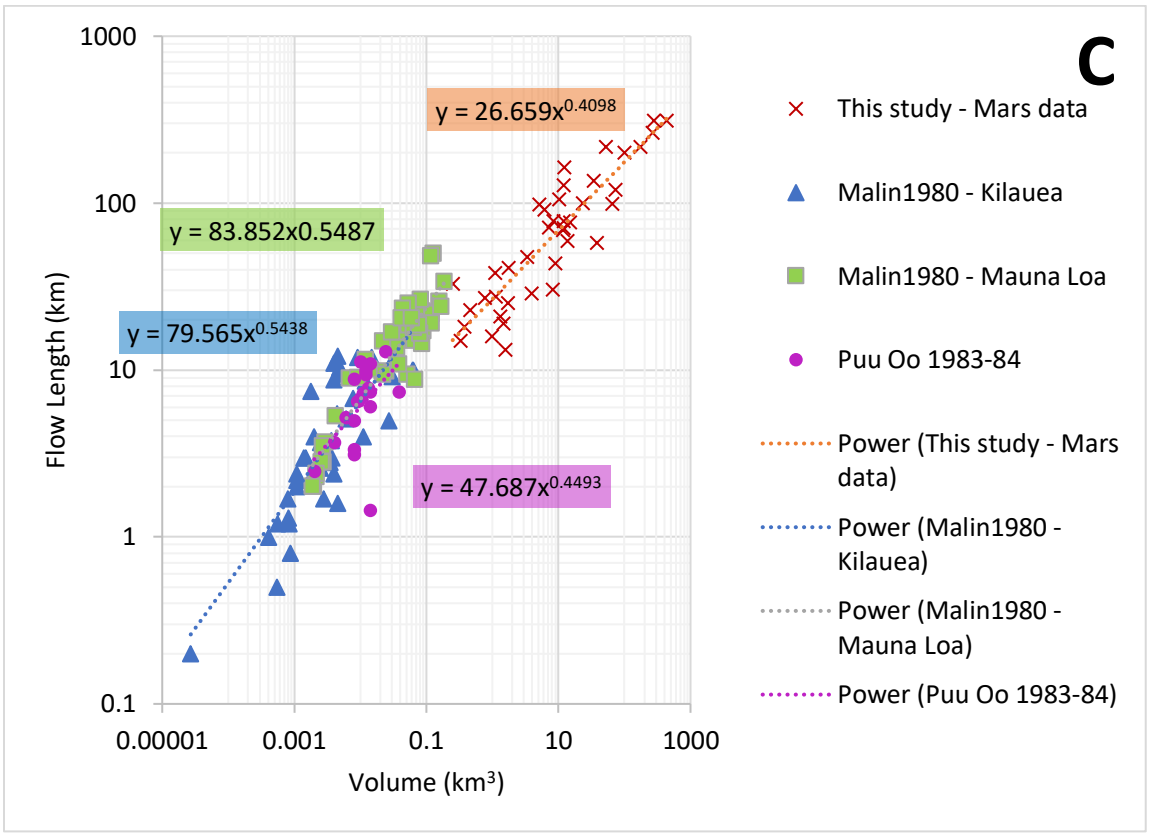

Figure 7: Volumes are expressed as a function of flow length and area covered. AM = Ascraeus Mons; OM = Olympus Mons; DP = Daedalia Planum; CRB = Columbia River Basalts. **(a)** The calculated volumes and area covered of the 40 lava flows observed in this study are plotted along with the 1983-1984 Pu'u O'o lava flows [Wolf et al.] and Columbia River Basalt [*Self* et al., 1997]. The smallest flows are not too dissimilar to the Pu'u O'o lava flows, while the largest flows are similar in size and volume to those erupted in the Columbia River basalts. **(b)** Measured flow length is plotted as a function of calculated volume for 40 lava flows on Mars. The data are compared to terrestrial flows in Hawai'i. The bulk of Martian flows are longer and volumetrically larger, however, a subset of flows primarily related to central volcanoes overlap in length with Mauna Loa flows. **(c)** Power law relationships for Hawaiian lava flows are compared to the Martian lava flows investigated in this study. *Malin* [1980] argued that an exponent equal to 0.5 indicated both length and cross-sectional area of the flows are controlled by volume. The Mars lava flows have an exponent ~0.4 indicating length and cross-sectional area are equally controlled by volume.


A
100000
10000
1000
100
10
1
Area Covered (km²)
1
10
100
1000
10000
100000
Eruption rate (m³/s)
West of AM (self-replicating)
OM (self-replicating)
Tharsis (self-replicating)
DP (self-replicating)
AM
West of AM
OM
South of OM
East of OM
Tharsis Plains
DP
Puu Ooo 1983-84

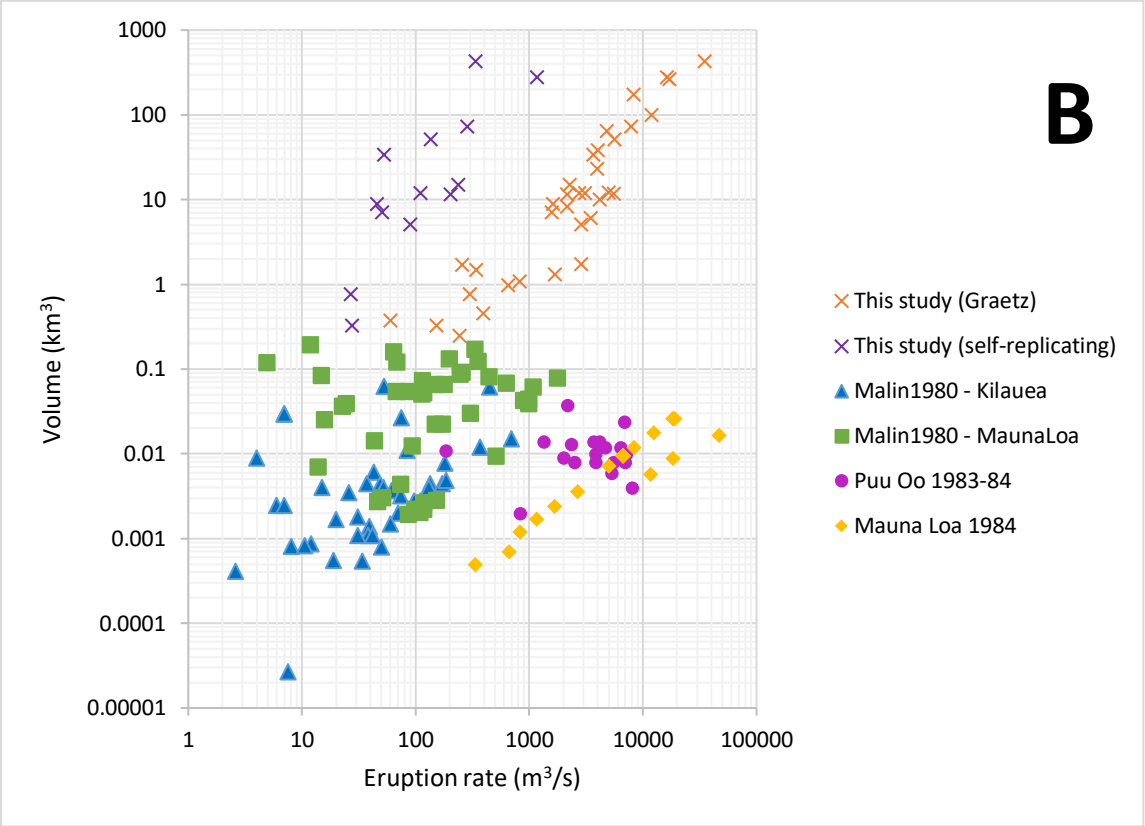

Figure 8: AM = Ascraeus Mons; OM = Olympus Mons; DP = Daedalia Planum. **(a)** Relationship between eruption rate and area covered. Large symbols denote values derived using self-replication model for long lava flows. Small symbols indicate values calculated using Graetz number. Large stars indicate values obtained for central volcanoes using self-replication model, while small stars indicate values for central volcanoes using Graetz number. This data supports the conclusion that eruption rates are controlled by subregions, with higher eruption rates calculated for the volcanic plains than central volcanoes. In general, the self-replication model produces lower eruption rates than using the Graetz number. The Mars flows are compared to flows erupted during the 1983-84 Pu'u O'o eruption in Hawai'i. **(b)** The relationship between eruption rate and total erupted volume. The eruption rates for the Mars lava flows are comparable to terrestrial values. The highest eruption rates calculated for Mars are similar to the highest values observed on Earth during the Mauna Loa eruption of 1984. Although the lower volume estimates are similar to those observed on Mauna Loa, most of the flow volumes are 2 – 4 orders of magnitude greater.

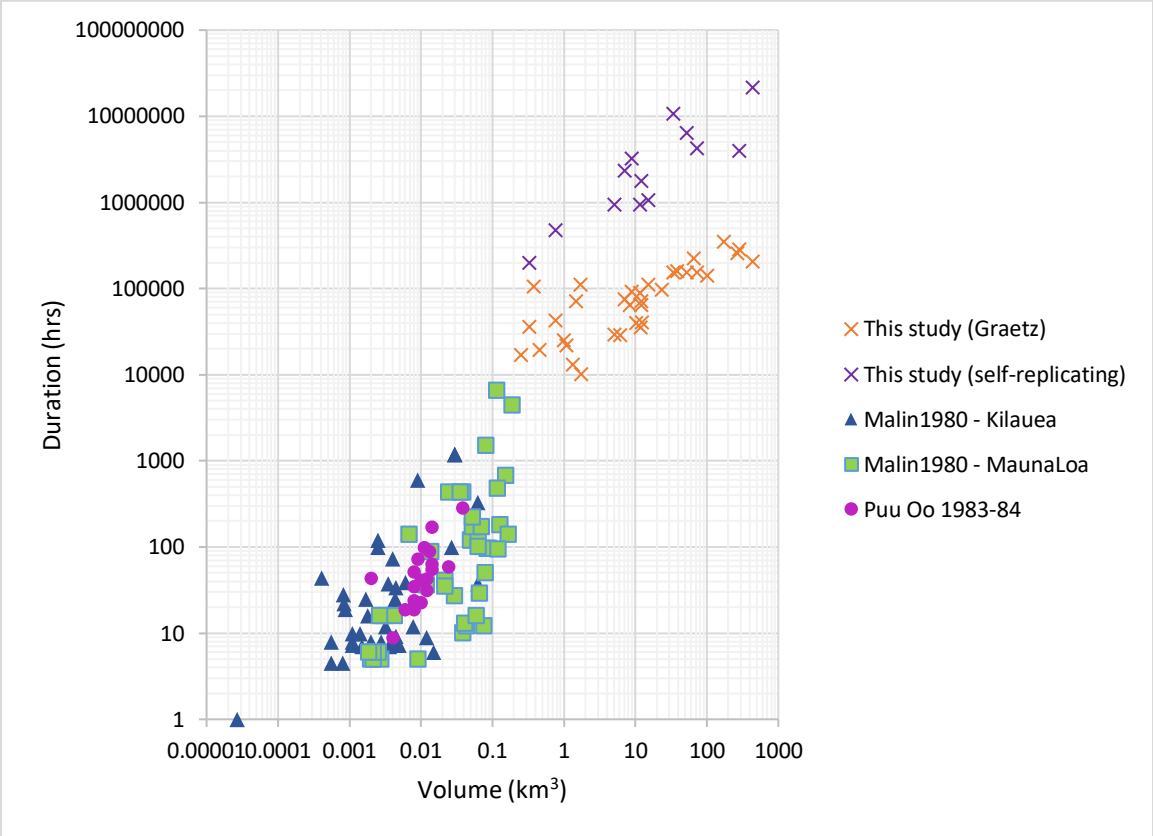

Figure 9: The calculated volume of Mars lava flows are compared to terrestrial flows as a function of duration of emplacement. The Mars lava flows are much larger in volume – although some values are similar to Mauna Loa – and erupted over greater lengths of time. This suggests that feeder dikes and other pathways necessary to producing these flows remained active and open for longer periods than pathways on Earth.

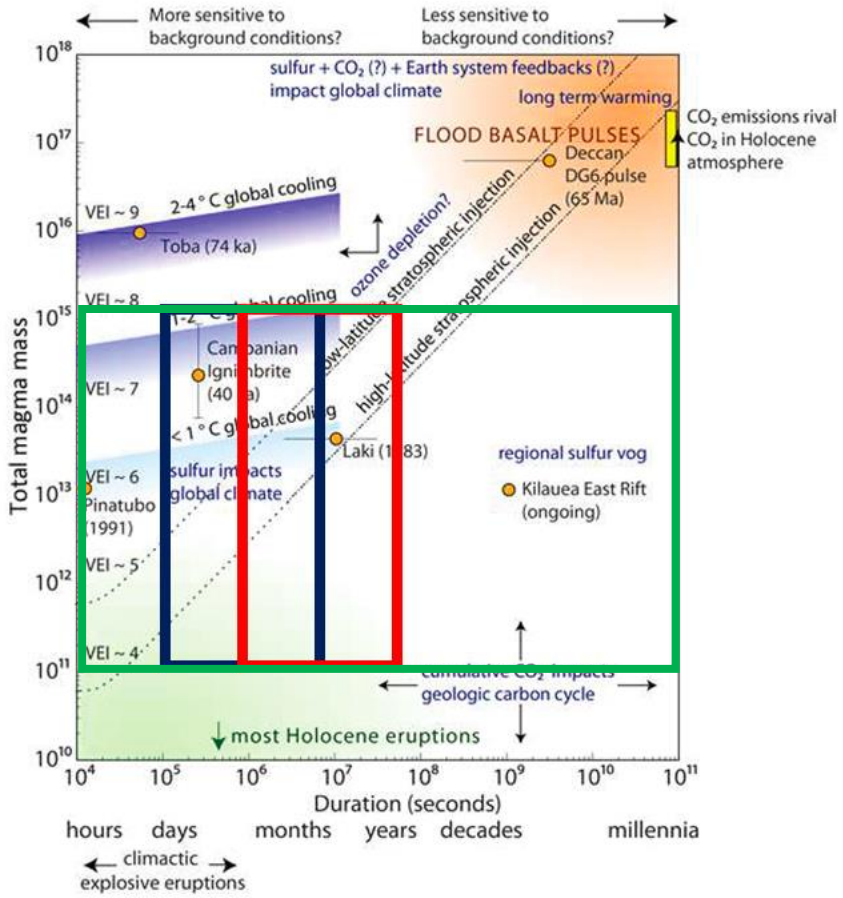

Figure 10: Mass of martian flows and emplacement times are compared with notable terrestrial eruptions. Blue box represents Graetz number minimum eruption durations, while red box represents self-replication model eruption durations. Green box represents eruption durations for full range of Ψ derived eruption rates. Image adapted from Black and Manga [2017].